WAVE PROPAGATION IN POROUS ROCK AND MODELS FOR CRUSTAL STRUCTURE

A DISSERTATION
SUBMITTED TO THE DEPARTMENT OF GEOPHYSICS
AND THE COMMITTEE ON GRADUATE STUDIES
OF STANFORD UNIVERSITY
IN PARTIAL FULFILLMENT OF THE REQUIREMENTS
FOR THE DEGREE OF
DOCTOR OF PHILOSOPHY

By
Terry Dean Jones

June 1983

TABLE OF CONTENTS

WAVE PROPAGATION IN POROUS ROCK AND MODELS FOR CRUSTAL STRUCTURE

Terry Dean Jones, Ph.D.

Stanford University, 1983

The physics of wave propagation and attenuation in porous rock is a critical input to crustal exploration seismology. New experimental results are reported on velocity and attenuation in wet sandstone at elevated temperature and pressure. Both velocity and attenuation decrease with increasing temperature at all pressures. This proves that thermal relaxation is not operating under these conditions. Rather dissipation is controlled by a viscous fluid flow mechanism, in which a sharp frequency peak in attenuation is shifted from 2 kHz at room temperature to 8 kHz at 120° *C* as the pore fluid viscosity is decreased with increasing temperature. The frequency dependence is not spread or suppressed with increased pressure, but the modulus defect is decreased.

A greater knowledge of Q in crustal rocks has aided interpretation of deep seismic reflection profiles of the Wind River mountains, Wyoming. Numerous reflections at long travel times are controversial because of the possible presence of multiples from the shallow sedimentary section. True amplitude synthetic seismograms are computed, using a Q structure controlled by spectral analysis of near surface reflections, and compared to true amplitude data records. It is found that multiples from sedimentary rocks do not arrive with sufficient amplitudes at long travel times to obscure true reflections from the crystalline basement of the lower crust. The deep reflection horizons observed at 6 to 15 seconds are primary events caused by a fine laminar structure of the crystalline section. Lamina thicknesses of 100 to 300 meters, each with reflection coefficient of 0.02 to 0.05 adequately model the data.

Some of these deep reflections are believed to be caused by ductile shear zones in the basement. Field studies of exhumed mylonite belts and laboratory measurement of physical properties of mylonites and their associated protoliths have shed light on the physical properties of dynamically

metamorphosed rocks responsible for their seismic signature. In rock containing significant amounts of phyllosilicates and little feldspar, strong anisotropy may develop during ductile deformation. True amplitude seismic modeling incorporating anisotropy and the fine layered structure of the fault zone indicates an anisotropy of 7% may produce strong seismic reflections even though the mean velocity of the mylonite is unchanged. It is also shown that zones of elevated pore pressure may produce seismic reflections in crystalline and sedimentary rocks if permeability is sufficiently low.

Chapter 1

INTRODUCTION

A portion of the COCORP Wind River profile is shown in Figure 1 (see chapter 3 for a full discussion). Several features in this line summerize the aims of this work, which involves the applications of rock physics principles to reflection seismology. What is the nature of the deep reflections from the crystalline basement, and how can we distinguish between multiple and primary events on a deep section? What is the effect of realistic attenuation structures on deep seismic reflection profiles? The Wind River thrust apparently is a strong reflector through 20 or 30 kilometers of the crust. What physical properties of the deformed rock are responsible for the seismic reflections? A zone of elevated pore pressure has been inferred in the sedimentary section from well logs. How does pore pressure effect seismic velocities and reflections and what range of in situ permeabilities are required to maintain high pore pressure in sedimentary and crystalline rock? More generally, what physical processes are responsible for wave propagation in crustal rocks?

The science of exploration geophysics generally involves four distinct processes. The measurement of some physical field is made at the surface of the earth. The measured field is presumably influenced by subsurface physical properties of some interest. Mathematical techniques are then used to invert or infer from the data the depth dependence of the relevant physical property. A geologic interpretation is made based on the inversion and drawing upon the interpretors experience in surface geology and previous interpretations which have been directly tested by drilling, other geophysical

methods, etc. Finally, and perhaps most rarely, the principles of rock physics are applied to infer from the measurements the rock type and in situ conditions to which the rock is subject. This is based primarily on laboratory measurements of physical properties of rocks under controlled conditions. Each of these steps is limited by various problems of non-uniqueness, stability, resolution, and lack of adequate testing of interpretations.

Reflection seismology continues to be by far the most widely used method for crustal exploration. The techniques for data acquisition and inversion of reflection data have been exceedingly well developed by the oil industry. Yet in the last decade as emphasis has shifted from structural traps to the more elusive stratigraphic traps interest has focused more on the direct detection of hydrocarbons. This work is hindered by our relatively poor understanding of the details of the physics of wave propagation and attenuation in porous, heterogeneous, anisotropic, inelastic, and multiphase rocks (Jones and Nur, 1983).

In recent years reflection seismology has been applied with increasing success to the study of the entire thickness of the continental crust (Oliver, 1982). The much greater resolution of this method over refraction seismology has markedly increased our understanding of the structure of the lower crust. A much greater degree of crustal heterogeneity has been found then was suspected from refraction work (Schilt et. al., 1979), and some long standing debates have been settled, such as the kinematics of crustal deformation at depth in the Laramide orogeny (Smithson et. al., 1979).

However many problems are associated with deep reflection work. While some of the techniques may be borrowed from the oil industry, the interpretation of deep seismic reflection profiles is not subject to direct tests by drilling. Much less is generally known about the geology and physical properties of the deep crust. Other problems are associated with the nature of the experiments. For example, the moveout from reflections recorded at very long travel times is insufficient to allow accurate velocity analysis at depth.

One controversy centers over the nature of deep reflections. It has been suggested in at least one instance that the deep events are predominantly multiples (Zawislak and Smithson, 1981). It is clearly a major problem to develop criteria to distinguish reflected energy at long travel times which is due to multiples from the overlying sedimentary section and true events generated within the deep basement. Another problem centers around the physical properties responsible for reflections from deep ductile shear zones (Jones and Nur, 1982).

This thesis contains four chapters dealing with the physics of wave propagation in rocks and the application of rock physics to the interpretation of reflection seismology.

Chapter 2 presents some new data on laboratory measurements of seismic wave velocity and attenuation at elevated temperatures and pressures in wet sandstones. This experiment is designed specifically to test the proposed thermoelastic mechanism of attenuation, which predicts a strong increase in attenuation with temperature (Kjartansson, 1979). In our experiment the opposite effect is observed. Attenuation of shear and extensional waves in partially and fully saturated sandstone increases with temperature. This effect was observed at confining and pore pressures to 200 bars. Velocity increases with temperature as well. The results prove that thermal relaxation is not operating under these conditions. Rather the velocity and attenuation data suggest a viscous fluid flow model, in which a frequency peak at 2 kilohertz at room temperature is shifted to higher frequencies as the increasing temperature decreases the fluid viscosity. We also find that the frequency dependence is fit quite well with the model of a standard linear solid with a single relaxation time. Although the modulus defect decreases with pressure the frequency peak is not spread out.

Chapter 3 involves the use of synthetic seismograms incorporating a depth variable attenuation, compared to true amplitude deep crustal reflection data, to model deep reflections. A Q structure for the crust in Wyoming near COCORP Wind River lines 1, 1a, and 2 is inferred by modeling the spectral content and amplitudes of the data. Synthetic seismograms are

generated incorporating this Q structure as well as velocities from borehole sonic logs. It is found that for any reasonable Q structure multiples generated in the sedimentary section of the upper crust do not have sufficient energy to show up as reflections at travel times corresponding to the deep crystalline basement. This is because multiples are traveling entirely within the sedimentary section which is much more attenuating than the crystalline section. Furthermore it is unlikely in general that multiples from a sedimentary section are a problem in deep crustal profiles, although multiples generated within crystalline rock may persist deeper in the section. Modeling of the amplitude and frequency content of the deep reflections indicates they are caused by thin laminations of alternating high and low velocity or anisotropy.

Chapter 4 deals with the effect of elevated pore pressures on seismic velocities and reflections. Laboratory data is summarized in an equation which relates velocity to confining pressure, pore pressure, temperature, and saturation. The equation involves several constants which are empirically determined for various rock types. Geologic conditions are postulated in which a zone of anomalously high pore pressure is created in either a sedimentary basin or the crystalline basement. The transient solution for pore pressure distribution in a heterogeneous material (corresponding to a geologic trap) is solved. At appropriate time intervals the depth and pore pressure distribution is used along with our empirically determined velocity pressure relation to compute the velocity profile, and then a synthetic reflection seismogram. It is found for this simple model that pore pressure distributions which give rise to significant velocity anomalies persist for geologically very short periods of time unless zones of very low permeabilities (less than a nanodarcy) exist.

In chapter 5 all these results are brought together to address the problem of seismic reflections from deep crustal fault zones (Jones and Nur, 1982). Exhumed zones of extensive ductile deformation in crystalline rock are examined. Samples of mylonites and their associated protolithic units have been collected for detailed study. Measurements of seismic velocity and

anisotropy at elevated pressure and petrographic work detail the conditions under which ductile shear zones may be seismic reflectors. Ductile deformation by itself does not strongly alter the velocity or density of a rock. It may however cause some rocks to become strongly anisotropic because ductile and anisotropic minerals, principally phyllosilicates, have strong preferred orientations of crystallographic axes in extensively deformed rocks. This effect is not strong in rock of granodioritic composition, but may be pronounced in rocks containing larger amounts of phyllosilicates. Seismic modeling of fault zones in the Wind River profile incorporating the crustal structure arrived at previously indicates that for suitable arrangement of laminations some of the mylonitic rocks measured can account for the reflections from the Wind River and Pacific Creek thrust faults.

REFERENCES

Jones, T. D., and A. Nur, Seismic velocity and anisotropy in mylonites and the reflectivity of deep crustal fault zones, Geology, 10, 260-263, 1982.

Jones, T. D., and A. Nur, Velocity and attenuation in sandstone at elevated temperatures and pressures, Geophys. Res. Lett., 10, 140-143, 1983.

Kjartansson, E., Attenuation of seismic waves in rocks, Ph. D. Thesis, Stanford University, Stanford, California, 147 p., 1979.

Oliver, J., Tracing surface features to great depths: A powerful means for exploring the deep crust, Tectonophysics, 81, 257-272, 1982.

Schilt, S., J. Oliver, L. Brown, S. Kaufman, D. Albaugh, J. Brewer, F. Cook, L. Jensen, P. Krumhans, G. Long, and D. Steiner, The heterogeneity of the continental crust: Results from deep crustal seismic reflection profiling using the Vibroseis program, Rev. Geophys. Space Physics, 17, 354-368, 1979.

Smithson, S. B., J. A. Brewer, S. Kaufman, J. E. Oliver, and C. A. Hurich, Structure of the Laramide Wind River uplift, Wyoming, from COCORP deep reflection data and from gravity data, J. Geophys. Res., 84, 5955-5972, 1979.

Zawislak, R. L., and S. B. Smithson, Problems and interpretation of COCORP deep seismic reflection data, Wind River range, Wyoming, Geophysics, 46, 1684-1701, 1981.

FIGURE CAPTION

Figure 1. True amplitude section of the COCORP Wind River line 1. Vertical scale is two way travel time in seconds. See chapter 3 for a full discussion.

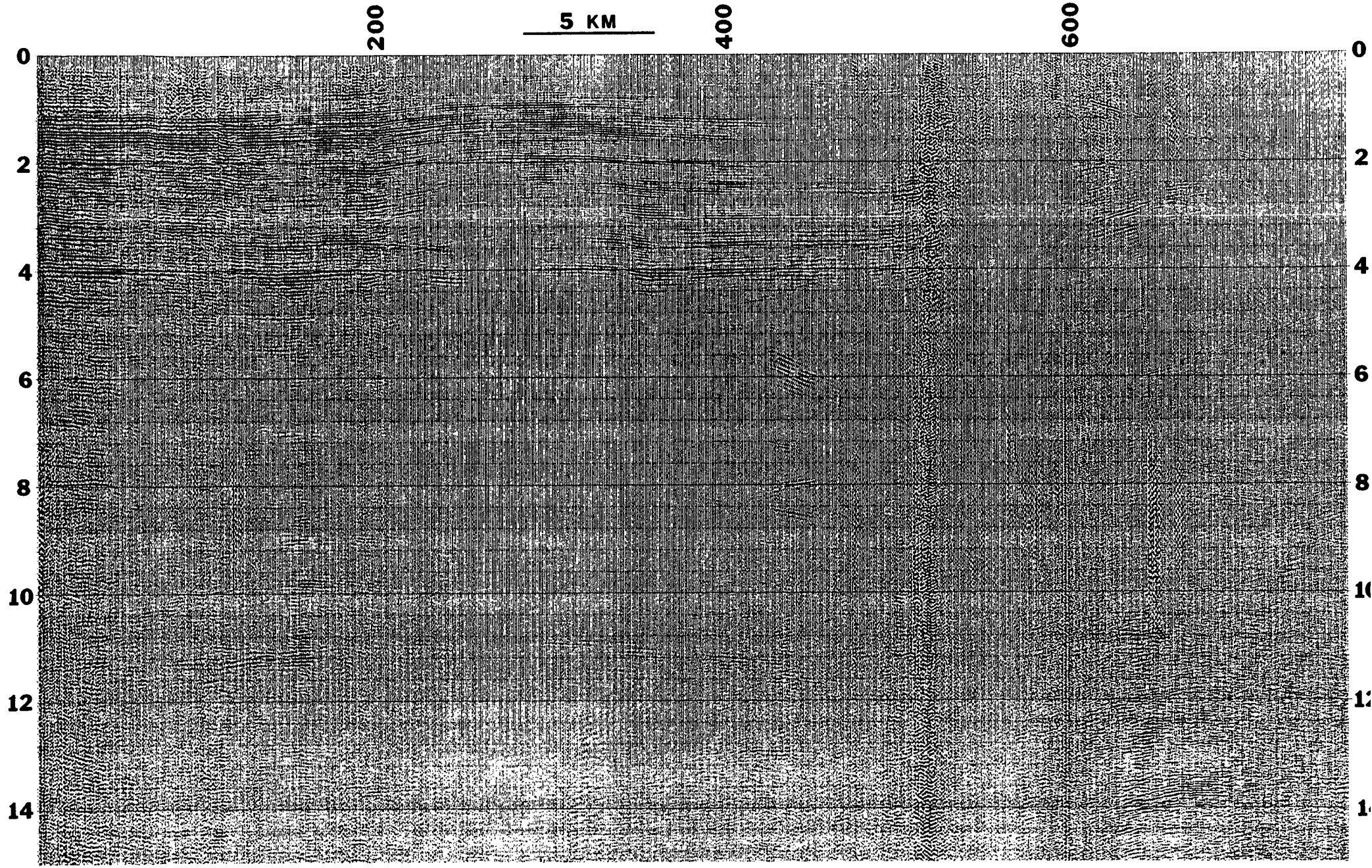
200
5 KM
400
600
0
2
4
6
8
10
12
14

Chapter 2

EFFECT OF TEMPERATURE, PORE FLUIDS, AND PRESSURE ON SEISMIC WAVE VELOCITY AND ATTENUATION IN ROCK.

ABSTRACT

New measurements of seismic wave velocity and attenuation are reported in the kiloHertz frequency range to temperatures of 140°C, confining and pore pressures to 200 bars in Berea sandstone. With increasing temperature, shear velocity and attenuation decrease at all pressures in a fully water saturated rock. In a partially saturated rock at low pressure, shear and extensional attenuation decrease with temperature to 130°C. Velocities first decrease, then increase with increasing temperature. The data show thermoelastic attenuation is not a significant loss mechanism under these conditions. We propose that dissipation is controlled by a viscous fluid flow mechanism, in which a sharp frequency peak in attenuation is shifted from about two kiloHertz at room temperature to about eight kiloHertz at 120°C as the pore fluid viscosity is decreased with increasing temperature. Frequency dependence is not significantly suppressed by the application of pressure. The velocity decrease is too great to be accounted for by a change of relaxation times. A non-dispersive temperature softening in shear and/or chemical effects may control the velocities. Mechanisms for attenuation of seismic waves under shallow crustal conditions which have a solid theoretical basis are evaluated in light of this data and results from other workers. Some form of wave induced fluid flow is the only mechanism which is consistent with most of the experimental evidence. A remaining problem is identifying the

geometrical or transport properties of the pore space which are responsible for the finely tuned nature of the loss mechanism. This may be related to upper and lower limits of pore aspect ratios beyond which losses are insignificant.

INTRODUCTION

Despite much attention in recent years, the mechanism by which seismic wave energy is dissipated in rocks in the form of heat and the relationship of attenuation to dispersion remain elusive. Laboratory data and theoretical work suggest that the interaction of pore fluids with the rock matrix is critical in controlling seismic attenuation. Yet the exact nature of the interaction is unclear (Winkler and Nur, 1982; Murphy, 1982a; Spencer, 1981; Johnston, 1981).

The anelastic component of seismic wave propagation is an important parameter because, when measured along with the seismic velocity it may provide an additional constraint on the in-situ state of subsurface formations. Specifically, attenuation is very sensitive to the relative amounts of fluid and gas in the pores (Winkler and Nur, 1982; Murphy, 1982a) and the effective pressure (Winkler and Nur, 1982). Furthermore attenuation is intimately associated with velocity dispersion.

Early observations that seismic wave attenuation was roughly independent of frequency over a large frequency range (Birch and Bancroft, 1938; Peselnick and Outerbridge, 1961; Pandit and Savage, 1973) suggested a rate independent process was controlling attenuation, such as sliding friction between contacts within the rocks (Walsh, 1966). Theory indicates a strong amplitude dependence for this mechanism (Mavko, 1979). Laboratory studies show proper amplitude dependence only at very low effective pressures and at strains greater than 10^{-6} (Gordon and Davis, 1968; Winkler and Nur, 1982), far in excess of seismic strain values. Furthermore the frictional mechanism cannot account for the strong effect of pore fluids in controlling seismic attenuation (Winkler and Nur, 1982; Clark et. al., 1980; Murphy, 1982a).

This has shifted emphasis to a mechanism in which energy is dissipated by relative motion of the pore fluid and the rock matrix induced by the strain wave. Numerous theories for fluid flow related mechanisms exist (Biot, 1956 a and b; Stoll, 1974; Mavko and Nur, 1975; White, 1975; O'Connell and Budiansky, 1977; Dutta and Ode, 1979 a and b; Dutta and Seriff, 1979; Mavko and Nur, 1979; Palmer and Traviolia, 1980; Mochizuki, 1982 and many others), but it is difficult to distinguish between say, inertial coupling, viscous relaxation, regional flow, local flow, etc. It has also become apparent in the last few years that seismic attenuation is in fact not frequency independent in rocks containing fluids, with a strong frequency peak in the kiloHertz range (Winkler and Nur, 1982; Spencer, 1981; Murphy 1982b; Jones and Nur, 1983). Depending on the model and the geometry of the pore structure, this provides an important, though as yet inadequately treated constraint on the attenuation mechanism and the matrix properties which are primarily responsible for driving the fluid flow.

Another theory for attenuation deals with thermoelastic relaxation of the fluid-rock system (Kjartansson and Nur, 1982). It is not possible to distinguish between this mechanism and some of the flow related mechanisms by room temperature measurements. However thermal mechanisms predict a strong dependence of attenuation on temperature. A number of measurements of attenuation have been made in rocks subjected to elevated temperature, either before or during the measurement (Kissell, 1972; Clark et. al., 1981; Johnston and Toksoz, 1980b). These have all been done on initially dry samples of uncontrolled fluid content, so the results are difficult to interpret. The decrease of attenuation with temperature generally observed is undoubtably dominated by the driving off of small amounts of losely bound volatiles, which are known to have a strong effect on attenuation (Clark et. al., 1980).

We present here new data on the temperature and pressure dependence of velocity and attenuation in water saturated sandstone. This experiment was designed specifically to distinguish between the thermal relaxation mechanism and fluid flow related mechanisms by observing the temperature

dependence. It has also yielded important new information about the viscosity and frequency dependence of attenuation, as well as the pressure dependence of attenuation.

EXPERIMENTAL TECHNIQUE

Experimental measurements of attenuation have been carried out by numerous techniques (for a review see Toksoz and Johnston, 1982). Our results are all obtained using the bar resonance method. The design and theoretical basis for this experiment have been discussed in detail by Winkler (1980).

Briefly, a cylindrical sample of rock about 30 centimeters long and 2 centimeters in diameter is clamped at the center, which becomes a node. It is then made to vibrate in either its extensional or torsional mode of resonance by means of electromagnetic transducers acting on permanent magnets attached to one end of the sample. A similar arrangement of permanent magnets and electromagnets at the other end of the sample receives the signal. The signal is amplified and displayed on an oscilloscope. The sinusoidal source signal fed into the electromagnets is abruptly shut off. The received signal then decays exponentially, the coefficient of the exponent being related to the quality factor Q of the rock. Our definition of Q is the fractional energy loss per wave cycle, following that of O'Connell and Budiansky (1978). By selecting appropriate materials for jacketing the sample and for the transducers, the entire apparatus may by slipped into an externally heated pressure vessel. A small tube attached to the node of the sample allows us to apply a pore pressure of fluid or gas.

We are able to independently control confining and pore pressure (to 200 bars) and temperature (to 140°C). Strains are well below the value (10^{-6}) above which non-linear effects may become noticeable (Winkler and Nur, 1982). Frequencies range from 1700 Hz to 3700 Hz depending on temperature, pressure, and mode of vibration. In all fluid saturated experiments samples were cycled through the temperature and pressure range of the anticipated experiment before any data was collected.

The rock is a Berea sandstone, a medium grained quartzose sandstone. It contains about 84% quartz, 6% clay (kaolinite and illite), 2% feldspar, and 8% amorphous silica. It has a porosity of about 21%. Permeabilities of the two samples discussed here are 617 millidarcies (Berea 500-600) and 1000 millidarcies (Berea 1000) (Nur et. al., 1980).

It is difficult to quantify the errors involved in our measurements. Precision of velocity data is better than 1%. Accuracy is much less due to uncertainties involved in correcting for the mass loading of the sample from the magnets and jacketing. Measurements on samples of aluminum and acrylic plastic of known properties indicate an accuracy of 5 to 10%. Calculation of precision of Q measurements from goodness of fit to the exponential decay yields values of 2 to 3%. It is probably more commonly 5 to 10% due to interference with spurious resonance peaks. Measurement of Q in a jacketed aluminum bar yielded values of about 500, independent of temperature and pressure. This implies accuracy errors from losses to the system of 20% for a Q of 100, less for lower Q. Measurements on acrylic plastic give Q values of 20 to 24, in agreement with values in the literature (Winkler, 1980).

RESULTS

Given the non-linear effects at high strain amplitudes (Winkler and Nur, 1982) it is important to ensure that our measurements are in the linear range. Figures 1-4 show the amplitude dependence of velocity and attenuation at temperatures of 25° C to 250° C. While we are unable to directly measure the strain amplitude, we infer from results of Winkler and Nur (1982) among others, that the strain amplitude independent portion of these curves is below a strain of about 10^{-6}. This extends previous work to indicate low strain attenuation is linear at high temperature. In all subsequent experiments care was taken to ensure each measurement was in the linear range.

Figures 5 and 6 detail the effect of volatiles on velocity and attenuation in 'dry' sandstone. The rapid increase in velocity with temperature cannot be explained by a density effect. A surface and chemical related effect on the

matrix by small amounts of absorbed water as proposed by Tittmann et. al. (1980) and Murphy (1982b) is probably more important. At temperatures above 200°C thermal cracking is most likely responsible for decreasing the velocities. The rapid initial decrease in attenuation from 25°C to 100°C is also likely due to driving off of volatiles (Clark et. al., 1981). Attenuation is then level to about 175°C where it again drops. More tightly bound volatiles, perhaps in the clays might be boiled off at this point. This is consistent with the results of Clark et. al. (1981). They found decreased attenuation in a Berea sandstone thermally cycled to 384°C over a sample cycled to 94°C.

More relevant to upper crustal exploration where a free fluid phase is generally present are measurements in a fluid saturated rock. Shear wave velocity and attenuation as a function of pressure and temperature are shown in Figure 7 for a water saturated sample (Berea 500-600). We also list the viscosity of water at the appropriate temperatures. The observed increase of velocity and decrease of attenuation with pressure is typical (i.e., Winkler and Nur, 1982). However, a new and surprising result is the strong decrease in velocity with temperature at all pressures; and the decrease in attenuation with increasing temperature. The attenuation decreases by a factor of 1.5 to 2.0 over the range 22°C to 110°C, roughly independent of pressure. Though this result appears similar to that of dry rock, the magnitudes of Q are drastically different and the temperature effects are probably controlled by different mechanisms.

Figures 8 through 11 show the effect of pore pressure on velocity and attenuation at 22°C through 110°C. The velocity at elevated pore pressure is slightly higher than at low pore pressure, hence confining pressure (P_c) is somewhat more efficient in increasing velocity than pore pressure (P_p) is in decreasing it. For effective pressure (P_e) defined as $P_e = P_c - \alpha P_p$, a value of $\alpha = 0.97$ fits the data reasonably well.

At low temperature there is no evidence for any anomalous effect of pore pressure on attenuation. At 85°C and 110°C the attenuation seems to be slightly higher at elevated pore pressures, particularly at low effective pressures. The lack of strong dependence of velocity or attenuation on pore

pressure, particularly at low pore pressures, indicates temperature induced phase transformations are not occurring.

Figure 12 shows velocity and attenuation as a function of temperature and pressure in Berea 1000 to 49°C. The effect of pore pressure on this sample was similar to that of the Berea 500-600 sample. Figure 13 shows velocity and attenuation as a function of temperature in Berea 1000. For this experiment the confining pressure was held at 100 bars and the pore pressure was held at 45 bars. The results are consistent with Figure 7. Velocity decreases with increasing temperature, although the decrease is not as great as that observed in the Berea 500-600 (Figure 7). Attenuation decreases strongly with temperature at about the same rate as in the Berea 500-600. At the lowest temperatures there may be an initial slight increase of attenuation with temperature before the decrease begins.

We have also measured velocity and attenuation in partially saturated rock at low pressures as a function of temperature (Figures 14 and 15). We are unable to accurately determine the degree of saturation of these samples. They were first fully saturated, then fluid pressure was released and a small amount of gas was pumped in to increase the pore pressure.

Both extensional and shear velocities decrease with temperature to about 110°C. At this point the velocities abruptly increase to very near their low temperature values by 130°C. These changes are much too large to be accounted for entirely by changes of saturation, although this may be a contributing effect. Furthermore pressure and temperature conditions for both this and the full saturation experiment are below the phase transition of water to steam. Upon decreasing the temperature the velocities do not retrace their low value, rather they stay nearly constant.

The large jump in the velocities at about 125°C occurred when the sample was held at constant temperature overnight. Previously measurements and temperature changes had been made about every three hours. This suggests some temperature activated and time dependent chemical reaction has been induced, perhaps silica dissolution and redeposition or alteration of the clays.

The extensional and shear attenuation in the partially saturated rock decreases with temperature by a factor of about five from 22°C to 110°C. There also appears to be a reversal in the relative magnitudes of attenuation at 100°C to 120°C. At low temperatures the extensional wave is more strongly attenuated, at high temperatures the shear attenuation is slightly greater. This effect may be within the experimental error. Nevertheless, it is significant that extensional and shear attenuation are so close at elevated temperature. With decreasing temperature the attenuation increases, although there is some hysteresis, with attenuation generally lower upon decreasing the temperature than on increasing it. We believe this is due to incomplete equilibrium of the sample, it has not fully cooled to the lower temperature between measurements.

The results at low temperatures are consistent with the data of Winkler and Nur (1982) which were obtained at slightly lower frequencies. In partially saturated rock extensional attenuation is greater than shear attenuation and shear attenuation increases on going from partial to full saturation. Our data indicate however, that at elevated temperature shear attenuation may be greater than, or very close to extensional attenuation in partially saturated rock.

INTERPRETATION OF THE DATA

The thermal relaxation mechanism (Kjartansson and Nur, 1982) models losses due to irreversible flow of heat induced by a strain wave in a heterogeneous material. This model predicts a strong increase in attenuation with temperature in a fluid saturated rock. It also predicts attenuation in bulk should dominate at high temperature. Our results are not consistent with this prediction. We observe decreasing attenuation with increasing temperature. It also appears that there is no strong increase in bulk loss in a partially saturated sample at elevated temperature. In fact, the results can be explained if most of the loss is in shear. Hence we conclude that thermoelastic attenuation is not a significant loss mechanism for the conditions under which the experiment was performed.

A number of theories have been proposed where attenuation is due to flow of pore fluids induced by the strain wave (Walsh, 1969; O'Connell and Budiansky, 1977; Mavko and Nur, 1979; Palmer and Traviolia, 1980). These models, although often of complex formulation, may be conceptually visualized as relating attenuation and velocity to the product of frequency and fluid viscosity and a term incorporating the local geometry and matrix properties, such as pore dimensions, matrix moduli, and local permeability.

Thus for losses due to a single matrix geometrical factor or transport property such as pore size or pore connectivity, there will be a single relaxation time or equivalently a frequency peak of attenuation depending on the fluid viscosity. A broadly spread pattern of frequency dependence or roughly frequency independent attenuation may be obtained by a wide distribution of matrix geometries. Recent data (Spencer, 1981; Winkler and Nur, 1982; Murphy, 1982b) shows that attenuation is strongly peaked in frequency at about one to ten kiloHertz, suggesting that a single, or very narrow distribution of relaxation times is controlling the loss mechanism.

If a fluid flow mechanism is controlling the dissipation, changing the temperature and hence the fluid viscosity will shift the attenuation peak to higher frequencies. This will cause attenuation to increase with temperature at frequencies above the peak. At any frequency below the attenuation peak, attenuation should decrease with increasing temperature.

We show how our data may be accounted for by such a shift in Figure 16, The attenuation for the fully saturated Berea 500-600 is plotted as a function of the product of frequency and dynamic viscosity for water at the appropriate temperature. The data is plotted at four different effective pressures. For reference we have plotted the theoretical attenuation for a standard linear solid with a single relaxation time of 5×10^{-4} seconds, for four different modulus defects to account for the decrease in attenuation with pressure. The phenomenological description of a loss peak by a standard linear solid is an excellent description of loss peaks in real materials in which loss mechanisms are linear (Zener, 1948).

A better fit could be obtained by using a narrow distribution of relaxation times to give a slightly broader peak. Regardless, all the attenuation data shown can be explained by the concept of a sharp frequency peak with a shift to higher frequencies proportional to fluid viscosity. We also note that increasing pressure does not suppress the frequency dependence nor does it change the relaxation time, rather it decreases the modulus defect of the rock. When the data at the four different pressures are normalized to the same peak value (Figure 17), the frequency dependence is fairly independent of pressure.

This interpretation is consistent with the data of Tittmann et. al. (1981) and Spencer (1981). Spencer's frequency peak shifts to lower frequencies on decreasing the temperature from 25°C to 4°C by about the same amount as the water viscosity increases over this range. The sample for this experiment was a water saturated Navajo sandstone. Spencer also found that the peak frequency was constant on changing pore fluids from water to ethanol to n-decane. The viscosity of each of these fluids is about the same. The magnitude of the peak attenuation is this experiment varied significantly however. The general behavior is also similar to the relative attenuation measurements by Nur and Simmons (1969) in a glycerol saturated Barre granite.

The viscous fluid interpretation also has implications for the velocity data. In Figure 16 we have also plotted the dynamic modulus vs. the product of frequency and dynamic viscosity for the Berea 500-600 velocity data. For comparison we have also plotted the theoretical dispersion using the modulus defects and relaxation times implied from the attenuation data. We have used ultrasonic measurements at a frequency of one megaHertz to constrain the experimental dispersion curve at high frequencies (see appendix).

Although the decrease of velocity with temperature has the correct sense, the predicted magnitude of the effect is much smaller than is observed, even if the ultrasonic measurements are disregarded. A non-dispersive temperature softening of the shear modulus, similar perhaps to that observed by Spencer and Nur (1976) or Timur (1977) is apparently controlling the

velocities, but not effecting the frequency dependent component of attenuation. The velocity decrease we observe is about 5 to 10% per 100°C at an effective pressure of about 50 bars. This is much greater than the 0.9% decrease in shear velocity per 100°C temperature increase observed by Timur (1977) in a Berea sandstone at similar pressures. Part of the difference, but not all may be accounted for by the frequency peak in the range of the lower frequency data. The effect of temperature on the bulk modulus of the frame and the pore fluid is small in this range and cannot even account for the smaller velocity temperature gradients observed by Timur (1977). Until more work is done the nature of this temperature dependence will remain unclear, though a chemical effect is suggested.

Figure 18 shows a similar fit for the Berea 1000 data (Figure 12). Again the attenuation data is well fit by a standard linear solid with a single relaxation time of 5×10^{-4} seconds at room temperature, shifting to higher frequencies at higher temperatures. Note that the attenuation data for this sample appears to go over the peak, although this is controlled by only one point. The decrease in the dynamic modulus is greater than the theoretical dispersion, though the fit is somewhat better than for the Berea 500-600. We have no ultrasonic data to constrain the unrelaxed modulus for the Berea 1000.

There is no obvious effect on velocity or attenuation of the different permeabilities of the two samples. However it may be that such a small change could not be resolved by our present data. More surprising is that possible permeability or pore geometry changes with pressure apparently do not affect the frequency dependence.

In Figure 19 we have added the partial saturation data to the plot of attenuation vs. the frequency-viscosity product. Considering that some changes in saturation may have occurred during the course of this experiment, the data also seem to be fit reasonably well with a frequency-viscosity peak at two kHz-cp.

THE MECHANISM

It seems relevant at this time to discuss what constraints our data, along with other work in the literature, may place on the attenuation mechanism. We will limit this discussion to consider mechanisms primarily responsible for attenuation in the upper crust at seismic to acoustic frequencies.

First we review the salient experimental observations. Differences between bulk and shear attenuation will be ignored for the moment because of possible coupling between bulk and shear losses (Budiansky and O'Connell, 1980).

1) Attenuation is linear (independent of strain) at seismic strains (Winkler and Nur, 1982; this paper).

2) Attenuation in vacuum dry rocks is negligible compared to upper crustal values, even at low pressure (Clark et. al., 1980; Tittmann, 1977; this paper. For a review of Q values in the upper crust see Jones, 1983).

3) Attenuation is strongly dependent on saturation in rocks containing a free fluid phase (Pandit and King, 1979; Winkler and Nur, 1982; Frisillo and Stewart, 1980; Murphy, 1982a).

4) Attenuation is independent of frequency in dry rocks (Winkler and Nur, 1982; Spencer, 1981; Murphy, 1982b).

5) Attenuation is strongly dependent on frequency in wet rocks with a frequency peak in the kiloHertz range. The peak can be adequately modeled by a single, or very narrow distribution of relaxation times (Winkler and Nur, 1982; Spencer, 1981; Murphy, 1982b; this paper).

6) Attenuation depends on the product of frequency and pore phase viscosity (this paper; Jones and Nur, 1983).

7) The frequency-viscosity dependence is not suppressed nor shifted significantly with increasing pressure. The modulus defect is however decreased with increased pressure (this paper).

8) The effect of temperature may be explained by volatiles in dry rocks, and by fluid viscosity in wet rocks (Clark et. al, 1980; Clark et. al., 1981; this paper).

9) The saturation dependence and frequency-viscosity dependence is apparently independent of rock type, from low porosity and permeability crystalline rock to high porosity and permeability clastic rock. Or at least the variation between rocks is small relative to the drastic changes in porosity, pore geometry, and permeability. This includes measurements on Vycor porous glass with a porosity of 28%, pore diameter of .005 microns, and a permeability of 0.01 millidarcies. (Murphy, 1982b; Spencer, 1981). See Table 1.

10) Attenuation depends on effective pressure (Winkler and Nur, 1982; this paper).

Table 2 lists the attenuation mechanisms most often discussed in the literature. We have also shown the predicted frequency dependence for fluid related mechanisms as well as the critical tests which allow us to evaluate each mechanism in light of the laboratory data, and our conclusions as to the role of each mechanism. A full discussion follows.

Attenuation mechanisms which rely on losses within the frame can be ruled out, primarily because there are negligible losses in the frame when all the volatiles have been removed (Clark et. al., 1980 and 1981; Tittmann, 1977). This includes frictional (Mavko, 1979), dislocation (Mason, 1969), and thermoelastic (Savage, 1966) mechanisms. The frictional mechanism which is still popular (Lockner et. al., 1977; Johnston, 1981; Johnston et. al., 1979) explains virtually none of the observations regarding frequency dependence, saturation dependence, viscosity dependence, and amplitude dependence. Similar arguments may be advanced against other mechanisms for losses to the dry matrix.

It seems clear that the correct mechanism must account for losses due to interaction of the matrix and the pore fluid. Of these, the thermal relaxation mechanism of Kjartansson and Nur (1982) can apparently be ruled out by the lack of appropriate temperature dependence, as shown in this paper. A related mechanism involves phase transformations in a two-phase system. While that mechanism has not been specifically tested here or elsewhere, the lack of a strong increase in bulk losses in the partial saturation experiment at

elevated temperatures indicates it is not important. The measurements of relative attenuation through the water-steam transition by Ito et. al. (1979) can be adequately explained by fluid flow mechanisms (Winkler and Nur, 1982).

The surface mechanism as proposed in different forms by Tittmann et. al. (1980) and Spencer (1982) cannot explain the strong saturation dependence in rocks containing large amounts of pore fluids (Pandit and King, 1979; Winkler and Nur, 1982; Murphy, 1982a). It may however be responsible for a small amount of frequency independent back-round attenuation in upper crustal rocks (Murphy, 1982a).

We are left with mechanisms which are based on flow of pore fluids. While it is possible that a number of these mechanisms may be operating, the strong frequency and saturation peaks seen in a variety of rock types at variable pressures and temperatures strongly suggest that one principal mechanism is dominant in rock containing fluids, at least in the seismic to acoustic range.

Viscous Shear Relaxation. Viscous relaxation of simple shear stresses in a rock containing fluid filled pores is likely the quickest local flow related dissipation mechanism. It has been shown by Walsh (1969), Nur (1971), and O'Connell and Budiansky (1977), that the frequency of peak dissipation (ω) is given by $\omega \approx \alpha\mu/\eta$ where α is the pore aspect ratio, μ is the matrix shear modulus, and η is the fluid viscosity. This formulation has the correct viscosity dependence to explain our data. However for typical values of these parameters in rock with water in the pores this mechanism yields a peak frequency of at least 10^9 Hz. This is far above the frequency range of interest. Furthermore there is such a large range of aspect ratios in common rocks as to make it unlikely that this mechanism could yield such a sharp peak.

Regional Fluid Flow. Flow of fluid between peaks and troughs of a strain wave can cause dissipation. The frequency for diffusion in a medium of hydraulic diffusivity (c) where $c=k/\varphi\beta\eta$ is given by $\omega = v^2/4\pi^2 c$. β is the compressibility of the pore fluid, φ is the porosity, v is the seismic velocity, and k is the permeability. All units are in the c.g.s. system. For values of k of 10^{-8} and φ of 0.1 this gives a frequency of about 50 kiloHertz, which is significantly above that inferred from our data. The values of permeability

and porosity in this mechanism are bulk values, similar to those that would be measured on a laboratory sample, so this mechanism should produce a pronounced dissipation peak. A problem is that it varies linearly with k and φ. Measurements in rocks samples have yet to confirm this. Samples of Vycor porous glass with a permeability of 10^{-13} cm^2, granite of unknown but likely much lower permeability, and Berea sandstone of permeability of 10^{-8} cm^2 all seem to yield frequency peaks in about the same range of one to ten kiloHertz. Furthermore the addition of confining pressure should decrease permeability, though this effect may be too small over the range of 200 bars to resolve with our present data (Nur et. al., 1980). A similar pressure experiment in granite where permeability is more influenced by pressure would be interesting. However as of now it appears that the lack of significant variation in the frequency peak with rocks of radically different permeabilities and porosities is further evidence against this mechanism. A final objection is that this mechanism has the opposite dependence on viscosity that we observe.

Solid-Fluid Inertial Coupling. The analysis of solid-fluid inertial coupling indicates dissipation by wave induced flow occurs in either a 'global' (Biot, 1956 a and b), or 'local' (Biot, 1962) mode. It has generally been found that this mechanism is unimportant at the low frequencies and permeabilities of interest to geophysical exploration (Johnston et. al., 1979; Stoll and Bryan, 1970; Murphy, 1982b). Most recently Mochizuki (1982) has shown that this mechanism yields attenuation values far too small to account for the data of Murphy (1982b). Inspection of the equations of Biot (1956 a and b) and Mochizuki (1982) show that the center frequency is directly proportional to fluid viscosity. Calculations show that increased viscosity causes smaller attenuation in the low frequency range. This is opposite of our experimental observations and opposite the prediction of other fluid flow mechanisms. Finally this mechanism should be inversely proportional to permeability and directly proportional to porosity. As discussed in the previous section this cannot account for the similarity of frequency peaks in the range of one to ten kiloHertz in materials varying in permeability by at least five orders of

magnitude.

A recent series of papers (Dutta and Ode, 1979 a and b; Dutta and Seriff, 1979) considers the inertial coupling mechanism's application to local flow (Biot, 1962), specifically the model of White (1976) of a partially saturated porous rock. This model predicts the correct overall frequency and viscosity dependence and the center frequency is at about the kiloHertz range for gas pockets on the order of one centimeter. However it is again linearly dependent on permeability and a length scale, here the gas pocket dimension.

Local Flow. This brings us to models which focus on the microgeometry of the pore space to describe viscous losses on this scale. A number of these models, also known as 'squirt' mechanisms exist (O'Connell and Budiansky, 1977; Mavko and Nur, 1979; Palmer and Traviolia, 1980; White, 1975). These models are attractive as they have the proper dependence on viscosity (center frequency is inversely proportional to viscosity) and the frequency peak is in the correct range of one to ten kiloHertz for high permeability and porosity sedimentary rocks. They also can explain the relative difference in bulk and shear attenuation at full and partial saturation (Winkler and Nur, 1982).

The problem with these models is that they also have a dependence in some form on local permeability and aspect ratio or pore dimension (O'Connell and Budiansky, 1977; Mavko and Nur, 1979; Dutta and Seriff, 1979; Palmer and Traviolia, 1979). As discussed previously it is difficult to reconcile this dependence with the observation of a very sharp frequency peak of attenuation in rock which contains a wide distribution of aspect ratios and pore connectivities, as well as the relative independence of the loss peak in rock types of radically differing permeabilities and pore geometries, unless for some as yet unspecified reason this mechanism may be operating only on a small portion of the pore structure, one which is fairly common to all rocks.

Although a quantitative model is currently lacking, this may be a reasonable idea. Two recent models of squirt attenuation in partially saturated rocks have been proposed by Palmer and Traviolia (1980) and Mavko and Nur (1979). They both note, on computing values of attenuation for their models based on reasonable aspect ratio distributions, that the smallest

aspect ratio pores (about 10^{-4} in both models where the distributions were cut off) dominate the dissipation, even though these pores are a relatively small percent of the total porosity. If there are insignificant quantities of pores below this range as some observations suggest (Sprunt and Brace, 1974; Hadley, 1976; Toksoz et. al., 1976) then the frequency peak in attenuation will be controlled by the lower cut off of the aspect ratio spectrum. This places an upper bound on aspect ratios contributing to attenuation.

Palmer and Traviolia (1980) predict a loss peak in frequency at $\omega \approx B\ \alpha^3/\eta$ where B is the bulk modulus of the rock. For values of B of 10^{11} or 10^{12} c.g.s. and an aspect ratio of 10^{-4} a loss peak in the kiloHertz range is predicted, similar to that observed experimentally. The cut off in aspect ratios at the low end is probably artificial and controlled by experimental difficulties in observing smaller cracks. An alternative model might propose that at smaller aspect ratios a much smaller mass of fluid is involved in viscous related losses, because for very small aspect ratio pores there will be little free water as most of the water will be bound in monolayers to the surface. For an aspect ratio of 10^{-4} and a typical crack length of 0.1 millimeters, the crack width would be 10^{-6} millimeters, which is about the same dimension as the 7 to 8 monolayers of water which would be bound to the surface (Olhoeft, 1976). Hence there can not be any free water in a crack of aspect ratio smaller then 10^{-4}. Either way, this places a lower bound on the aspect ratios contributing to dissipation. If the upper and lower bounds of relevant aspect ratios are sufficiently close, a sharp frequency peak results. Figures 20 and 21 shows how the fluid squirt models of Mavko and Nur (1979) and Palmer and Traviolia (1980) may be adapted to quantitatively explain our observations.

Small aspect ratio (10^{-4}) cracks are presumably present in all rock types, and hence could account for the similar frequency dependence of attenuation in various rocks. This could also explain the pressure dependence of attenuation, pressure decreasing the amount of small aspect ratio cracks, and the variation of the magnitude of attenuation among different samples, perhaps having different concentrations of cracks or pores of the critical aspect ratio.

Furthermore Palmer and Traviolia (1980) interpret aspect ratio as the angle of convergence of contacts, which avoids arbitrary assumptions regarding the elliptical shape of the pores.

CONCLUSIONS

New experimental results in the kiloHertz frequency range show shear velocity and attenuation decrease with temperature to 140°C in fully and partially water saturated rock. The data indicate thermal relaxation is not an important loss mechanism under these conditions.

Fluid flow mechanisms where the relaxation time is controlled by a pore phase viscosity may explain the attenuation data as the attenuation peak shifts from about two kiloHertz at room temperature to about eight kiloHertz at 120°C, as temperature decreases the viscosity of water. Increasing effective pressure apparently does not eliminate the frequency dependence nor shift the relaxation time, rather it decreases the modulus defect.

The shifting frequency peak should also decrease the velocity, although the predicted effect is too small to fully account for the data. A non-dispersive temperature softening in shear may also be effecting the velocity data, perhaps related to a chemical interaction of the pore fluid and the rock matrix.

This interpretation implies a very narrow distribution of relaxation times which are relatively uneffected by pressure changes. A review of theories of attenuation indicates that some form of local fluid flow or squirt is likely to be controlling attenuation. Yet theories of attenuation by fluid flow which are formulated in terms of the microgeometry of the pore system or the bulk transport properties are difficult to reconcile with data on a variety of rock types reported in the literature. The attenuation peak in frequency (Spencer, 1982) and saturation (Murphy, 1982b) seems to be relatively independent of rock type, and from the data presented here is relatively independent of pressure. This implies that a single element which is similar in most rocks is controlling dissipation. A fluid squirt model whereby smaller aspect ratio pores cause substantially more losses than larger aspect ratio pores down to

some cut off where there are insufficient amount of pores or volume of fluids involved in dissipation may quantitatively explain the data. An obvious test of this would be measurements in some artificial material containing only spherical fluid inclusions. Other mechanisms which involve losses in the rock frame, surface mechanisms, or thermoelastic relaxation do not seem to be relevant to rocks in the upper crust at seismic to acoustic frequencies, which are inevitably at least wetted, if not saturated.

We also note that crude oils could have a viscosity of one to two orders of magnitude higher than water (Hobson and Pohl, 1973), especially for very heavy tar sands. This will shift the attenuation peak and the strong dispersion effect into the seismic band for sedimentary rocks containing sufficiently viscous oils. Measurements of the frequency dependence of velocity or attenuation could be a useful test for pore phase viscosity. Furthermore a frequency peak in attenuation between the borehole and surface seismic frequencies implies a much greater difference in velocity between well logging and seismic reflection measurements than would be predicted by a constant or nearly constant Q model.

ACKNOWLEDGEMENTS

This research was supported by grant #DEAT03-76 ER71045 from the Department of Energy and the industrial sponsors of the Stanford Rock Physics Project. I am grateful to Peter Gordon for invaluable assistance in the experimental design.

REFERENCES

Biot, M.A., 1956a, Theory of elastic waves in a fluid-saturated porous solid. I. Low-frequency range, J. Acous. Soc. Am., 28, 168-178.

Biot, M.A, 1956b, Theory of elastic waves in a fluid-saturated porous solid. II. Higher frequency range, J. Acous. Soc. Am., 28, 179-191.

Biot, M.A., 1962, Generalized theory of acoustic propagation in porous dissipative media, J. Acous. Soc. Am., 28, 1254-1264.

Birch, F., and D. Bancroft, 1938, Elasticity and internal friction in a long column of granite, Bull. Seism. Soc. Am., 28, 243-254.

Budiansky, B., and R.J. O'Connell, 1980, Bulk dissipation in heterogeneous media, in Solid Earth Geophysics and Geotechnology, S. Nemat-Nasser, Ed., Appl. Mech. Div. Vol., ASME, New York.

Clark, V. A., T. W. Spencer, and B. R. Tittmann, 1981, The effect of thermal cycling on the seismic quality factor Q of some sedimentary rocks, J. Geophys. Res., 86, 7087-7094.

Clark, V. A., B. R. Tittmann, and T. W. Spencer, 1980, Effect of volatiles on attenuation (Q^{-1}) and velocity in sedimentary rocks, J. Geophys. Res., 85, 5190-5198.

Dutta, N. C., and H. Ode, 1979a, Attenuation and dispersion of compressional waves in fluid-filled rocks with partial gas saturation (White model)-Part I: Biot theory, Geophysics, 44, 1777-1788.

Dutta, N.C., and H. Ode, 1979b, Attenuation and dispersion of compressional waves in fluid-filled rocks with partial gas saturation (White model)-Part II: Results, Geophysics, 44, 1789-1805.

Dutta, N.C., and A.J. Seriff, 1979, On White's model of attenuation in rocks with partial gas saturation, Geophysics, 44, 1806-1812.

Frisillo, A.L., and T.J. Stewart, 1980, Effect of partial gas/brine saturations on ultrasonic absorption in sandstone, J. Geophys. Res., 85, 5209-5211.

Gordon, R.B., and L.A. Davis, 1968, Velocity and attenuation of seismic waves in imperfectly elastic rock, J. Geophys. Res., 73, 3917-3935.

Hadley, K., 1976, Comparison of calculated crack densities and seismic velocities in Westerly granite, J. Geophys. Res., 81, 3484-3494.

Hobson, G.D., and W. Pohl, 1973, Modern Petroleum Technology, 4th edition, John Wiley and Sons, Inc., New York.

Ito, H., J. DeVilbiss, and A. Nur, 1979, Compressional and shear waves in saturated rock during water-steam transition, J. Geophys. Res., 84, 4731-4736.

Johnston, D.H., 1981, Attenuation: A state of the art summary, Seismic Wave Attenuation, S. E. G. geophysics reprint series no. 2, 123-135.

Johnston, D.H., and M.N. Toksoz, 1980a, Ultrasonic P and S wave attenuation in dry and saturated rocks under pressure, J. Geophys. Res., 85, 925-936.

Johnston, D.H., and M.N. Toksoz, 1980b, Thermal cracking and amplitude dependent attenuation, J. Geophys. Res., 85, 937-943.

Johnston, D.H., M.N. Toksoz, and A. Timur, 1979, Attenuation of seismic waves in dry and saturated rocks: II: Mechanisms, Geophysics, 44, 691-711.

Jones, T.D, 1983, The nature of seismic reflections from the crystalline basement: COCORP Wind River line, Wyoming, chapter 3, this volume, submitted to Journal of Geophysical Research.

Jones, T.D., and A. Nur, 1983, Velocity and attenuation in sandstone at elevated temperature and pressure, Geophys. Res. Lett., 10, 140-143.

Kissell, F.N., 1972, Effect of temperature on internal friction in rocks, J. Geophys. Res., 77, 1420-1423.

Kjartansson, E., and A. Nur, 1982, Attenuation due to thermal relaxation in porous rocks, Geophysics, submitted.

Lockner, D., J.B. Walsh, and J. Byerlee, 1977, Changes in seismic velocity and attenuation during deformation of granite, J. Geophys. Res., 82, 5374-5378.

Mason, W.R., 1969, Internal friction mechanism that produces an attenuation in the earth's crust proportional to frequency, J. Geophys. Res., 74, 4963-4966.

Mavko, G.M., 1979, Frictional attenuation: An inherent amplitude dependence, J. Geophys. Res., 84, 4769-4776.

Mavko, G.M., and A. Nur, 1975, Melt squirt in the aesthenosphere, J. Geophys. Res., 80, 1444-1448.

Mavko, G.M., E. Kjartansson, and K. Winkler, 1979, Seismic wave attenuation in rocks, Rev. Geophys. Space Physics, 17, 1155-1164.

Mavko, G.M., and A. Nur, 1979, Wave attenuation in partially saturated rocks, Geophysics, 44, 161-178.

Mochizuki, S., 1982, Attenuation in partially saturated rocks, J. Geophys. Res., 87, 8598-8604.

Murphy, W., 1982a, Effects of partial water saturation on attenuation in Massillon sandstone and Vycor porous glass, J. Acous. Soc. Am., 71, 1458 -1468.

Murphy, W., 1982b, Effects of microstructure and pore fluids on the acoustic properties of granular sedimentary materials, Ph.D. Thesis, Stanford University, Stanford, California, 255 p.

Nur, A., 1971, Viscous phases in rocks and the low-velocity zone, J. Geophys. Res., 76,1270-1277.

Nur, A., and G. Simmons, 1969, The effect of viscosity of a fluid phase on velocity in low porosity rocks, Earth Planet. Sci. Lett., 7, 99-108.

Nur, A., J.D. Walls, K. Winkler, and J. DeVilbiss, 1980, Effects of fluid saturation on waves in porous rock and relation to hydraulic permeability, Soc. of Pet. Eng. J., 20, 450-458.

O'Connell, R.J., and B. Budiansky, 1977, Viscoelastic properties of fluid-saturated cracked solids, J. Geophys. Res., 82, 5719-5736.

O'Connell, R.J., and B. Budiansky, 1978, Measures of dissipation in viscoelastic media, Geophys. Res. Lett., 5, 5-8.

Olhoeft, G.R., 1976, Electrical properties of rocks, in The Physics and Chemistry of Minerals and Rocks, K.G.J. Sterns, editor, John Wiley and Sons, Inc., p. 261-278.

Palmer, I.D., and M.L. Traviolia, 1980, Attenuation by squirt flow in undersaturated gas sands, Geophysics, 45, 1780-1792.

Pandit, B.I., and M.S. King, 1979, The variation of elastic wave velocities and quality factor of a sandstone with moisture content, Can. J. Sci., 16, 2187-2195.

Pandit, B.I., and J. Savage, 1973, An experimental test of Lomnitz's theory of internal friction in rocks, J. Geophys. Res., 78, 6097-6099.

Peselnick, L., and W.F. Outerbridge, 1961, Internal friction in shear and shear modulus of Solenhofen limestone over a frequency range of 10^{-7} cycles per second, J. Geophys. Res., 66, 581-588.

Savage, J., 1966, Thermoelastic attenuation of seismic waves by cracks, J. Geophys. Res., 71, 3929-3938.

Spencer, J.W., 1981, Stress relaxations at low frequencies in fluid saturated rocks: Attenuation and modulus dispersion, J. Geophys. Res., 86, 1803-1812.

Spencer, J.W., and A. Nur, 1976, The effects of pressure, temperature, and pore water on velocities in westerly granite, J. Geophys. Res., 81, 899-904.

Sprunt, E.S., and W.F. Brace, 1974, Direct observations of microcavities in crystalline rocks, Int. J. Rock Mech. Min. Sci. and Geomech. Abstr., 11, 139-150.

Stoll, R.D., 1974, Acoustic waves in saturated sediments, in Physics of Sound in Marine Sediments, L. Hampton, Ed., New York, Plenum Press, 19-39.

Stoll, R.D., and G.M. Bryan, 1970, Wave attenuation in saturated sediments, J. Acous. Soc. Am., 47, 1270-1277.

Tittmann, 1977, Internal friction measurements and their implications in seismic Q structure models of the crust, A.G.U. Monograph, 20, 197-213.

Tittmann, V.A. Clark, J.M. Richardson, and T.W. Spencer, 1980, Possible mechanism for seismic attenuation in rocks containing small amounts of volatiles, J. Geophys. Res., 85, 5199-5209.

Tittmann, B.R., H. Nadler, V.A. Clark, and L.A. Albeny, 1981, Frequency dependence of seismic dissipation in saturated rocks, Geophys. Res. Lett., 8, 36-38.

Toksoz, M.N., C.H. Cheng, and A. Timur, 1976, Velocities of seismic waves in porous rocks, Geophysics, 41, 621-645.

Toksoz, M.N., D.H. Johnston, and A. Timur, 1979, Attenuation of seismic waves in dry and saturated rocks: I. Laboratory measurements, Geophysics, 44, 681-696.

Toksoz, M.N., and D.H. Johnston, 1981, Seismic Wave Attenuation, S.E.G. geophysics reprint series no. 2, 459p.

Timur, A., 1977, Temperature dependence of compressional and shear wave velocities in rocks, Geophysics, 42, 950-957.

Walsh, J.B., 1966, New analysis of attenuation in partially melted rock, J. Geophys. Res., 74, 4333-4337.

Walsh, J.B., 1969, Attenuation of seismic waves in rock due to friction, J. Geophys. Res., 71, 2591-2599.

White, J.E., 1975, Computed seismic speeds and attenuation in rocks with partial gas saturation, Geophysics, 40, 224-232.

Winkler, K.W., 1980, Effects of pore fluids and frictional sliding on seismic wave attenuation in rocks, Ph.D. Thesis, Stanford University, Stanford, California.

Winkler, K.W., and A. Nur, 1982, Seismic attenuation: Effects of pore fluids and frictional sliding, Geophysics, 47, 1-15.

Zener, C., 1948, Elasticity and Anelasticity of Metals, University of Chicago Press, 170 p.

TABLE 1

Frequency Dependence of Attenuation in Various Rock Types

Sample	ϕ	k	ω	Reference	Conditions
Berea Sandstone	20%	617 md.	~ 2 kHz	Jones & Nur (1983)	P_c and P_p (water) to 200 bars
Berea Sandstone	20%	1000 md.	~ 2 kHz	Jones & Nur (1983)	P_c and P_p (water) to 200 bars
Navajo Sandstone	11%		0.7 to 2.1 kHz	Spencer (1981)	Saturated - various fluids
Navajo Sandstone	11%		6.5 kHz	Spencer (1981)	Low saturation
Spergen Limestone	14%		0.017 kHz	Spencer (1981)	Water saturated
Oklahoma Granite	1%		2.5 kHz	Spencer (1981)	Water saturated
Massilon Sandstone	23%	737 md.	4-6 kHz	Murphy (1982)	Variable saturation
Vycor porous glass	28%	0.01 md.	7-9 kHz	Murphy (1982)	Variable saturation
Berea Sandstone	20%	500 md.	3-6 kHz	Winkler & Nur (1982)	Water saturated, to 100 bars

ϕ Porosity

k Permeability (millidarcies)

ω Frequency of peak attenuation

TABLE 2

Attenuation Mechanisms

MECHANISM	CRITICAL TEST	VERDICT
Frame losses i.e., friction	Viscosity, amplitude, saturation, frequency	NO
Thermoelastic	Q^{-1} $\propto$ temp viscosity dependence	NO
Surface	Saturation dependence	NO
Viscous relax.	$\omega_o \simeq \mu\alpha/\eta$ Freq to high	NO
Biot inertial flow	$\omega_o \propto k\eta$ Freq to high magnitude to low	NO
Viscous regional flow	$\omega_o = \frac{v^2\phi\eta\beta}{4\pi^2 k}$ Freq to high	NO
Local viscous squirt	$\omega \simeq B\alpha^3/\eta$	YES ???

ω Frequency of peak attenuation

μ Shear modulus of matrix

α Aspect ratio

η Viscosity of fluid

k Permeability

v Velocity

ϕ Porosity

β Compressibility of fluid

B Bulk modulus of matrix

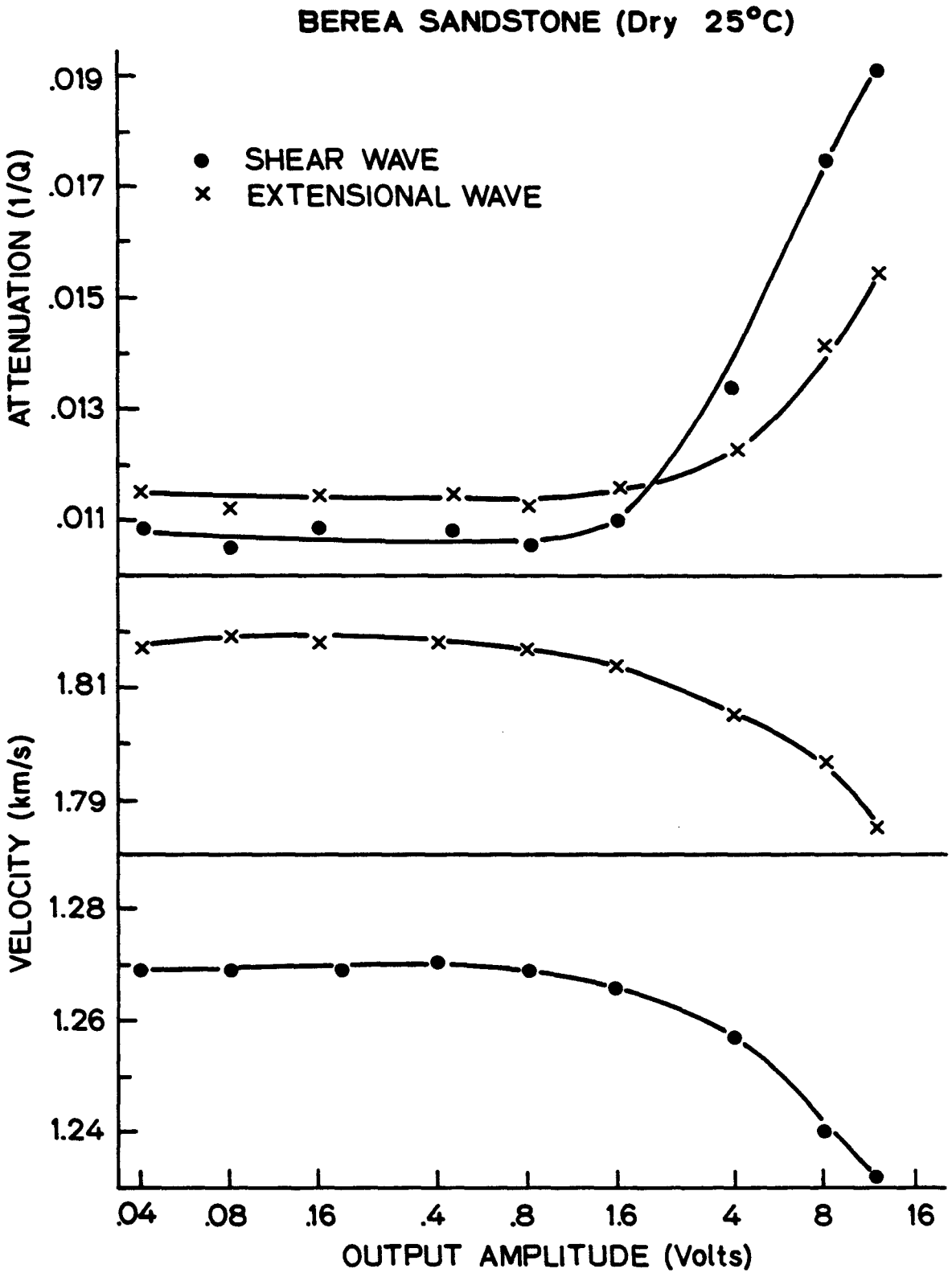

Figure 1. Dependence of shear and extensional velocity and attenuation on strain amplitude in a dry Berea sandstone. No pressure. 25°C.

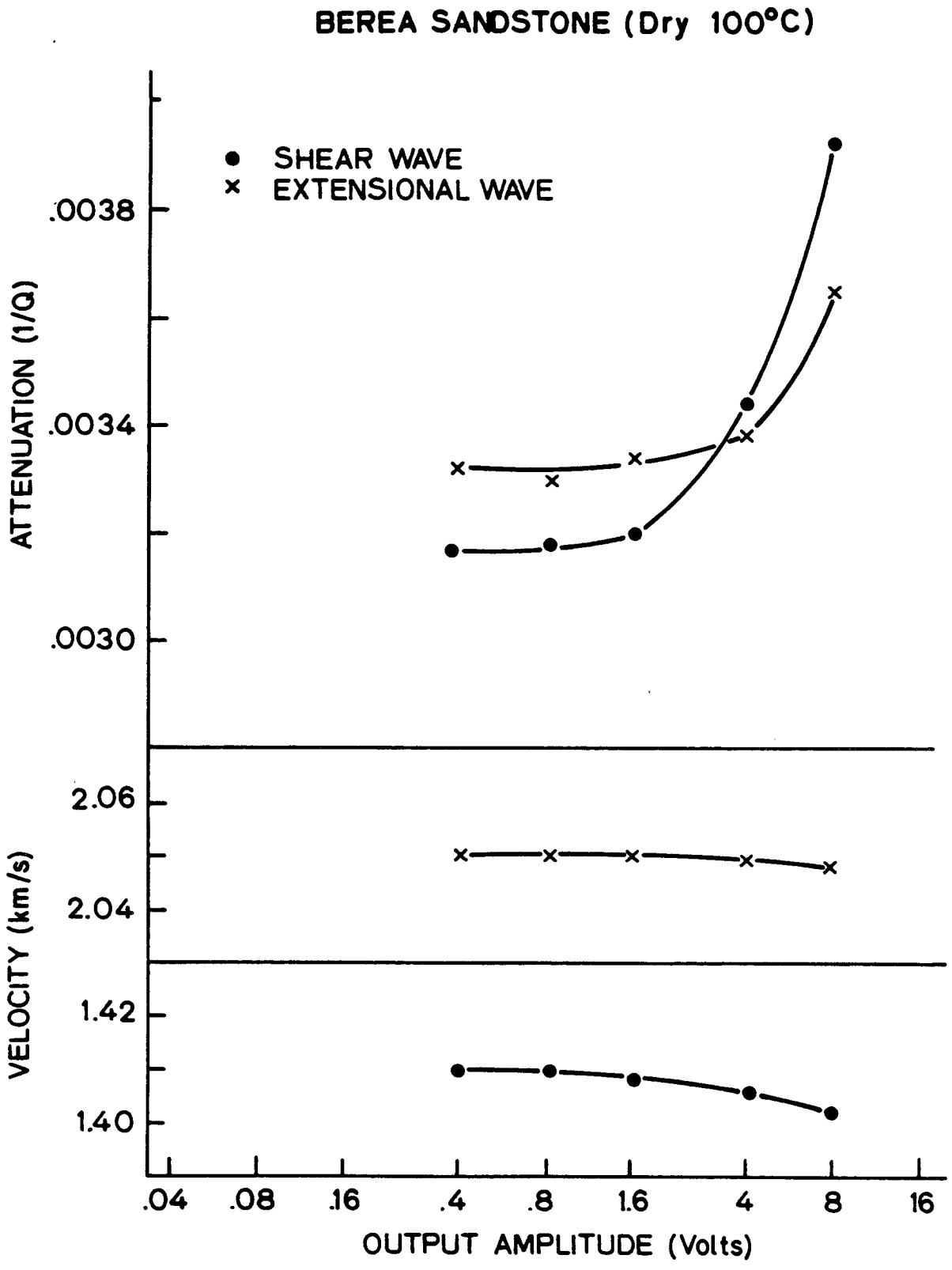

Figure 2. Dependence of shear and extensional velocity and attenuation on strain amplitude in a dry Berea sandstone. 100° C.

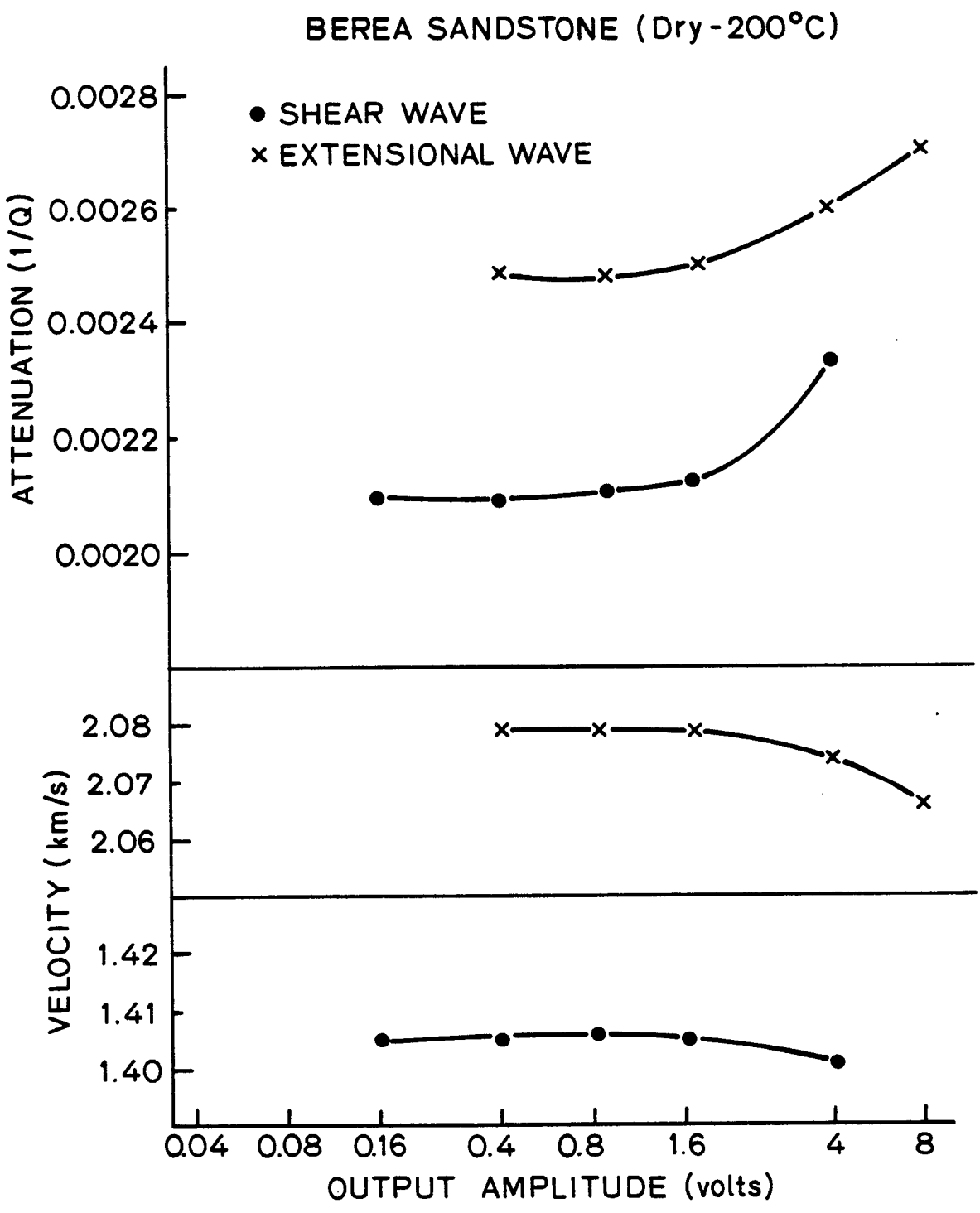

Figure 3. Dependence of shear and extensional velocity and attenuation on strain amplitude in a dry Berea sandstone. 200° C.

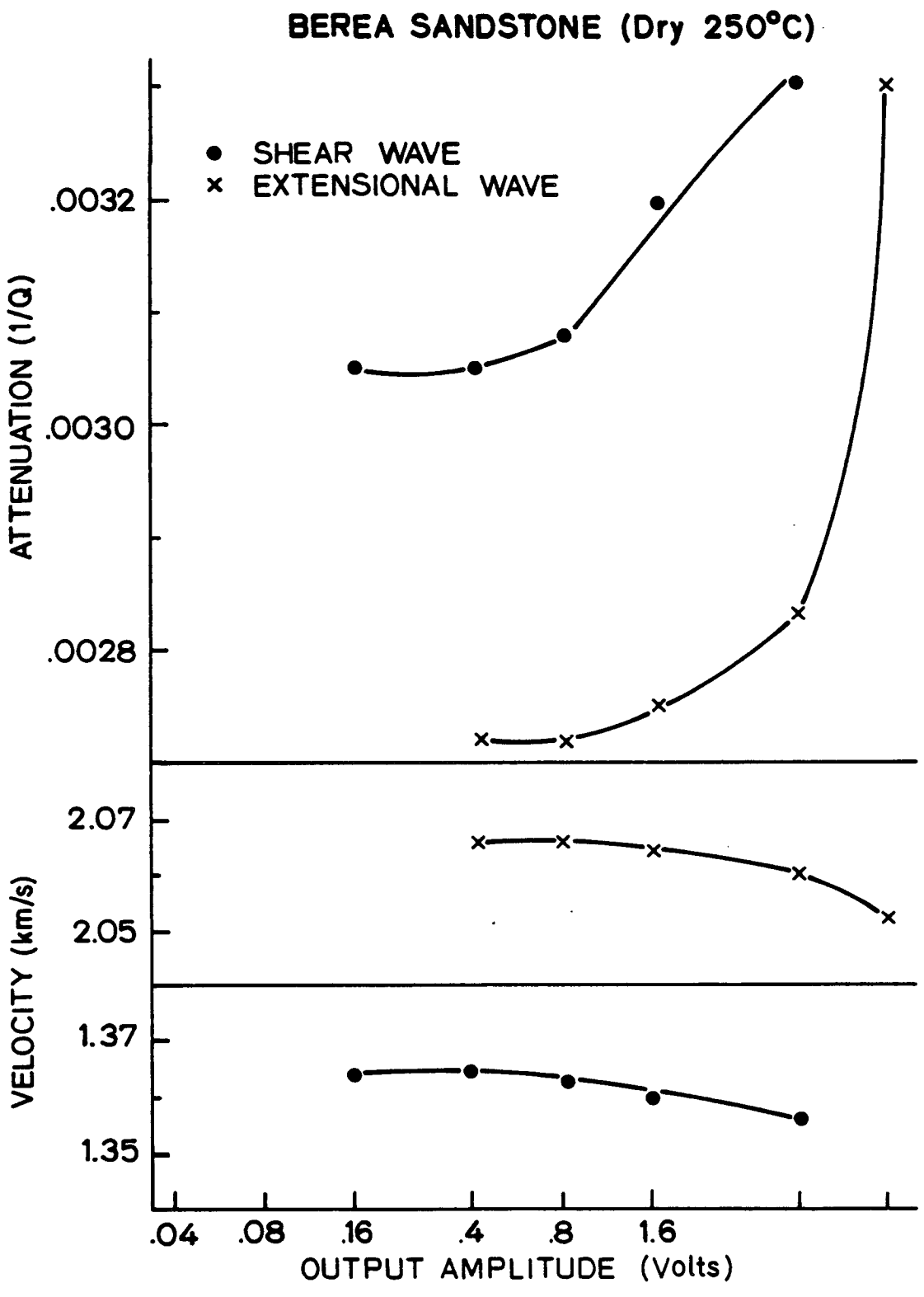

Figure 4. Dependence of shear and extensional velocity and attenuation on strain amplitude in a dry Berea sandstone. 250° C.

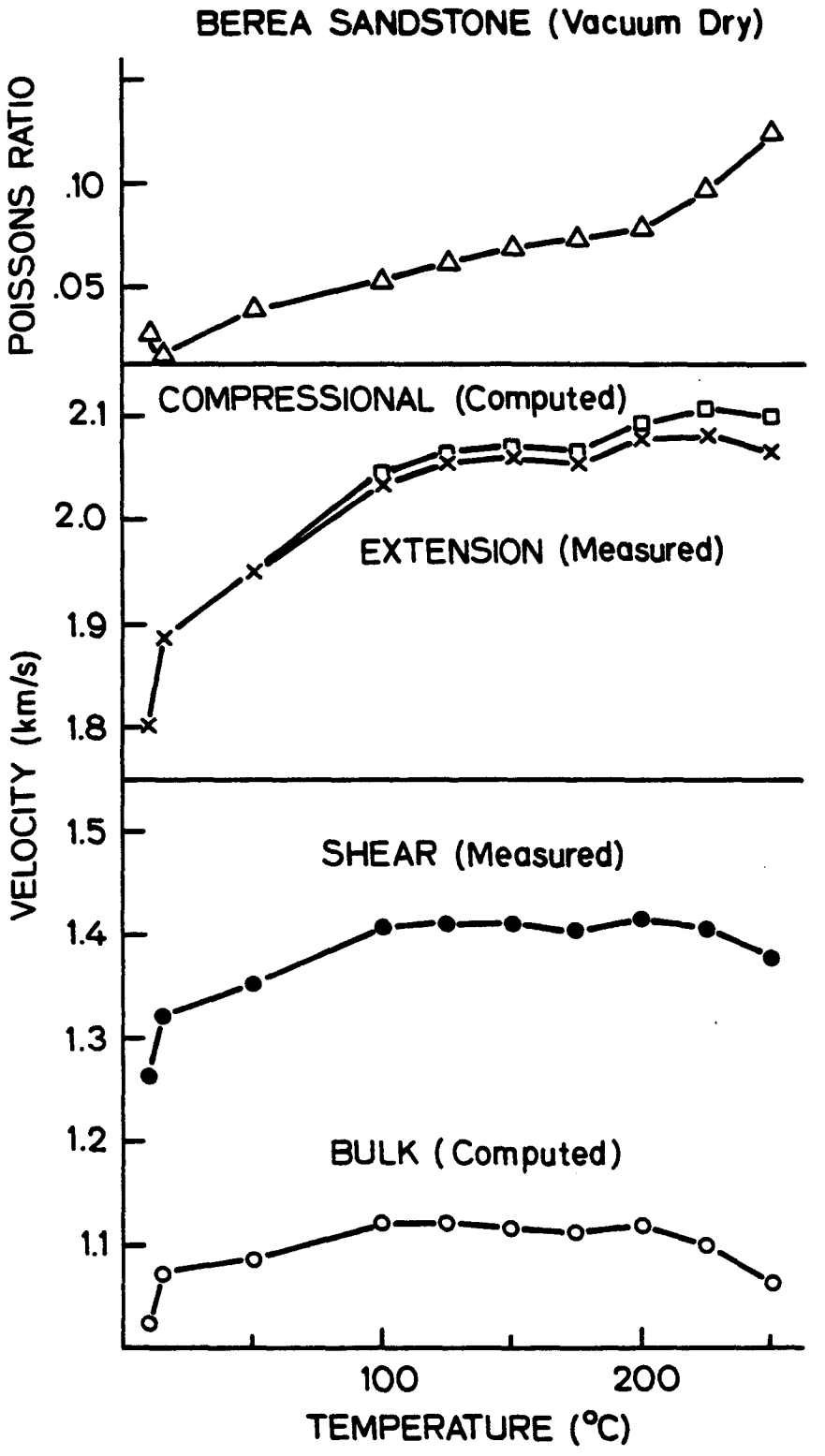

Figure 5. Velocity and Poisson's ratio as a function of temperature in a vacuum dry (10^{-3} Torr) Berea sandstone.

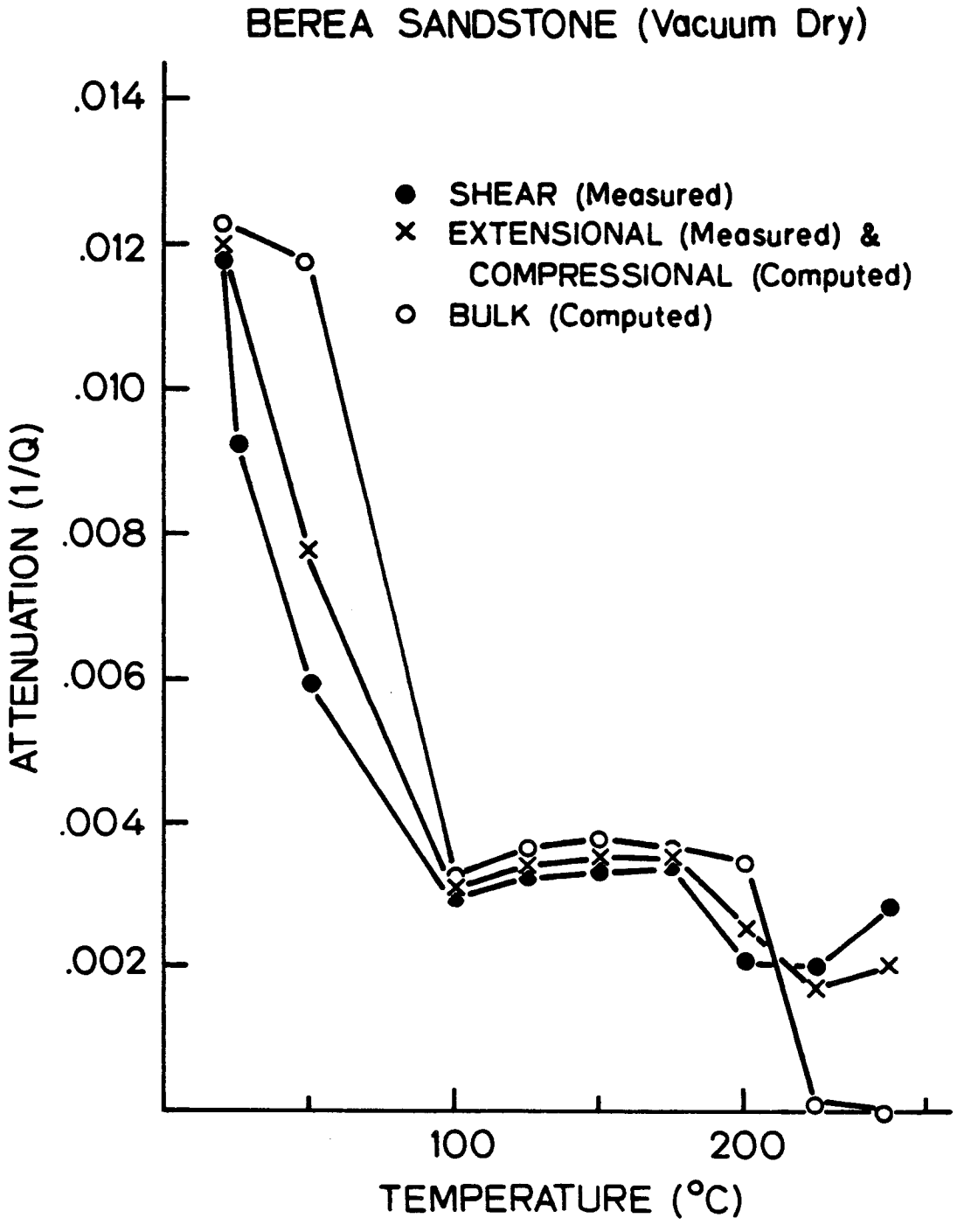

Figure 6. Attenuation as a function of temperature in a vacuum dry (10^{-3} Torr) Berea sandstone.

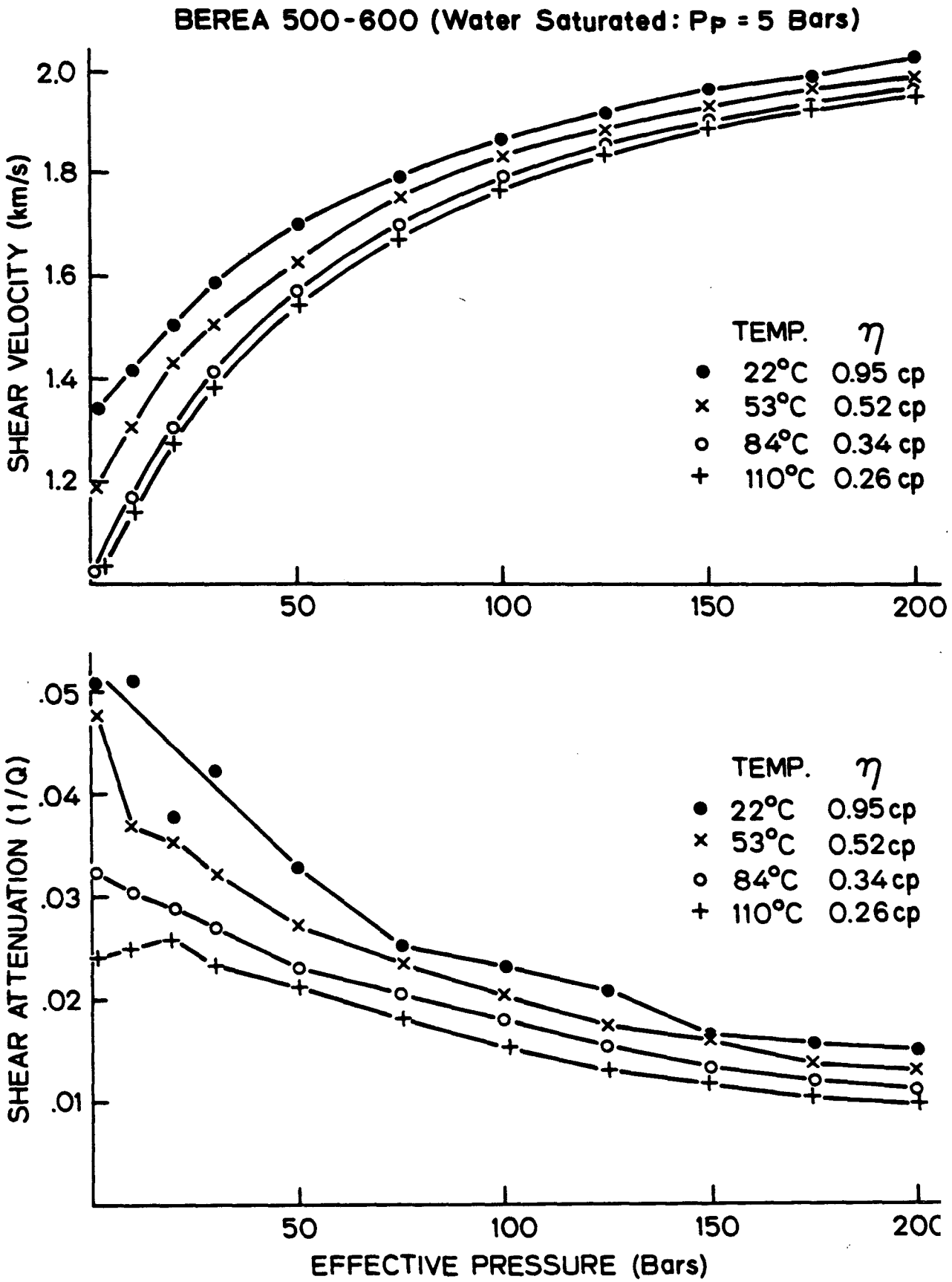

Figure 7. Shear velocity (top) and attenuation (bottom) as a function of effective pressure and temperature. Water saturated Berea 500-600.

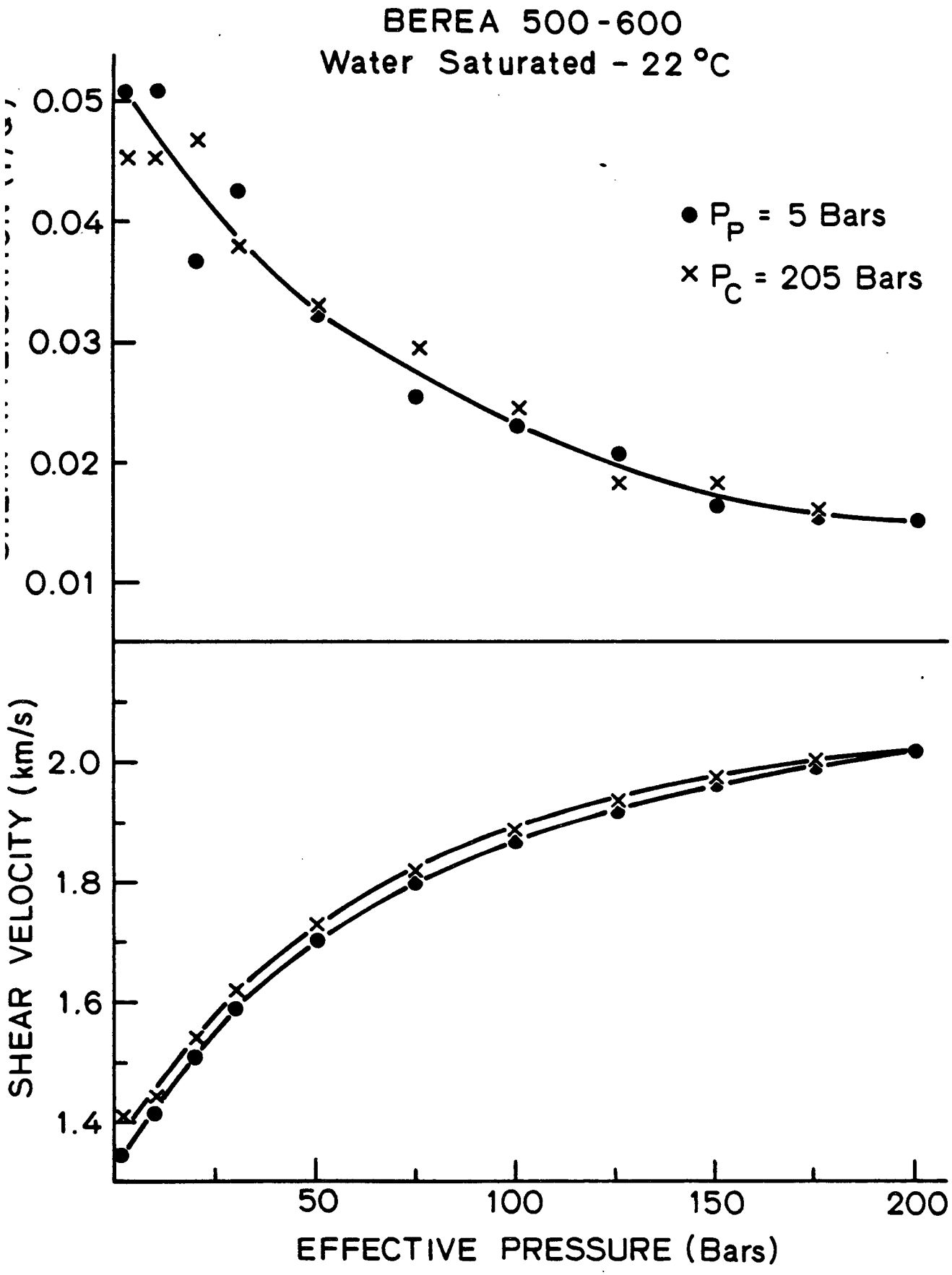

Figure 8. Effect of pore pressure on velocity and attenuation at 22°C. Pore pressure was held at 5 bars while confining pressure was raised to 205 bars, where it was held as pore pressure was raised to 205 bars.

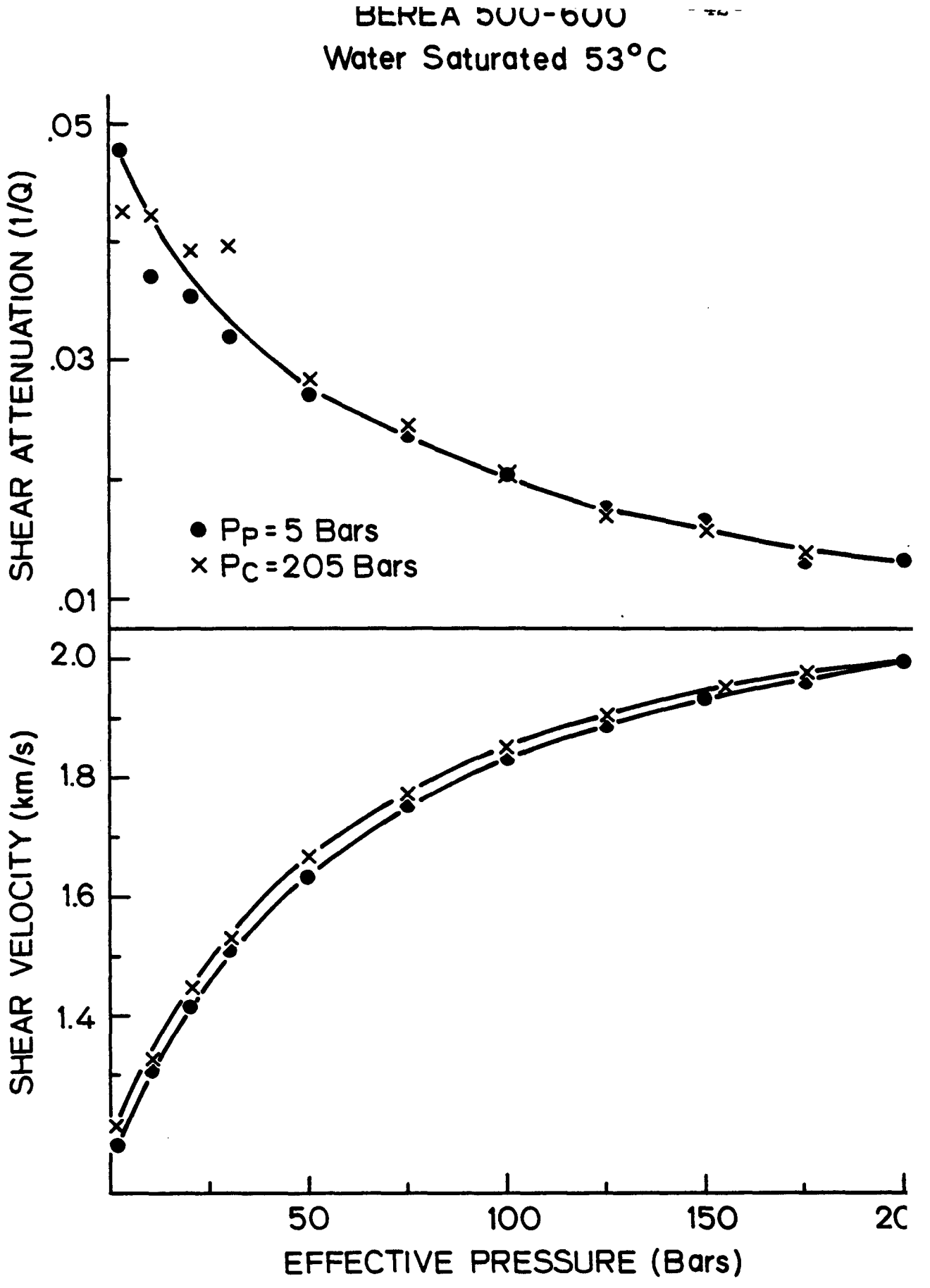

Figure 9. Effect of pore pressure on velocity and attenuation at 53°C. Same pressure changes as in Figure 8.

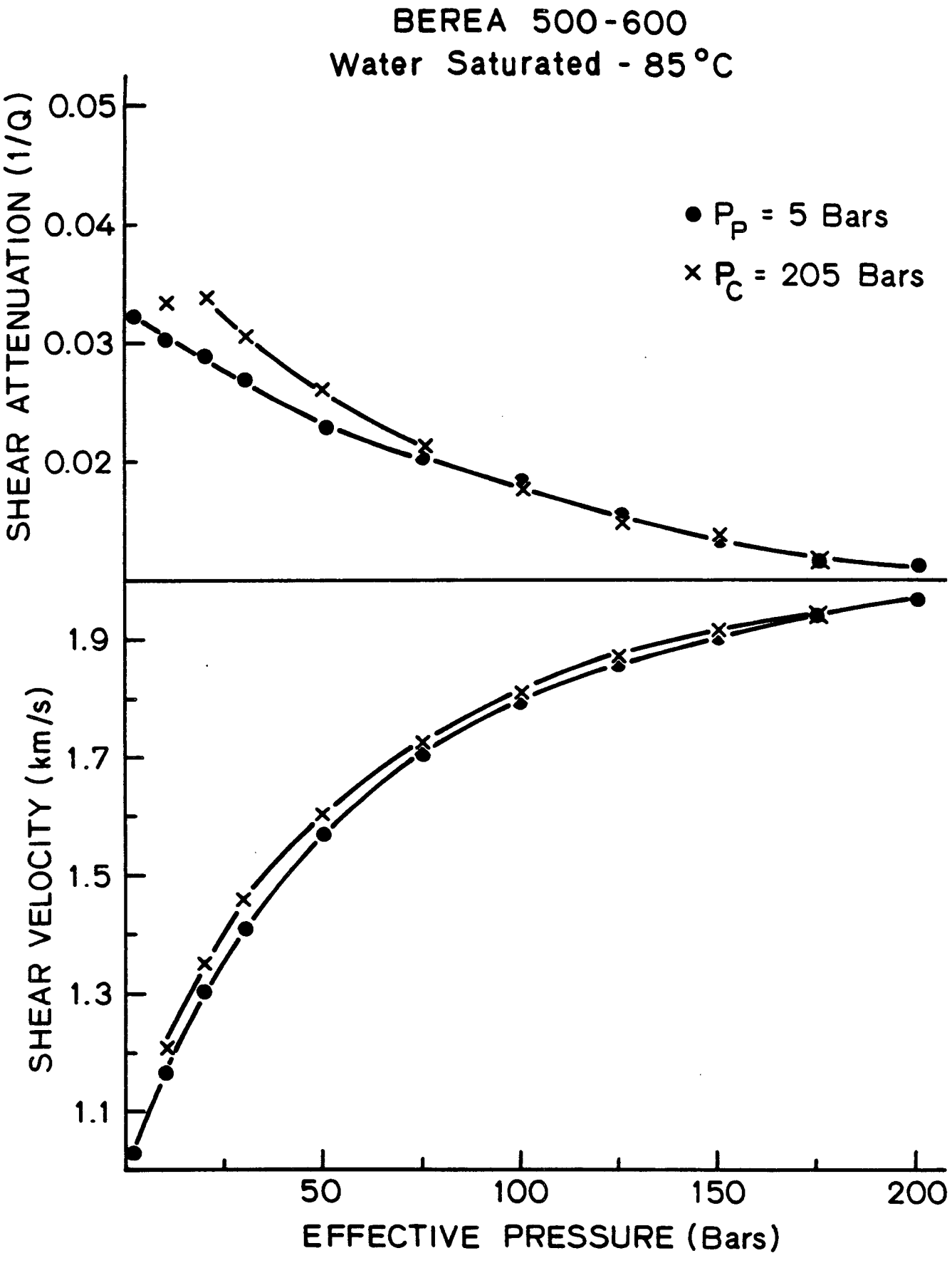

Figure 10. Effect of pore pressure on velocity and attenuation at 85°C. Same pressure changes as in Figure 8.

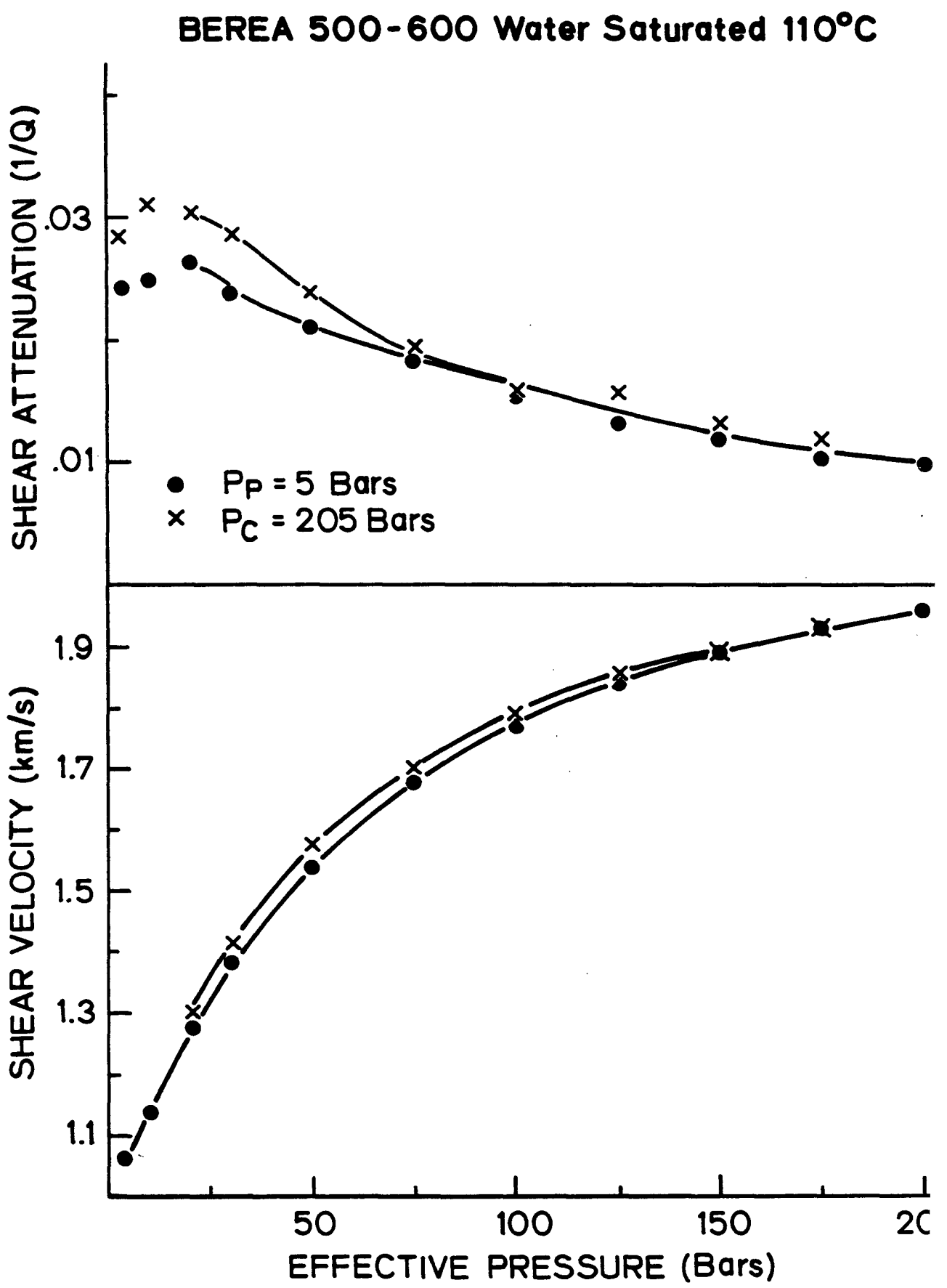

Figure 11. Effect of pore pressure on velocity and attenuation at 110°C. Same pressure changes as in Figure 8.

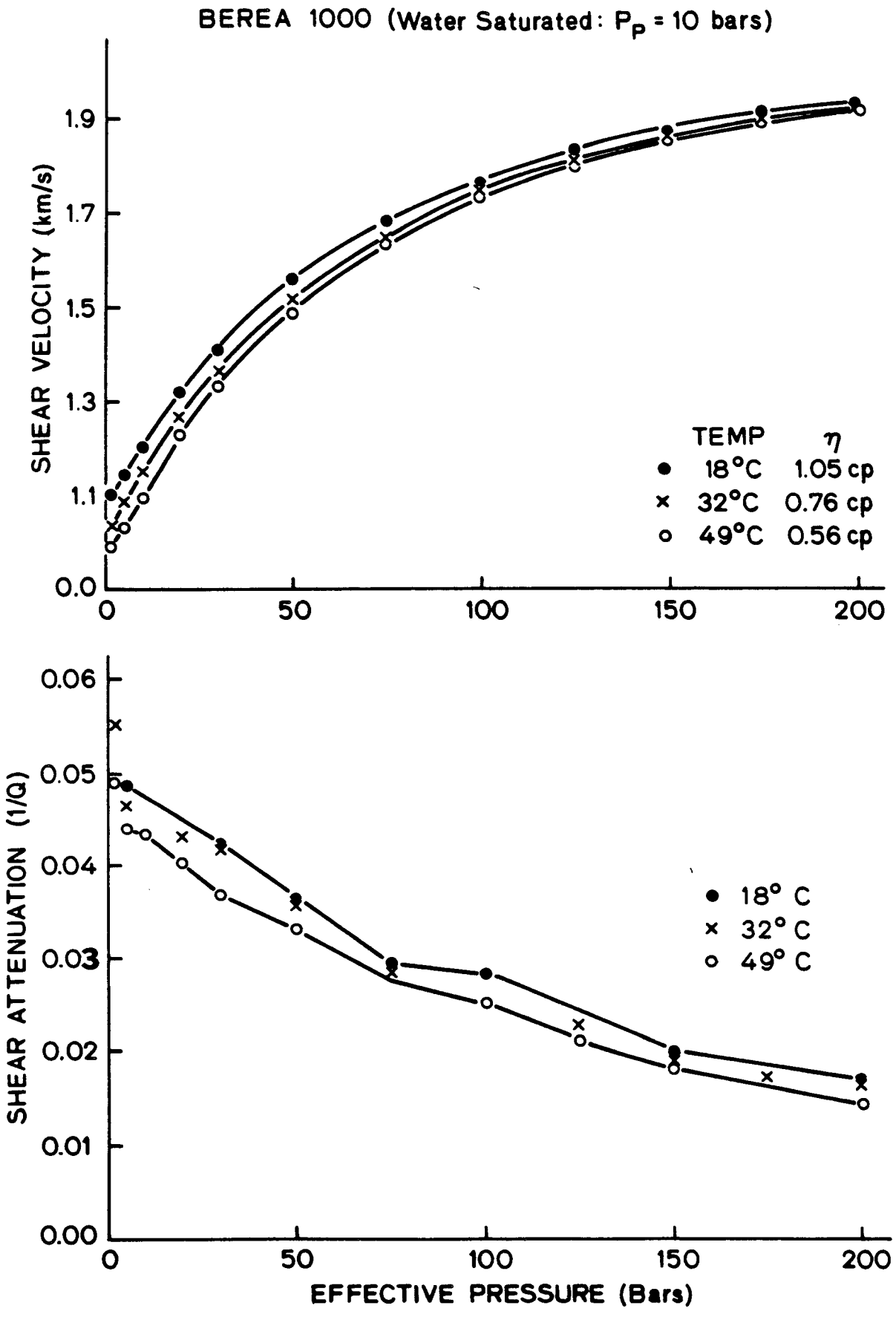

Figure 12. Shear velocity (top) and attenuation (bottom) as a function of effective pressure and temperature. Water saturated Berea 1000.

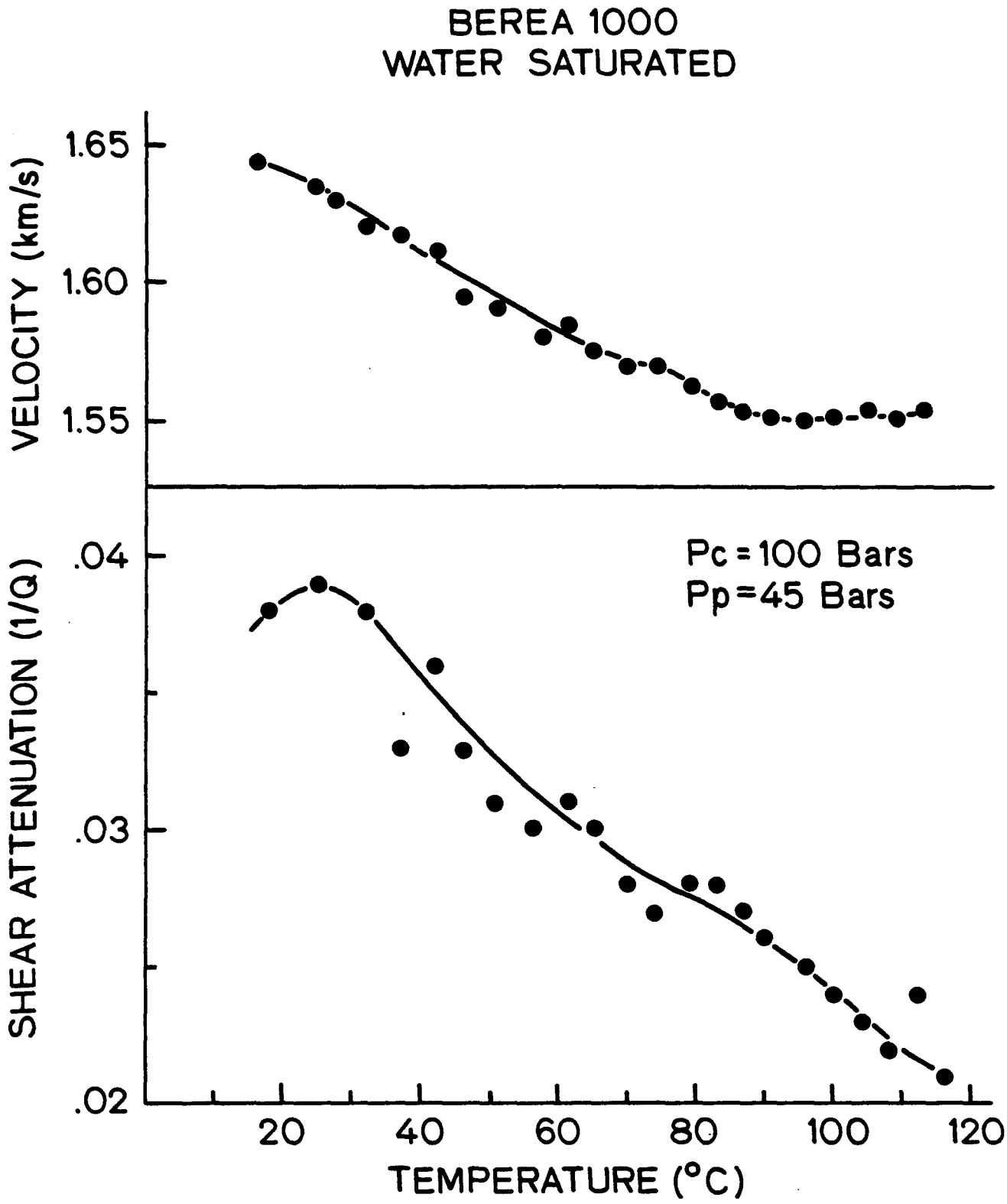

Figure 13. Effect of temperature on velocity and attenuation. Confining and pore pressure were held constant throughout the experiment. Water saturated Berea 1000.

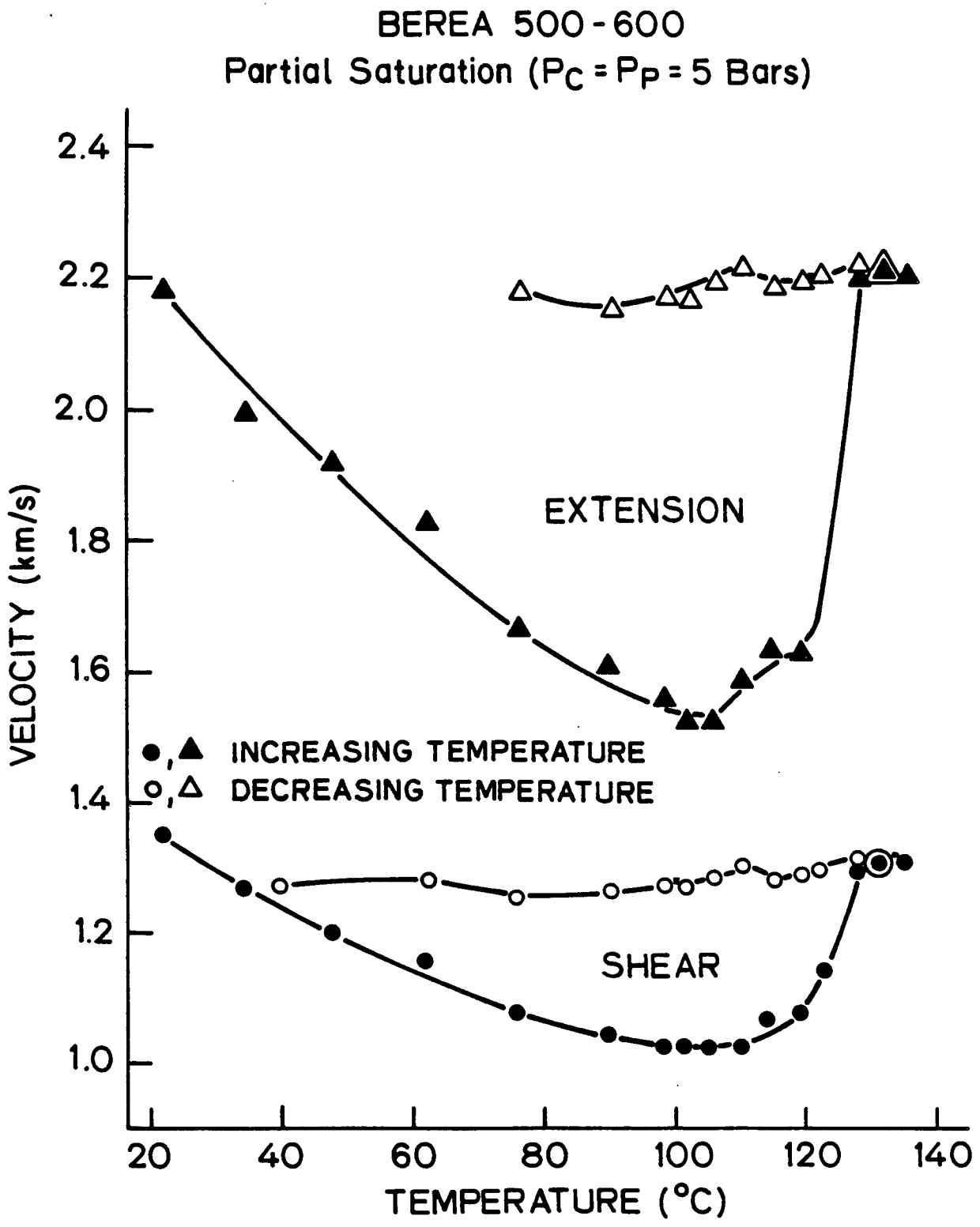

Figure 14. Effect of temperature on extensional and shear velocity to 140° C. Confining and pore pressure were held at 5 bars throughout the experiment. Partially saturated Berea 500-600.

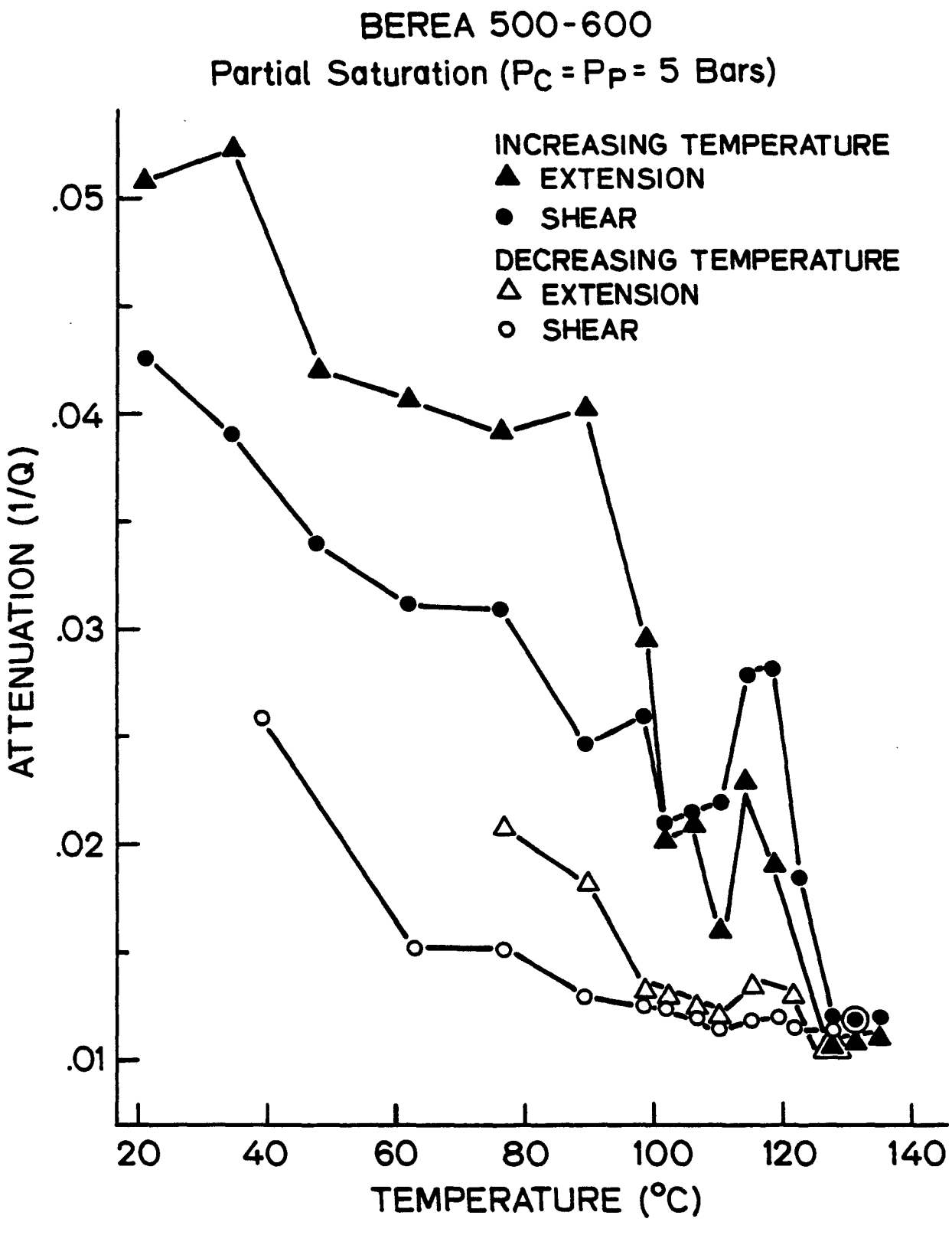

Figure 15. Effect of temperature on extensional and shear attenuation to 140°C. Same conditions as Figure 14.

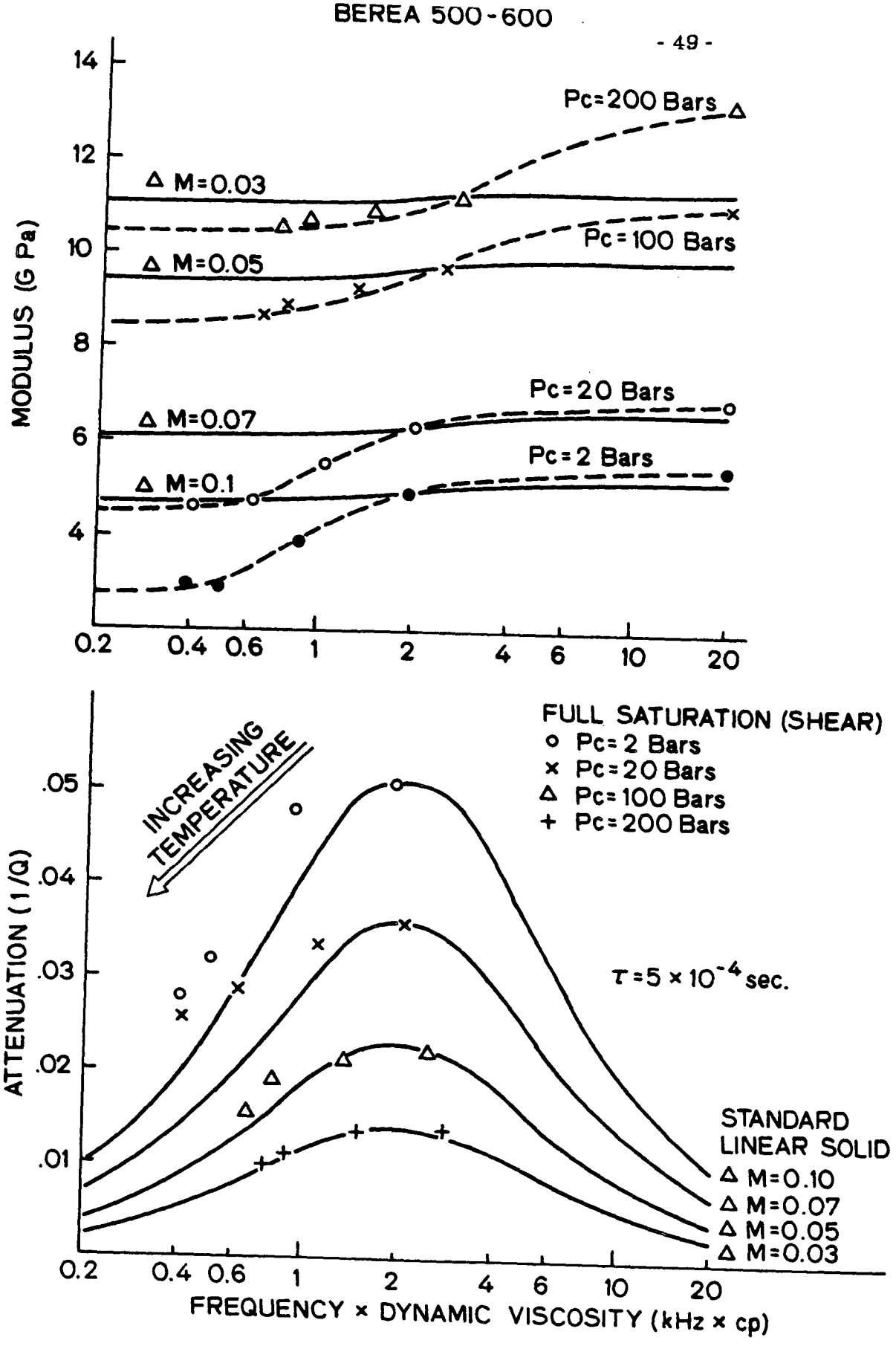

Figure 16. Dynamic shear velocity (top) and attenuation (bottom) vs. the product frequency and dynamic viscosity for the Berea 500-600 sample. For comparison we have plotted the theoretical modulus and attenuation (solid lines) for a standard linear solid with a single relaxation time (τ) of 5×10^{-4} seconds, and for four different modulus defects (ΔM). Ultrasonic measurements at one megaHertz constrain the unrelaxed modulus.

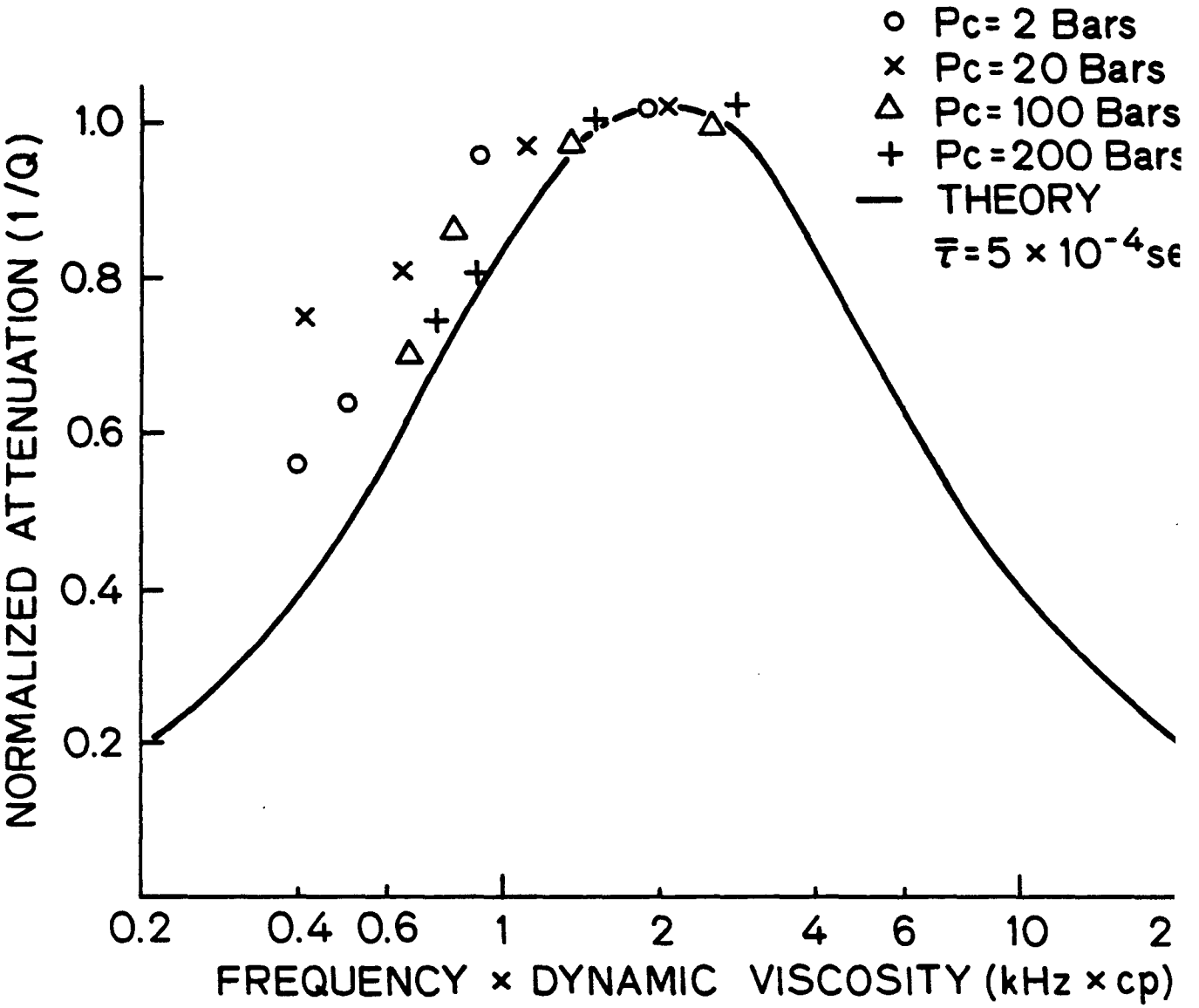

Figure 17. Normalized shear attenuation vs. the product frequency and dynamic viscosity for the Berea 500-600 sample. For comparison we have also shown the attenuation for a standard linear solid with a relaxation time of 5 x 10^{-4} seconds.

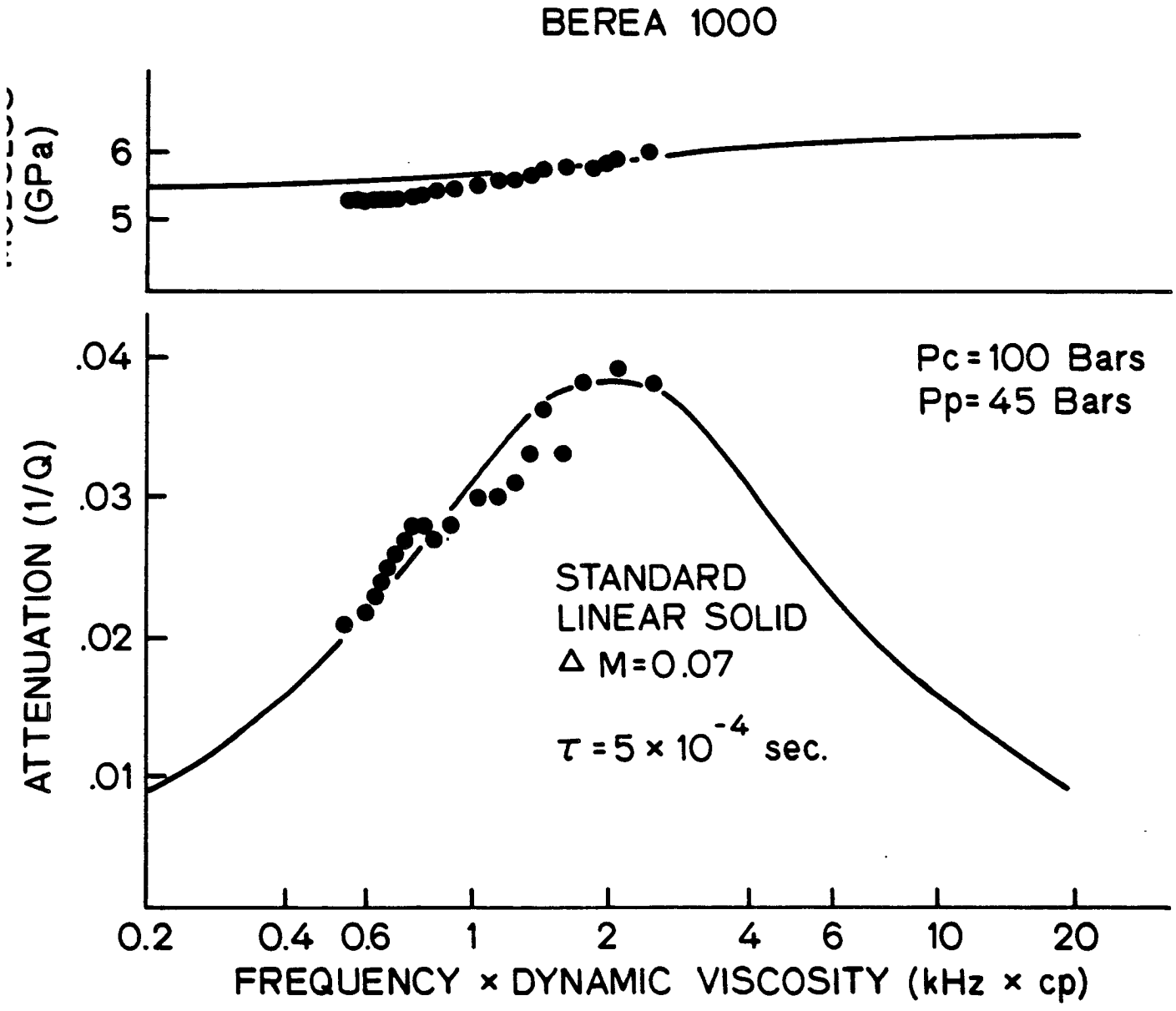

Figure 18. Shear attenuation and dynamic modulus vs. frequency times dynamic viscosity for the Berea 1000 sample. Solid lines are the theoretical attenuation and dispersion for a standard linear solid with a single relaxation time of 5×10^{-4} seconds and a modulus defect of 0.07.

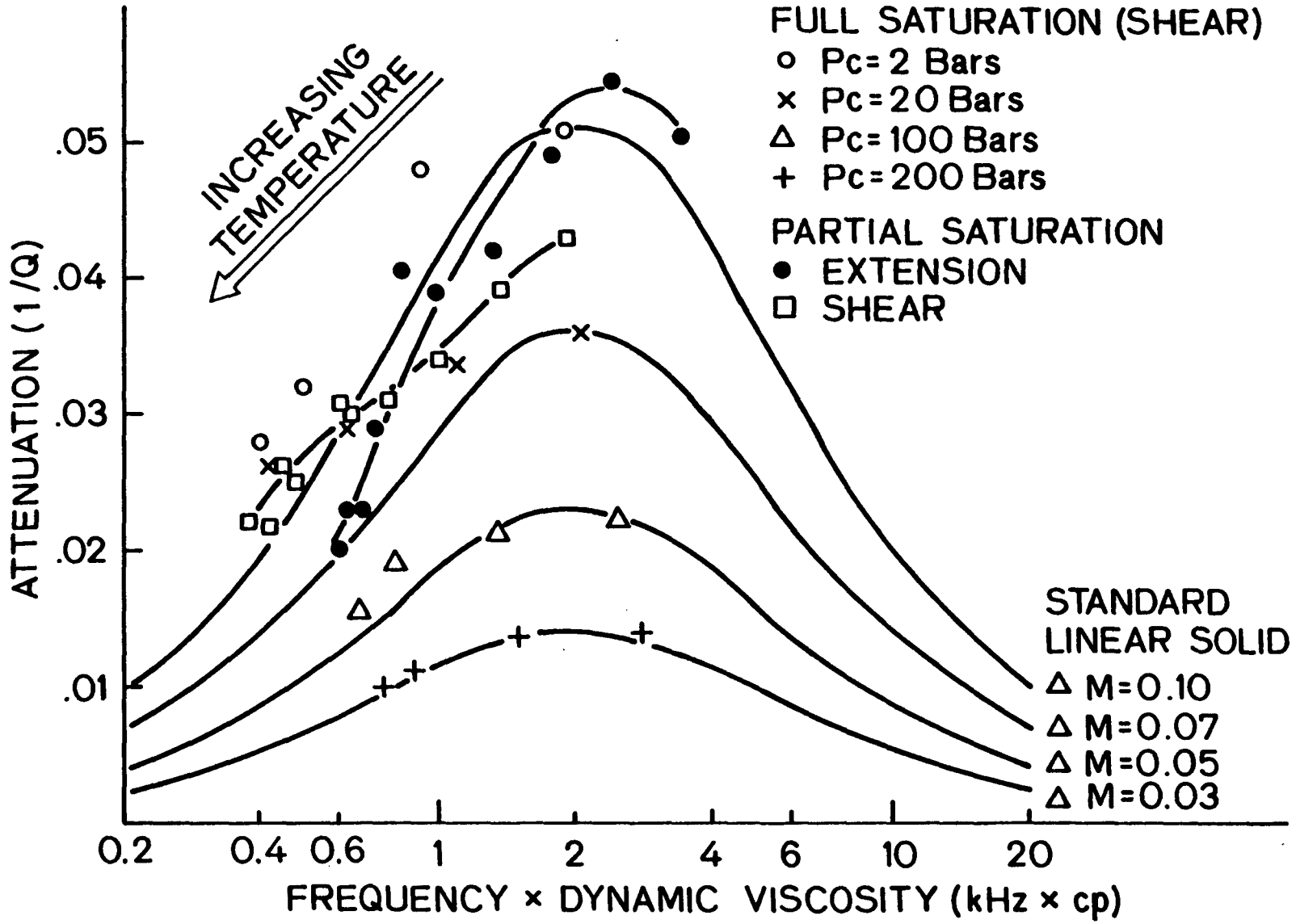

Figure 19. Shear attenuation vs. the product frequency and dynamic viscosity for Berea 500-600 data. Same as Figure 16 with the partially saturated data included.

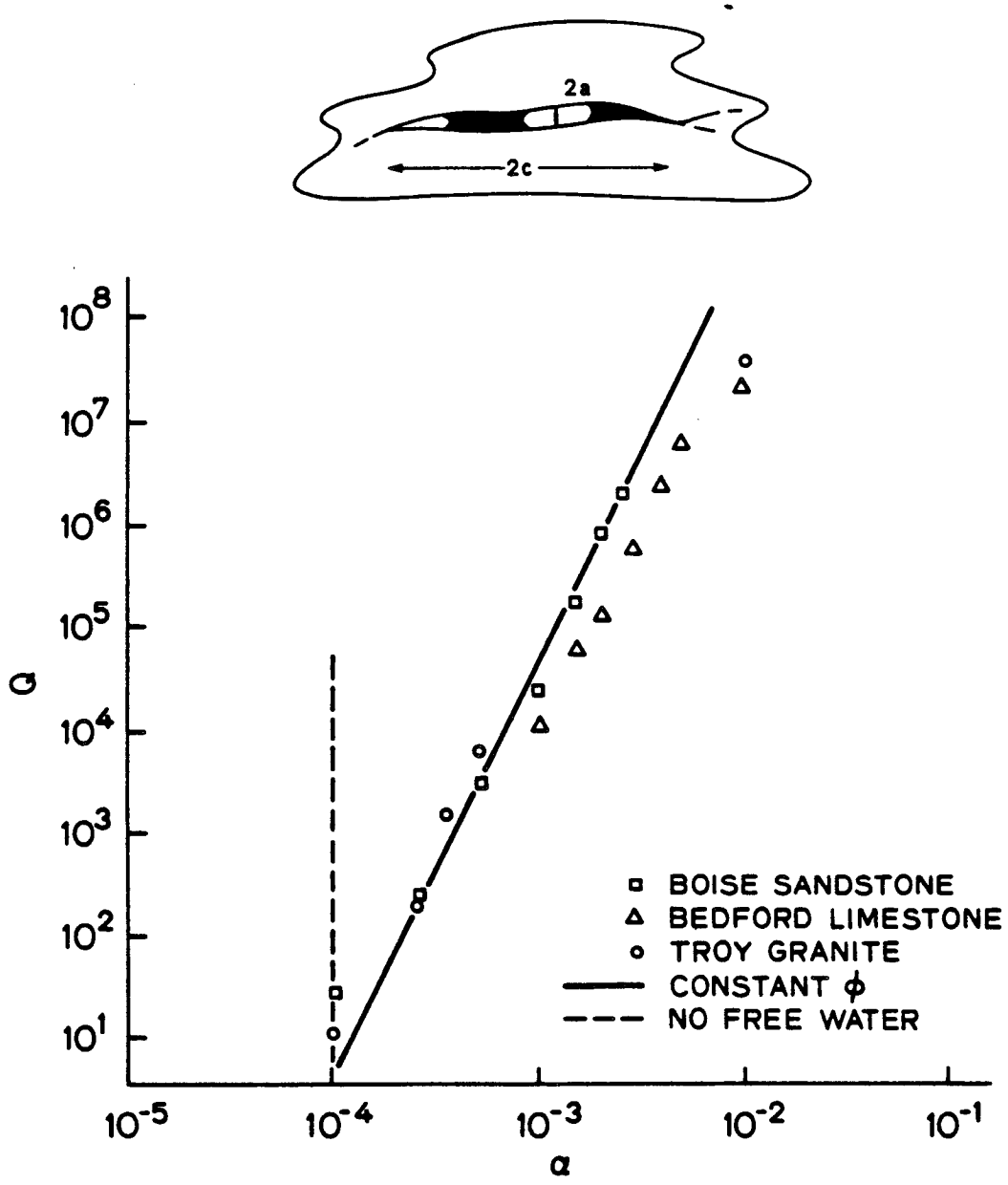

Figure 20. Model of Mavko and Nur (1979) for squirt attenuation in partially saturated rock. Top shows geometry of pore space and water droplets. The bottom graph plots Q values for each crack geometry as a function of aspect ratio. Crack aspect ratio distributions for the three rocks listed are taken from velocity-pressure inversions by Toksoz et. al. (1976). Solid line is computed for the case where each aspect ratio makes the same contribution to total porosity. For a typical crack length of 0.1 millimeter, when the aspect ratio becomes less then 10^{-4} there is no free water in the crack, it is all bound to the surface in monolayers. Hence only cracks of aspect ratio about 10^{-4} contribute significantly to attenuation. Dashed line represents this cutoff. This gives a strong frequency peak in attenuation in the kiloHertz range.

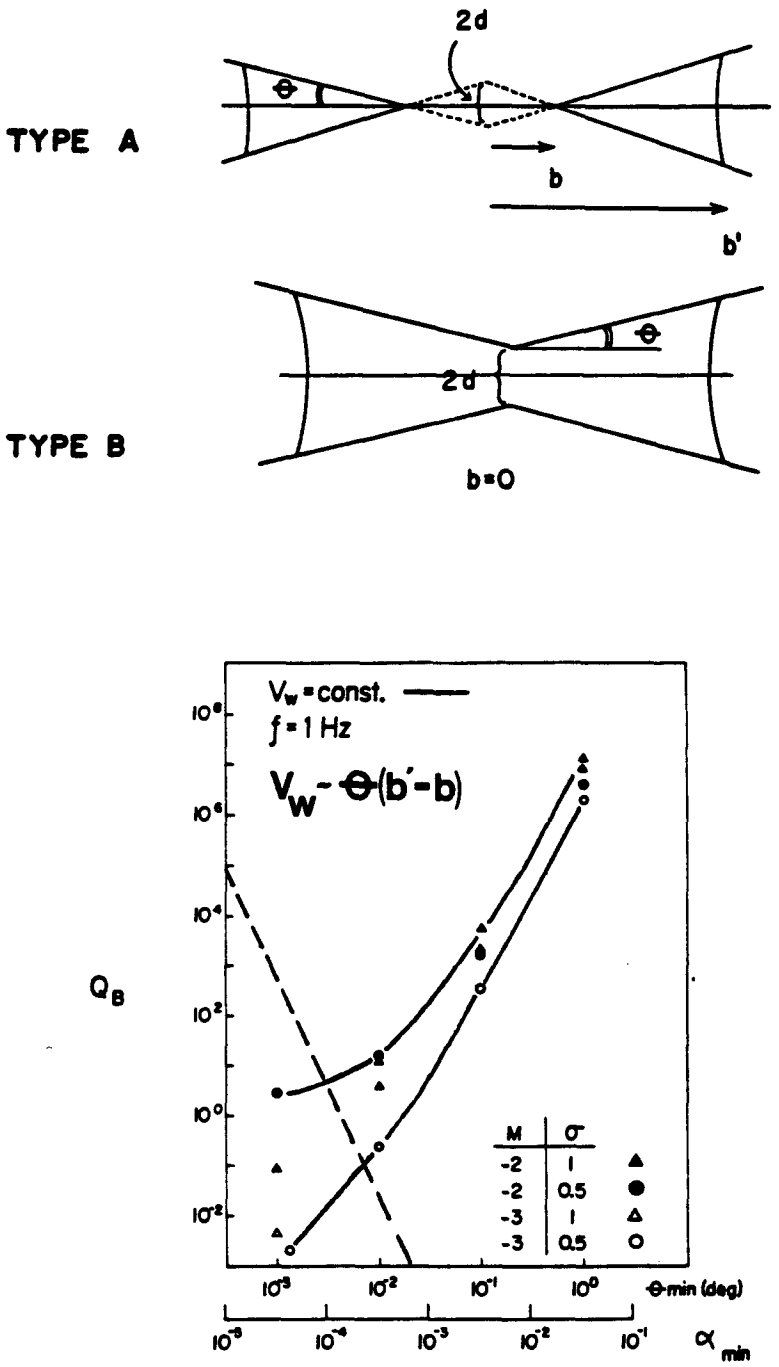

Figure 21. Model of Palmer and Traviolia (1980) for squirt attenuation in partially saturated rock. Top shows geometry of pore space, modeled by contacts, and water droplets. The bottom graph plots Q values as a function of aspect ratios for various aspect ratio distributions. As with the model of Mavko and Nur (1979), the smaller aspect ratios contribute much more to dissipation. Taking into account the reduced volume of free water in the very small aspect ratio pores due to bound monolayers might cause a correction similar to that shown by the dashed line. This would have the effect of allowing significant contributions to attenuation only from 10^{-4} aspect ratio pores, again producing an attenuation peak in the kiloHertz range.

APPENDIX

Ultrasonic Velocity Measurements

Ultrasonic velocity measurements in some popular laboratory rocks are given here for comparison to low frequency measurements. Standard ultrasonic techniques were used. Resonant frequency of transducer was 1 megaHertz. Precision is estimated at better than 1%, accuracy better than 3%. Pore fluid was de-ionized water. Samples were saturated, pore pressure was held constant at 1 bar as confining pressure was raised to 800 bars, where it was held as pore pressure was raised to 800 bars. Physical properties of the samples (as available) are summarized in Table 1. Description of samples is given below.

Berea sandstone. Medium grained sandstone, obtained from Cleveland Quarries, Amherst, Ohio. Contains about 84% quartz, 6% clay (kaolinite and illite), 2% feldspar, 8% amorphous silica.

Sierra White granite. Fine grained muscovite-biotite granite, obtained from Raymond Quarry, Raymond, California.

Massillon sandstone. Medium grained sandstone, obtained from Briar Hill Stone Co., Glenmont, Ohio. Contains 88% quartz, 5% clay (kaolinite), 3% feldspar, and 4% amorphous silica.

St. Peters sandstone. Medium grained quartzose sandstone. 0.5% clay.

TABLE 1

Sample	Orientation to bedding	Percent porosity	Permeability (md)	Velocity at 800 Bars P(km/s)	Velocity at 800 Bars S	Anisotropy Percent P	Anisotropy Percent S
Berea 1a	⊥	20	52**	4.04	2.51	0.2	0.8
1α	∥	20	52**	4.03	2.49		
2a	⊥	22	363**	3.96	2.42	3.3	1.0
2α	∥	22	363**	3.83	2.39		
3a	⊥	22	382**	3.79(dry) 3.76(wet)	2.45 2.35	7.2	3.4
3α	∥	22	382**	4.03	2.43		
4	none	22	400*	3.86	2.36		
5a	⊥	21	617**	4.13	2.65	2.9	2.6
5α	∥	21	617**	4.25	2.72		
Massilon 1a	⊥	23		3.82	2.35	2.4	0.9
1α	∥	23	737**	3.91	2.33		
2	none			3.76	2.18		
St. Peter N	⊥	20.0	944**	4.77	3.06		
Granite	—	0.8	—	5.98	3.51		

*Measured by Cleveland Quarries, Amherst, Ohio.

**Measured by Nur et al., 1980.

BEREA 1A

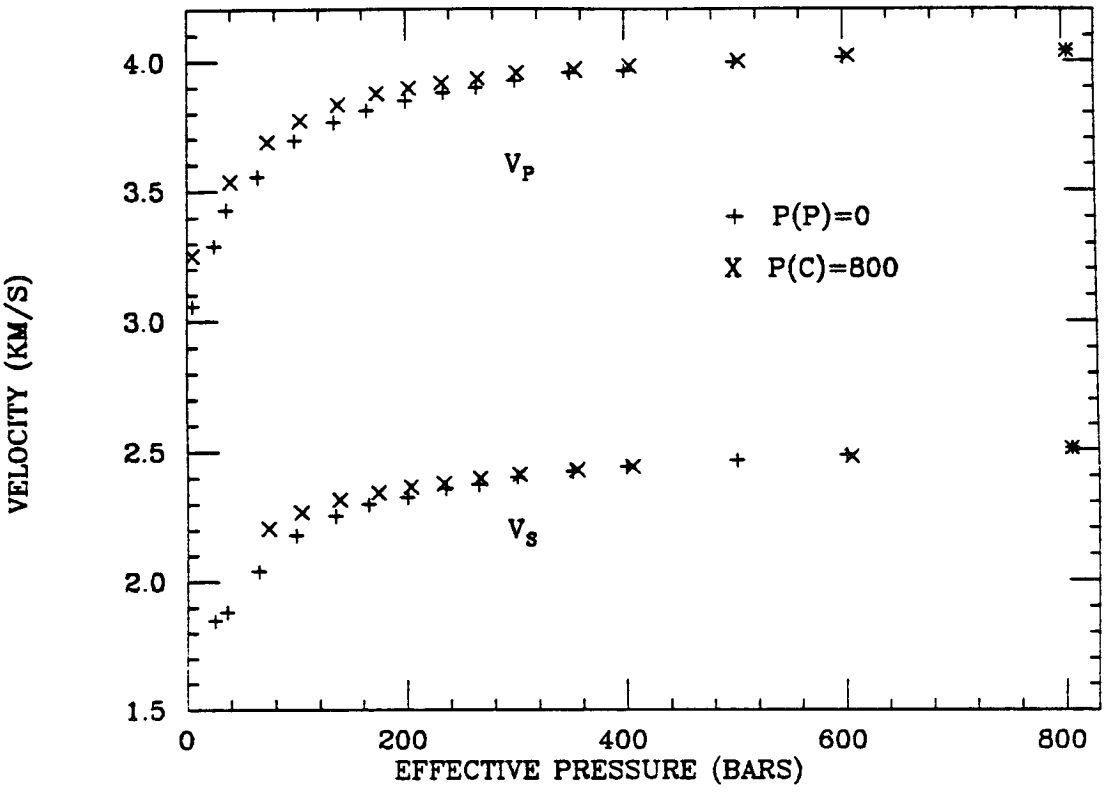

BEREA 1α

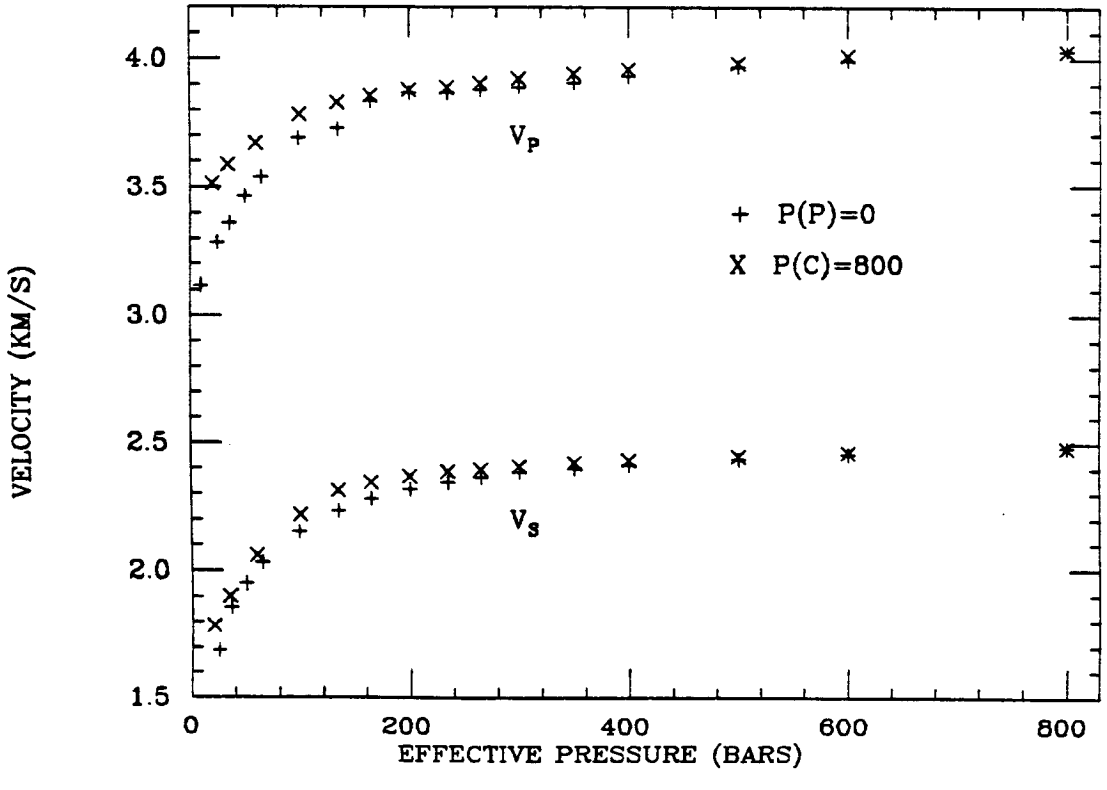

BEREA 2A

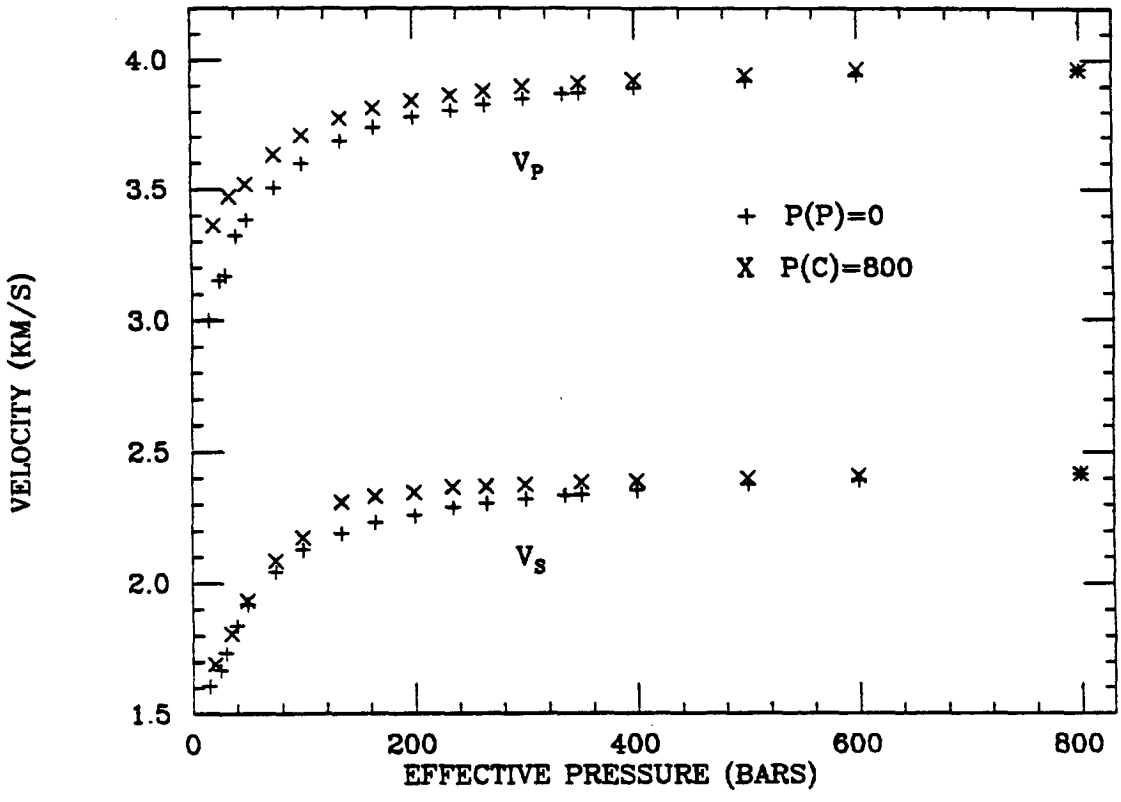

BEREA 2α

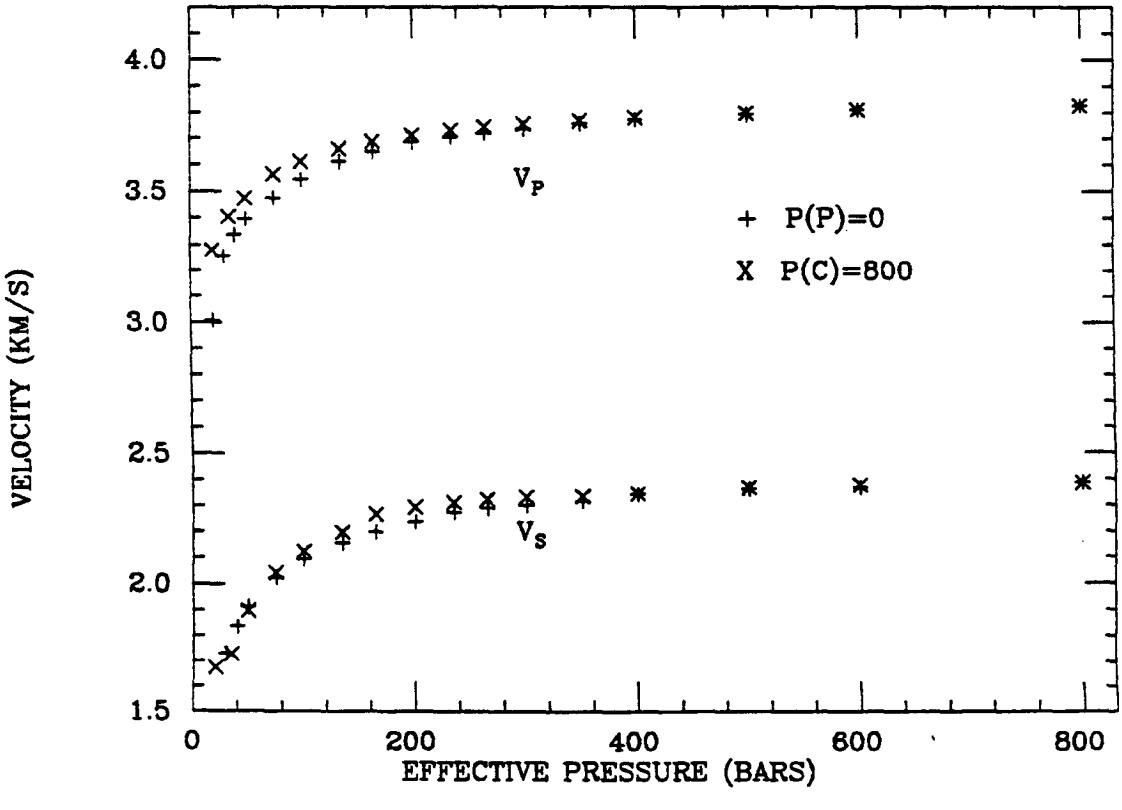

BEREA 3a

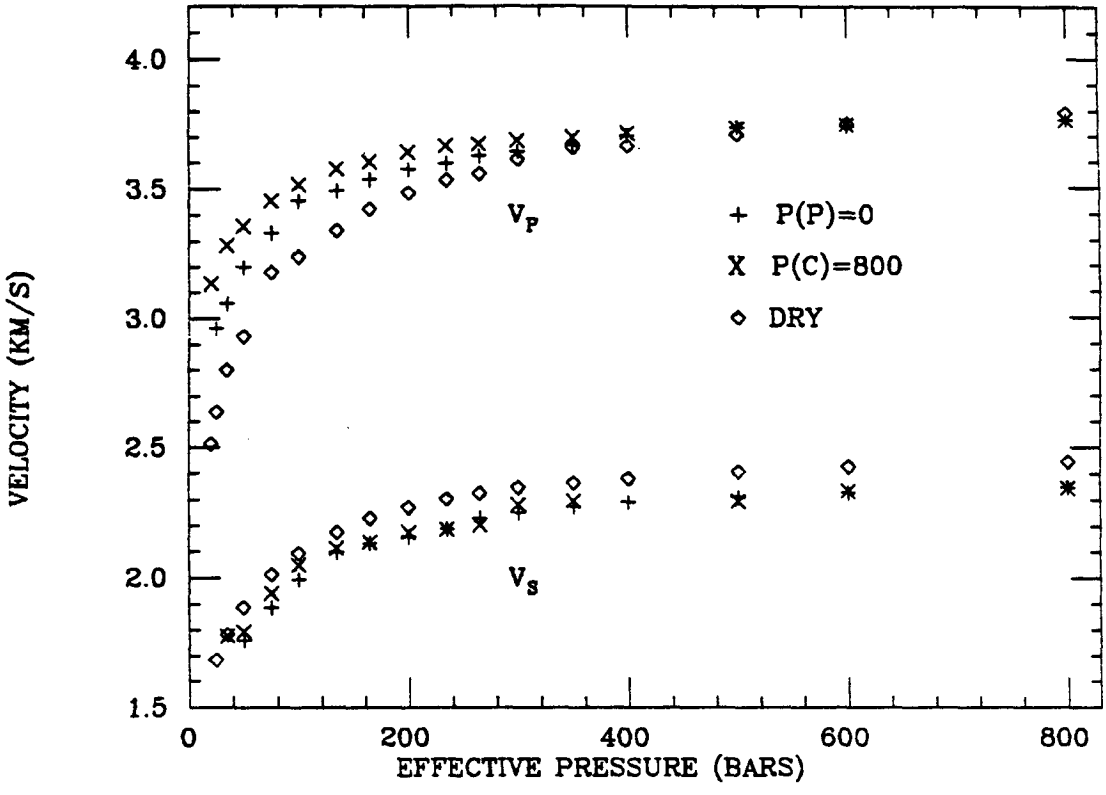

BEREA 3α

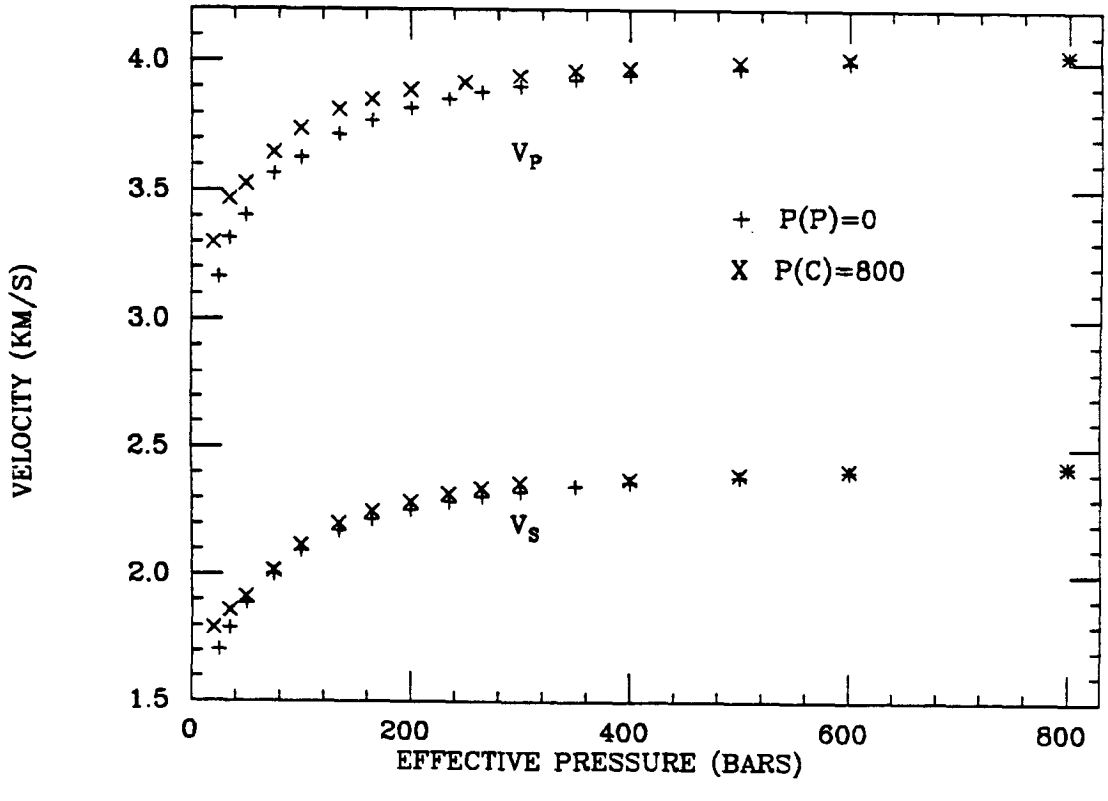

BEREA 4

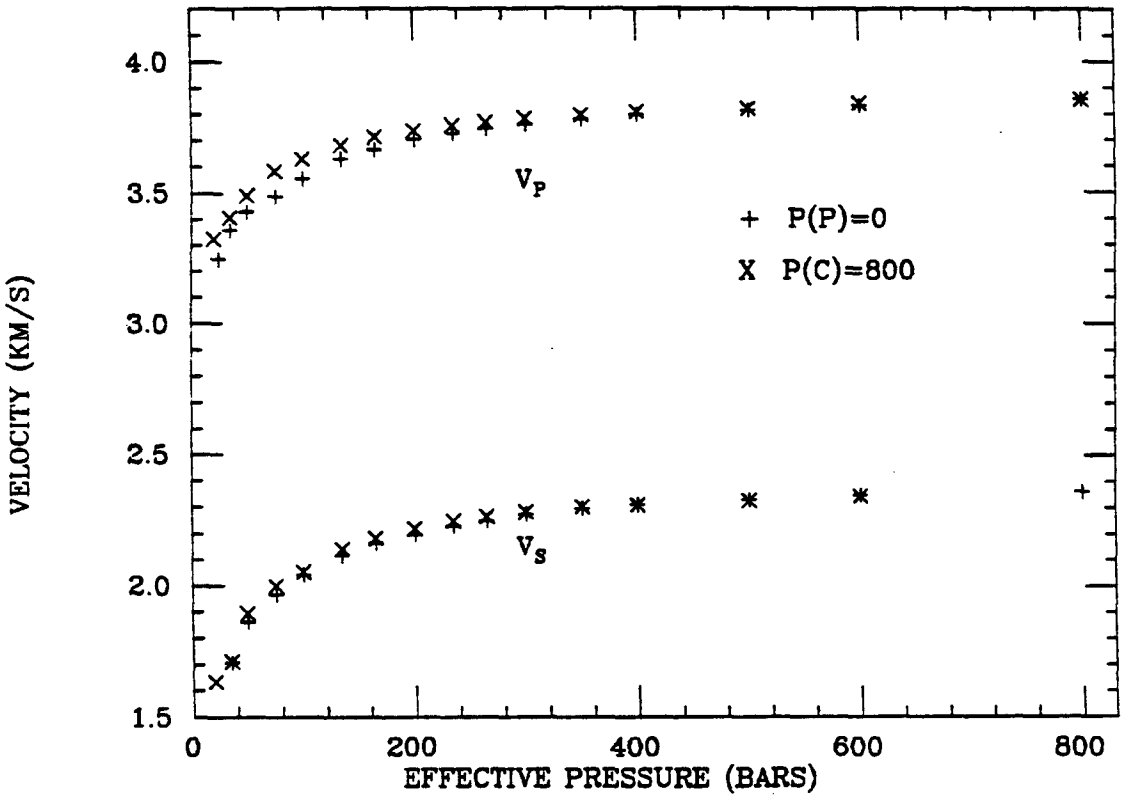
4.0
3.5
3.0
2.5
2.0
1.5
VELOCITY (KM/S)
0
200
400
600
800
EFFECTIVE PRESSURE (BARS)
V_P
V_S
+ P(P)=0
X P(C)=800

BEREA 5A

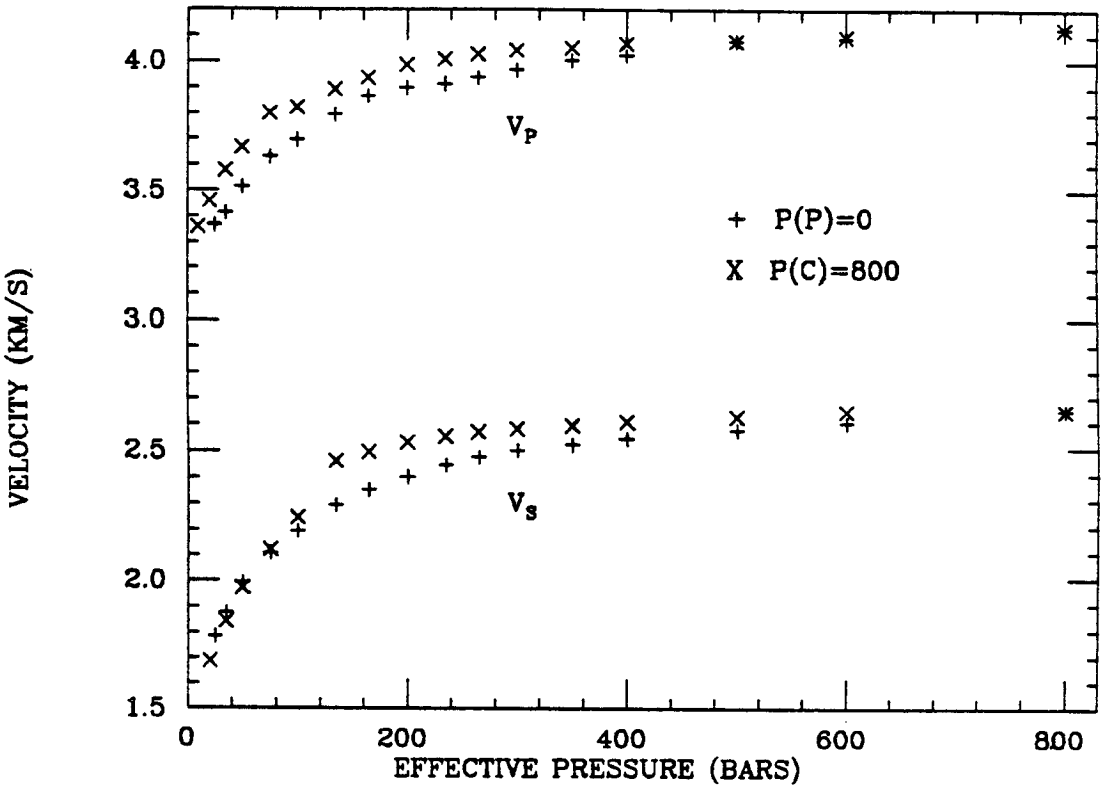

BEREA 5α

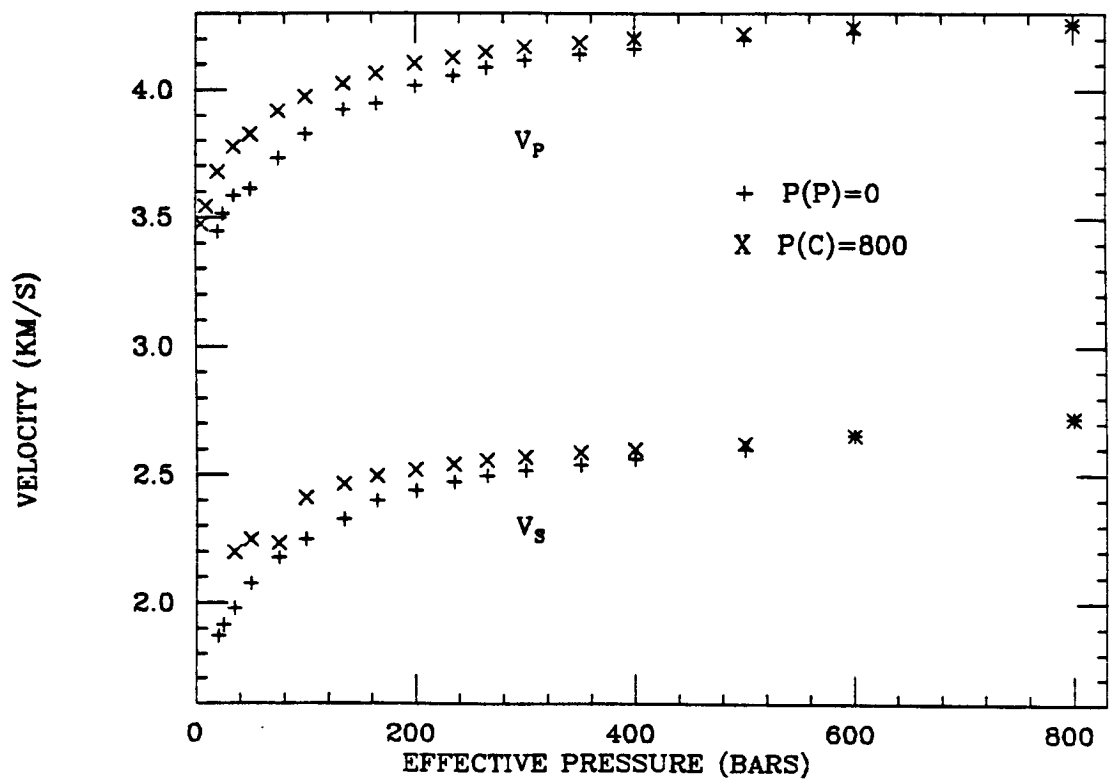

MASSILON 1A

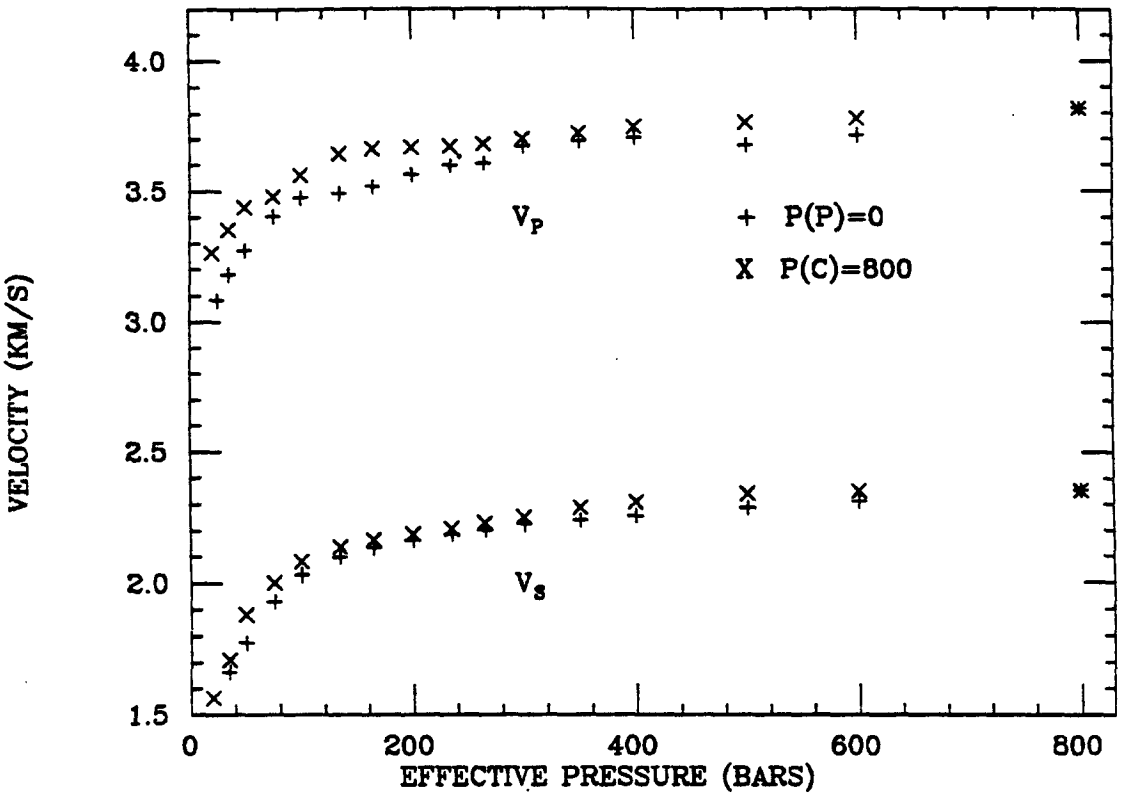

MASSILON 1α

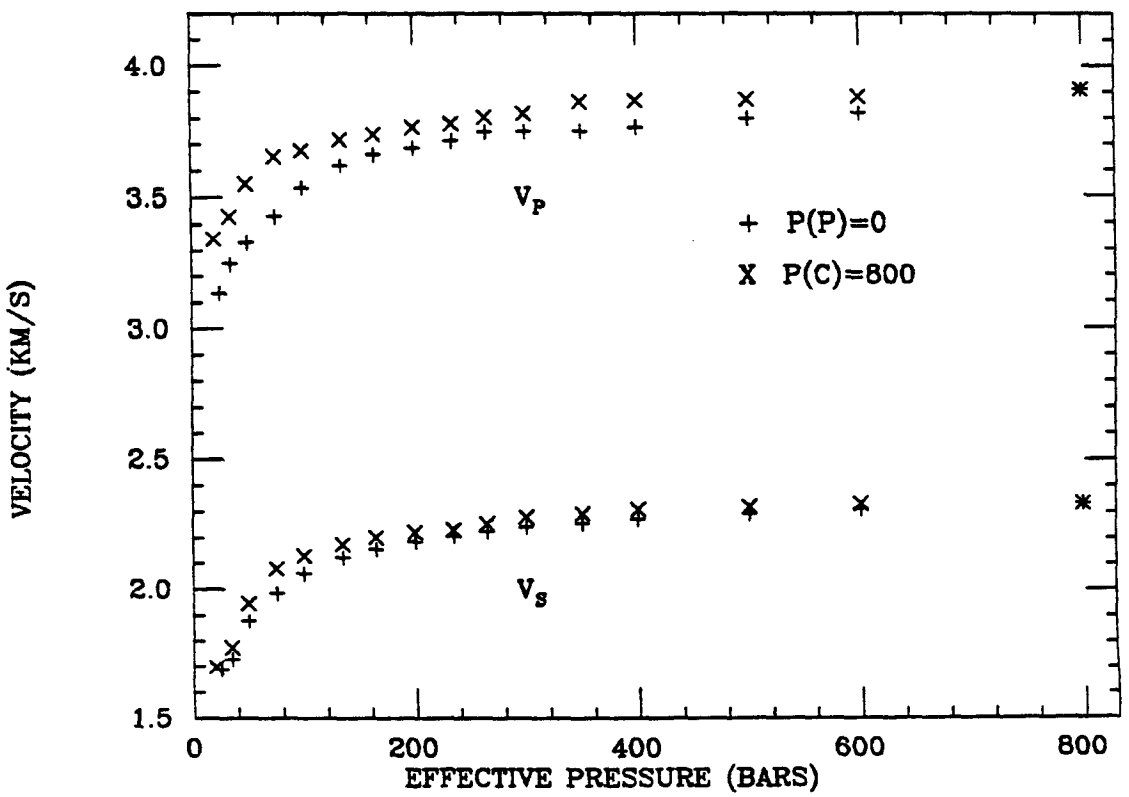

MASSILON 2

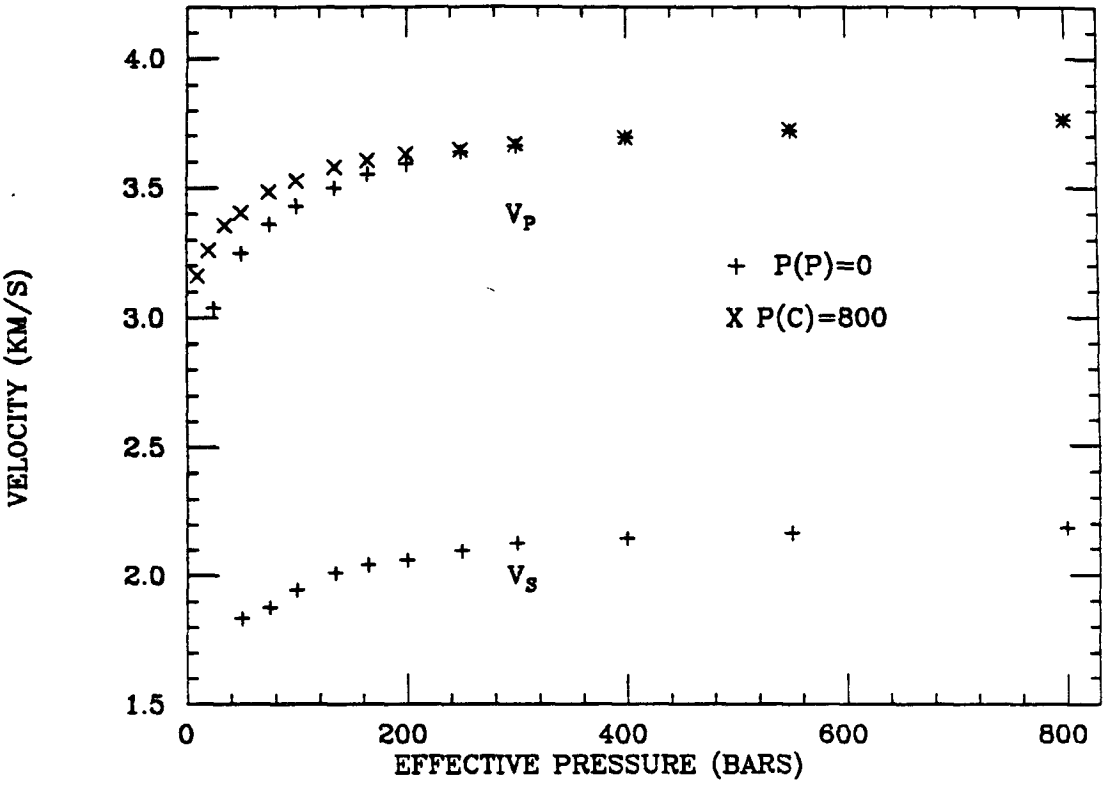

ST. PETER N

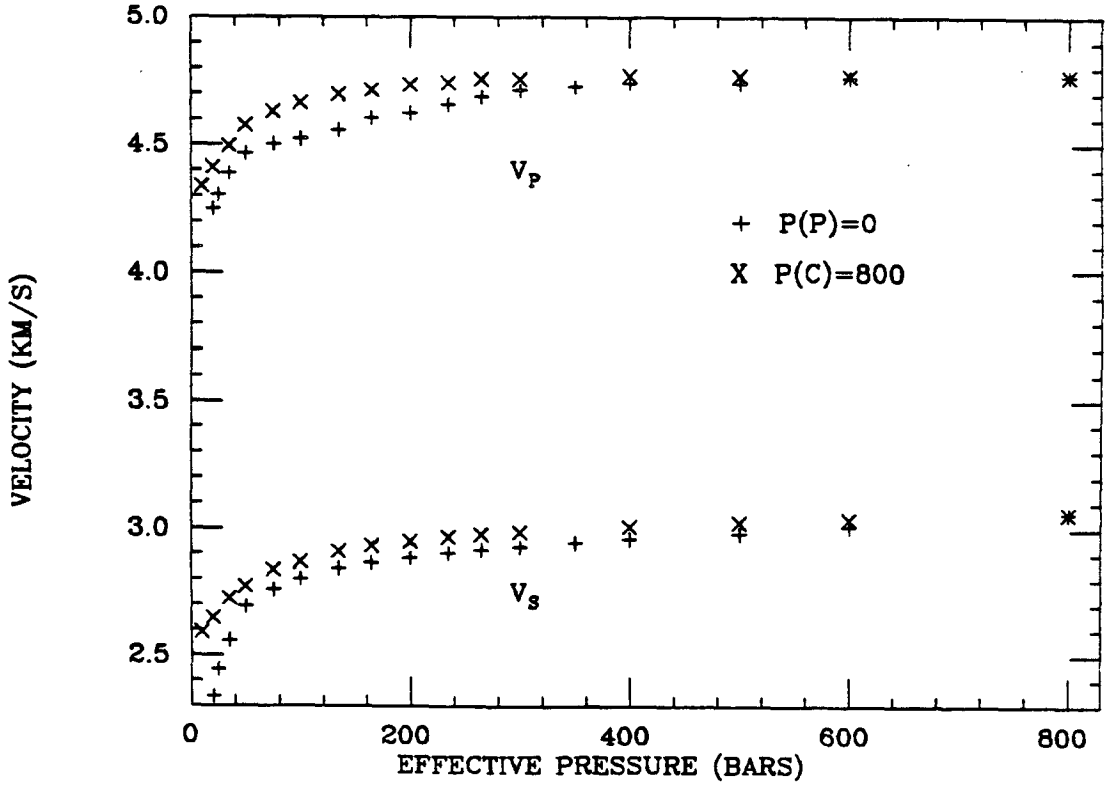

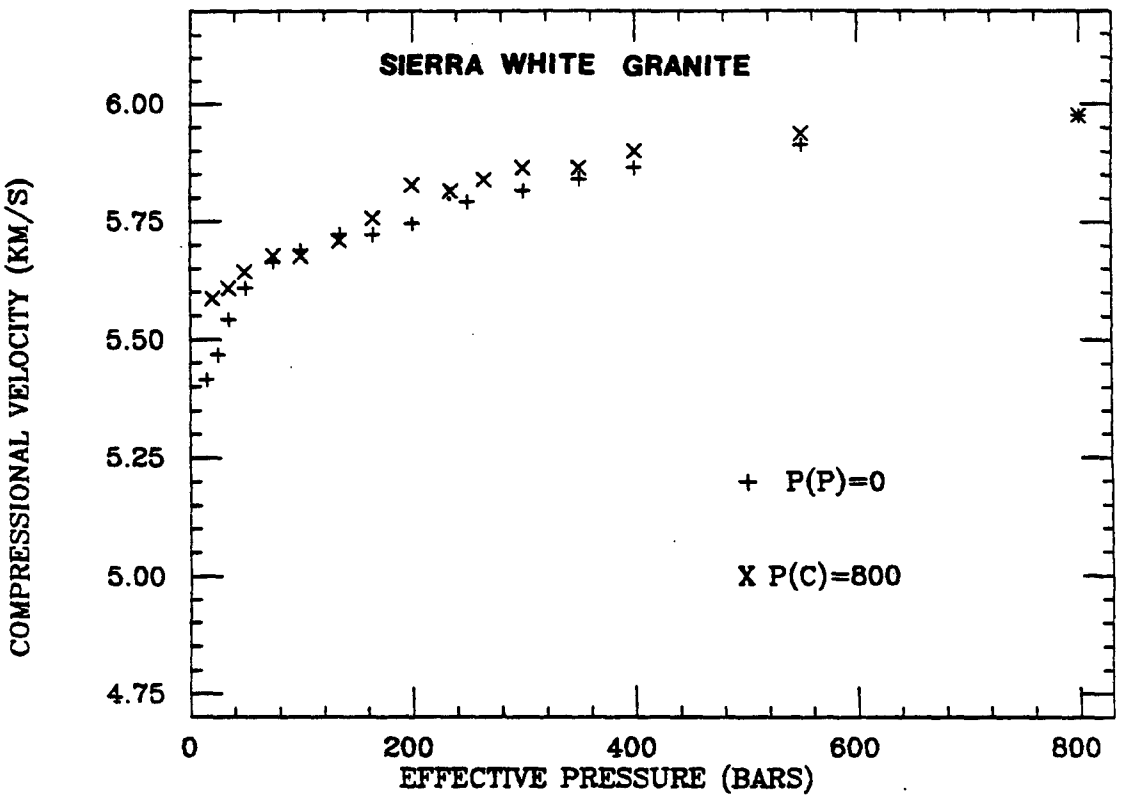
SIERRA WHITE GRANITE
COMPRESSIONAL VELOCITY (KM/S)
6.00
5.75
5.50
5.25
5.00
4.75
0
200
400
600
800
EFFECTIVE PRESSURE (BARS)
+ P(P)=0
X P(C)=800

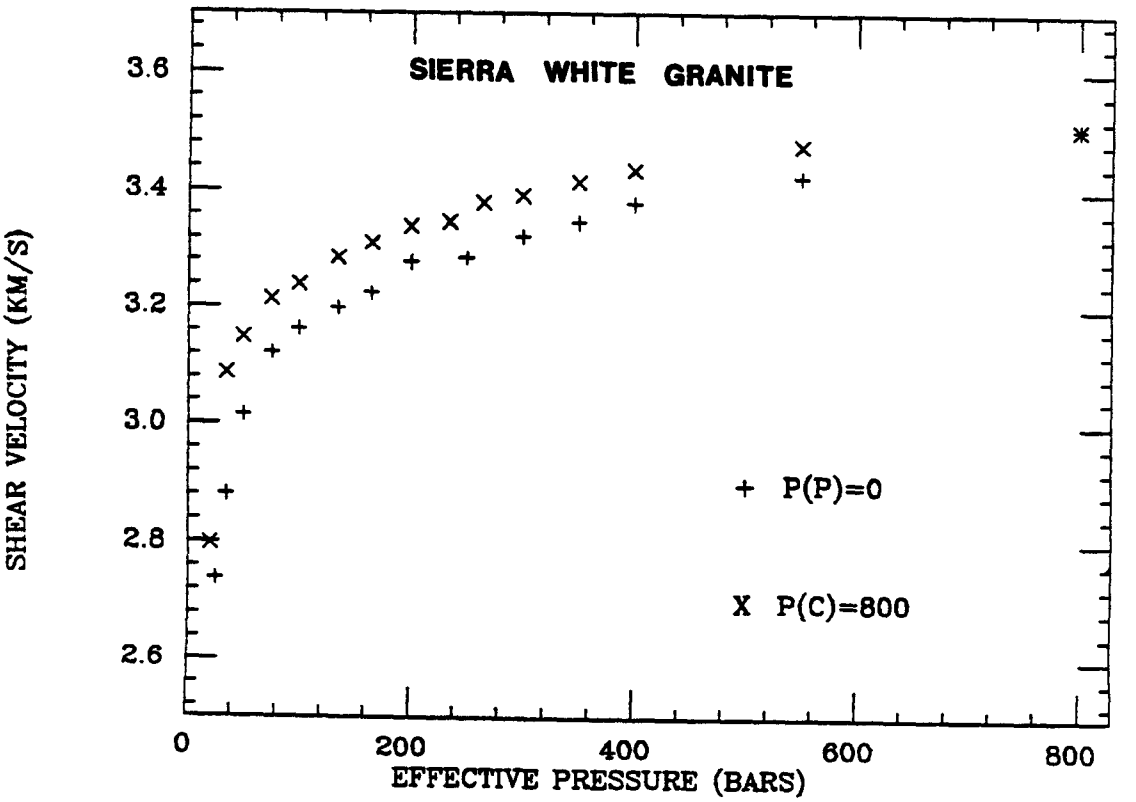
SIERRA WHITE GRANITE
SHEAR VELOCITY (KM/S)
3.6
3.4
3.2
3.0
2.8
2.6
0
200
400
600
800
EFFECTIVE PRESSURE (BARS)
+ P(P)=0
X P(C)=800

Chapter 3

THE NATURE OF SEISMIC REFLECTIONS FROM THE CRYSTALLINE BASEMENT: COCORP WIND RIVER LINE, WYOMING

ABSTRACT

Seismic reflection experiments designed to explore the lower continental crust have raised the problem of distinguishing multiples generated within the shallow sedimentary section arriving at long travel times from primary events in the lower crystalline crust as the cause for deep reflection horizons. This issue must be resolved before a geologic interpretation may be made of deep reflection profiles. Traditional techniques of analyzing for multiples are inappropriate because of the very long travel times and small moveouts involved. This problem is investigated for the particular case of the COCORP Wind River profile in Wyoming, where numerous reflections from 6 to 14 seconds have been suspected of being multiples. A one dimensional seismic modeling technique is used where seismic losses due to depth variable attenuation are accounted for. Sonic logs from boreholes near the line constrain the velocity structure in the shallow crust. By modeling the amplitude and spectrum of the reflections we arrive at a Q structure for the crust in this area. The Q in the sedimentary section varies from 40 to 300 increasing with depth. Q in the crystalline basement is about 2000. When synthetic seismograms are generated using a realistic Q structure and compared to true amplitude records it is found that the amplitudes of multiples generated from within the sedimentary section are far too small to account for the observed deep reflections. This is due to the fact that

multiples are traveling entirely in the much more attenuating sedimentary section. In general we do not expect multiples to be present in the crystalline basement below a sedimentary section of relatively low Q. Multiples generated within the crystalline section may however be observed in the deep record at greater travel times than the primary event due to the higher Q of crystalline rocks. Hence the deep reflection horizons found in the Wind River profile are mostly primary events from impedance contrasts deep within the crystalline basement. Spectral analysis indicates that these reflection horizons are not due to simple step discontinuities, but are caused by multiple thin laminations of alternating high and low velocity or anisotropy, where the thickness of laminations varies from 40-400 meters.

INTRODUCTION

In the past decade the seismic reflection technique has been applied with success to the study of the entire thickness of the continental crust, using primarily techniques developed by the oil industry for shallow crustal exploration (Schilt et. al., 1979; Oliver, 1982). The COCORP Wind River reflection experiment (Smithson et. al., 1979) is an example of a high quality deep reflection profile which has increased our understanding of the structure of the deep continental crust. Yet some problems remain in interpreting these data.

One of the prominent features of the Wind River profile is the significant amount of coherent reflected energy arriving at travel times of 6 to 14 seconds, corresponding to depths well within the crystalline basement. Zawislak and Smithson (1981) suggest that these events are multiples from the overlying sedimentary section and are not due to impedance contrasts within the Precambrian basement. Their argument is based on the observation that deep events are more common under the Green River and Wind River basins where substantial thicknesses of sediments have accumulated, than under the Wind River mountains where Precambrian rocks outcrop. Also cited is evidence from autocorrelograms and synthetic studies. However this interpretation of the deep events as multiples is not shared by

all (Wallace, 1980; Lynn, 1979; Jones and Nur, 1982). This is an important problem which must be resolved before many of the deep reflection profiles which show reflection events in crystalline basement below sedimentary sections may be interpreted.

A simple calculation shows some problems with the interpretation of the deep events in the Wind River profile as multiples. Zawislak and Smithson (1981) calculate that multiple reflections from an interface with a reflection coefficient of 0.35 at 4.5 kilometers depth in a sedimentary section of 8 kilometers thickness may arrive at travel times corresponding to depths of about 9 kilometers, just within the basement, with amplitudes similar to a primary reflection from an interface of reflection coefficient of 0.13 in the crystalline basement at 9 kilometers. In this calculation and in their synthetic modeling they do not take into account the attenuation structure of the crust.

However evidence is accumulating, both from in situ (Mitchell, 1980) and laboratory work (Johnston, 1981; Tittmann, 1977) that attenuation of seismic waves is much stronger in sedimentary rocks than in crystalline rocks. Multiple reflections generated within the sedimentary section travel entirely in the highly attenuating sediments so we would expect them to lose energy much more rapidly with time than events originating within the crystalline basement. Consider a Q in the sedimentary section of 100 and a Q in the basement of 1000. The Wind River basin is about 8 kilometers thick. Assuming a reflection coefficient of 0.2 in the sedimentary section, and taking the fewest number of bounces for a surface multiple to arrive at a time of 11 seconds, the amplitude of a multiple will be approximately four orders of magnitude less then the amplitude of a primary event of reflection coefficient 0.05 in the basement at about 30 kilometers in depth. In shallower sedimentary basins with multiples at similar travel times is even more energy is lost with each additional bounce.

Figure 1 illustrates the effect of attenuation contrast on decay of amplitude with depth. Normalized amplitude on a logarithmic scale for a reflection from a step interface is plotted versus the depth to the interface for

two frequencies, 13 Hz and 32 Hz, and for Q values from 30 to 10,000. Note the significant effect at large depths of attenuation on the amplitude of the reflected wave.

The possible presence of multiples arriving at travel times corresponding to the lower crust has been considered by several other workers (Junger, 1951; Widess and Taylor, 1959; Narans et. al., 1961; Robertson, 1963; Dohr and Fuchs, 1967; Kanasewich and Cumming, 1965; Pavlenkova and Smelyanskaya, 1970). In each of these cases the conclusion was that multiples generated from the sedimentary section of the shallow crust do not significantly contribute to reflection horizons observed at travel times corresponding to the lower crust. These studies usually cite a lack of correspondence between shallow and deep reflections, lack of intermediate multiple events, or insufficient amplitudes expected from sedimentary multiples to account for the deep reflections.

More recently Lynn (1979) and Wallace (1980) argue specifically against the presence of multiples in the deep section of the Wind River profiles. However most of these arguments are based on qualitative reasoning. It would be useful to develop a quantitative tool to distinguish the relative importance of multiple and primary events in deep seismic sections. Methods developed for shallow crustal reflection experiments such as velocity analysis are not appropriate because the small effective aperture of a deep reflection experiment yields small moveouts.

In this paper we use one dimensional synthetic seismograms and true amplitude data records to analyze quantitatively the case for multiples in the COCORP Wind River profile, specifically taking into account the attenuation structure of the crust. Since the problem hinges critically on the Q structure of the crust we also attempt to constrain the depth dependence of Q in this area. It is found that multiples from the overlying sedimentary section do not arrive at times corresponding to the deep basement with significant amplitudes. True amplitude sections show a distinct lack of features which are expected from multiples and a lack of correlation of shallow events with deep events. Unless some specific multiple ray path is proposed which gives

rise to the features observed on the data it must be concluded that multiples from the sedimentary section are not important at long travel times.

A number of studies of deep reflections from within the crust and the Moho have found that a thinly laminated structure is required to account for the amplitude and spectral content of deep reflections (Meissner, 1973; Clowes and Kanasewich, 1970; Fuchs, 1969; Hale and Thompson, 1982; Pavlenkova and Selyanskaya, 1970; Davydova et al, 1972; Kosminskaya and Kapustian, 1979). A similar result is found here. Thin laminations of alternating high and low velocities are required in the models. Reflection coefficients we infer for these laminations are reasonable for typical lithologic variations in a heterogeneous granulitic complex.

WIND RIVER REFLECTION DATA

The location of the COCORP Wind River profile is shown in Figure 2 along with the simplified geology. The major feature traversed is the Wind River range, where Precambrian crystalline rocks have been uplifted along the Wind River thrust fault. On either side of the mountain range is a sedimentary basin. Sonic logs in boreholes near the line (Zawislak and Smithson, 1982; Smithson and Ebens, 1971) constrain the velocities in the shallow crust. Details of the data acquisition and processing as well as geologic interpretations of the data are given by Lynn (1979) and Smithson et. al., (1979).

As waves propagate in the earth they lose energy and decrease in amplitude primarily due to two causes, spherical divergence and inelastic absorption. If we know approximately the velocity and attenuation structure of the crust we can correct a reflection profile for these effects as a function of time along the section. This "true amplitude" section has an advantage over an automatic gain control section of preserving the relative strength of reflection horizons.

Wind River lines 1, 1a, and 2 are displayed in true amplitude sections in Figures 3, 4, and 5. The velocity and attenuation structures used to gain the data are given in Figure 6. A three layer gain function (g) was used, with gain

a linear function of velocity and travel time (g=vt), and an exponential function of Q at the dominant frequency ($g=e^{\pi f t/Q}$) in each layer. This gain function was found to yield high quality records and corresponds to a reasonable velocity and attenuation structure for each of the three lines. No trace equalization has been applied nor has there been any attempt to suppress bad traces. The only processing has been the Vibroseis correlation, static corrections, velocity analysis for common depth point stacking, and the true amplitude gain recovery.

The data quality is remarkably good (compare to automatic gain control sections shown in Smithson et. al., 1979; Lynn, 1979). All the prominent features are still present, the strong reflections from the Wind River and the Pacific Creek thrust faults, the layered reflections from the Green River and Wind River basins, and most importantly here, the deep reflections below 10 seconds. Note particularly the reflector at 11 seconds on the left side of line 1 and the reflections at 10 to 12 seconds on line 2.

Some simple observations apply to the multiples problem. That the deep events show up at all on a true amplitude section is evidence against their being multiples. As discussed earlier multiples from the sedimentary section should be of relatively low amplitudes at long travel times due to loss of energy from the low Q sediments and multiple bounces, whereas the true amplitude section has been gained assuming the deep events are attenuated significantly less by the higher Q lower crust. Multiples might be expected on an automatic gain control section if the basement was highly transparent, but not on a true amplitude section.

In line 2 there is an apparent shadow zone of no energy from two to five seconds just below the sediments of the Wind River basin. This would be expected if the section had an automatic gain control applied as the early gain factors would be controlled by the strong sedimentary primary reflections, but such is not the case here. It seems inconceivable that the strong events on the true amplitude section at 10 to 12 seconds can be multiples with no evidence of intermediate multiples, particularly immediately below the sedimentary section. At 10 to 12 seconds they have undergone five

or six bounces and the amplitude level would be far to small to observe. Furthermore the deep events have a similar dip to the shallow events implying that they would have to be interbed rather than surface multiples, further reducing their likely amplitudes.

Figure 7 shows detail of the line 1 true amplitude data for stations 50 to 190. Note the very strong reflection at 11 seconds, a kind of bright spot in the basement, as well as many laminar reflections from 11 to 15 seconds. The strong event at 11 seconds is directly below an anomalously weak series of reflections from the sedimentary section. It is difficult to explain this lack of correlation between strength of deep reflections and strength of shallow reflections if the deep events are multiples. Again no evidence of intermediate multiples are seen on the true amplitude record, although they do appear on automatic gain control records (Smithson et. al., 1979). The sedimentary section in this area is very flat lying and uniform so anomalous focusing effects are not likely.

Figure 8 is detail from a portion of line 1a, stations 580 to 710. The strong events at 6 to 8 seconds are from the Wind River thrust fault. On viewing the section from the side a number of events from 12 to 14 seconds may be seen. In this portion of the line only a very thin layer of Mesozoic and Paleozoic sediments cover the Precambrian basement. There would have to be 20 to 25 bounces of surface multiples to get an event at this depth. Again no evidence of intermediate multiples is seen. These observations argue strongly against the deep events being multiples.

ATTENUATION STRUCTURE OF THE CRUST

Both the display of true amplitude seismic sections and quantitative modeling of amplitudes from deep reflections require estimates of the Q structure of the crust. In situ attenuation is much more difficult to measure than velocity and hence the variation of Q with depth in the crust is poorly constrained. However a number of attempts have recently been made to invert seismic data for depth dependent Q. Additional information from laboratory measurements of attenuation in rocks at elevated temperatures

and pressures allow us to estimate a typical Q structure for the crust.

Herrmann and Mitchell (1975), Mitchell (1975), Mitchell, (1973), Mitchell (1980), Canas and Mitchell (1978), and Lee and Solomon (1975) present inversions of surface wave data for shear Q determinations in North America. They inevitably find relatively low values of Q (100 to 300) in the upper crust (5 to 15 kilometers). Attenuation is very small in the lower crust, with Q values of 1000 to 2000.

Clowes and Kanasewich (1970) analyzing spectral content of reflection data, and Braile (1977), studying amplitudes of refracted waves, find Q values on the order of 50-300 for the upper crust and 1000 to 2000 for the lower crust. Aki (1980) also finds very high Q values (about 3000) for the basement.

Detailed determination of Q by spectral analysis and modeling in sedimentary basins (Kan et. al., 1981) gives values of 28 to 110. In situ measurements on shale (McDonal et. al., 1958) gives a Q of 32. Hauge (1981) measured Q in sedimentary basins of 30 to 273, generally increasing with depth.

Laboratory measurements of various rock types are in rough accord with these observations. Q values in wet sedimentary rocks under shallow crustal conditions are as low as 20 up to about 100 (Johnston, 1981; Winkler and Nur, 1982). In vacuum dry crystalline rocks Tittmann (1977) has measured Q values of several thousand, similar to values inferred for the lower crust. A model emerges of a relatively highly attenuating sedimentary section with very low attenuation in the crystalline section, and Q generally increasing with depth, both due to increasing pressure and the presence of lower porosity rocks.

A more specific estimate of the Q structure in the area of the Wind River reflection profile is required. The method will be to use available near surface velocity information to compute synthetic seismograms for depth variable Q. The synthetics are one dimensional, computed by the wave equation method (Ganley, 1981). We then compare the amplitude level and the frequency content of the synthetic record to the true amplitude data record after both have been gained identically with the factors in Figure 6.

The source used for the Wind River survey was a Vibroseis 8 to 32 Hz sweep. There was very little energy in the low frequency end of this spectrum. A 13 to 32 Hz zero phase wavelet was found to correspond most accurately to the data.

We are fortunate to have very good velocity control from sonic logs in this area. Several exploratory holes drilled in the Green River basin provide velocity information through essentially the entire nine kilometer thickness of sedimentary section (Zawislak and Smithson, 1979). The velocity profile is shown in Figure 9. Also available is a sonic log from a three kilometer deep hole in the Precambrian rock of the Wind River range (Smithson and Ebens, 1971). This is also plotted in Figure 9. Sonic logs from the sedimentary section were digitized at 15 meter intervals so approximately 600 layers were used in the calculation of the synthetic seismograms from the sedimentary section.

No velocity information is available in the shallower Wind River basin to the east. Since the stratigraphy is probably similar to that of the Green River basin we used the same velocity profile, but half the thickness for each layer. On the north eastern flank of the Wind River range it might be more appropriate to use the lower half of the sedimentary section from the Wind River basin. However in this case (the Wind River basin) we are only interested in a representative sedimentary section so the details of the seismic stratigraphy are not important.

In Figure 10 we show true amplitude single traces from three typical stations in line 1. Reflections which were relatively distinct were windowed and the amplitude spectrum was computed. Also shown in Figure 10 are six examples of frequency content from well defined reflections in the sedimentary section. Spectral analysis was done on well defined reflections for over 100 individual traces on the three reflection lines.

If we assume that the velocity profiles in Figure 9 are representative and the source is known and constant, then the Q dependence with depth is the only unknown in determining the frequency content of the individual reflections. Synthetics were computed using various Q structures until a

reasonable fit was obtained for the amplitude and frequency content of representative traces for each line. Of course errors in the sonic logs and lateral heterogeneities complicate the procedure.

The preferred Q model for each line is shown in Figure 11. The Q models are compatible with in situ and laboratory measurements discussed earlier. Q is fairly low in sedimentary rocks, about 40 near the surface, increasing to 300 near the bottom of the sedimentary basin. There is very little control on basement Q values, though they must be high (greater than 1000). A value of 2000 will be used here. In fact the results are rather insensitive to the Q value of the basement. Values as low as 600 have also been used as test cases and these values do not change substantially the gained data or the synthetics and hence do not effect the conclusions.

Figure 12 shows the synthetic seismogram and frequency content of various reflections from the sedimentary section for the preferred Q model e1, corresponding to line 1. The same gain was used on these traces as was used on the data. The general level of amplitudes is similar to the data on Figure 10, although exact correspondence of individual events is not expected due to the problem of lateral heterogeneity. The frequency content of the individual records is a reasonable match to the data, both in the shape of the spectrum and the frequency of peak energy.

For comparison also shown are synthetics for Q models which do not fit as well. Figure 13 is for Q model e12, with a Q of 50 throughout the sedimentary section. Note that the amplitude level is generally too small in the lower part of the sedimentary section and the energy is concentrated at lower frequencies than the data. Figure 14 was computed for Q model e20 with a Q of 300 through the sedimentary section. The amplitudes are larger in the lower part of the record compared to the shallow record. Too much high frequency energy was present in most of the windowed reflections, note particularly A, D, and F.

The Q model e1 is a reasonable approximation for line 1. A similar model but with half the thickness of each layer was used for line 2 through the sedimentary section. This model proved to adequately account for the data in

line 2.

Very little control is available for modeling the Q structure for line 1a where Precambrian crystalline rocks are exposed. Figure 11 shows a Q model which is consistent with the data. Note that high values of Q are achieved at much shallower depths.

It is interesting to note the similarity between the Q models inferred from spectral analysis and modeling of the data and those which were found to yield the highest quality true amplitude records when used as gain factors. In both instances a Q in the range of hundreds in sediments and a Q of thousands in the basement were appropriate. This implies the gain function is predominantly removing effects of spherical divergence and attenuation and not amplifying noise or sedimentary multiples.

SEISMIC AMPLITUDE MODELING

Using the Q structure previously determined for the crust in this area, and the velocity profiles of the sedimentary section, we may compute true amplitude synthetic seismograms which incorporate multiples. The synthetics are gained using the same gain function as was applied to the data. We may then match the general level of amplitudes from the sedimentary record on the synthetics to the amplitudes of the data and determine if multiples generated from the sedimentary section arrive with significant amplitudes at long travel times.

Figure 15 shows a detailed portion of Wind River line 1, stations 420 to 460, true amplitude data. The dipping event at 5.5 to 6 seconds is from the Pacific Creek thrust fault. Other reflections in the basement may be seen at 7.5, 8, 8.5, 11 to 12, and 13 seconds. The traces on the right are synthetic sections computed using Q model e1 and the velocity structure determined from sonic logs. For each synthetic three identical traces are plotted to facilitate comparison to the data.

Synthetic A is for primary events only. In addition to the sedimentary section a series of impedance contrasts were used to model basement events. At 6 seconds and 11 seconds a series of 15 layers of alternating high and low

velocity, each of thickness 110 meters and reflection coefficient 0.05 were used.

Synthetic B includes multiples from the sedimentary section as well as primary events, but no basement reflectors. The multiples from the sedimentary section are visible with low amplitudes to about 6 seconds but there is definitely no multiple energy at depths corresponding to the deep reflections at 11 to 13 seconds.

Synthetic D is the same as synthetic B, but the entire trace has been multiplied by a factor of 10. This causes the primary sedimentary events to be strongly clipped. Even with this amount of amplification the multiple energy falls off rapidly, and is not present below 9 seconds.

Trace C contains primary and multiple events with the basement reflectors added. Again the multiples from the sedimentary section decay rapidly, but multiples generated from impedance contrasts in the basement may be clearly seen. It is possible for the dipping events on the data at 7.5 and 8.5 seconds to be multiples from shallower basement events, based on comparison to the synthetics. The reflection on the data at 13 seconds fits well with multiples from the laminated basement event at 11 to 12 seconds on the synthetic.

It is reasonable that multiples are more likely to be present when generated in the crystalline section than when generated in the sedimentary section because of the much lower attenuation of crystalline rocks. The laminar structure of the basement reflections causes them to have significantly higher amplitudes than would be expected from a step interface when the appropriate wavelength to thickness ratio is present to produce constructive interference. It also causes the beating phenomenon seen in synthetic C, causing the multiples to appear fairly strong a short distance below the primary.

Figure 16 shows similar synthetic traces computed with different Q structures. Model e12 is for a Q in the sedimentary section of 50. When the gain is applied there is no significant energy anywhere in the lower section, even where basement impedance contrasts are present, implying this Q value

is too low to account for the data.

Model e20 is for a Q in the sedimentary section of 300. Multiples persist for somewhat greater times than for model e1, but there is still no multiple energy below 9 seconds that would be above the noise level. Model e8 was computed neglecting attenuation effects (infinite Q). No gain was used on this trace or the lower part of the record would be strongly clipped. In this case multiples are present nearly throughout the record and would be even stronger if the synthetic was gained. This emphasizes the importance of properly accounting for attenuation contrasts. Note for Q models e20 and e8 which use higher Q values in the sedimentary section that the frequencies of events arriving at long travel times are much higher than is indicated by the data.

Figure 17 shows a detailed portion of line 1a, stations 650 to 690. The synthetics are computed for the same cases as for Figure 15. Basement events on the data at 6 to 8 seconds and 12 to 13 seconds were modeled on the synthetic by an alternating series of high and low velocities each corresponding to a reflection coefficient of 0.05 and having a thickness of 150 meters.

The shallow velocity structure is provided by the sonic logs in the Wind River range (Figure 9). The sedimentary section is very thin here and no multiples can be expected to explain the event at 12 to 13 seconds, and indeed no energy is present on the synthetics to these times. The deep events on this line are clearly not multiples. No strong multiples from the basement events are indicated on the synthetics here because the different thicknesses of the layers and the frequency content in the deep section due to the different Q structure causes predominantly destructive interference in the multiples, as opposed to the constructive interference obvious in Figure 16.

In Figure 18 we examine Wind River line 2 in the Wind River basin. The sedimentary section is thinner here, about 2 seconds on the record. Several deep reflections are seen at 11 to 12 seconds. The sedimentary basin velocity profile and Q model e2 were used for the model.

Synthetics B and C which incorporate multiples show no significant sedimentary multiple energy below 4 seconds. Even when the synthetic incorporating multiples is increased in amplitude by two orders of magnitude (synthetic D) sedimentary multiple energy cannot explain the deep events at 11 to 12 seconds. Trace C which includes basement events, again as a number of thin layers, does fit quite well with the data showing the deep events. Note again that multiples generated from impedance contrasts within the basement may be present.

The one dimensional, true amplitude synthetic seismogram models the data quite well using the shallow crust velocity profile from sonic logs and a Q structure for the crust inferred from spectral analysis of the data. It is observed that multiples generated from within the sedimentary section cannot explain the deep events as they do not arrive with significant energy at long travel times. This is due to the much higher attenuation of sedimentary rocks.

The deep reflection horizons in the Wind River line must then be due to impedance contrasts within the crystalline basement. Due to the higher Q of the deep crust multiples generated within the crystalline section may be present on the record for short times below the primary events, if the proper seismic wavelength to layer thickness ratio occurs.

MODELING OF DEEP REFLECTIONS

As reflection experiments have yielded higher resolution in studies of the crystalline basement, the concept of major boundaries in the crust, including the Moho, as step discontinuities in seismic velocity has been refined. A number of studies have shown deep interfaces to be gradational, generally with many thin layers of alternating high and low velocity zones (Meissner, 1973; Fuchs, 1969; Davydova et. al., 1977; Clowes and Kanasewich, 1970; Hale and Thompson, 1982; Pavlenkova and Smelyanskaya, 1970, Dohr and Meissner, 1975; Kosminskaya and Kapustian, 1979; O'Brian, 1964). This "laminar" model of the crust is required to explain both the high amplitudes and frequency content of deep crustal reflections and refractions. Reflections from laminar structures in basement rocks have also been confirmed by seismic studies and

drilling of uplifted Precambrian rocks (Rief and Robinson, 1981)

The deep reflections in the Wind River profile also indicate many thin laminations of alternating high and low velocities are causing the deep reflection horizons. Figure 19 shows some windowed reflections at intermediate depths from various traces in Wind River line 1, and the corresponding spectrum. It was not possible to adequately model either the time record in terms of its amplitude and ringing character or the amplitude spectrum with a step discontinuity. Rather a series of laminations of alternating high and low velocities of thickness (L) ranging from 40 to 110 meters was required. Each of the layers in the model has a reflection coefficient of 0.05. At thicknesses of 110 meters for the basement laminations constructive interference causes much higher amplitude of reflections (Morlet et. al., (1982) provide a theoretical analysis of this problem).

Figure 20 shows some deeper reflections in line 1. Also shown are synthetic models using laminations varying from 40 to 400 meters thick. Figure 21 shows a reflection from the Wind River thrust (station 644). Both the time and amplitude section are fit remarkable well by basement reflections from approximately 25 layers of alternating high and low velocity, each of reflection coefficient 0.05 and thickness of 150 meters. Figure 22 models some deep events in Wind River line 2 using basement lamination thickness of 300 meters. In all these cases the appropriate Q structure and shallow crustal velocity structure for each line was used to generate the synthetics.

Although models using reflection coefficients of 0.05 are shown here, by tuning the layer thickness to get maximum constructive interference a reflection coefficient as low as 0.02 could account for some of the deep reflections. This range of reflection coefficients requires velocity or density contrasts in the basement of 4% to 11%.

Others have speculated on the geologic significance of a laminar structure in the crystalline basement (Hale and Thompson, 1982; Lynn et. al., 1981; Kay and Kay, 1981; Meissner, 1973; Oliver et. al., 1983). The reflection coefficients implied by the modeling are well within the range of variations in a

typical terrain of gneissic granulitic rocks (Hall and Simmons, 1979; Christensen and Fountain, 1975). Eroded Archean metamorphic terrains commonly have strong layering (Windley et. al., 1981). Variations of thickness of layers in the deep basement as well as complex folding of these rocks could easily produce the laminar and discontinuous nature of basement reflectors. The small aperture of the array effectively dip filters events arriving from the lower crust so only horizontal or gently dipping layers of appropriate thickness will be seen. Although lamina thicknesses of 40 to 400 meters were used in the models, this does not prove that this is the only scale at which heterogeneities occur. For the wavelengths used in this experiment it is only these lamina scales which produce strong reflections. Other lamina dimensions are probably present but not resolvable.

Another possibility is variations in orientation of anisotropic rocks. Metamorphic rocks of high grade are commonly anisotropic (Christensen and Fountain, 1975; Hall and Simmons, 1979), related to deformation. Variations in the orientation of principal axes could produce a strong contrast in physical properties for a nearly vertically propagating seismic wave (Jones and Nur, 1982 and 1983). Strong seismic anisotropy has been measured in situ (Meissner and Fluh, 1979; Rezanov and Galdin, 1967). Again layering of deformed high grade and anisotropic metamorphic rocks in uplifted Archean terrains (Bayley et. al., Windley et. al., 1981) appears, when dip filtered and appropriate wavelength to thickness ratios are considered to be remarkably similar to the deep reflections in the COCORP Wind River line.

CONCLUSIONS

A number of lines of evidence have been presented for the interpretation of the deep reflection horizons in the COCORP Wind River profile being primary reflections from interfaces deep within the crystalline basement. A multiple orogin for these events may be ruled out. True amplitude sections show a lack of any intermediate multiples, a distinct shadow zone in the basement just below the sedimentary section, and a lack of correlation between the strength of shallow events and deep events. Deep seismic reflections are also seen

where there is little or no sedimentary cover.

It is also shown that the attenuation structure of the crust is critical to this problem. Modeling of the amplitude and frequency content of the Wind River data allow us to estimate the Q structure in this area. Q is about 40 near the surface, increases to 300 at the bottom of the sedimentary basin, and is much higher in the crystalline basement, about 2000. These results are consistent with other in situ and laboratory measurements of attenuation in rocks under the appropriate conditions.

When synthetic seismograms incorporating losses due to depth variable attenuation are computed using the attenuation structure found for the crust in this area and velocity profiles in the shallow crust from sonic logs it is found that multiples from the sedimentary section do not arrive at travel times corresponding to the deep reflections observed in the Wind River line with sufficient energy to be observed. Furthermore we can say that in general multiple events from sedimentary units are not likely to be a problem in interpretation of deep reflection profiles. This is due to the fact that sedimentary rocks attenuate seismic energy much more rapidly than crystalline rock. Multiples generated within the crystalline section may however be observed, and some of the events in Wind River line 1 may be crystalline multiples.

Problems with the change of character of deep events between line 1 in the Green River basin and line 1a in the Wind River mountains (Zawislak and Smithson, 1981) are probably due to stacking related problems in the much more rugged terrain the line traversed and stronger lateral heterogeneities beneath the Wind River range (Wallace, 1980). Other evidence for multiples in the deep section (Zawislak and Smithson, 1981) is circumstantial in nature.

Other possible explanations for the deep events in the Wind River line are sideswipe and refracted reflections. Since the line crosses perpendicular to the main trend of the structural and topographic features of the area sideswipe and refracted reflections off of the most prominent features would be removed during stacking. Out of plane reflections traveling perpendicular to the line in the sedimentary section are again subject to the high

attenuation and would likely not have sufficiently large amplitudes to show up in the deep section. It is concluded that the deep horizons in the Wind River line are predominantly due to impedance contrasts deep within the crystalline basement with some energy due to multiples generated within the basement.

Modeling of amplitudes and frequency content of deep reflection events indicates that they are laminar in nature, composed of many alternating zones of high and low velocities. Thicknesses of laminations in the models varied from 40 to 400 meters. Reflection coefficients could be from 0.02 to 0.05, consistent with laboratory measurements of velocity variations in gneissic granulitic terrains (Hall and Simmons, 1979; Christensen and Fountain, 1975). Impedance contrasts could also be related to variations in the orientation of principal axes in anisotropic metamorphic rocks (Jones and Nur, 1982). The layered, undulating, and discontinuous nature of the deep reflections is just what would be expected from field observations of layering in Archean granulitic complexes (Windley et. al., 1981). The reflection character may also be effected by strong folding of layered basement terrains, as the deep reflection data is dip filtered due to the narrow effective aperture of the array with respect to these deep reflections. One of the deep reflections, the 11 second event on Wind River line 1, is remarkably pervasive in lateral extent and horizontal. On detailed sections of line 1 this event may be followed nearly continuously extending over about 30 kilometers. This suggests a relationship to pressure and temperature profiles and perhaps a phase transition. Most of the other deep events are probably due to layering or structure within the Archean rocks because their predominant dips usually match the large scale tilting of the crustal blocks in line 1a and 2, and are nearly horizontal in line 1. Deep seismic reflection data are clearly yielding valuable information about the structure of the lower crust.

ACKNOWLEDGEMENTS

I thank George Thompson, Dave Okaya and Amos Nur for critical discussions. Dave Hale wrote the synthetic seismogram program. The Stanford Exploration Project provided computer facilities. This research was funded by grant #EAR81-09294 from the National Science Foundation, and grant #DEAT03-76 ER71045 from the Department of Energy.

REFERENCES

Aki, K., Scattering and attenuation of shear waves in the lithosphere, J. Geophys. Res., 85, 6496-6504, 1980.

Bayley, R. W., P. D. Proctor, and K. C. Condie, Geology of the South Pass area, Fremont County, Wyoming, Geological Survey Professional Paper 793, 39p., 1973.

Braile, L. W., 1977, Interpretation of crustal velocity gradients and Q structure using amplitude corrected refraction profiles, The Earths Crust: A. G. U. Geophysical Monograph 20, 427-439, 1977.

Canas, J. A., and B. J. Mitchell, Lateral variation of surface-wave anelastic attenuation across the Pacific, Bull. Seismol. Soc. Am., 68, 1637-1650, 1978.

Christensen, N. I., and D. M. Fountain, Constitution of the lower continental crust based on experimental studies of seismic velocities in granulite., Geol. Soc. Am. Bull., 86, 227-236, 1975.

Clowes, R. M., and E. R. Kanasewich, Seismic attenuation and the nature of reflecting horizons within the crust, J. Geophys. Res., 75, 6693-6705, 1970.

Davydova, N. I., I. P. Kosminskaya, N. K. Kapustian, and G. G. Michota, Models of the earth's crust and M-boundary, Zeitschrift fur Geophysik, 38, 369-393, 1972.

Dohr, G. P., and K. Fuchs, Statistical evaluation of deep crustal reflections in Germany, Geophysics, 32, 951-967, 1967.

Dohr, G. P., and R. Meissner, Deep crustal reflections in Europe, Geophysics, 40, 25-39, 1975.

Fuchs, K., On the properties of deep crustal reflectors, Zeitschrift fur Geophysik, 35, 133-149, 1969.

Ganley, D. C., A method for calculating synthetic seismograms which include the effects of absorption and dispersion, Geophysics, 46, 1100-1107, 1981.

Hale, L. D., and G. A. Thompson, The seismic reflection character of the Mohorovicic discontinuity, J. Geophys. Res., 87, 4625-4635, 1982.

Hall, J., and G. Simmons, Seismic velocities of Lewisian metamorphic rocks at pressures to 8 kbar: Relationship to crustal layering in North Britain, Geophys. J. R. Astr. Soc., 58, 337-347, 1979.

Hauge, P. S., Measurements of attenuation from vertical seismic profiles, Geophysics, 46, 1548-1559, 1981.

Herrmann, R. B., and B. J. Mitchell, Statistical analysis and interpretation of surface wave anelastic attenuation data for the stable interior of North America, Bull. Seismol. Soc. Am., 65, 1115-1128, 1975.

Johnston, D. H., Attenuation: A state of the art summary, Seismic Wave Attenuation, Geophysics Reprint Series no. 2, 123-135, 1981.

Jones, T. D., The nature of seismic reflections from deep crustal fault zones, chapter 5, this volume, submitted to J. Geophys. Res., 1983.

Jones, T. D., and A. Nur, Seismic velocity and anisotropy in mylonites and the reflectivity of deep crustal fault zones, Geology, 10, 260-263, 1982.

Jones, T. D., and A Nur, Nature of seismic reflections from fault zones and the crystalline basement, S. E. G. Technical Program, 52nd annual meeting, 92-93, 1982.

Junger, A., Deep basement reflections in Big Horn county, Montana; Geophysics, 16, 499-505, 1951.

Kan, T. K., D. Corrigan, and P. D. Huddleston, Attenuation measurement from vertical seismic profiles, Geophysics, 47, 466, 1982.

Kay, R. W., and S. M. Kay, The nature of the lower continental crust: Inferences from geophysics, surface geology, and crustal xenoliths, Rev. Geophy. Space Physics, 19, 271-297, 1981.

Kanasewich, E. R., and G. L. Cumming, Near-vertical-incidence seismic reflections from the 'Conrad' discontinuity, J. Geophys. Res., 70, 3441-3446, 1965.

Kosminskaya, I. P., and N. K. Kapustian, The wave field associated with a fine structured Moho in continents and oceans, J. Geophys., 45, 159-170, 1979.

Lee, W. B., and S. C. Solomon, Inversion schemes for surface wave attenuation and Q in the crust and the mantle, Geophys. J. R. Astr. Soc., 43, 47-71, 1975.

Lynn, H. G., Migration and interpretation of deep crustal seismic reflection data, Ph.D., Thesis, Stanford University, Stanford, California, 159p., 1979.

Lynn, H. B., L. D. Hale, and G. A. Thompson, Seismic reflections from the basal contacts of batholiths, J. Geophys. Res., 86, 10,644-10,638, 1981.

McDonal, F. J., F. A. Angona, R. L. Mills, R. L. Sengbush, R. G. Van Nostrand, and

J. E. White, Attenuation of shear and compressional waves in Pierre shale, Geophysics, 23, 421-439, 1958.

Meissner, R., The 'Moho' as a transition zone, Geophysical Surveys, 1, 195-216, 1973.

Meissner, R. O., and E. R. Fluh, Probable relations between seismic anisotropy and a fine structure of the lithosphere, J. Geophys. 45, 349-352, 1979.

Mitchell, B. J., Radiation and attenuation of Rayleigh waves from the southeastern Missouri earthquake of October 21, 1965, J. Geophys. Res., 78, 886-899., 1973.

Mitchell, B. J., Regional Rayleigh wave attenuation in North America, J. Geophys. Res., 80, 4904-4916, 1975.

Mitchell, B. J., Frequency dependence of shear wave internal friction in the continental crust of eastern North America, J. Geophys. Res., 85, 5212-5218, 1980.

Morlet, J., G. Arens, E. Fourgeau, and D. Giand, Wave propagation and sampling theory-Part I: Complex signal and scattering in multilayered media, Geophysics, 47, 203-221, 1982.

Narans, H. D., J. W. Berg, and K. L. Cook, Sub-basement seismic reflections in Northern Utah, J. Geophys. Res., 600-603, 1961.

O'Brien, P. N. S., A note on normal incidence reflections from the Mohorovicic discontinuity, Geophys. J. R. Astr. Soc., 9, 541-545, 1965.

Oliver, J., Tracing surface features to great depths: A powerful means for exploring the deep crust, Tectonophysics, 81, 257-272, 1982.

Oliver, J., F. Cook, and L. Brown, COCORP and the continental crust, J. Geophys. Res., 88, 3329-3347, 1983.

Pavlenkova, N. I., and T. V. Smelyanskaya, The nature of the group of reflected seismic waves from the base of the earth's crust, Izv., Earth Physics, 1, 17-27, 1970.

Reif, D. M., and J. P. Robinson, Geophysical, geochemical, and petrographic data and regional correlation from the Arizona state A-1 well, Pinal county, Arizona, Ariz. Geol. Soc., Digest, 13, 99-109, 1981.

Rezanov, I. A., and N. Y. Galdin, Geological significance of anisotropy of seismic velocities in earths crust, Internat. Geology Rev., 9, 1424-1429, 1967.

Robertson, G., Intrabasement reflections in southwestern Alberta, Geophysics, 28, 910-915, 1963.

Schilt, S., J. Oliver, L. Brown, S. Kaufman, D. Albaugh, J. Brewer, F. Cook, L. Jensen, P. Krumhansl, G. Long, and D. Steiner, The heterogeneity of the continental crust: Results from deep crustal seismic reflection profiling using the Vibroseis program, Rev. Geophys. Space Physics, 17, 354-368, 1979.

Smithson, S. B. and R. J. Ebens, Interpretation of data from a 3.05-kilometer borehole in Precambrian crystalline rocks, Wind River mountains, Wyoming, J. Geophys. Res., 76, 7079-7087, 1971.

Smithson, S. B., J. A. Brewer, S. Kaufman, J. E. Oliver, and C. A. Hurich, Structure of the Laramide Wind River uplift, Wyoming, from COCORP deep reflection data and from gravity data, J. Geophys. Res., 84, 5955-5972, 1979.

Tittmann, B. R., Internal friction measurements and their implications in seismic Q structure models of the crust, A. G. U. Geophysical Monograph 20, 197-214, 1977.

Wallace, M., Deep basement reflections in Wind River line 1, Geophys. Res. Lett., 7, 729-732, 1980.

Widess, M. B., and G. L. Taylor, Seismic reflections from layering within the Precambrian basement complex, Oklahoma, Geophysics, 17, 417-425, 1959.

Windley, B. F., F. C. Bishop, and J. V. Smith, Metamorphosed layered igneous complexes in Archean granulite-gneiss belts, Ann. Rev. Earth Planet. Sci., 9, 175-198, 1981.

Winkler, K. W., and A. Nur, Seismic attenuation: Effects of pore fluids and frictional sliding, Geophysics, 47, 1-15, 1982.

Zawislak, R. L., and S. B. Smithson, Problems and interpretation of COCORP deep seismic reflection data, Wind River range, Wyoming, Geophysics, 46, 1684-1701, 1981.

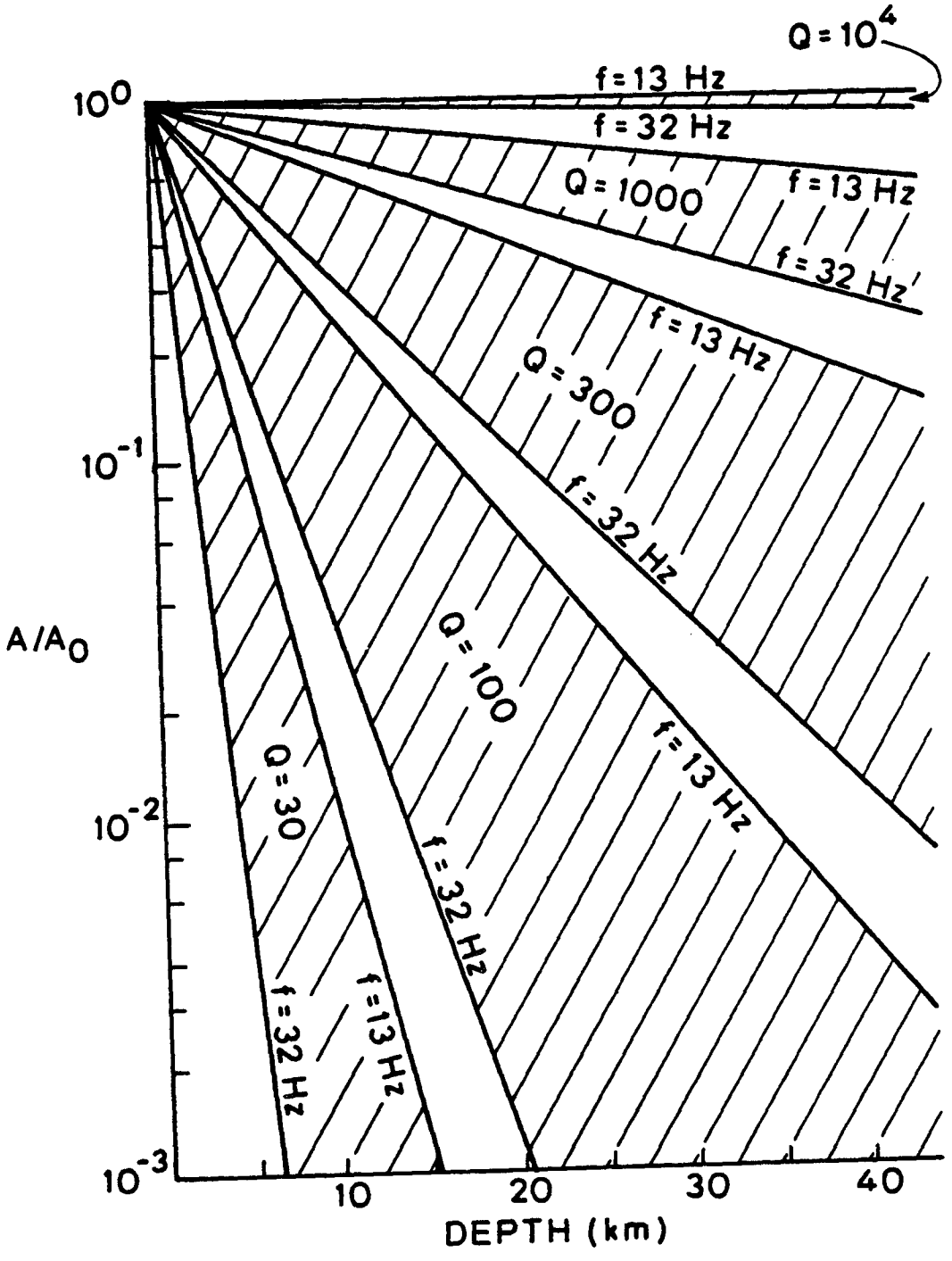

Figure 1. Normalized amplitude from a reflection off a step discontinuity plotted as a function of depth to the discontinuity for a range of Q values and frequencies of 13 Hz and 32 Hz.

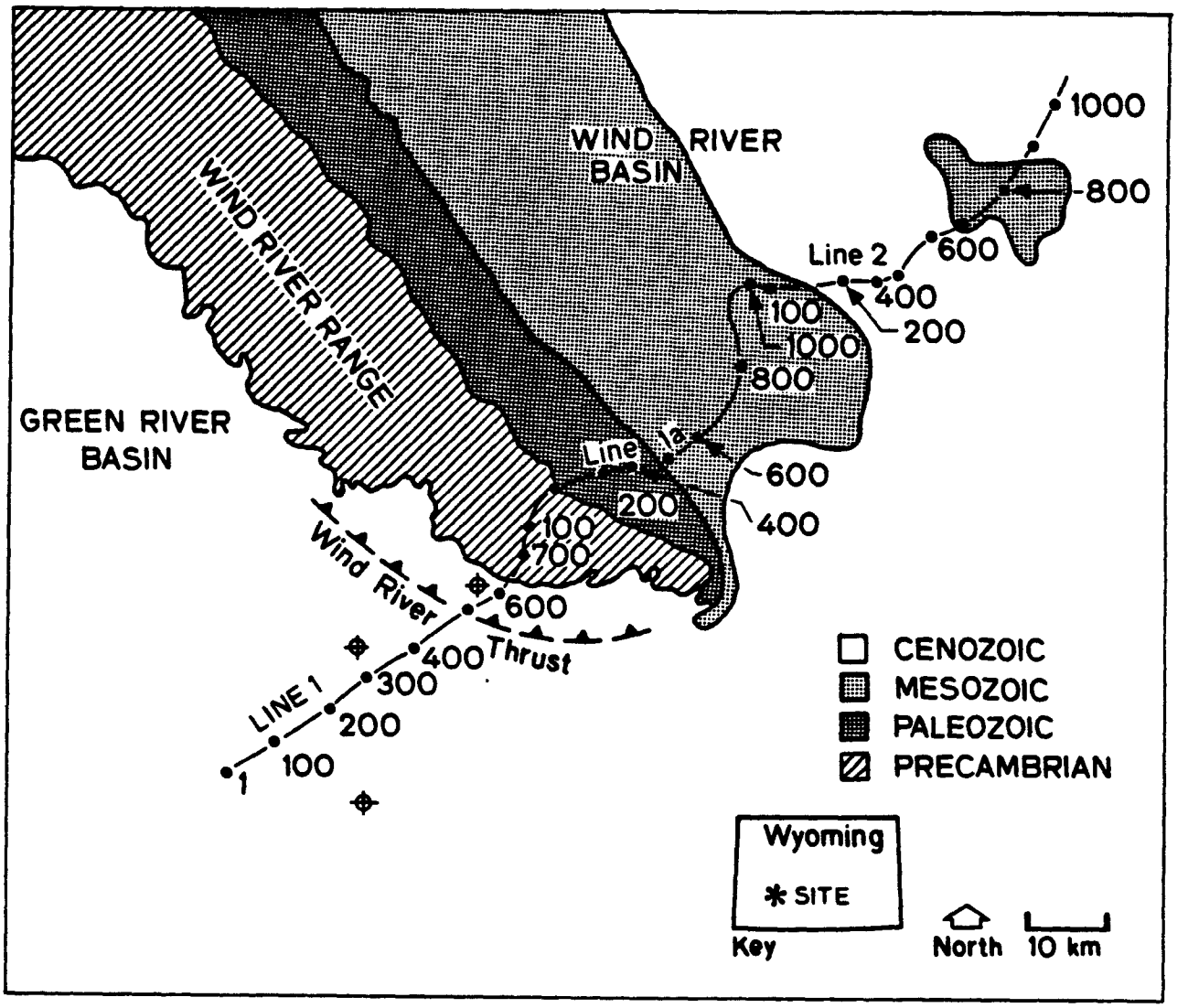

Figure 2. Generalized geologic map of the southern Wind River Range, Wyoming, showing the location of the COCORP lines 1, 1a, and 2. Also shown are the locations of nearby exploratory holes which provided sonic logs.

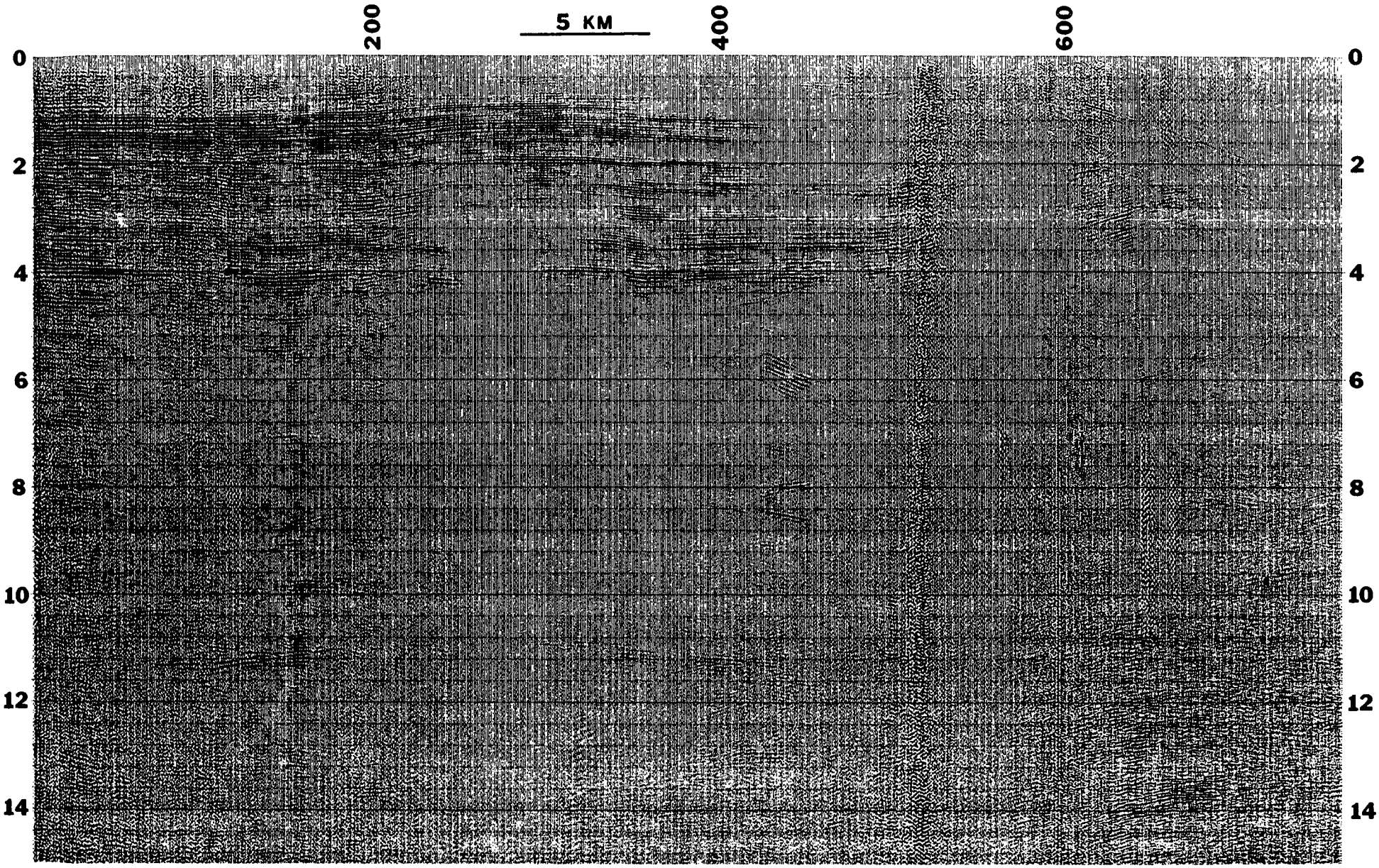

Figure 3. True amplitude time section for Wind River line 1. Vertical scale is two way travel time in seconds. The gain used on this data is shown in Figure 6.

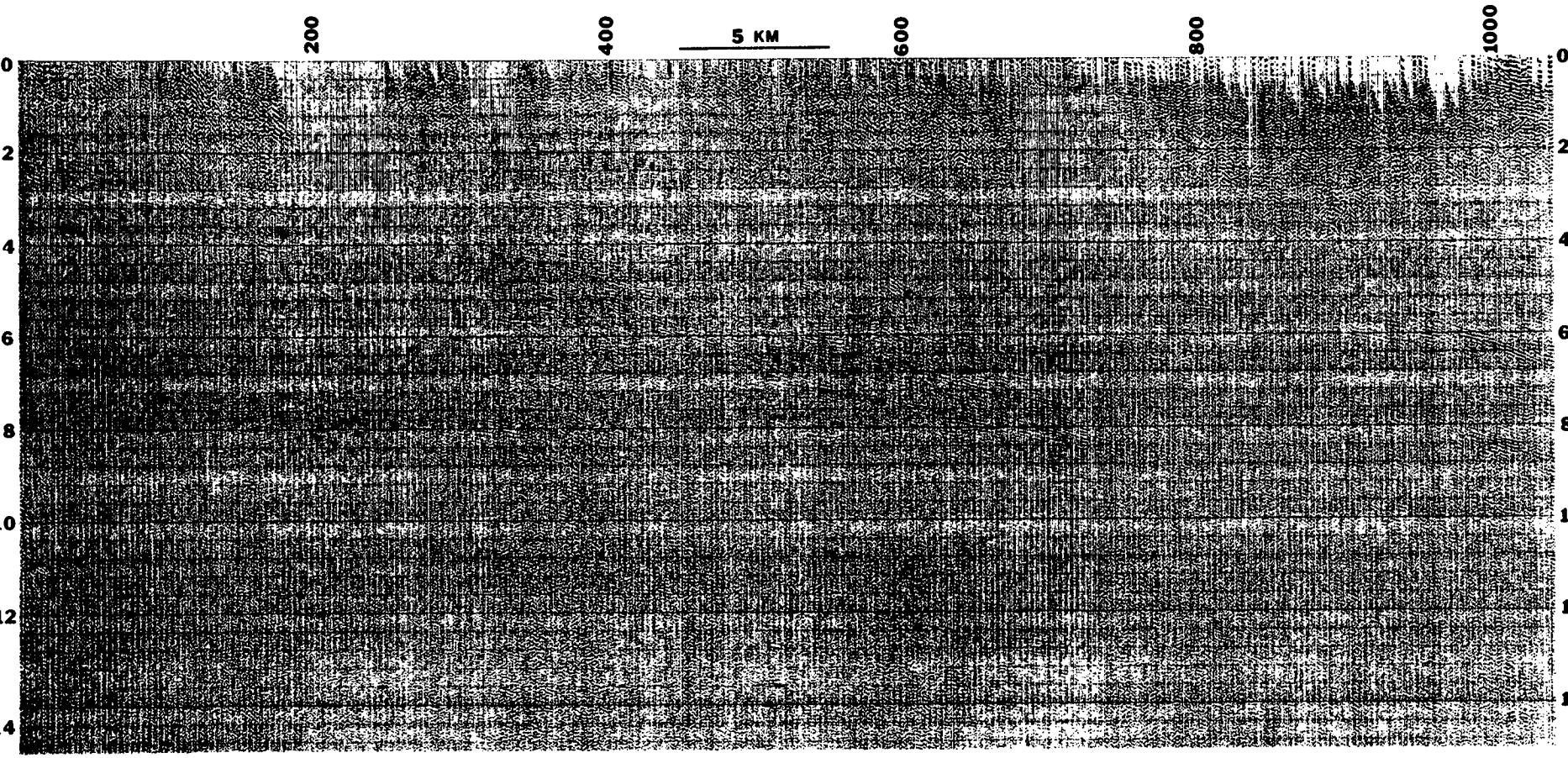

Figure 4. True amplitude time section for Wind River line 1a. Vertical scale is two way travel time in seconds. The gain used on this data is shown in Figure 6.

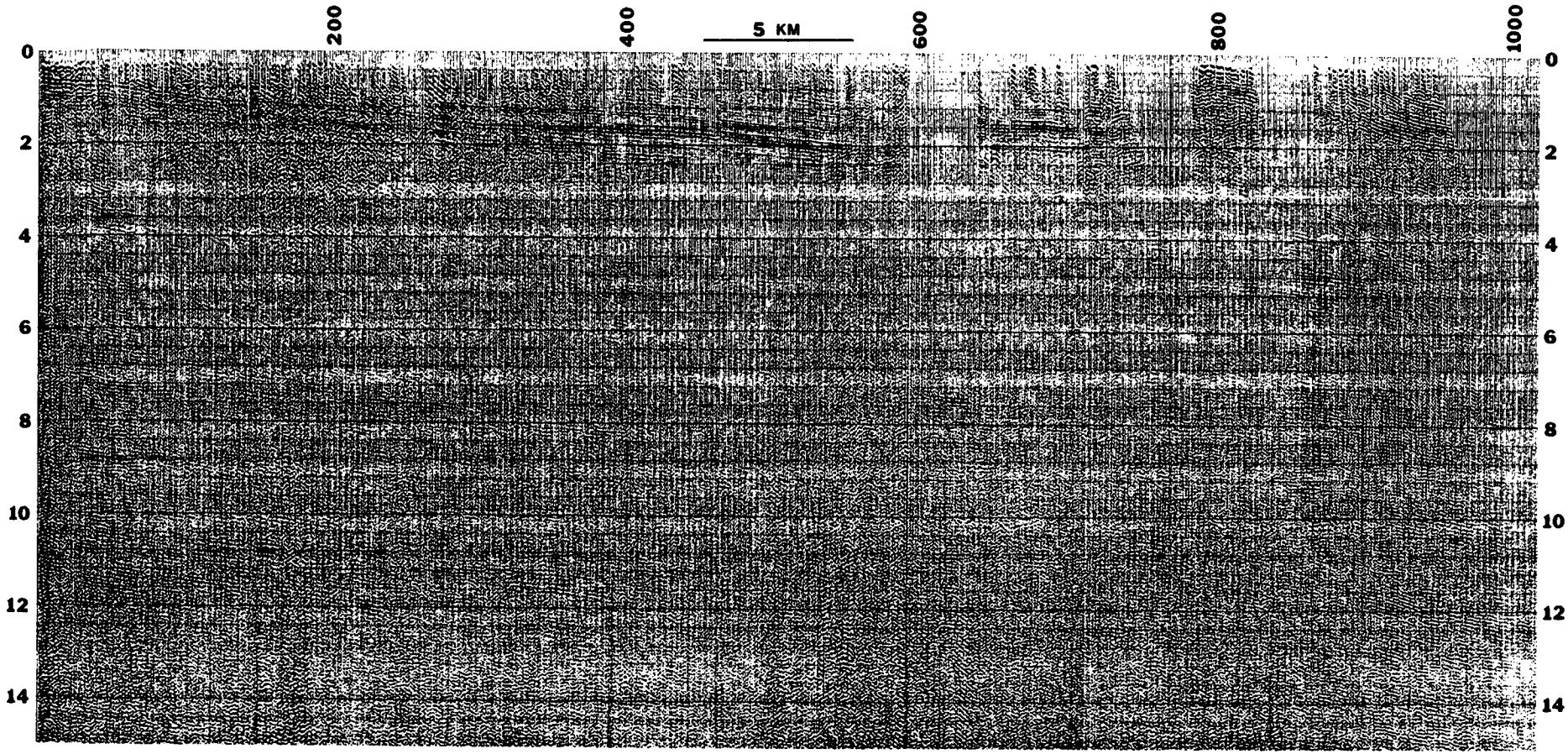

Figure 5. True amplitude time section for Wind River line 2. Vertical scale is two way travel time in seconds. The gain used on this data is shown in Figure 6.

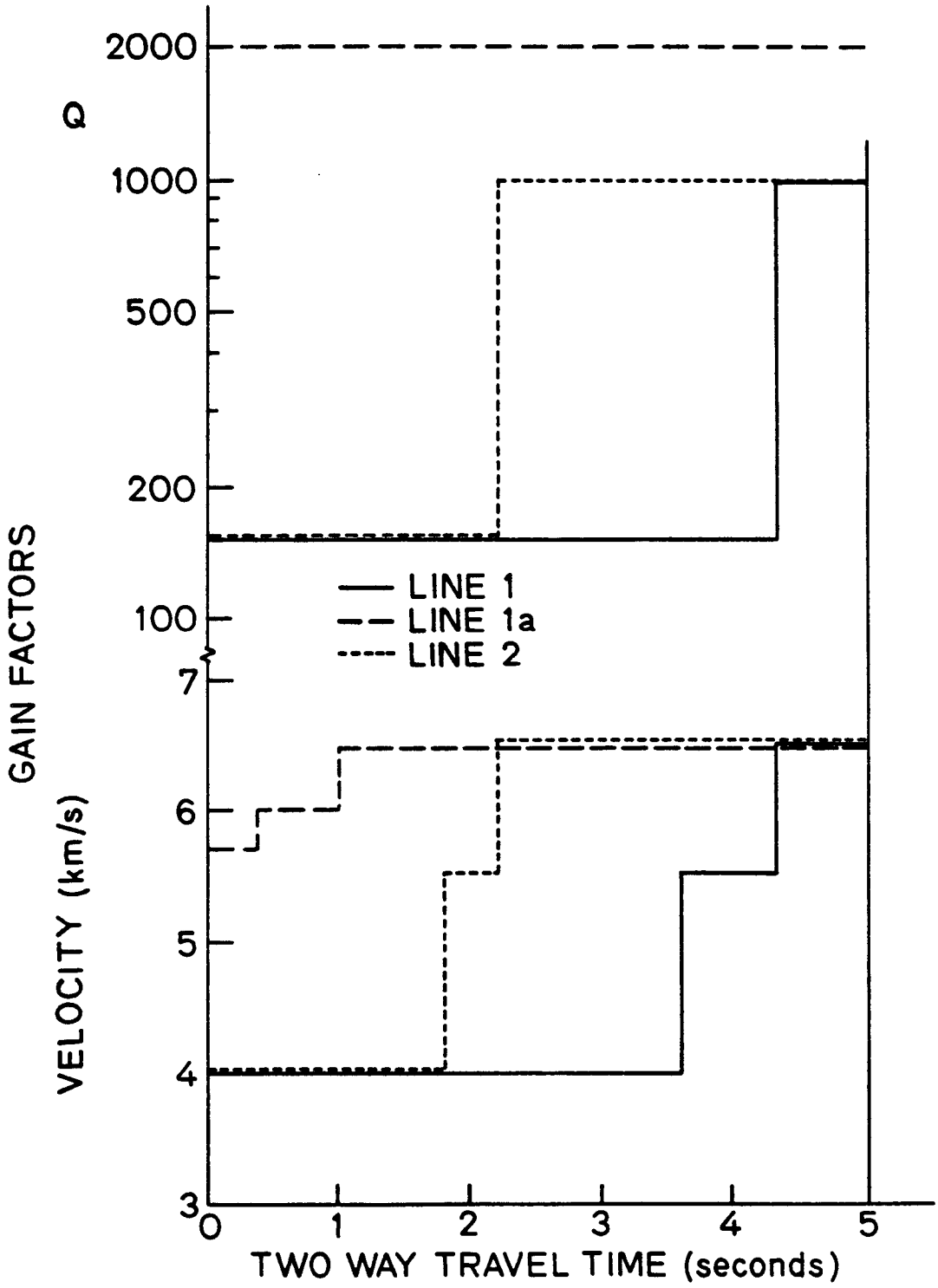

Figure 6. Velocity and attenuation functions of depth which were used to gain the data in Figures 3, 4, and 5.

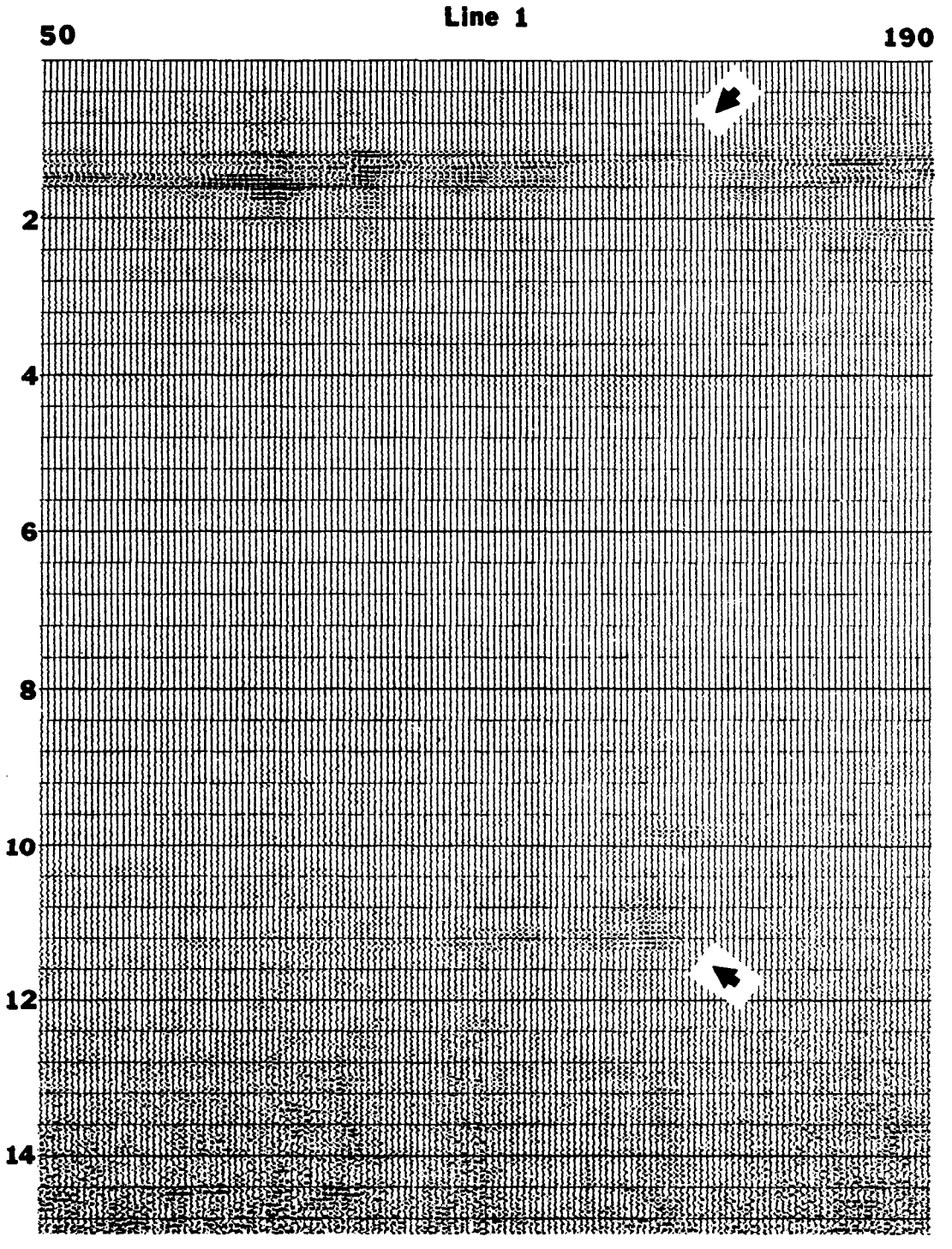

Figure 7. Detail from true amplitude display of line 1, stations 50 to 190. The strong event at 11 seconds (bottom arrow) is directly below a section of anomalously weak events in the overlying sedimentary section (top arrow).

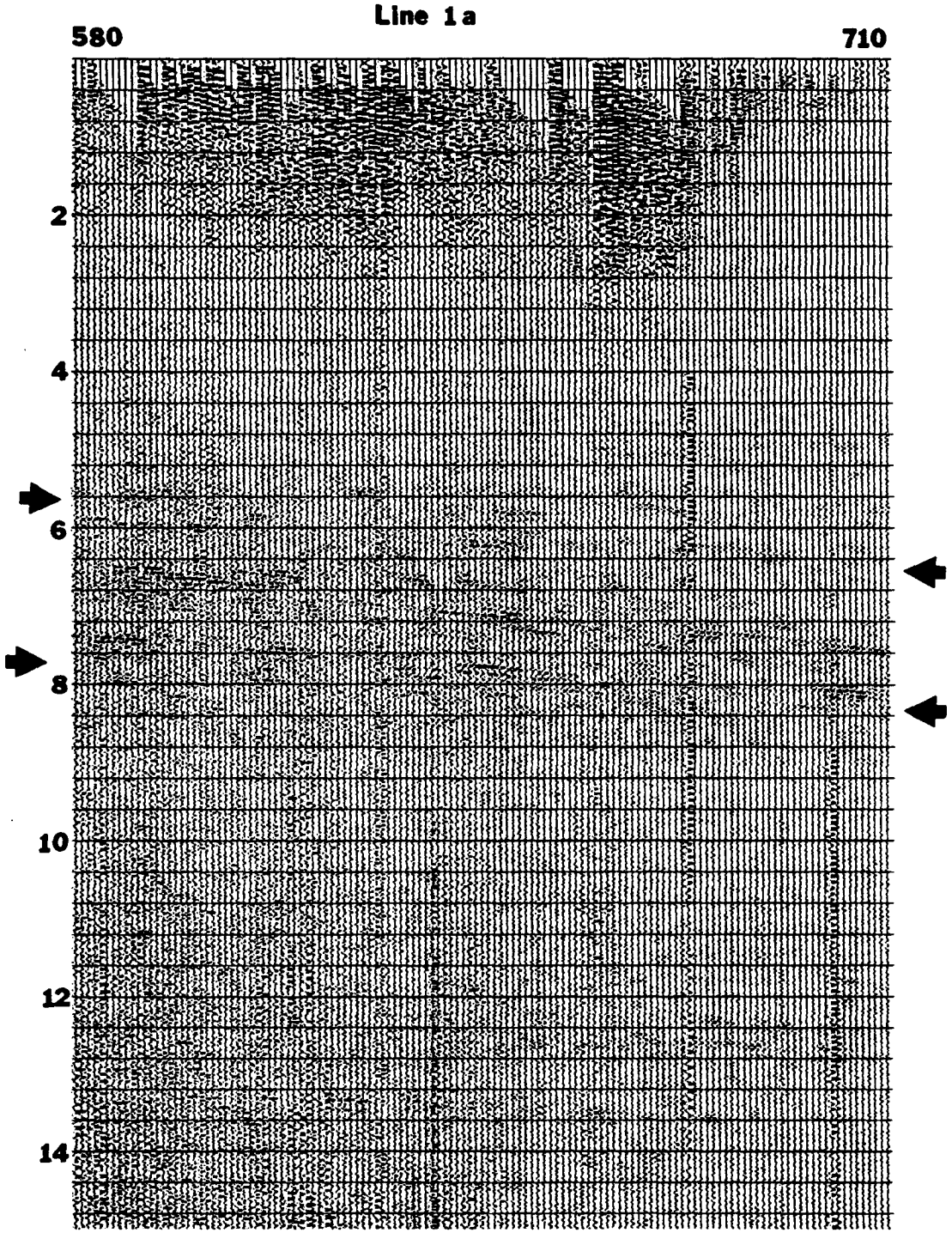

Figure 8. Detail from true amplitude display of line 1a, stations 580 to 710. The Wind River thrust is prominent from 6 to 8 seconds. There is some reflected energy at 12 to 14 seconds as well. Only a thin layer of Mesozoic and Paleozoic sediments cover the crystalline basement here.

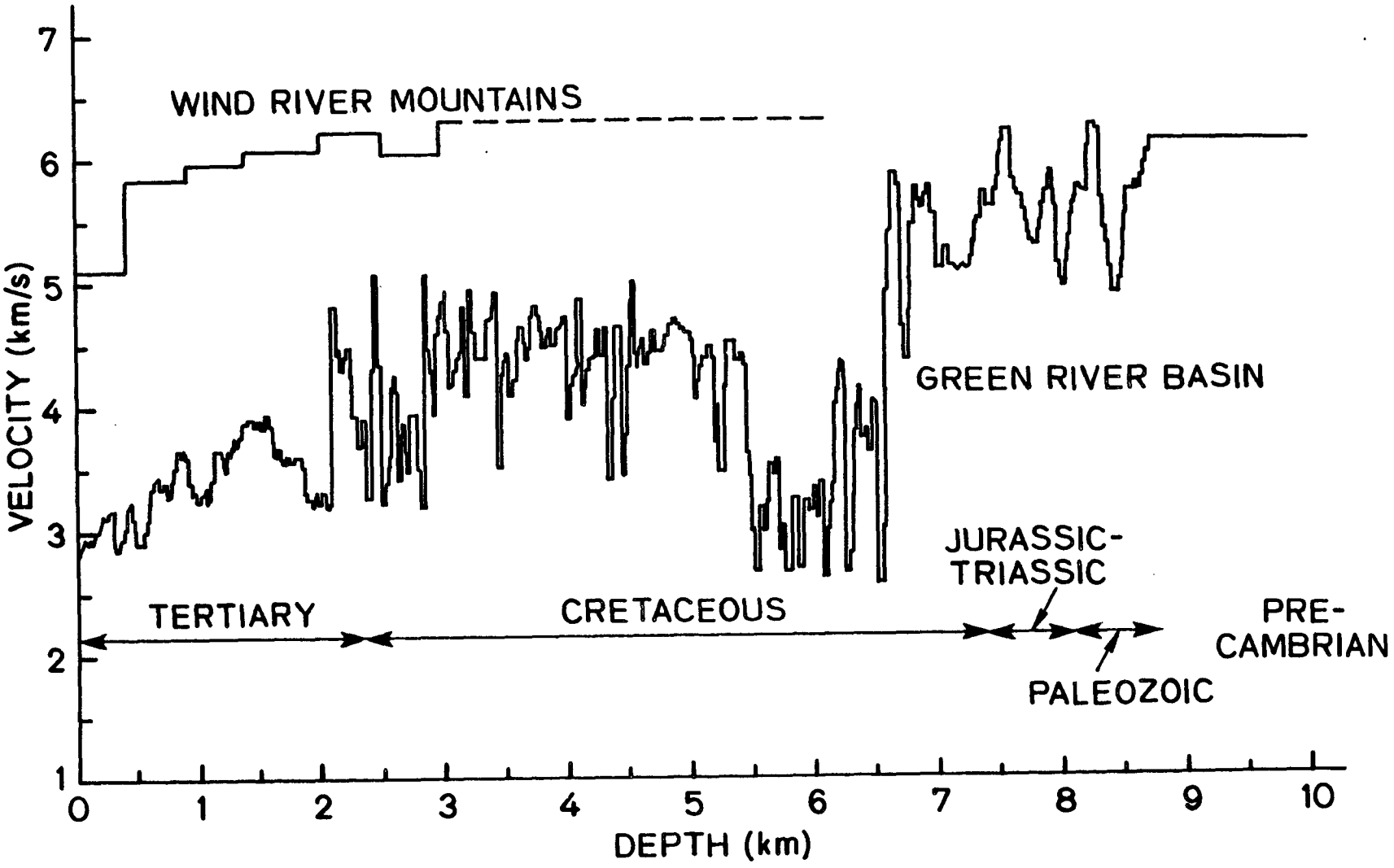

Figure 9. Velocity profiles for the Green River basin and the Wind River mountains taken from sonic logs near the reflection line, as reported by Zawislak and Smithson (1981) and Smithson and Ebens (1971).

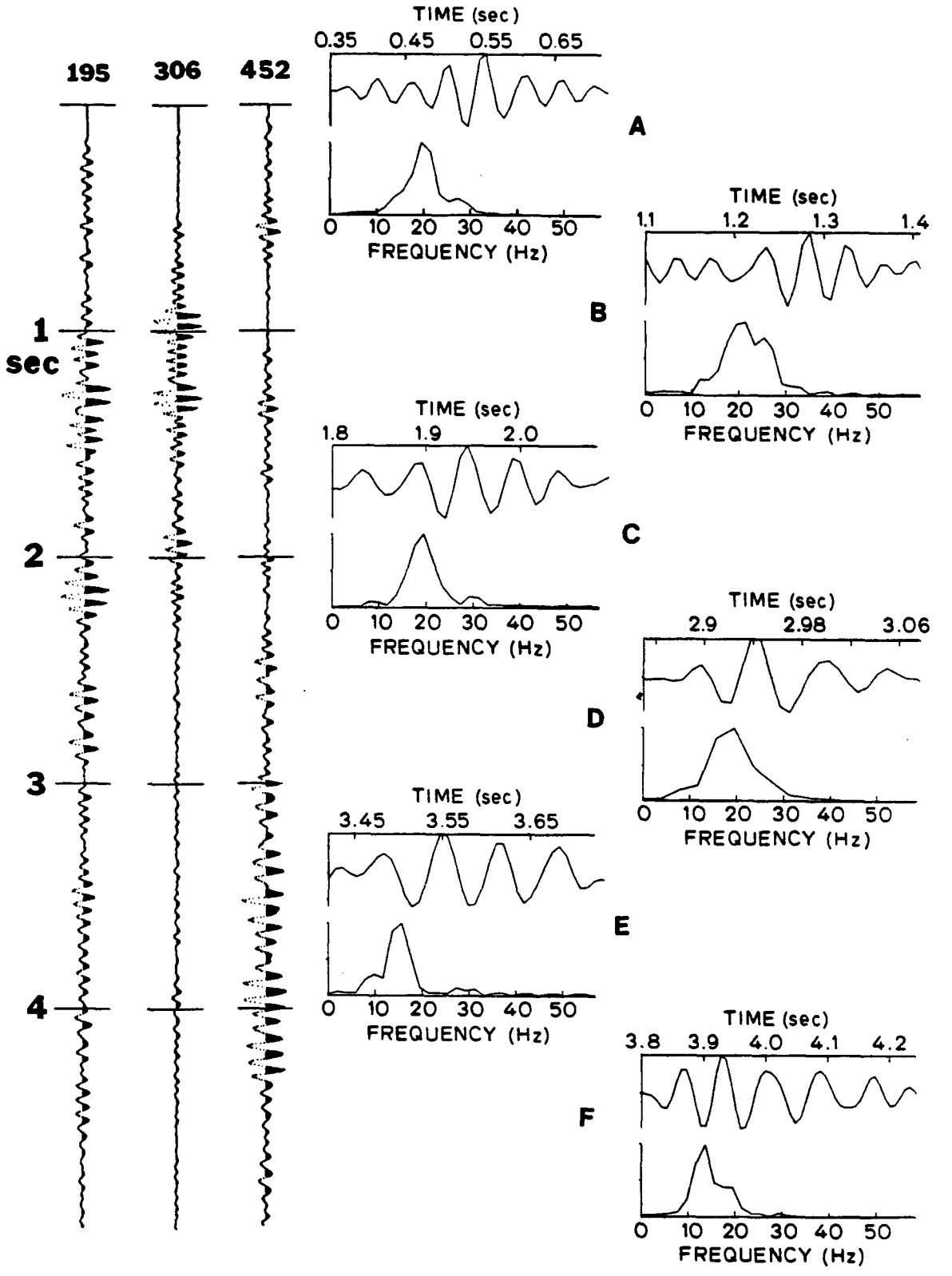

Figure 10. True amplitude data to 5 seconds for three representative traces (195, 306, 452) from line 1. Plots A through F show the detailed time section and amplitude spectrum from windowed reflections from these traces, and others, through the sedimentary sections.

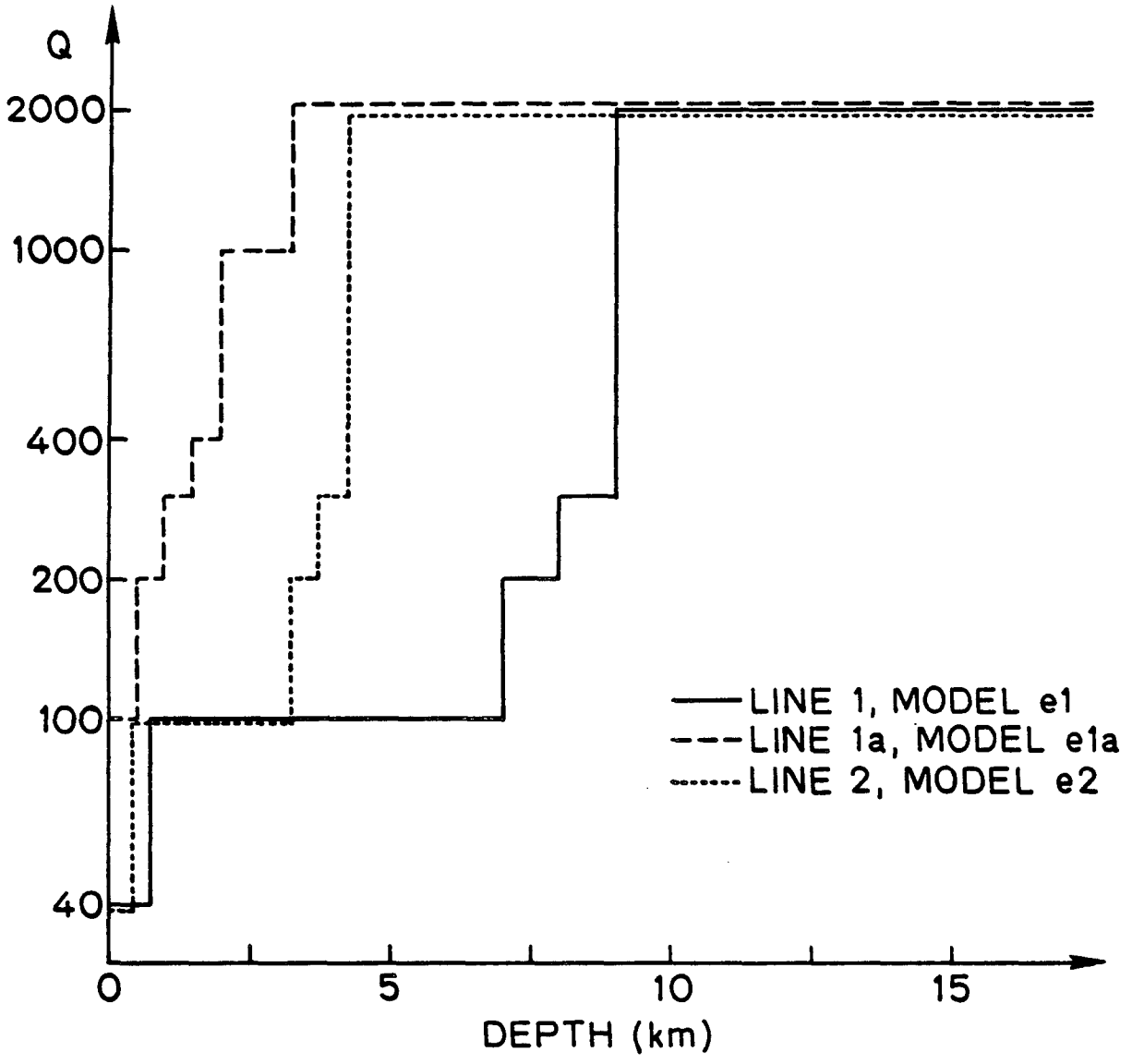

Figure 11. Q structures chosen for lines 1, 1a, and 2 based on modeling amplitude and frequency content of the data.

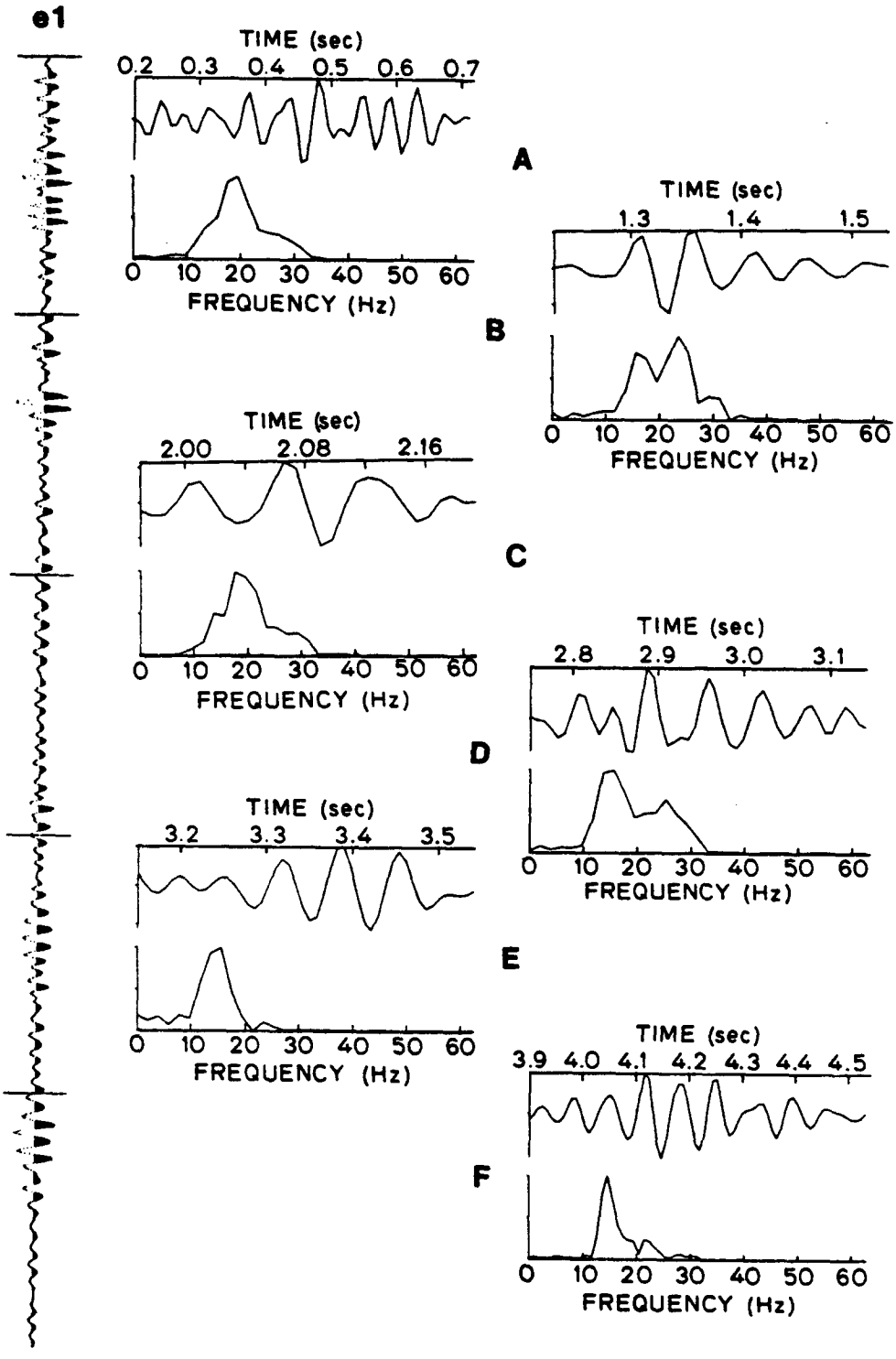

Figure 12. Synthetic data, including time section to 5 seconds and amplitude spectrum for various reflections. This figure uses Q model e1, which was chosen as the best fit to the data.

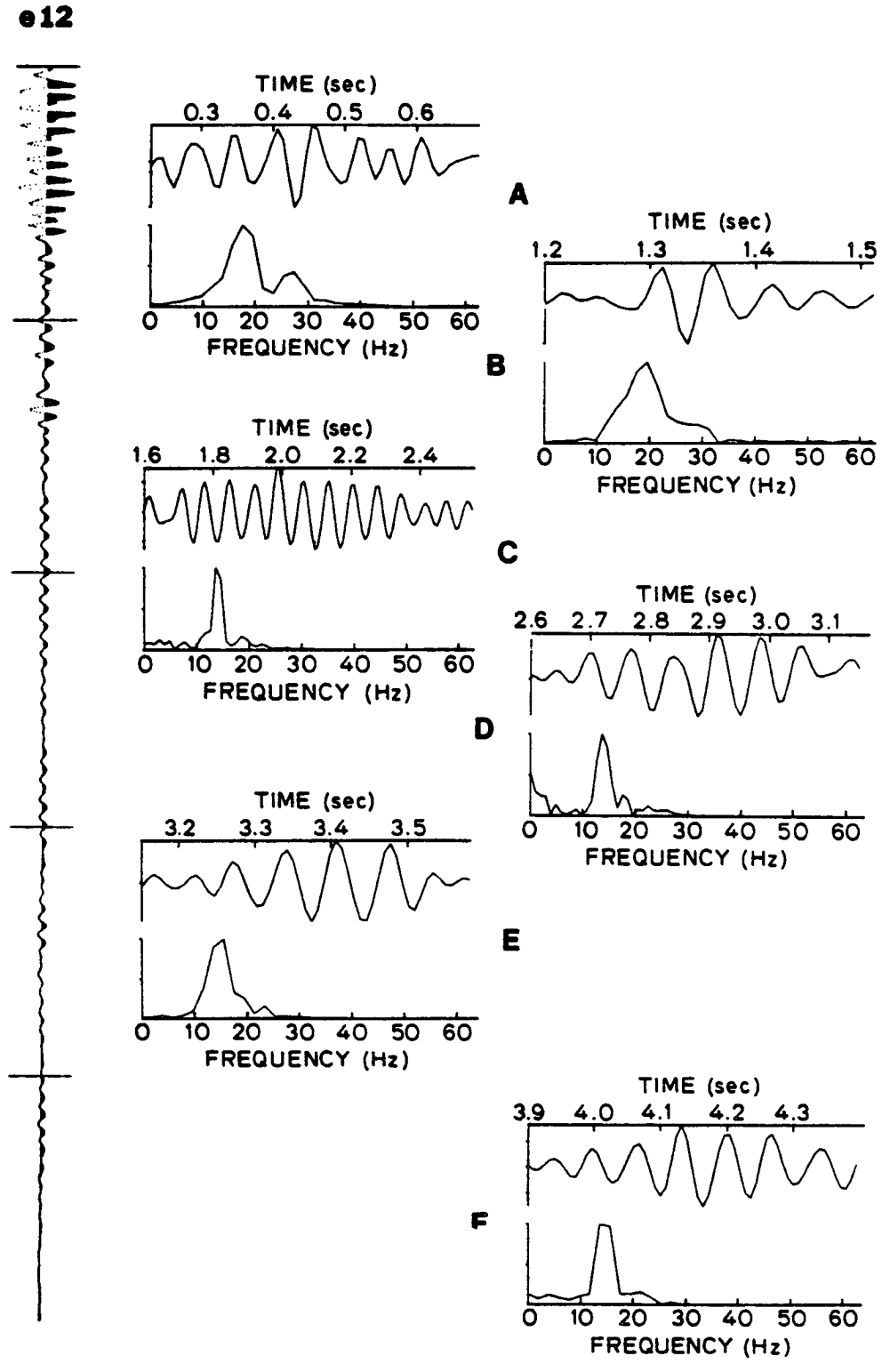

Figure 13. Synthetic data for Q model e12, using the same velocity structure but higher attenuation in the sedimentary section (Q=50). Frequency content of individual reflections is generally too low in this model to account for the data in Figure 10.

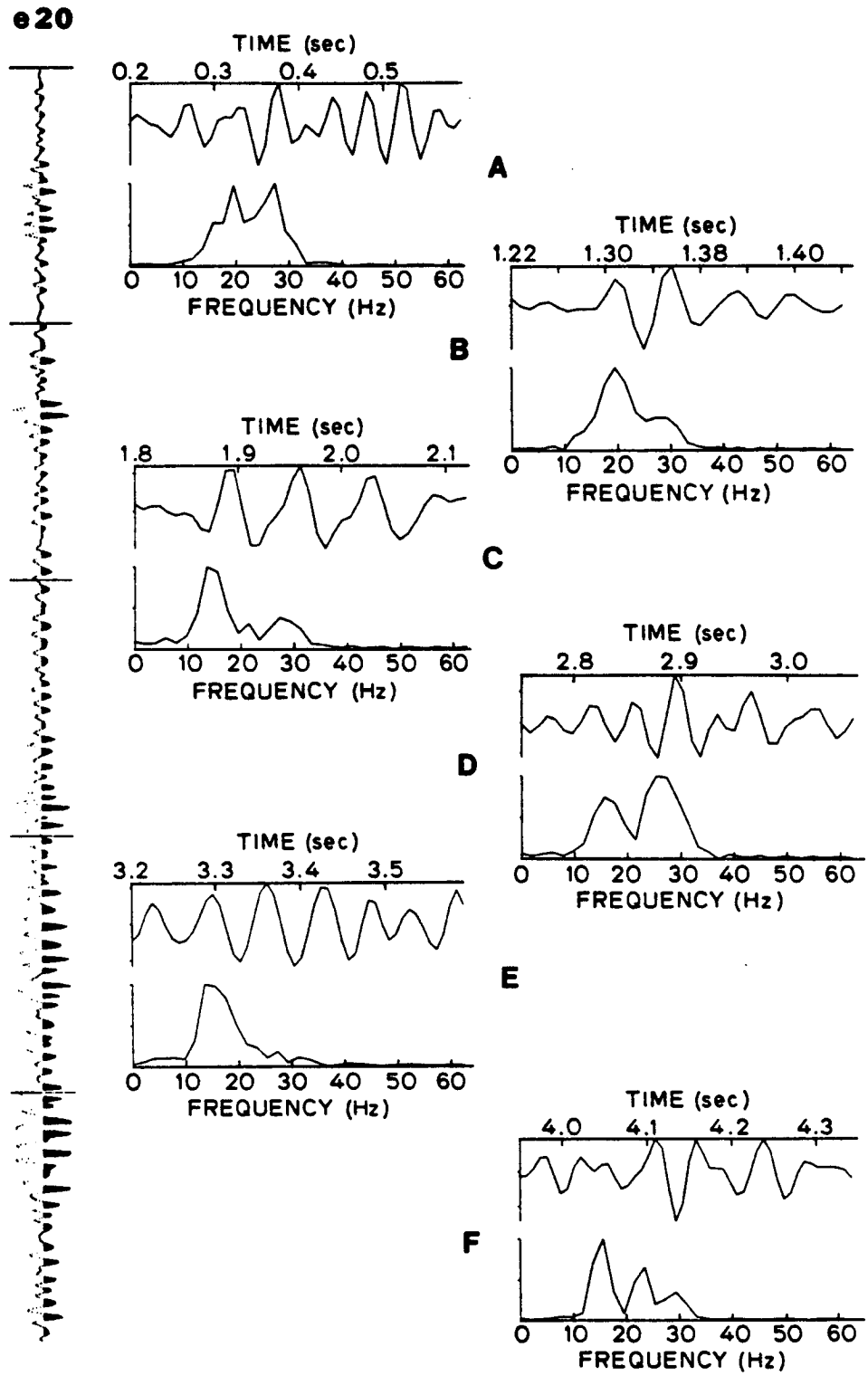

Figure 14. Synthetic data for Q model e2, using the same velocity structure but lower attenuation in the sedimentary section (Q=300). Frequencies of individual reflections are generally too high to account for the data in Figure 10.

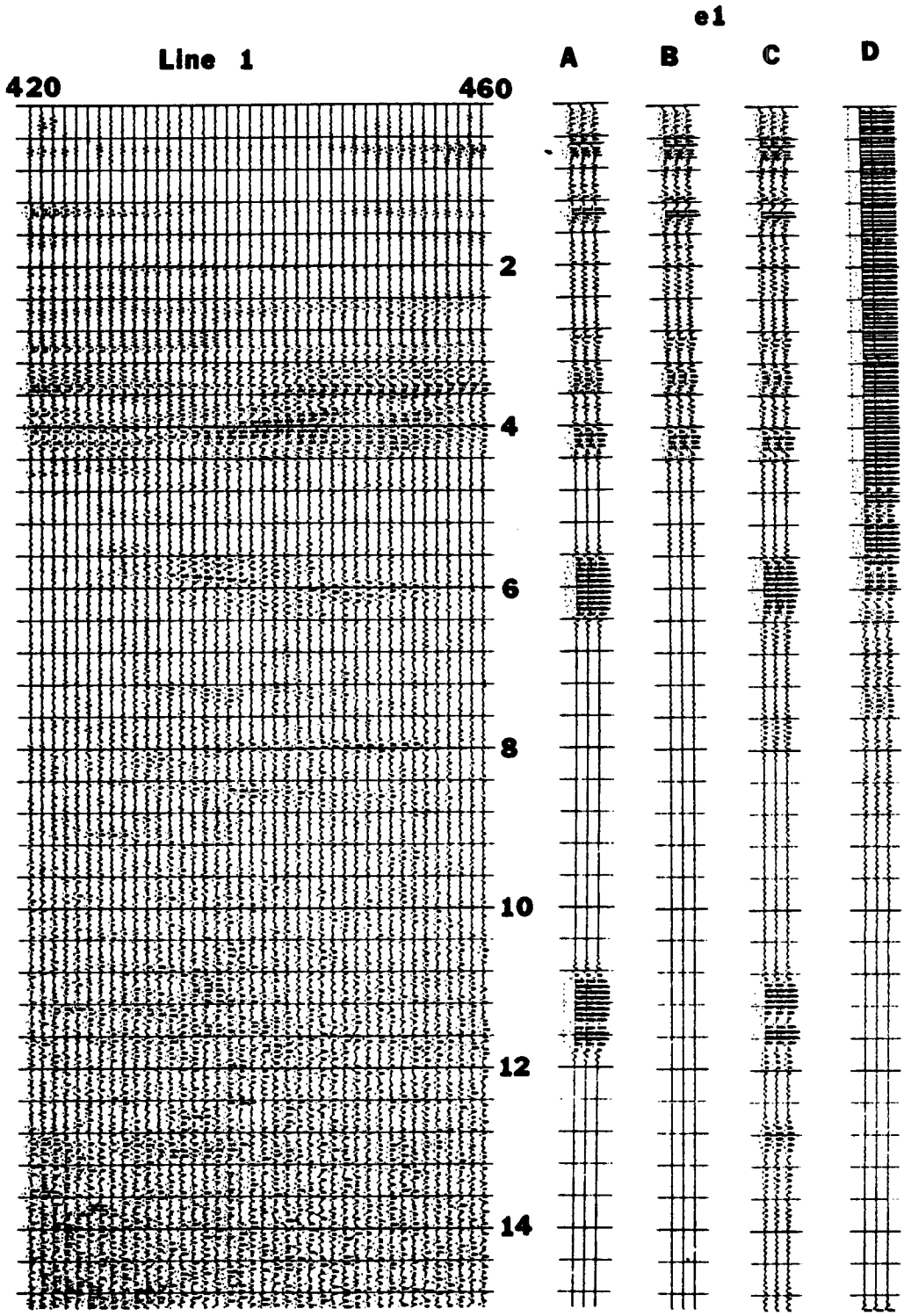

Figure 15. Detail portion of line 1, stations 420-460, true amplitude data. On the right are synthetic traces computed using the velocity profile given in Figure 9, the Q profile given in Figure 11, and gained using the same gain function as was used on the data. Three identical traces are plotted for each case to enhance comparison with the data. A: No multiples, basement reflections are from 15 layers 110 meters thick, each with a reflection coefficient of 0.05, and arranged as alternating zones of high and low velocity. B: No basement reflectors, multiples from the sedimentary section included. C: Basement reflectors and multiples for all events. D: Same as synthetic B but the entire trace has been multiplied by a factor of 10.

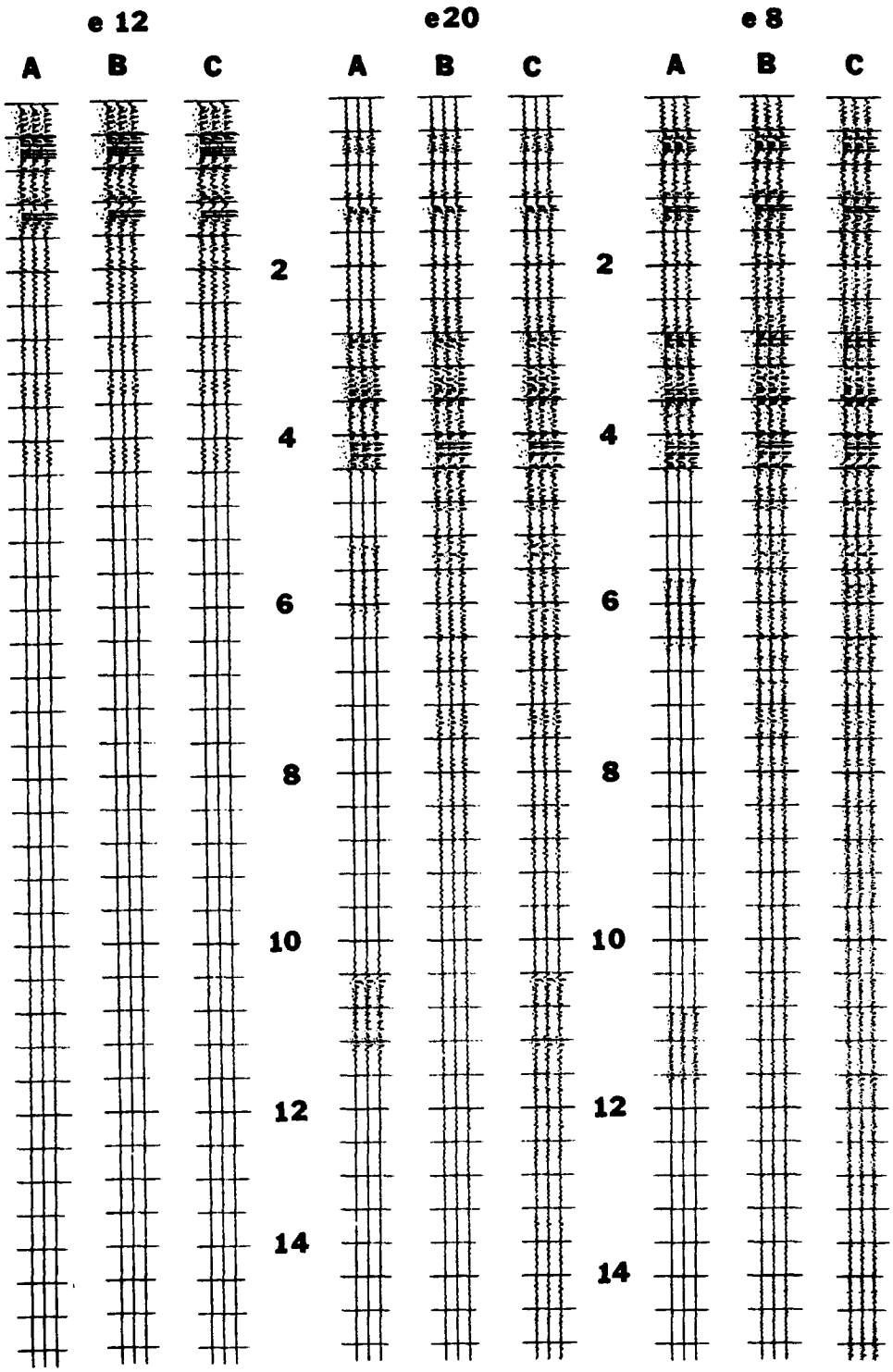

Figure 16. Synthetic traces for the same conditions as Figure 15 for Q model e12 (Q=50 in sedimentary section), and Q model e20 (Q=300 in sedimentary section), and Q model e8 (no attenuation).

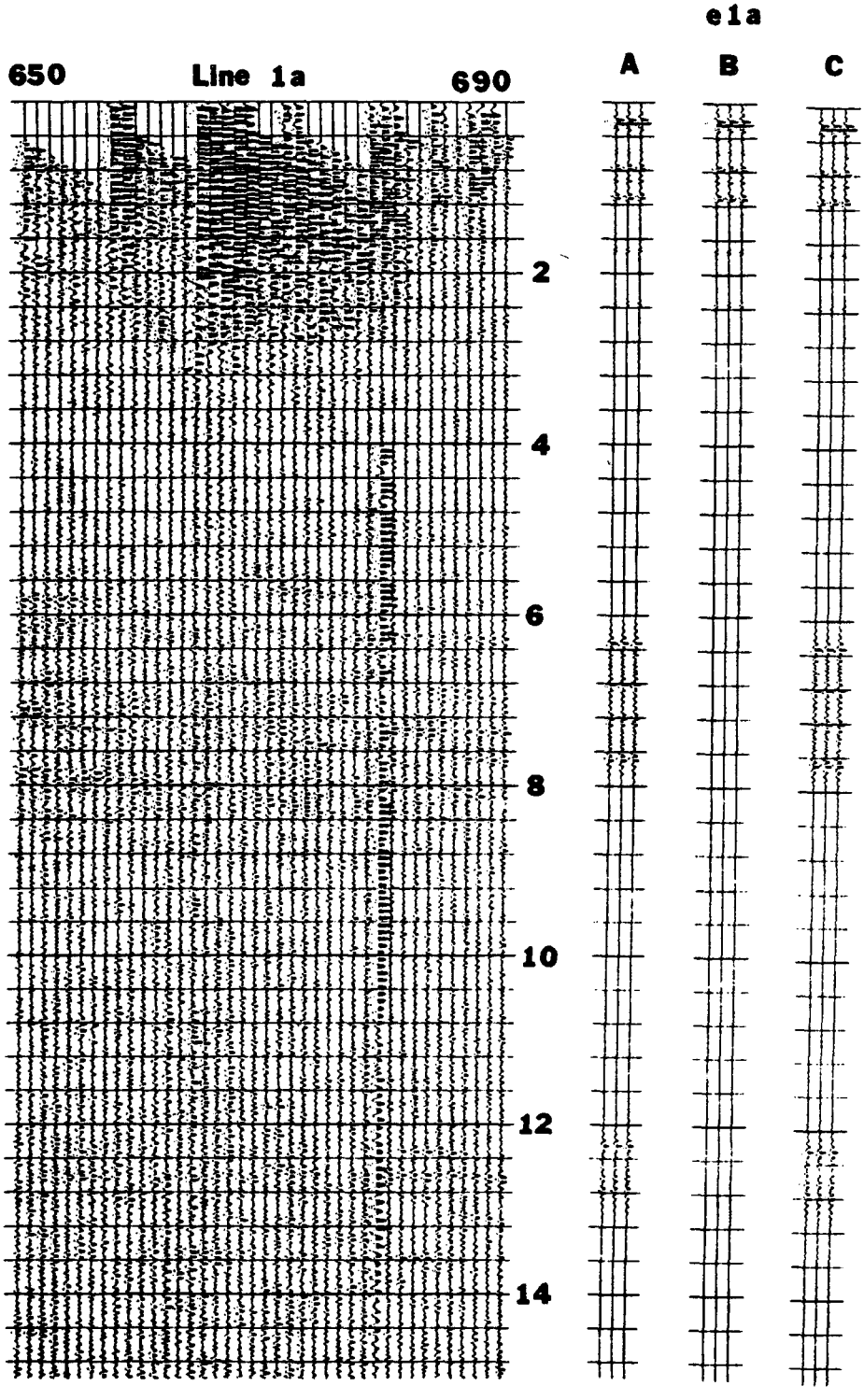

Figure 17. Detailed portion of line 1a, stations 650 to 690, true amplitude data. Synthetics generated for the same cases and in the same manner as in Figure 16, using Q model e1a.

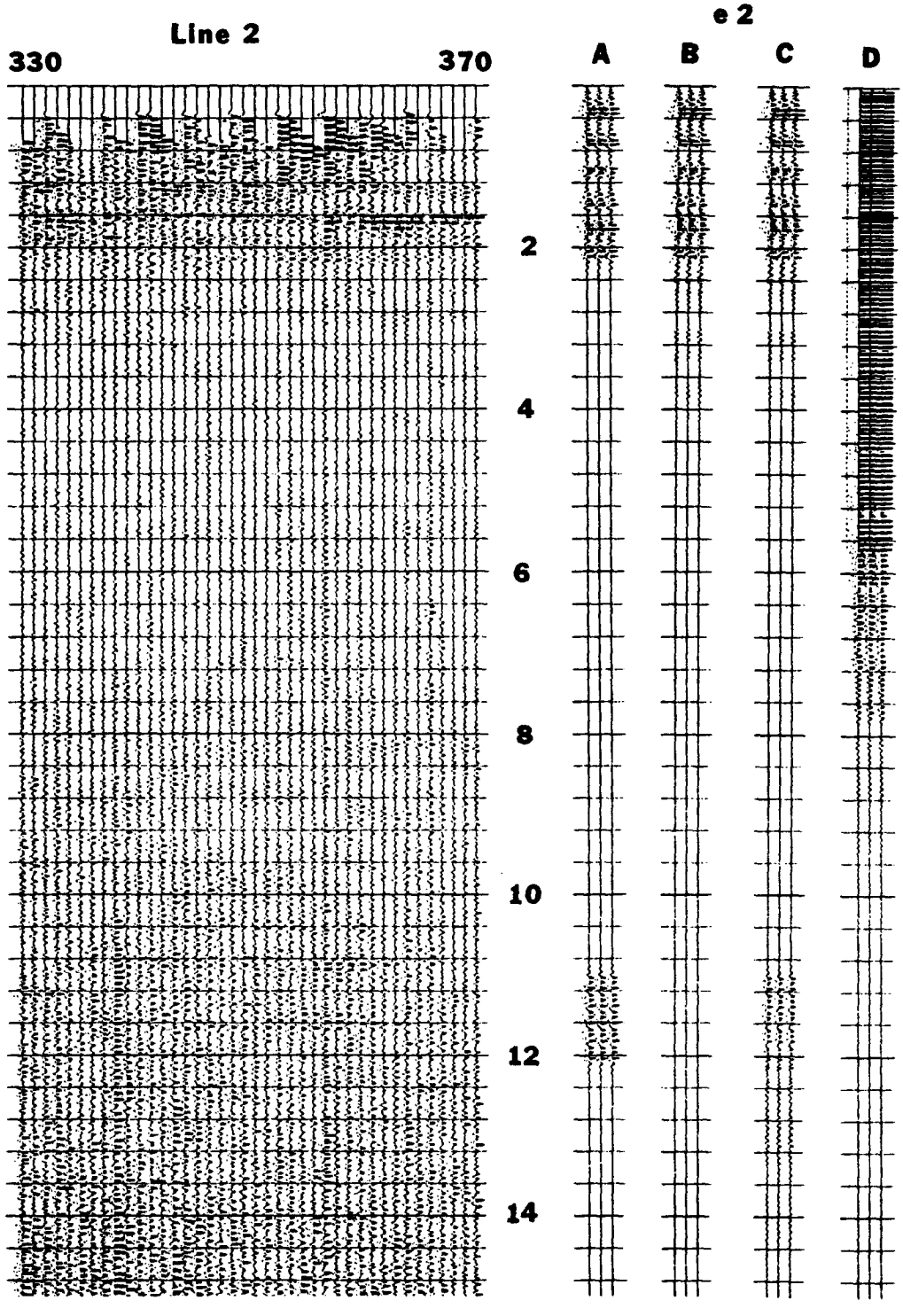

Figure 18. Detailed portion of line 2, stations 330-370, true amplitude data. Synthetics generated for the same cases and in the same manner as Figure 15, using Q model e2, and the same velocity structure as was used in line 1, but with half the thickness.

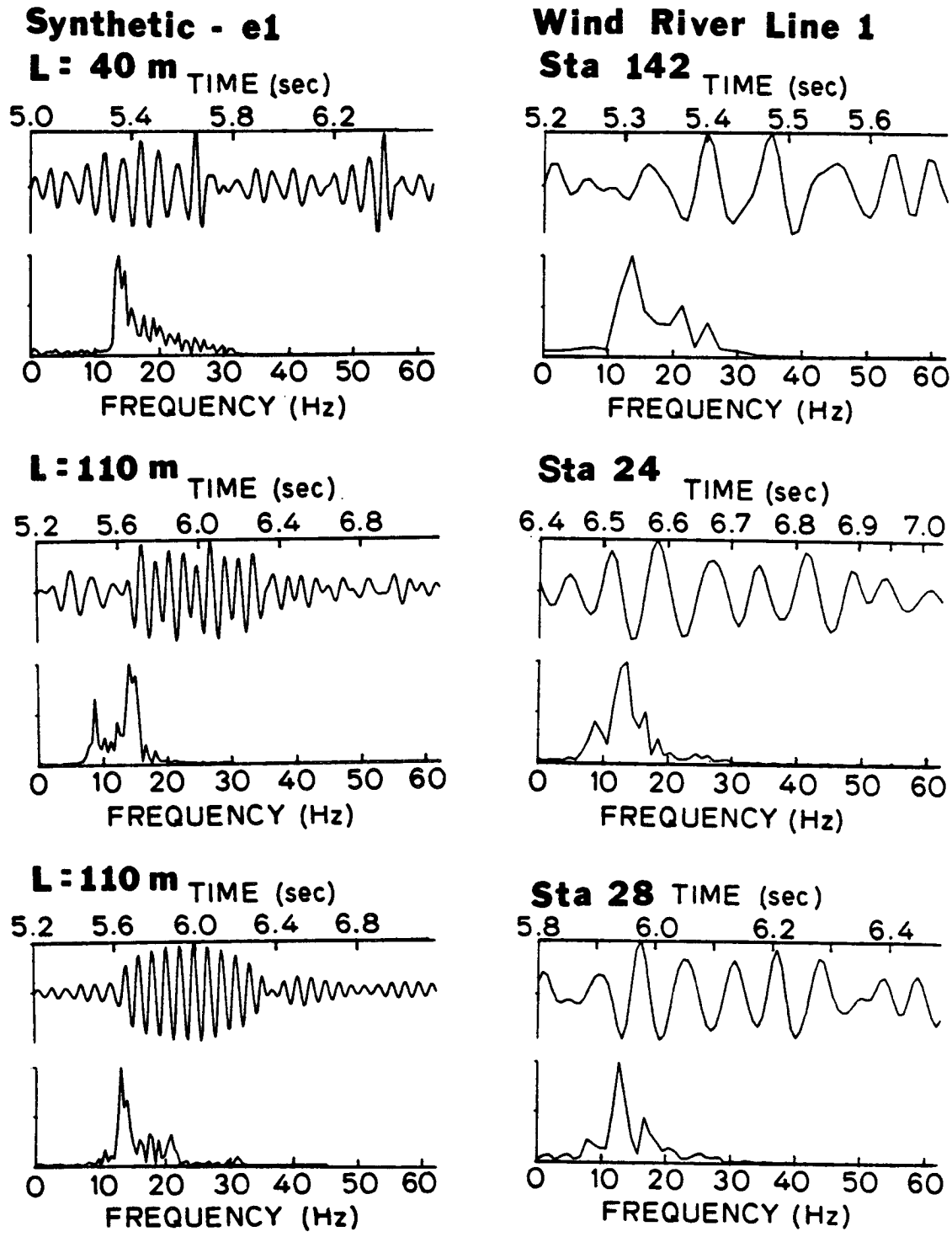

Figure 19. Time section and amplitude spectrum of some events from the Pacific Creek fault reflection in line 1. Also shown are the synthetic time section and amplitude spectrum for deep events using model e1, sedimentary velocity profile for line e1, and laminations of 40 to 150 meters in thickness, each with a reflection coefficient of 0.05

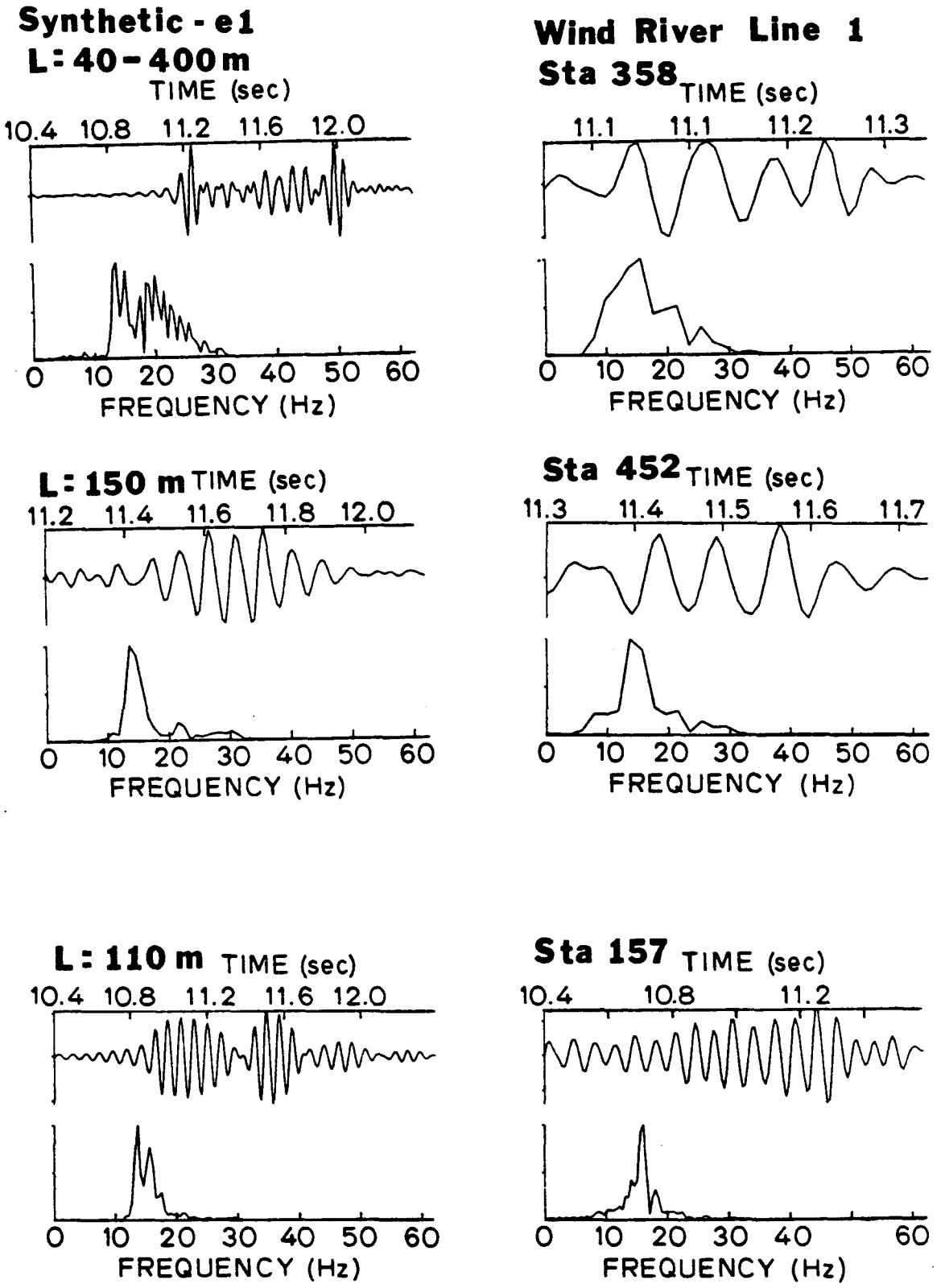

Figure 20. Time section and amplitude spectrum of some deep events in line 1. Also shown are the synthetic time section and amplitude spectrum for deep events using model e1, sedimentary velocity profile for line e1, and laminations of 40 to 400 meters in thickness, each with a reflection coefficient of 0.05

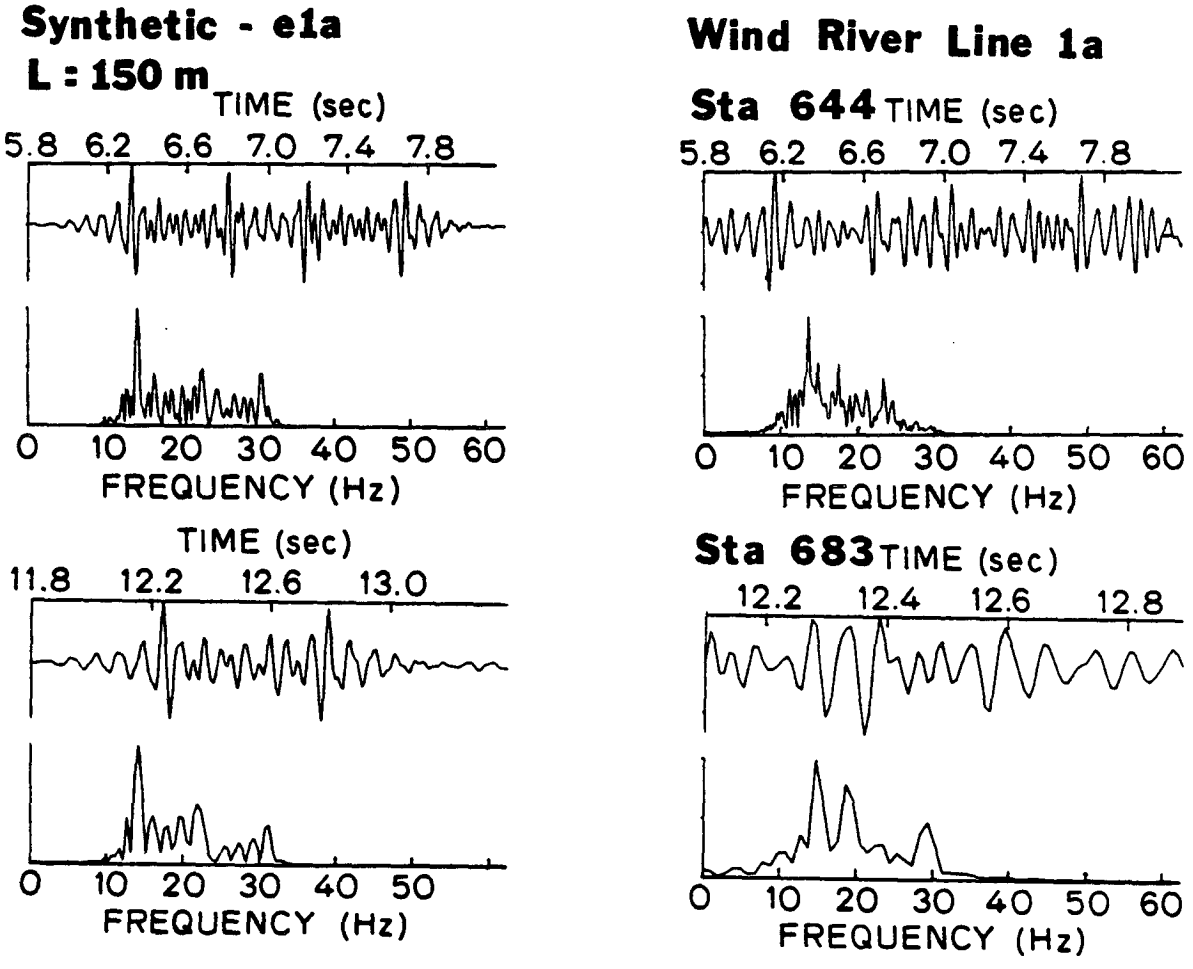

Figure 21. Time section and amplitude spectrum for some deep events in line 1a. Also shown are the synthetic time and amplitude spectrum generated using the appropriate velocity and Q structure, for laminations of from 150 to 300 meters, each with a reflection coefficient of 0.05

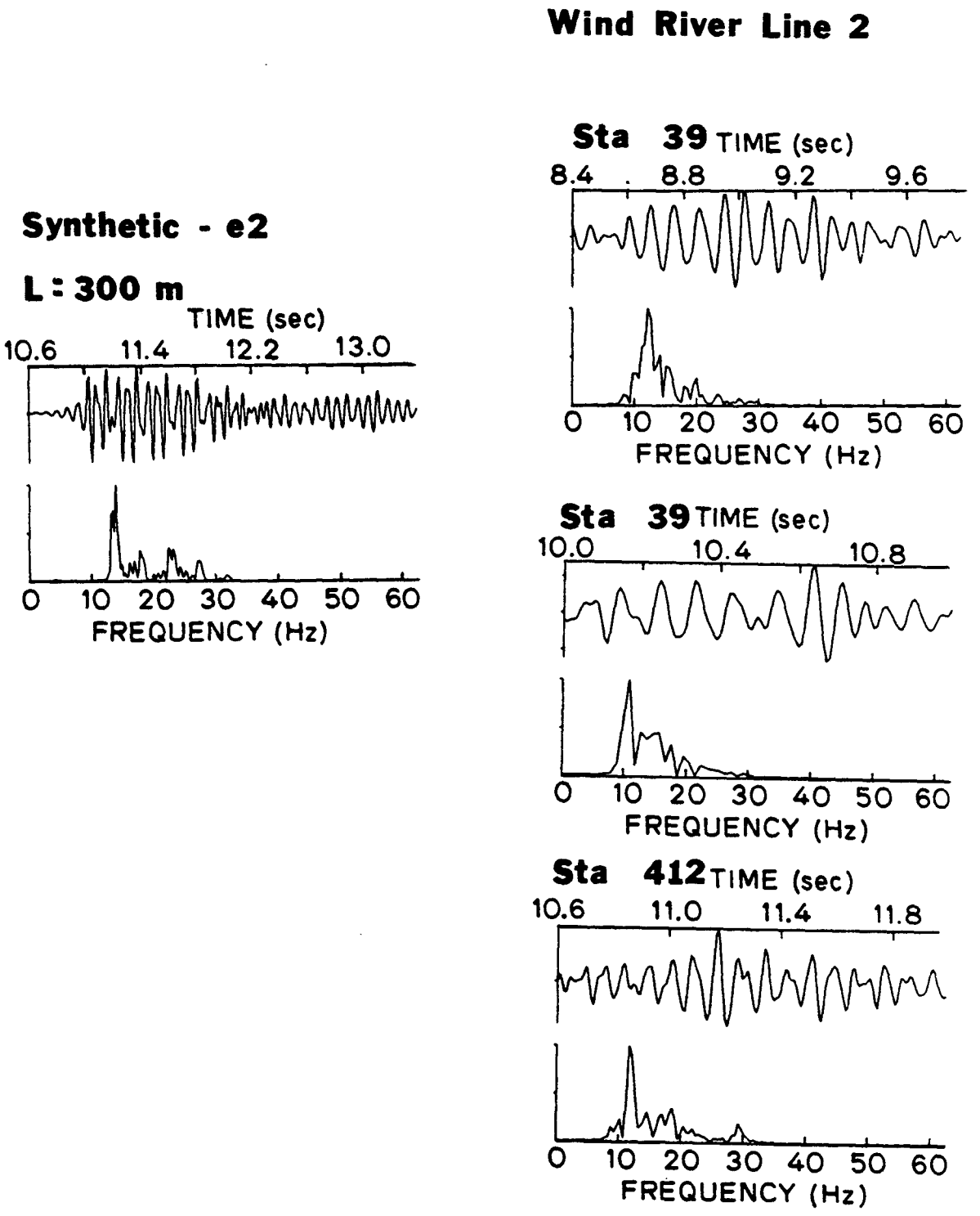

Figure 22. Time section and amplitude spectrum for some deep events in line 2. Also shown are the synthetic time and amplitude plots generated using the appropriate velocity and Q structure, for laminations of from 150 to 300 meters, each with a reflection coefficient of 0.05.

Chapter 4

THE SEISMIC SIGNATURE FROM CRUSTAL ZONES OF ELEVATED PORE PRESSURE

ABSTRACT

Models for the distribution of pore pressure in a permeable crust and empirical relationships of seismic velocity to depth of burial and pore pressure are combined to produce velocity profiles and synthetic seismic reflection traces for overpressured zones in sedimentary and crystalline rock. Pore pressure can significantly effect the existence and amplitude of reflected waves. However for models which ignore compaction, porosity reduction, or fluid sources at depth the effect is visible for geologically significant periods of time only for a permeability lower than that generally observed in laboratory measurements on crustal rocks. The effect of pore pressure on the amplitude of reflected waves may have decayed to a negligible amount while pore pressure is yet sufficiently high to significantly effect the strength of crustal rock units.

INTRODUCTION

The distribution and pressure of a free fluid phase in the earth's crust will be an important factor in the distribution of energy resources, the strength of crustal rocks, the velocity structure of the crust, and petrogenesis. In this paper we consider some models for permeability of crustal rocks, the distribution of pore pressure, and the effect of pore pressure on seismic velocity and reflection data.

Figure 1 shows a portion of the COCORP Wind River seismic reflection profile (see Jones, 1983 for a full discussion). The velocity structure of the Green River sedimentary basin which comprises the upper 4.3 seconds of this record is shown in Figure 2. This was compiled from sonic logs in the area (Zawislak and Smithson, 1982). The anomalously low velocity between 5.5 and 6.5 seconds is suggestive of a zone of high pore pressure. High pore pressure is commonly observed directly in sedimentary basins which have been drilled (Berry, 1973; Moore et. al., 1982; Yeats, 1983).

In the crystalline section elevated pore pressure has been proposed as a partial explanation for velocity reversals commonly observed in refraction experiments (Mueller and Landisman, 1966), and reflection data (McEvilly, 1981). Localized zones of high pore pressure have also been suggested as an explanation for the strong reflections observed from the Pacific Creek and Wind River thrust faults in the Wind River seismic data (Jones and Nur, 1982).

Mechanical consideration of stresses involved in forming thin but laterally extensive overthrust sheets may require zones of elevated pore pressure to drastically reduce the strength of rock in the detachment zone (Hubbert and Rubey, 1959). More recently Rayleigh and Evernden (1982) have invoked elevated pore pressure associated with fault zones to explain the low deviatoric stresses which are thought to be present along major plate boundary faults.

By elevated or abnormal pore pressure we mean pore pressure above the hydrostatic gradient, perhaps approaching the lithostatic gradient. The strength of rock is controlled by an effective stress law (Handin et. al., 1963), hence increasing pore pressure decreases the strength of rock. For the crystalline basement and undrilled sedimentary basins it is desirable to detect overpressured zones with geophysical techniques. As seismic velocity also depends on an effective stress law (Jones and Nur, 1983a), low velocity zones may in some cases be related to overpressured zones, but a unique interpretation is seldom possible due to unknown variations in lithology.

Related to the distribution of pore pressure in the crust is the problem of the permeability structure of the crust. Very low permeability is needed,

unless there is a source for the fluids at depth, to maintain high pore pressure for geologically significant periods of time. Thus high pore pressure may be related to low permeability shale zones, compaction of sedimentary rocks (Sprunt and Nur, 1977), or extensive ductile deformation in crystalline rocks (Bernabe et. al., 1982). Permeability also depends on effective pressure (Brace et. al., 1968), so that high pore pressure tends to increase permeability unless one of the previously mentioned processes are acting.

THE MODEL

In order to determine the seismic effect of overpressured zones we require a model for the relationship of pore pressure to permeability, and seismic velocity to pore pressure. When the velocity profile is obtained we may then compute a synthetic reflection seismogram to show the effect of localized pore pressure on reflected waves. Ignoring effects of compaction, fluid sources at depth, and time or pressure dependent permeability we can model changes in pore pressure over time, and the resulting change in seismic velocity.

The transient solution in one dimension for pore pressure as a function of time, with initial pressure over a distance (X) of -L<X<L is given by Carslaw and Jaeger (1959). The time scale (t) over which pressure decays may be estimated by $t=L^2/c$, where c is the hydraulic diffusivity. A more complicated solution for pore pressure in a material of heterogeneous hydraulic diffusivity and the same initial conditions is given by Lovering (1936). For layers of radically differing hydraulic diffusivities the time for decay of pore pressure is about the same as for the homogeneous case, controlled by the lower value of diffusivity. Some values of permeability of crustal rocks are given by Bredehoeft and Hanshaw (1968), Brace (1982), Brace et. al., (1968), and Trimmer et. al., (1980).

An empirical relationship is used to model the dependence of seismic velocity on pressure, $V = A + B(P_e) - Ce^{-DP_e}$ where $P_e = P_c - \alpha P_p$. Some values for the constants A, B, C, D, are given in Table 1 determined from laboratory data on common crustal rocks. Nur and Byerlee (1971) show that α is in

general a little less than one, hence increasing pore pressure is slightly less effective in lowering velocity than decreasing confining pressure. They also show that α is related to the bulk modulus of the rock and the bulk modulus of the mineral constituents. There is in general insufficient data to evaluate this for most rocks. We have instead used the data of Todd and Simmons (1972), and Jones and Nur (1983a and b) to form an empirical relationship of α to pore pressure, $\alpha = E - Fe^{GP_p}$. Where data is not available on water saturated samples or at sufficiently high pressures and temperatures we can use Gassman's relation (Brown and Korringa, 1975) and data for the compressibility of water (Burnham et. al., 1968) to extrapolate. Temperature derivatives of velocity in water saturated rocks are given by Spencer and Nur (1976) and Timur (1976). Using this data and our empirical relationships we may estimate the velocity as a function of depth and pore pressure within the crust.

Finally, in some cases of localized pore pressure gradients it will prove interesting to compute a synthetic reflection seismogram to detail the comparative effects of pore pressure and lithology on seismic reflections. We will use the one-dimensional wave equation algorithm (Ganley, 1982).

RESULTS

We will first consider effects of localized zones of pore pressure on reflections from within crystalline rocks. In particular we will consider the possibility of reflections from the Pacific Creek thrust fault due to zones of elevated pore pressure. A full discussion of this problem is given in Jones and Nur (1983a and b).

Figure 3 shows the distribution of pore pressure around a zone of width 2L, as the parameter kt/L^2 increases. For this illustration we have used a porosity of 1% and representative values for the compressibility and viscosity of water (Burnham et. al., 1969).

Figure 4 is the velocity model we will use for a rock of roughly gabbroic composition. The data was taken from Christensen and Salisbury (1975). A value of L of 55 meters was inferred from spectral and amplitude modeling of

reflections from the fault zone (Jones, 1983). We then may compute the velocity profile through this zone, assuming an initial lithostatic pore pressure inside and zero pore pressure outside. Since time scales exactly as the permeability we have done this for increasing values of time (t) and permeability (k) in Figure 5.

Figure 6 is a portion of the true amplitude data record from COCORP Wind River line 1. Note the strong reflections from the Pacific Creek thrust fault at 5.5 to 6.5 seconds. The synthetics were computed using the velocity structure of the sedimentary basin (Figure 2), and a number of equally spaced zones of elevated pore pressure in the basement to model the Pacific Creek thrust. Initially where the pore pressure is lithostatic strong reflections are seen on the synthetics comparable to the data. As the pressure diffuses out amplitudes of reflected waves decrease rapidly. For a value of $tk=10^{-9}$ (c.g.s.) where some reflections are still seen, we can evaluate the permeability which would be required to maintain high pore pressure, assuming pore pressure was initially lithostatic until Laramide deformation ceased on the fault. If this was about 40 million years ago (10^{+15} seconds) a permeability of 10^{-24} cm^2 or 10^{-16} darcy is required. This is about three orders of magnitude lower than the lowest values found in the literature for laboratory measurements on low porosity crystalline rock (Timmer et. al., 1980) and it is on the order of permeability for volume diffusion in oxides and silicates of no porosity (Brace et. al., 1968). While ductile deformation may help to create and maintain low permeability (Bernabe et. al., 1982) it seems unlikely that such low values could be maintained for such long periods of time, particularly as high pore pressure would tend to increase permeability (Brace et. al., 1968).

Figure 7 was computed for the same case as Figure 6 except that the initial pore pressure was only 90% lithostatic. The amplitudes are much smaller due to the strong non-linear relationship of velocity to pressure at low effective pressure. Amplitudes decay at about the same rate as in Figure 6.

In Figure 8 we attempt to model the fault zone reflections with a 2 kilometer thick zone of lithostatic pore pressure. Since the decay of pore pressure scales as L^2/c we would expect significant pore pressure to be

maintained in time about two orders of magnitude longer than in the thinner zone. However the reflected energy is influenced primarily by the large pore pressure gradients at the outer part of the zone, which do not exist substantially longer for a thicker zone. As the velocity decrease is strongest only at very high pore pressures, amplitudes of reflected waves decay at very near the same rate as for the thinner zone, although in terms of rock strength, the pore pressure is significant for much longer periods of time. Note also that a single thick zone does not produce strong amplitudes of reflected waves due to lack of constructive interference and does not display the ringing character nor appropriate frequency content (Jones, 1983).

Several cases have also been considered for sedimentary sections. Figure 9 shows the velocity profile through a 500 meter thick section of Berea sandstone as an initial lithostatic pore pressure decays. A confining pressure of one kilobar was used. Figure 10 shows the decay of reflection amplitudes from the top and bottom of the pressurized sandstone layer as pressure decays with increasing tk. For reference we have inserted arbitrarily reflection coefficients of 0.05 above and below the sandstone layer. Note that not only does the amplitude of the reflections decay, but the reflection from the top of the layer moves down, and the reflection from the bottom of the layer moves up as the strong velocity gradients on the edges of the zone are decreasing and moving in towards the center. Note also that the bottom event with constant amplitude and depth moves up in the time section as the pressure decays outwards. The greatest move upwards occurs between tk of 10^{-7} and 10^{-6}. This follows from the velocity profiles in Figure 9, as this time interval is where the pore pressure throughout the zone drops below the range of strong non-linear effects on velocity. Also the greatest decrease in amplitude of the reflected waves occurs before much of the velocity pull-up has taken place.

A similar calculation has been made for a Pierre shale. Figure 11 shows the velocity profiles through a zone 110 meters in thickness as pressure decays with increasing tk. Figure 12 shows reflections obtained from a number of thin shale zones arranged so as to give strong constructive

interference. Figure 13 shows reflections from the top and bottom of a thick pressurized shale zone. In both Figures 12 and 13 a reflection coefficient of 0.05 was inserted above and below the pressurized shale layers for reference. In each of these figures the reflected wave amplitudes decay at similar rates due to the non-linear effect of pressure on velocities. Again the amplitudes decrease and move in towards the center of the zone. Similarly to Figure 10 the velocity pull-up of the bottom reference reflector occurs predominantly after most of the decay of amplitude has taken place.

Perhaps of more geologic relevance would be the case in Figure 14, an interbedded shale and sandstone sequence. The transient solution for pore pressure is controlled in the short term by the permeability of the shale layer and its thickness. Eventually the pressure between the sand and shale will equilibrate. Because of the drastic changes in permeability likely to exist between these two units there will not be significant pressure or velocity gradients in the sandstone compared to the shale. The case in this illustration was computed for a permeability of 10^{-9} darcy for the shale and 10^{-1} darcy for the sandstone. At much longer times the fluid will escape from the entire system and the pressure will go to zero for both units.

Figure 15 shows the velocity profiles in one sandstone-shale layer as pore pressure decays with increasing time. The solid lines were computed for the case of initially high pore pressure in the shale and low pore pressure in the sandstone. The synthetics for this case are shown in Figure 16. Again the top and bottom reflections are from a reflection coefficient of 0.05 at constant depth for reference. The leftmost synthetic was computed for the case of lithostatic pore pressure in both units.

Initially when pore pressure is high only in the shale there will be a very strong reflection from each interface due to the higher velocity in the sandstone, and the lower velocity in the shale made still lower because of the high pore pressure. With time the pressure decreases and the velocity increases in the shale, the reverse happening in the sandstone. This causes the decrease in reflection amplitudes with increasing tk, and velocity pull-up. Again we note that after most of the amplitude decrease has occurred further

velocity pull-up takes place as there is still significant excess pore pressure in each layer, but it is gradational so as not to significantly increase reflected wave amplitudes.

A second case is shown by the dashed lines in Figure 15 and the synthetics in Figure 17. Initially the pore pressure is low in the shale and high in the sandstone. This causes very small reflection coefficients at each interface. As tk increases pore pressure decreases and velocity increases in the sandstone and vice verse in the shale. Hence the amplitudes of reflected waves increase with increasing time. After equilibrium is reached between individual layers and pressure begins to diffuse out of the system as a whole the reflected wave amplitudes decrease slightly.

We would also like to consider briefly the significance of the variation in velocity shown on the sonic log of the Green River basin in Figure 2. Figure 18 summarizes the constraints experimental velocity determinations place on velocity depth profiles. We have plotted velocity as a function of depth for rock types likely to be present within and immediately below the Green River basin. Included in the conversion of pressure to depth is the assumption of hydrostatic pore pressure throughout the basin and a temperature gradient of 20° C per kilometer. The general trend of velocity in the Green River basin is fit reasonably well by the Berea sandstone velocity depth profile. The majority of variations from this, including low velocity zones may be explained by lithologic variations.

Figure 19 combines the experimentally determined velocity depth profiles to produce an analogous velocity depth profile to that of the Green River Basin. Zones of shale or overpressured sandstone produce low velocity zones in the upper portion of the basin. The lower portion of the basin, below about 6.6 kilometers, is known to contain carbonates from lithology logs. Data on limestones fits well the higher velocity in this region. Carbonates or siltstones higher in the section can also produce high velocity zones. The pronounced low velocity zone at about 5.5 to 6.5 seconds seems to require an overpressured shale zone to produce the strong velocity reversal. This is supported by lithology logs which show substantial amounts of shale at these

depths. The shales, when overpressured, have appropriate velocity and may provide the low permeability required to maintain high pore pressure.

CONCLUSIONS

Models for seismic velocity in overpressured zones show that localized pore pressure gradients may strongly contribute to velocity variations with depth and may effect amplitudes of reflected waves in either crystalline or sedimentary rock. However the effect of pore pressure on the amplitude of a reflected wave is short lived in comparison to the existence of fluid pressures large enough to significantly affect the strength of crustal rock units. It was found that, relatively independent of rock type and dimension of the pressurized zone the effect on amplitude of reflected waves is small for tk greater than about 10^{-9} or 10^{-8} (c.g.s.). For this to be a significant effect for 1 million years requires a permeability of about 10^{-13} darcy, well below that generally observed experimentally. These simple models predict a very low permeability is required to maintain pore pressure sufficient to effect seismic velocity for geologically significant periods of time. Most likely this is due our lack of consideration of additional processes for which inadequate constraint is presently available to incorporate in our models. These effects could include compaction of unconsolidated sedimentary layers, fluid sources at depth due to dehydration reactions, reduction of porosity and permeability through pressure solution, and permeability reduction due to ductile deformation in crystalline rocks. In principal these effects could be incorporated into this model. For the present our results may apply primarily to shorter time scales, such as artificial draw-down of reservoirs.

ACKNOWLEDGEMENTS

The synthetic seismogram program was written by Dave Hale. Thanks are due to the Stanford Exploration Project and Jon Claerbout for the use of computing facilities. This research was supported by grant DEAT03-76 ER71045 from the Department of Energy.

REFERENCES

Bernabe, Y., W. F. Brace, and B. Evens, Permeability, porosity, and pore geometry of hot pressed calcite, Mechanics of Materials, 1, 173-183, 1982.

Berry, F. A. F., High fluid potentials in California coast ranges and their tectonic significance, Bull. Am. Assoc. Pet. Geol., 57, 1219-1249, 1973.

Brace, W. F., Permeability of crystalline and argillaceous rocks: Status and problems, Int. J. Rock. Mech. and Min. Sci., in press, 1982.

Brace, W. F., J. B. Walsh, and W. T. Frangos, Permeability of granite under high pressure, J. Geophys. Res., 73, 2225-2236, 1968.

Bredehoeft, J. D., and B. B. Hanshaw, On the maintenance of anomalous fluid pressures: I. Thick sedimentary sequences, Geol. Soc. Am. Bull., 79, 1097-1106, 1968.

Brown, R. J. S., and J. Korringa, On the dependence of the elastic properties of a porous rock on the compressibility of a pore fluid, Geophysics, 40, 608-616, 1975.

Burnham, C. W., J. R. Holloway, and N. F. Davis, Thermodynamic properties of water to 1000°C and 10,000 bars, Geol. Soc. Am., special paper 132, 96p., 1969.

Carslaw, H. S., and J. C. Jaeger, Conduction of heat in solids, 2nd edition, London, Oxford University Press, 510 p., 1959.

Christensen, N. I., and M. H. Salisbury, Structure and constitution of the lower oceanic crust, Rev. Geophys. and Space Physics, 13, 57-86, 1975.

Ganley, D. D., A method for calculating synthetic seismograms which include the effects of absorption and dispersion, Geophysics, 46, 1100-1107, 1981.

Handin, J., R. V. Hager, M. Friedman, and J.N. Feather, Experimental deformation of sedimentary rocks under confining pressure: Pore pressure tests, Bull. Am. Assoc. Pet. Geol., 47, 717-755, 1963.

Hubbert, M. K., and W. W. Rubey, Role of fluid pressure in mechanics of overthrust faulting, I. Mechanics of fluid-filled porous solids and its application to overthrust faulting, Geol. Soc. Am. Bull., 77, 741-760, 1959.

Jones, T. D., The nature of seismic reflections from the crystalline basement, submitted to J. Geophys. Res., chapter 3, this volume, 1983.

Jones, T. D., and A. Nur, Velocity and attenuation in sandstone at elevated temperature and pressure, Geophys. Res. Lett., 10, 140-143, 1983a.

Jones, T. D., and A. Nur, The nature of seismic reflections from deep crustal fault zones, submitted to J. Geophys. Res., chapter 5, this volume, 1983b.

Jones, T. D., and A. Nur, Seismic velocity and anisotropy in mylonites and the reflectivity of deep crustal fault zones, Geology, 10, 260-263, 1982.

Lovering, T. S., Heat conduction in dissimilar rocks and the use of thermal models, Geol. Soc. Am. Bull., 47, 87-100, 1936.

McEvilly, T. V., Extended reflection seismic survey of the San Andreas fault zone, U. S. Geological Survey Open File Report no. 81-388, 28p., 1981.

Moore, J. C., and others, Offscraping and underthrusting of sediment at the deformation front of the Barbados Ridge: Deep Sea Drilling Project leg 78A, Geol. Soc. Am. Bull., 11, 1065-1077, 1982.

Mueller, S., and M. Landisman, Seismic studies of the earth's crust in continents, I: Evidence for a low-velocity zone in the upper part of the lithosphere, Geophys. J. R. Astr. Soc., 10, 525-538, 1966.

Nur, A, and J. D. Byerlee, An exact effective stress law for elastic deformation of rock with fluids, J. Geophys. Res., 76, 6444-6419, 1971.

Nur, A., and G. Simmons, The effect of saturation on velocity in low porosity rocks, Earth and Planet. Sci. Lett., 7, 183-193, 1969.

Raleigh, B., and J. Evernden, Case for low deviatoric stress in the lithosphere, Mechanical behavior of crustal rocks, A. G. U., 173-186, 1982.

Spencer, J., and A. Nur, The effects of pressure, temperature, and pore water on velocities in Westerly granite, J. Geophys. Res., 81, 899-904, 1976.

Sprunt, E., and A. Nur, Destruction of porosity through pressure solution, Geophysics, 42, 726-742, 1977.

Timur, A., Temperature dependence of compressional and shear wave velocities in rocks, Geophysics, 42, 950-957, 1977.

Todd, T., and G. Simmons, Effect of pore pressure on the velocity of compressional waves in low-porosity rocks, J. Geophys. Res., 77, 3731-3743, 1972.

Tosaya, C., Acoustical properties o clay bearing rocks, Ph.D. Thesis, Stanford University, Stanford, California, 136 p., 1982.

Trimmer, D., B. Bonner, H. C. Heard, and A. Duba, Effect of pressure and stress on water transport in intact and fractured gabbro and granite, J. Geophys. Res., 85, 7059-7071, 1980.

Yeats, R. S., Large-scale Quaternary detachments in Ventura Basin, Southern California, J. Geophys. Res., 88, 569-585, 1983.

Zawislak, R. L., and S. B. Smithson, Problems and interpretation of COCORP deep seismic reflection data, Wind River range, Wyoming, Geophysics, 46, 1684-1701, 1981.

TABLE 1

Constants in Velocity-Pressure Relations

ROCK TYPE	POROSITY	A	B	C	D	E	F	G	REFERENCE
Pierre shale	14.5%	2.95	$5.0\ 10^{-4}$	0.28	0.017	1	0.3	400	Tosaya, 1982
Cotton Valley siltstone	4.2%	4.34	$4.0\ 10^{-4}$	0.28	0.008	1	0.7	400	Tosaya, 1982
Berea sandstone	21.0%	4.04	$1.6\ 10^{-4}$	0.8	0.009	1	0.3	400	Jones and Nur, 1983
Solenhofen limestone	4.7%	5.72	$2.6\ 10^{-5}$	0.04	0.003	1	0.5	400	Nur and Simmons, 1969
Westerly granite	0.9%	5.98	$6.8\ 10^{-5}$	0.5	0.005	1	0.5	400	Nur and Simmons, 1969

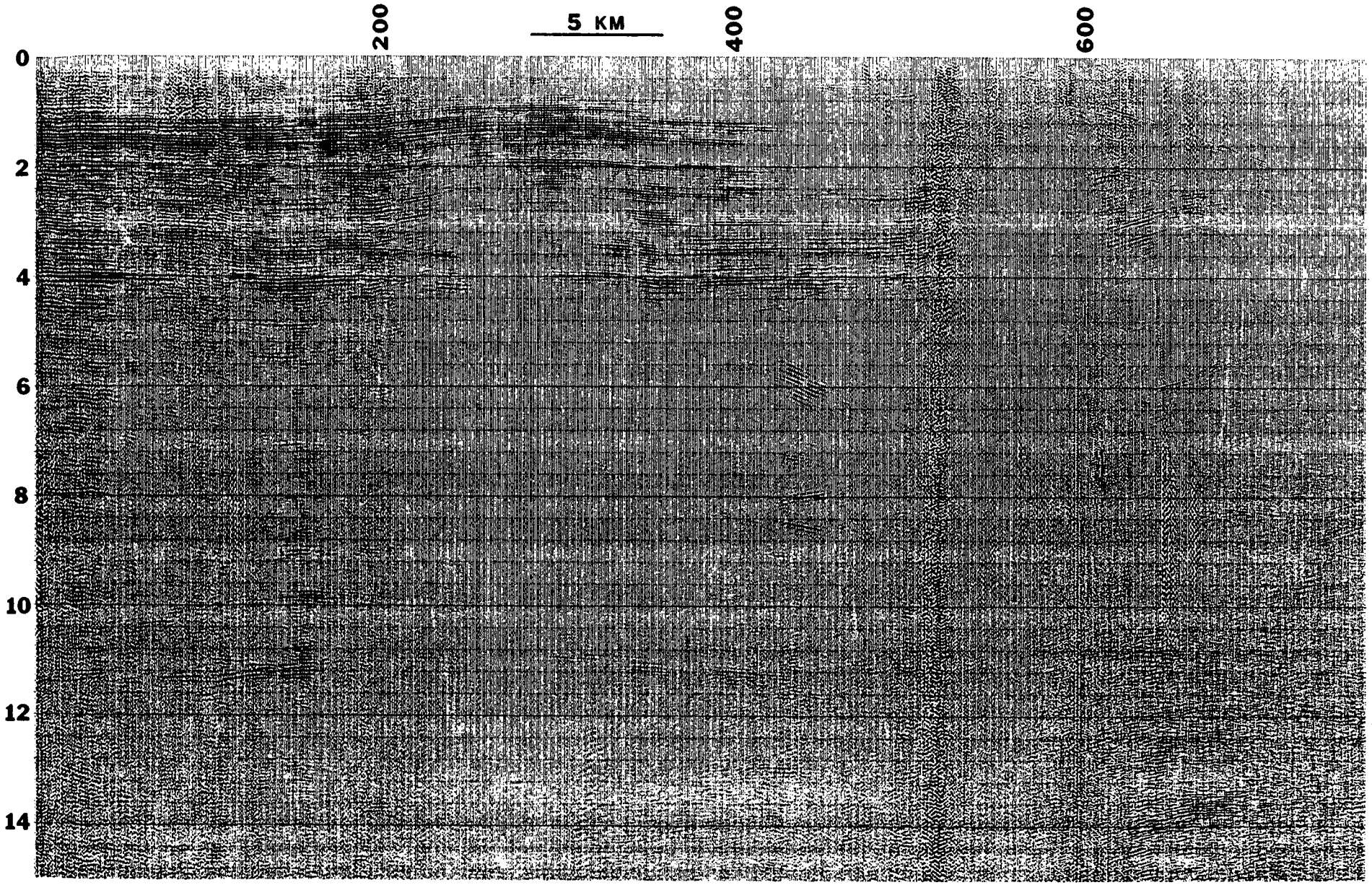

Figure 1. COCORP Wind River line 1, true amplitude data. Vertical scale is two-way travel time in seconds. See Jones (1983) for a discussion of processing of this line.

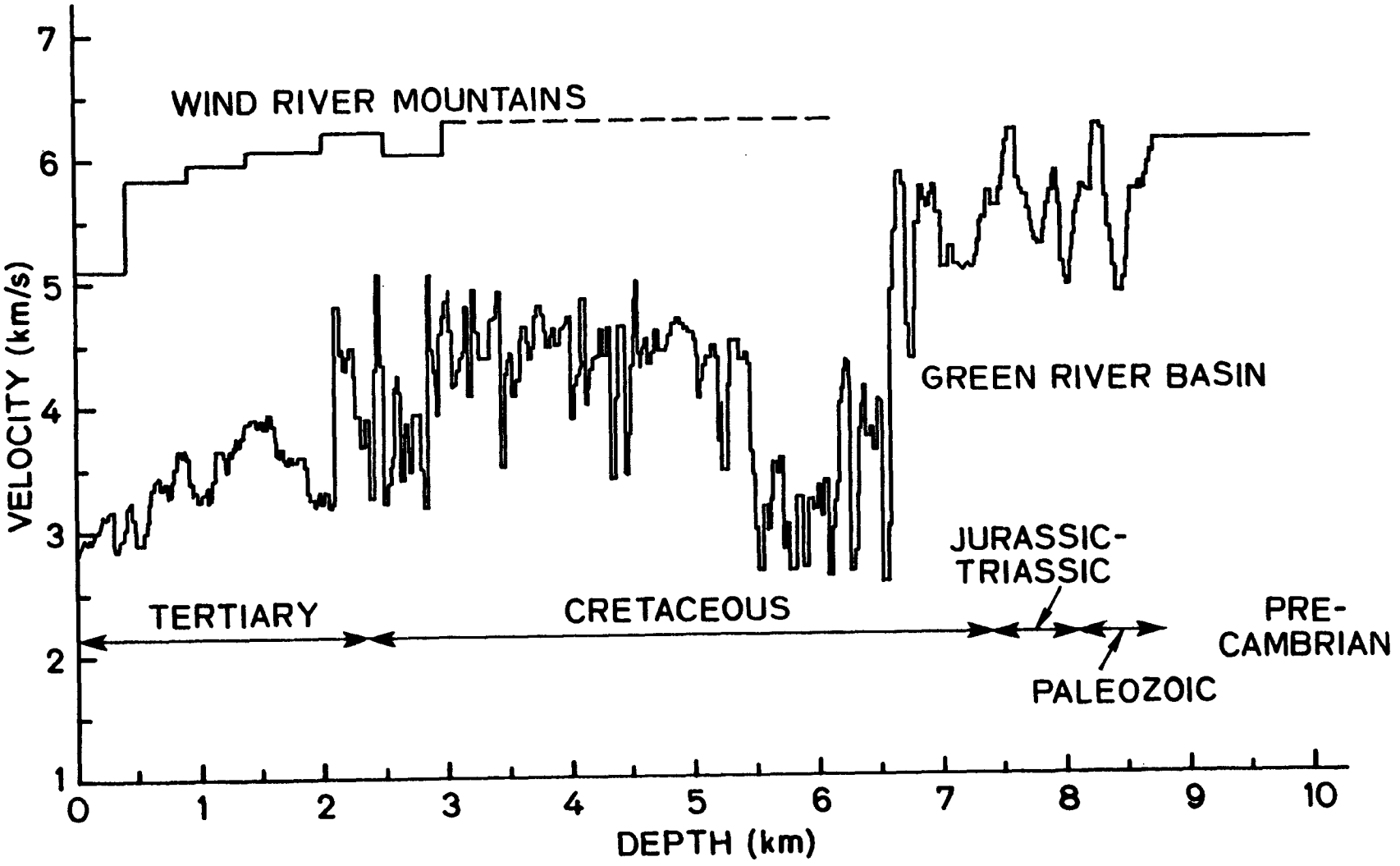

Figure 2. Velocity structure through the Green River basin, as determined from sonic logs.

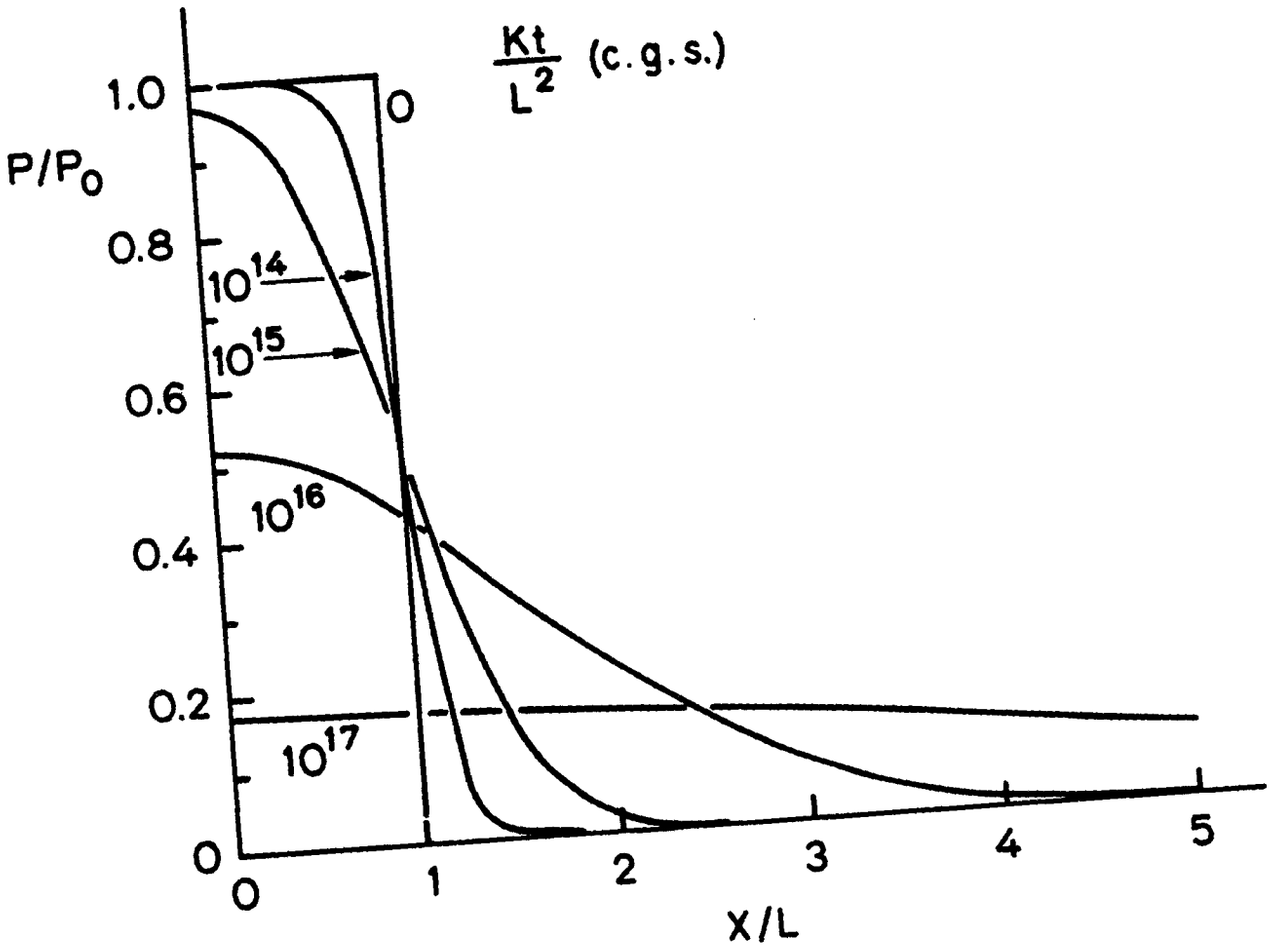

Figure 3. Transient solution for pore pressure in a material of permeability k. Initial conditions are pore pressure of P_0 in a zone of width 2L, and pore pressure of zero elsewhere. Curves plotted for given values times kt/L^2. A porosity of 1% was used. Compressibility and viscosity of water are taken as 10^{-11} and 10^{-3} c.g.s., respectively.

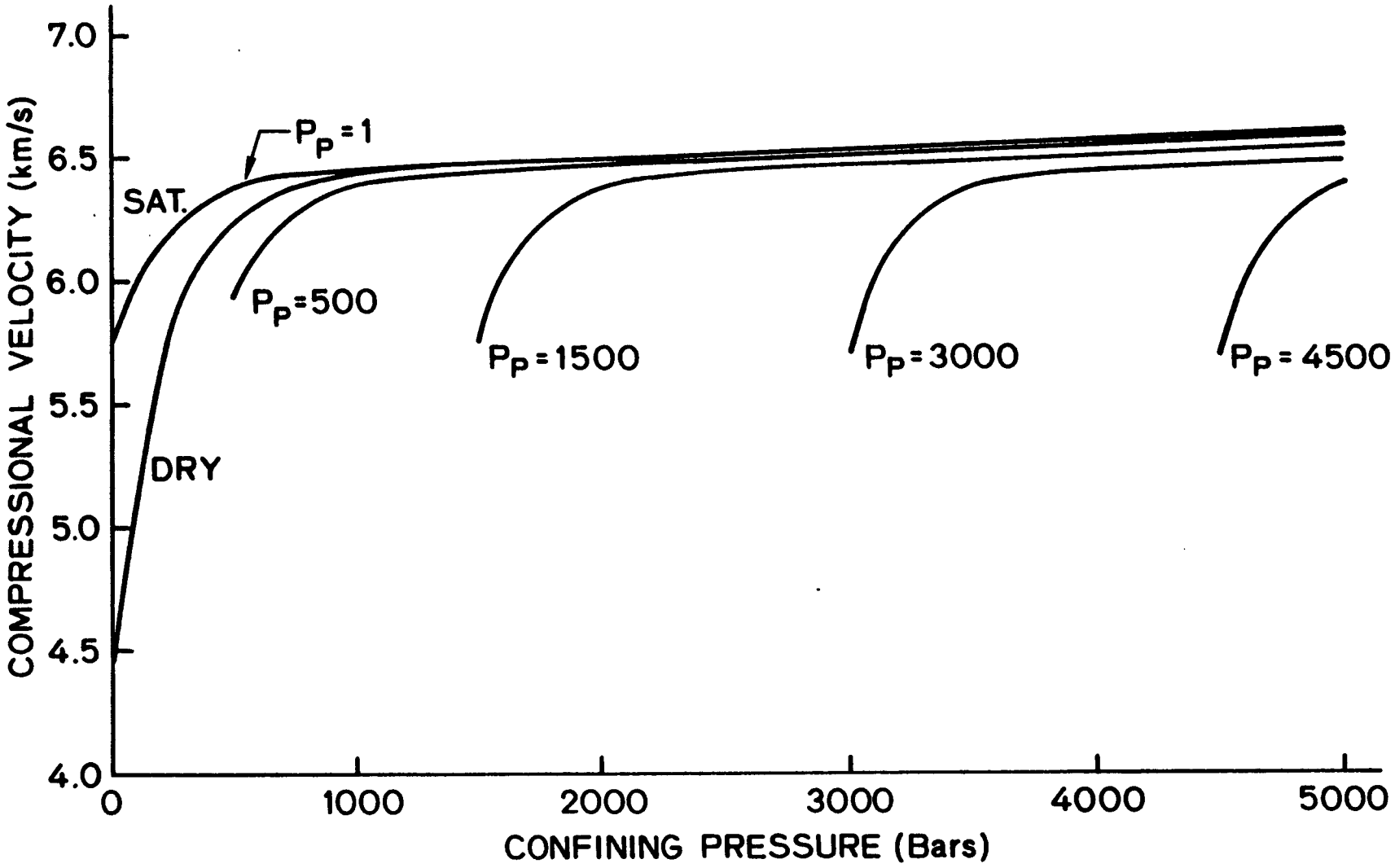

Figure 4. Empirical model for the effect of confining pressure and pore pressure on compressional velocity in a low porosity rock of approximately gabbroic composition.

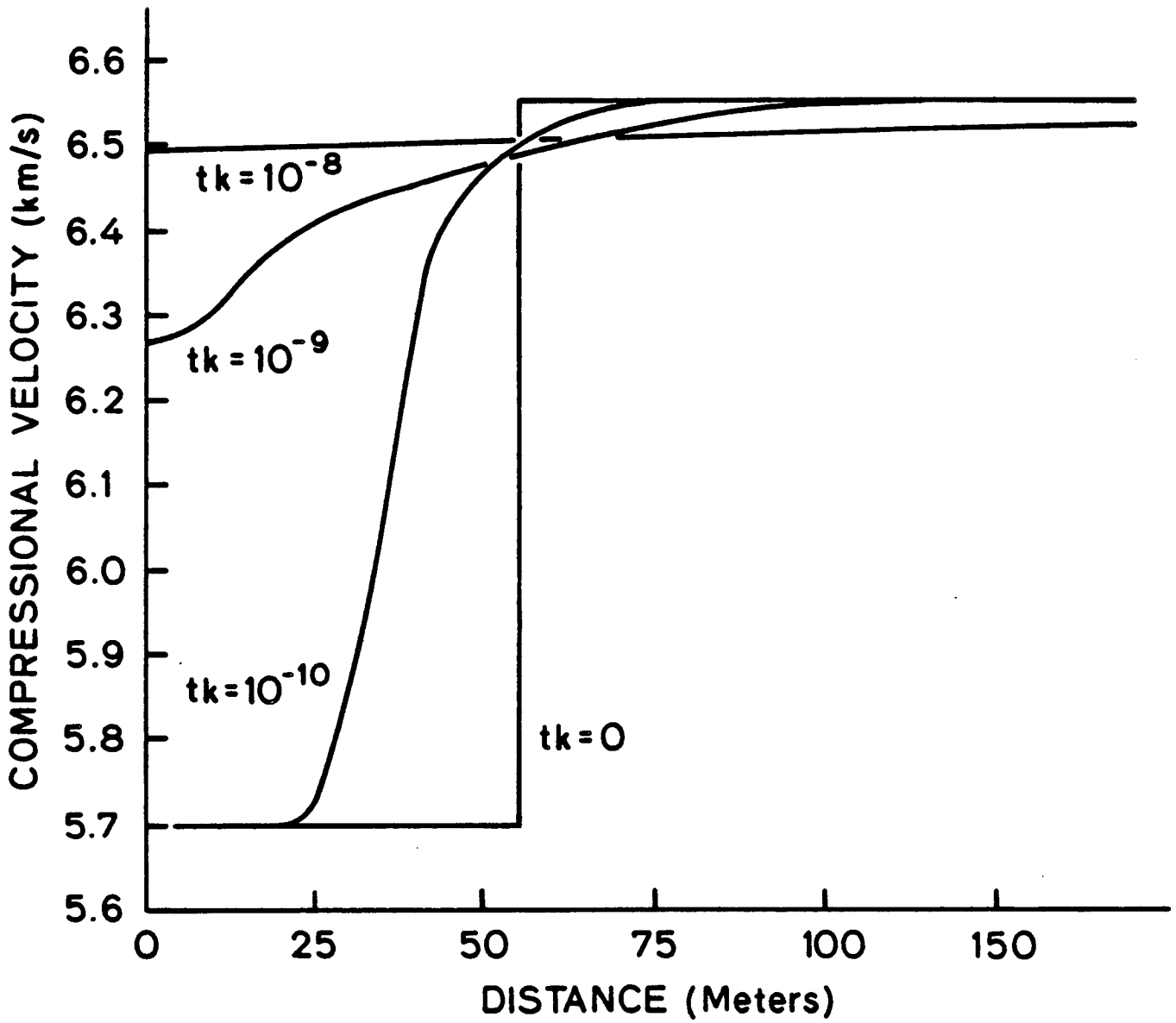

Figure 5. Velocity profile across a zone 110 meters thick as initial lithostatic pore pressure diffuses out. Pore pressure model based in Figure 3, and velocity model based on Figure 4. Curves are plotted for values of the product of time (in seconds) and permeability (in cm^2).

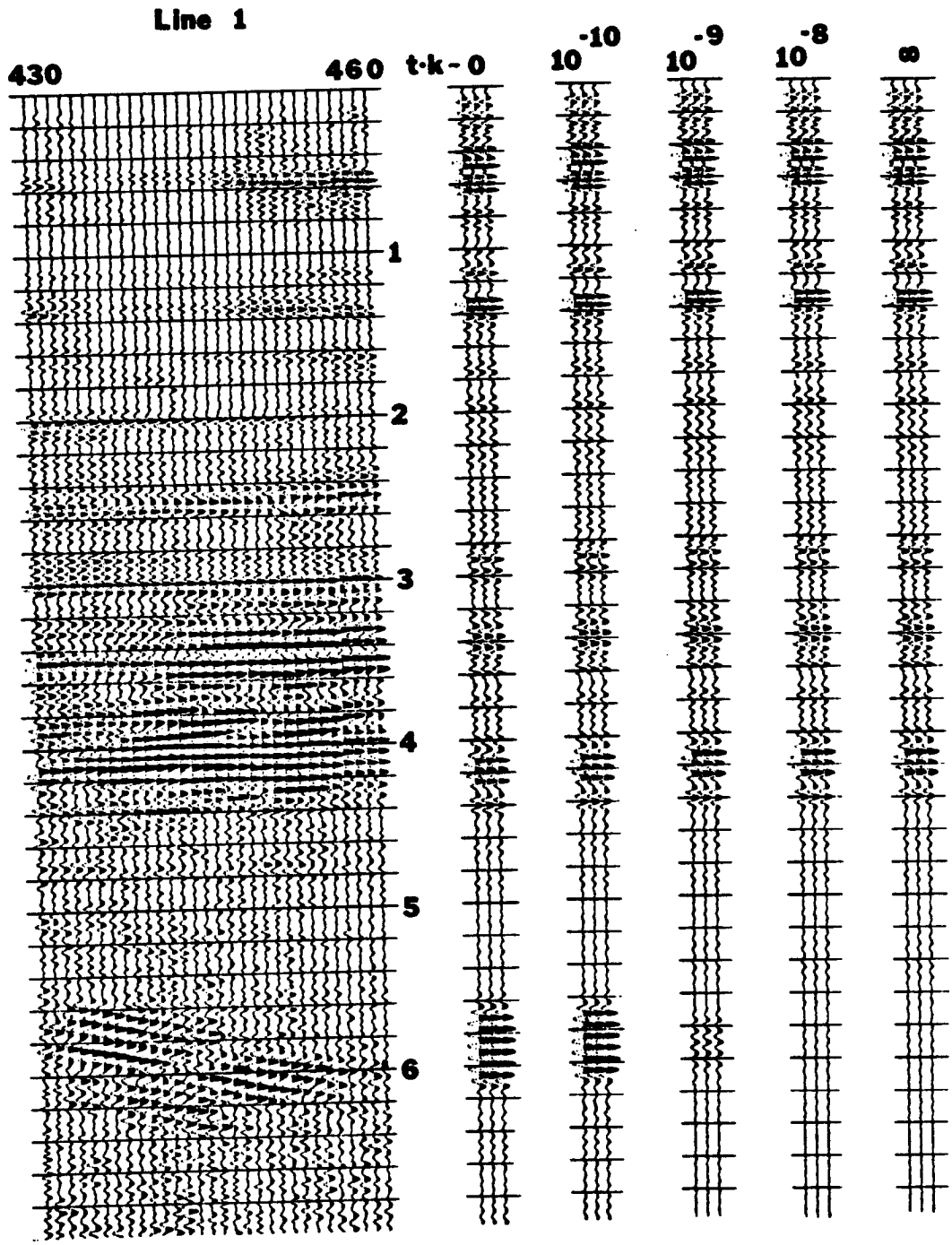

Figure 6. Portion of Wind River line 1 on the left, showing reflections from the Pacific Creek thrust at 6 seconds. Synthetics computed for a series of zones 110 meters in thickness, alternating ones which have an initial lithostatic pore pressure. Several cases show the change in reflectivity as the pore pressure diffuses out as the product tk increases.

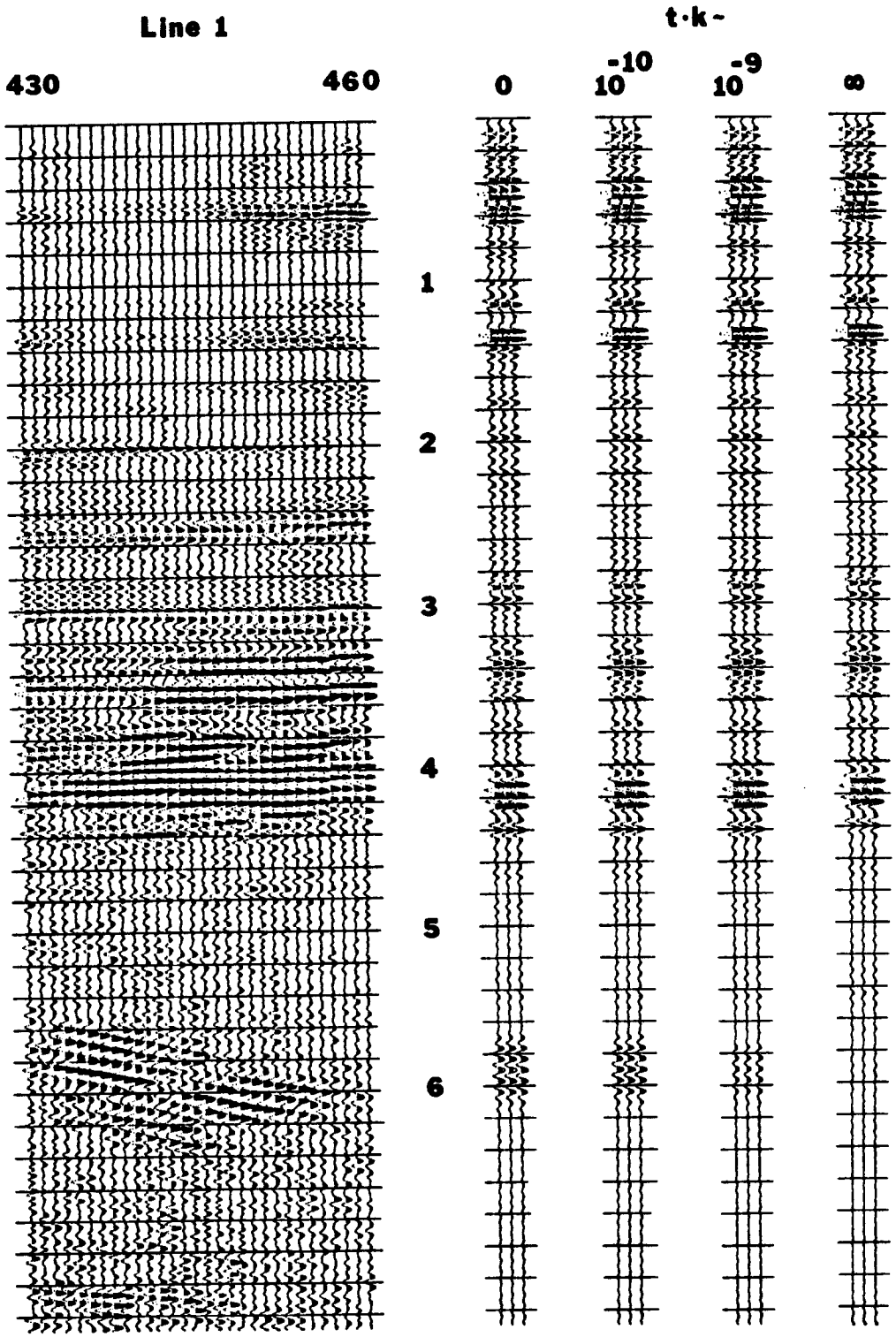

Figure 7. Same as Figure 6, but initial pore pressure is 90% of lithostatic.

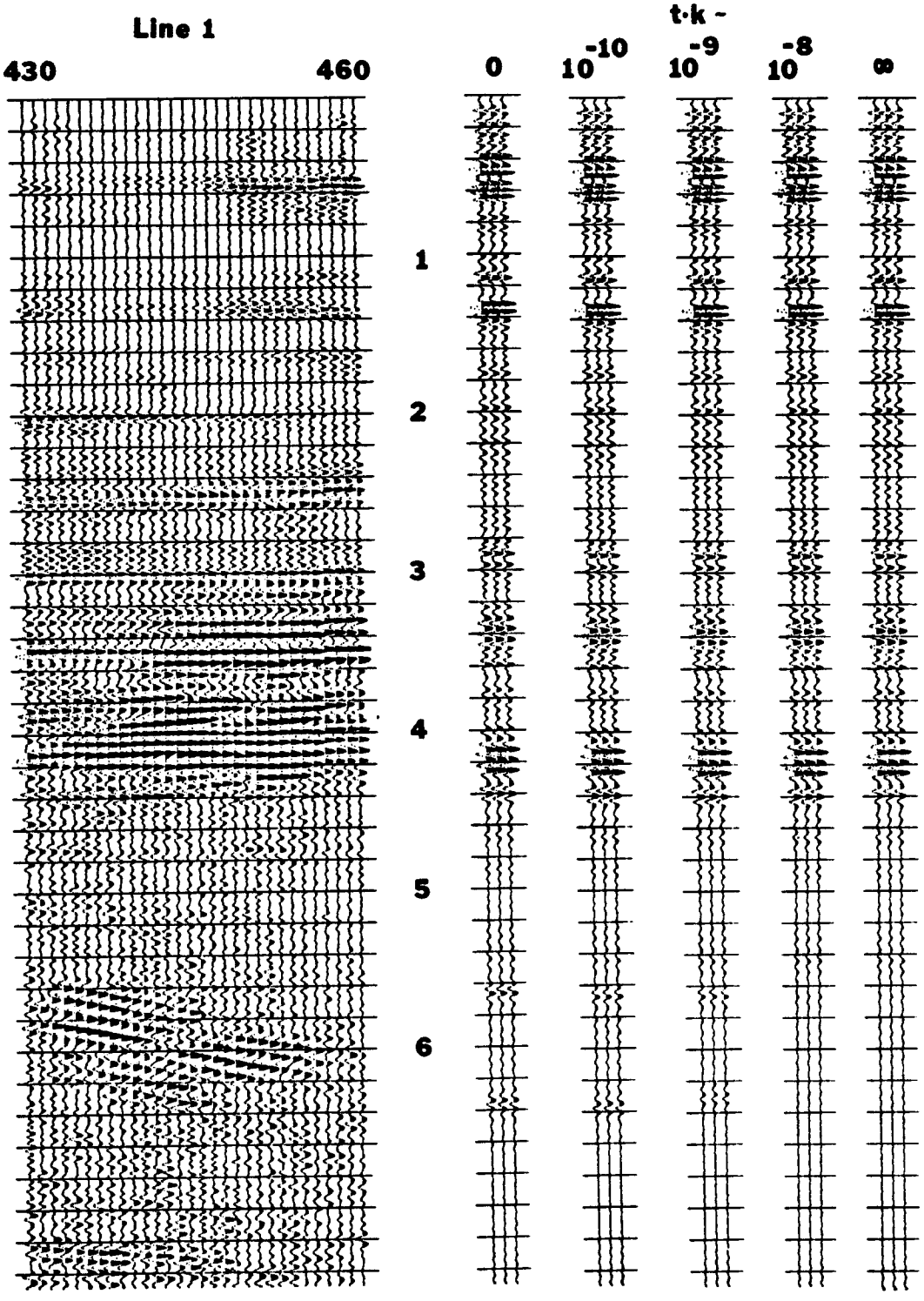

Figure 8. Same as Figure 6, but a single pressurized zone two kilometers thick was used.

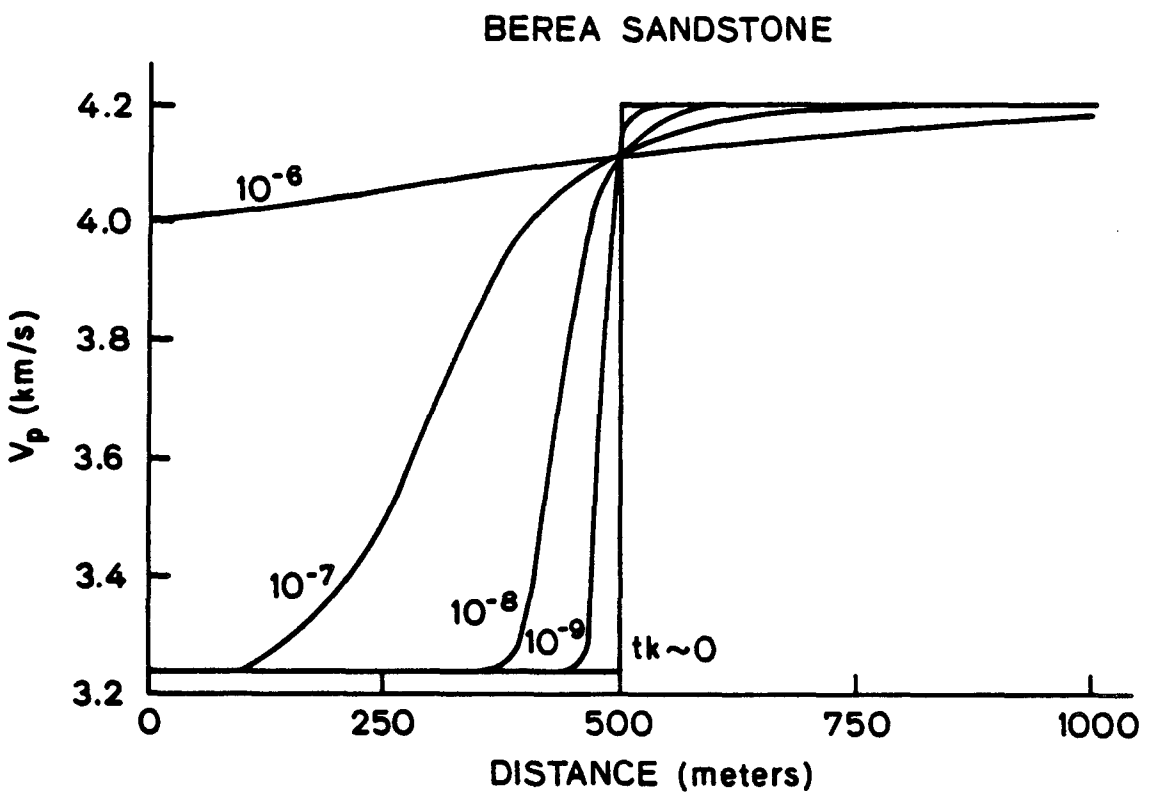

Figure 9. Velocity profile in a 1000 meter thick section of Berea sandstone as pressure diffuses out as the product tk increases.

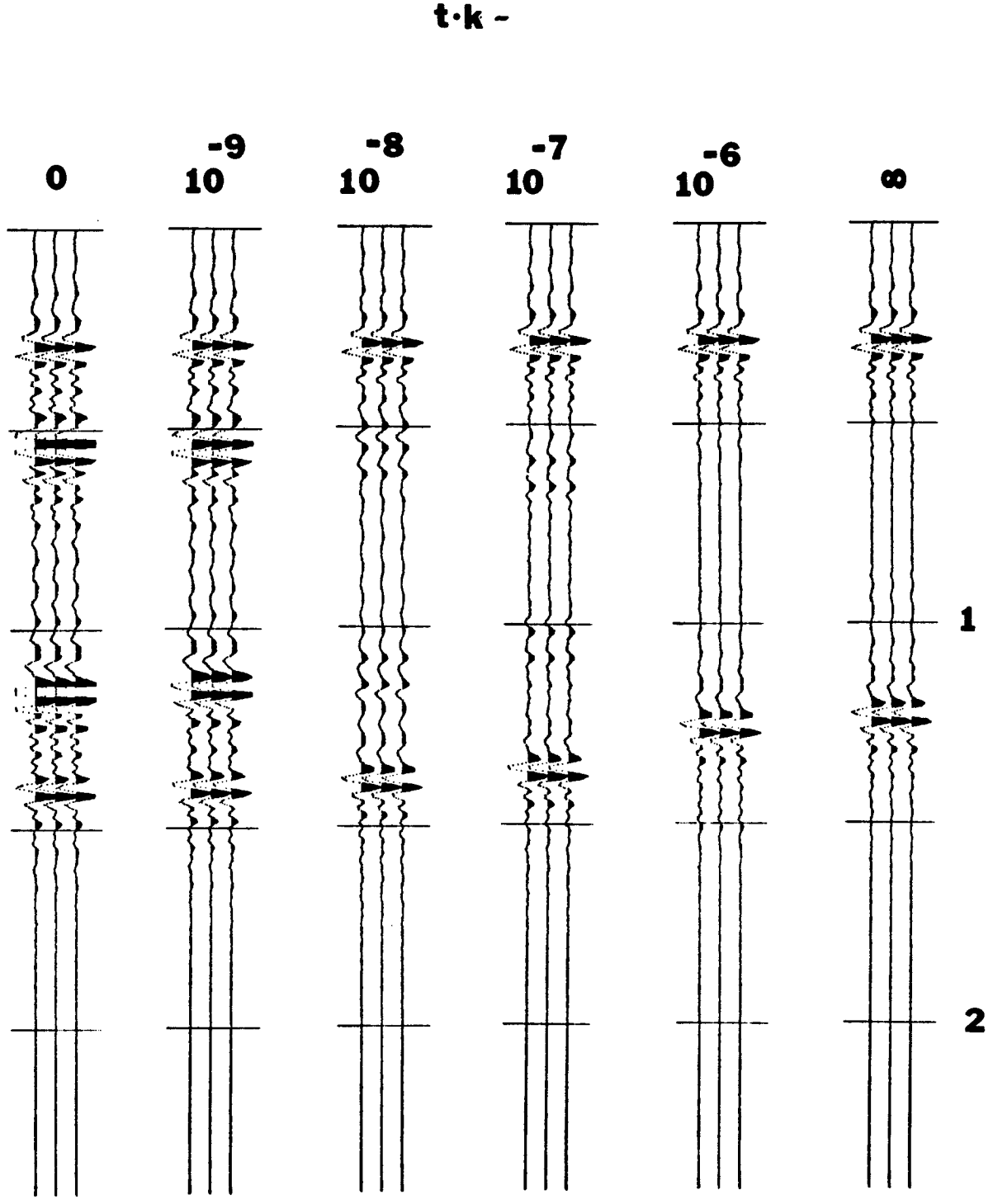

Figure 10. Synthetic seismograms computed over a thick section of Berea sandstone as the pore pressure decays. The top and bottom reflections are from a 0.05 reflection coefficient for reference. The middle events are from the top and bottom of the pressurized zone.

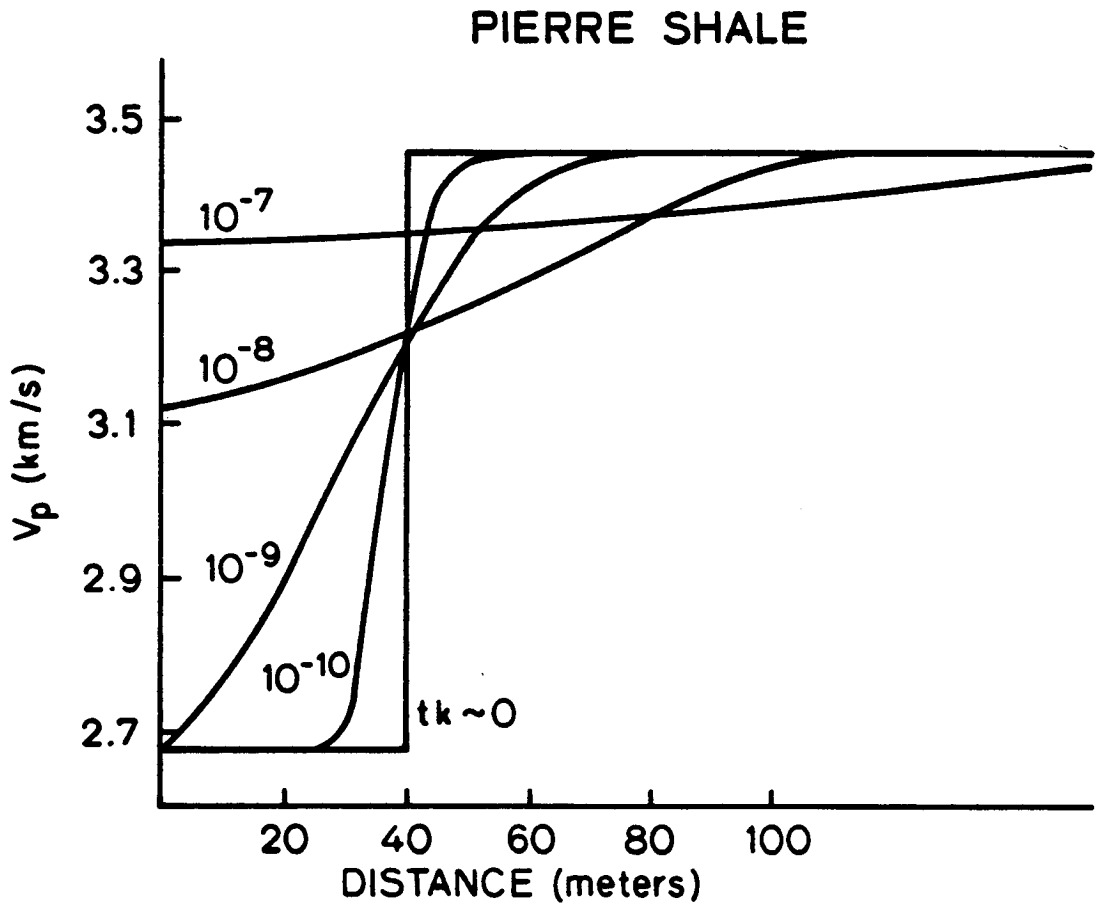

Figure 11. Velocity profile in a 110 meter thick section of Pierre shale as pressure diffuses out as the product tk increases.

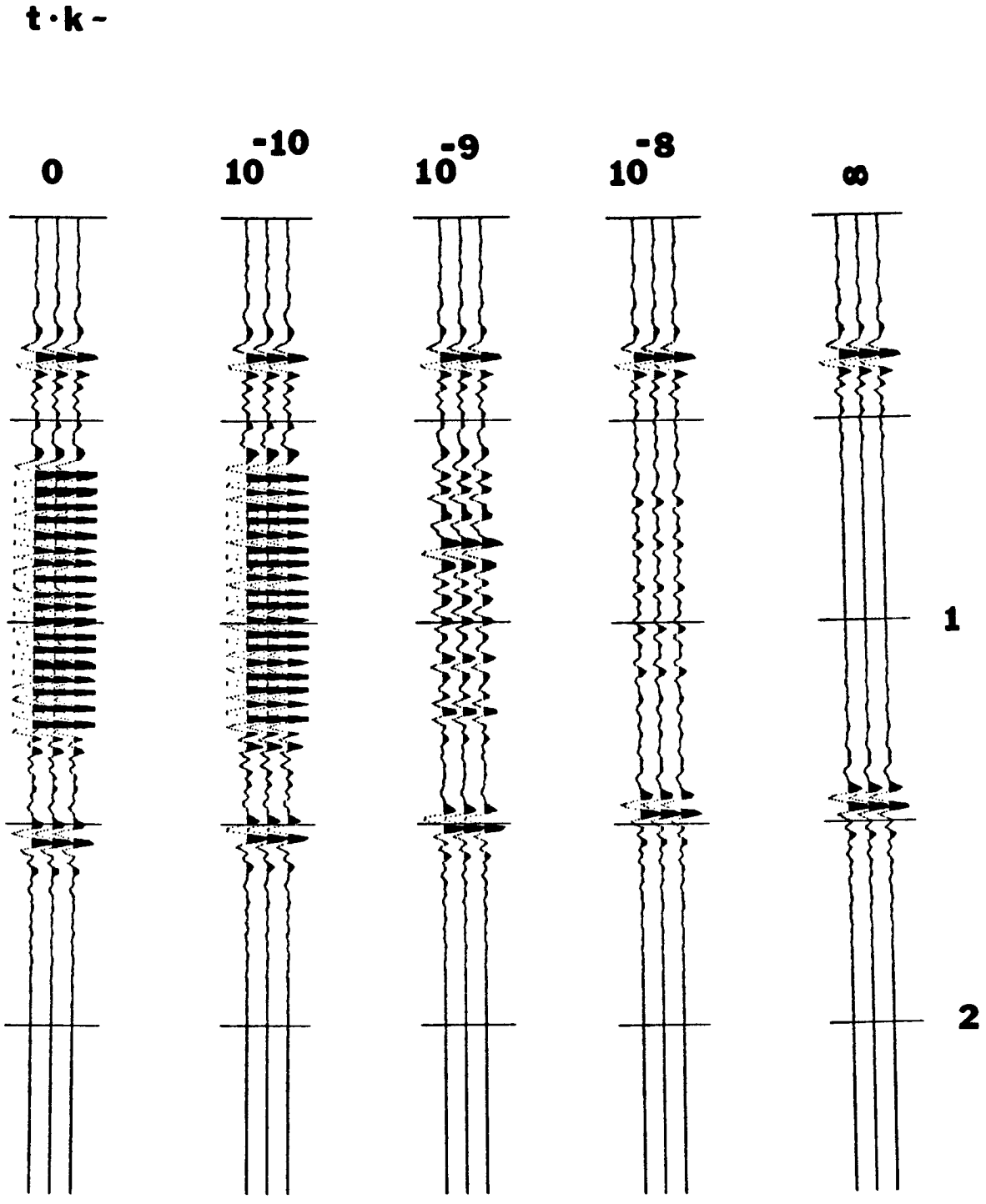

Figure 12. Synthetic seismograms computed for many thin zones of pressurized shale as the pore pressure decays. The top and bottom reflections are from a 0.05 reflection coefficient for reference. The middle events are from the thin pressurized zones.

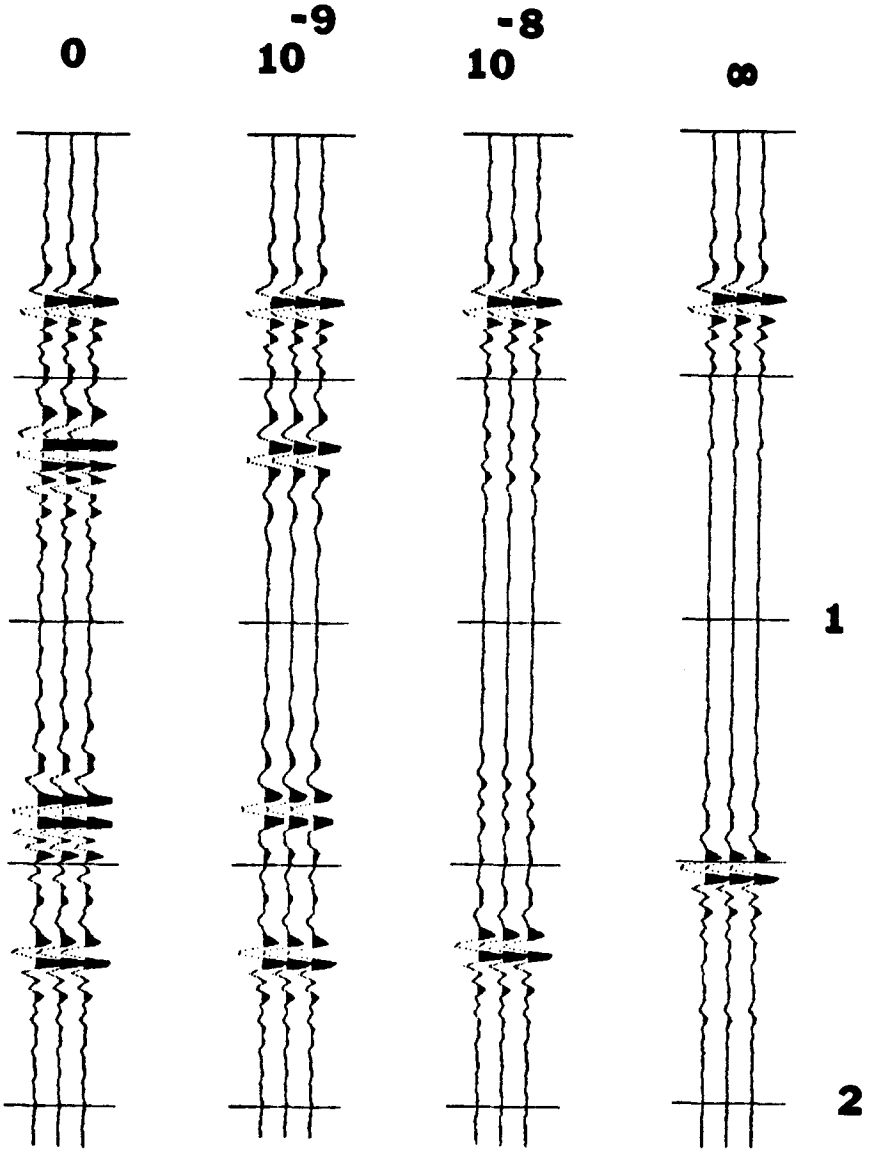

Figure 13. Synthetic seismograms computed for a single zone of pressurized shale as the pore pressure decays. The top and bottom reflections are from a 0.05 reflection coefficient for reference. The middle events are from the top and bottom of the pressurized shale zone.

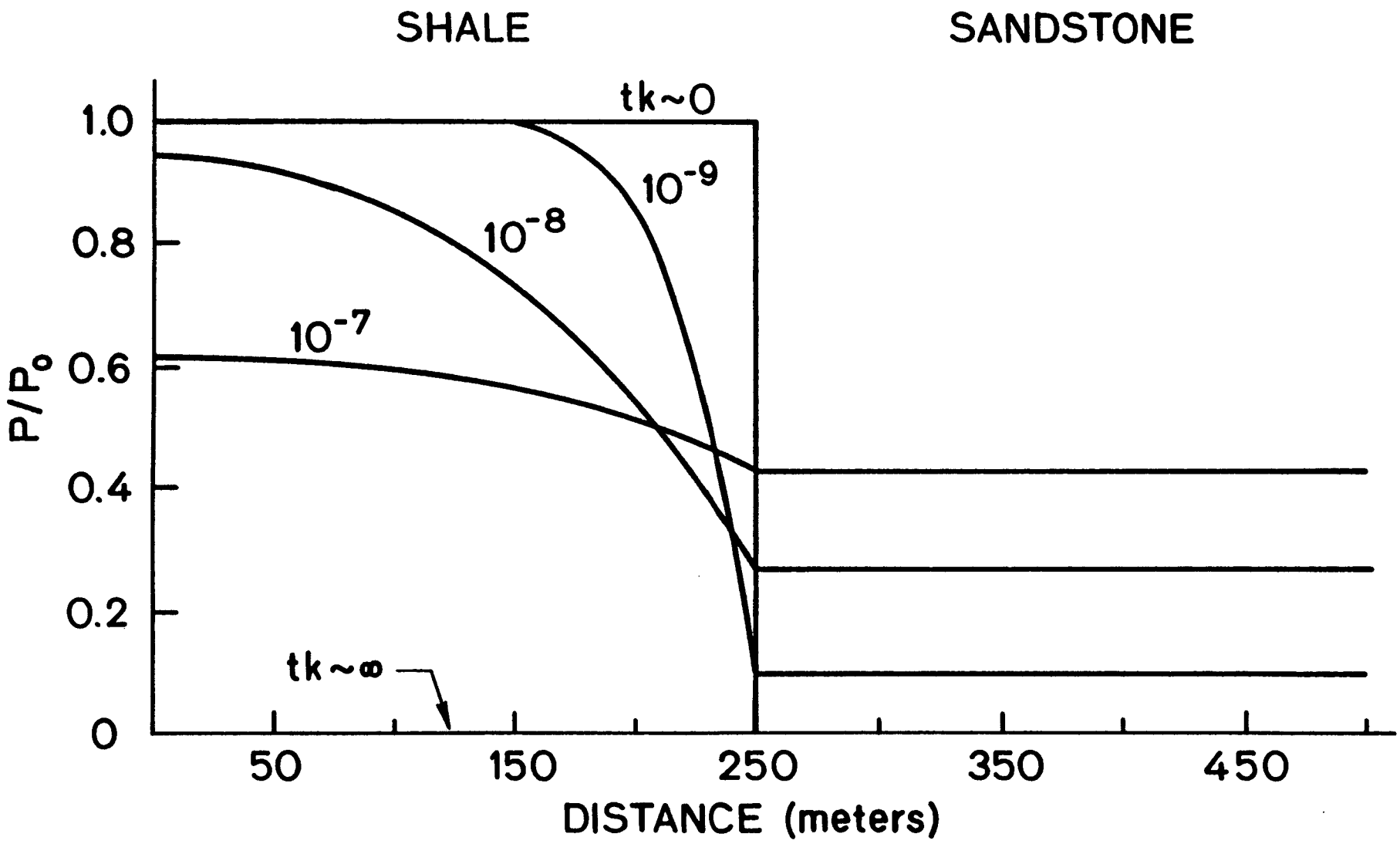

Figure 14. Distribution of pore pressure in an interbedded sand-shale sequence, where the sandstone has permeability several orders of magnitude higher then the shale.

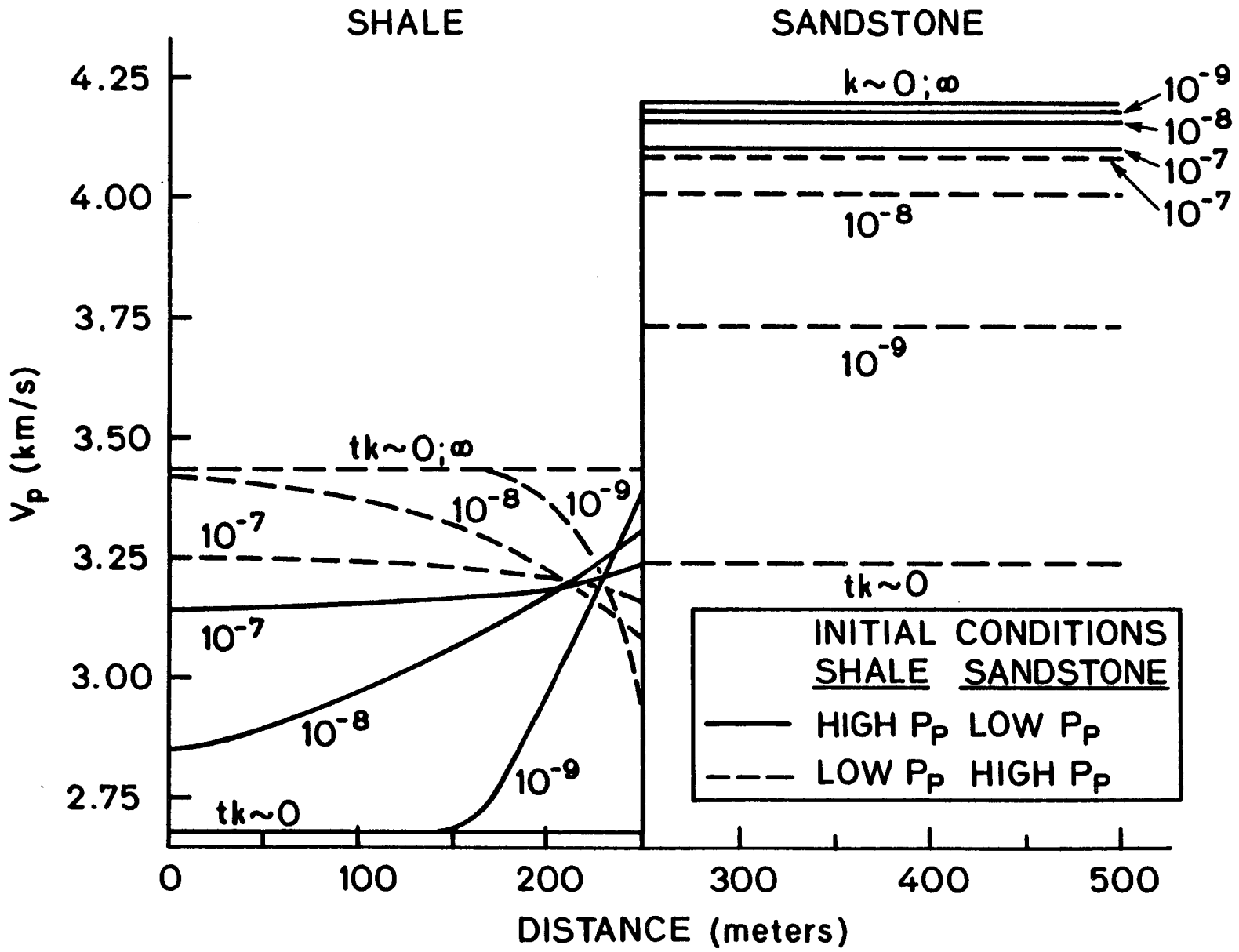

Figure 15. Velocity profiles in an interbedded sand-shale sequence computed for two cases. The first case (solid lines) is for high pore pressure in the shale and low pore pressure in the sandstone. The second case (dashed lines) is for high pore pressure in the sandstone and low pore pressure in the shale. The low value of permeability in the shale controls the decay of pore pressure.

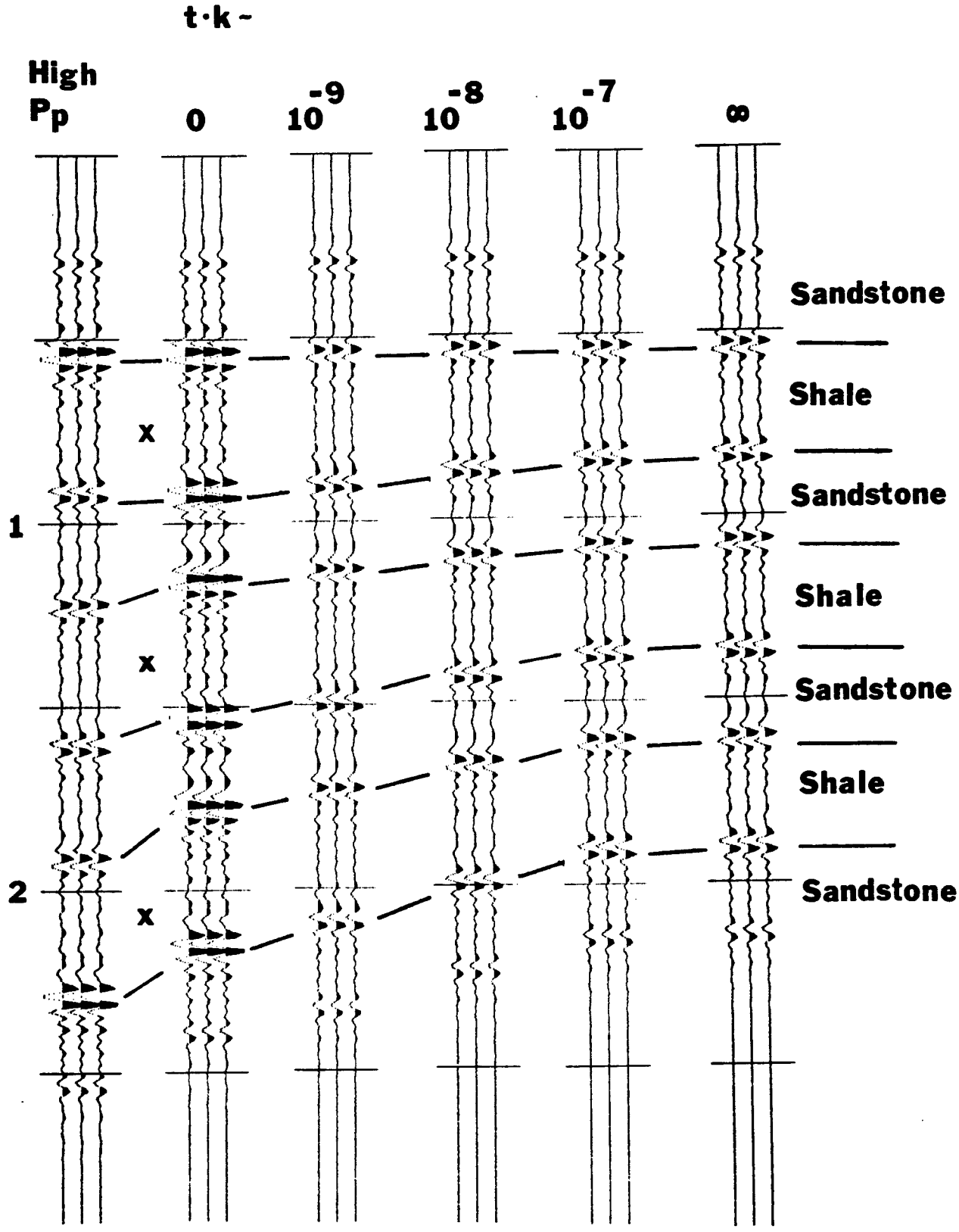

Figure 16. Synthetic seismograms computed for the interbedded sand-shale sequence as pore pressure decays. This case is for initial high pore pressure in the shale and low pore pressure in the sandstone.

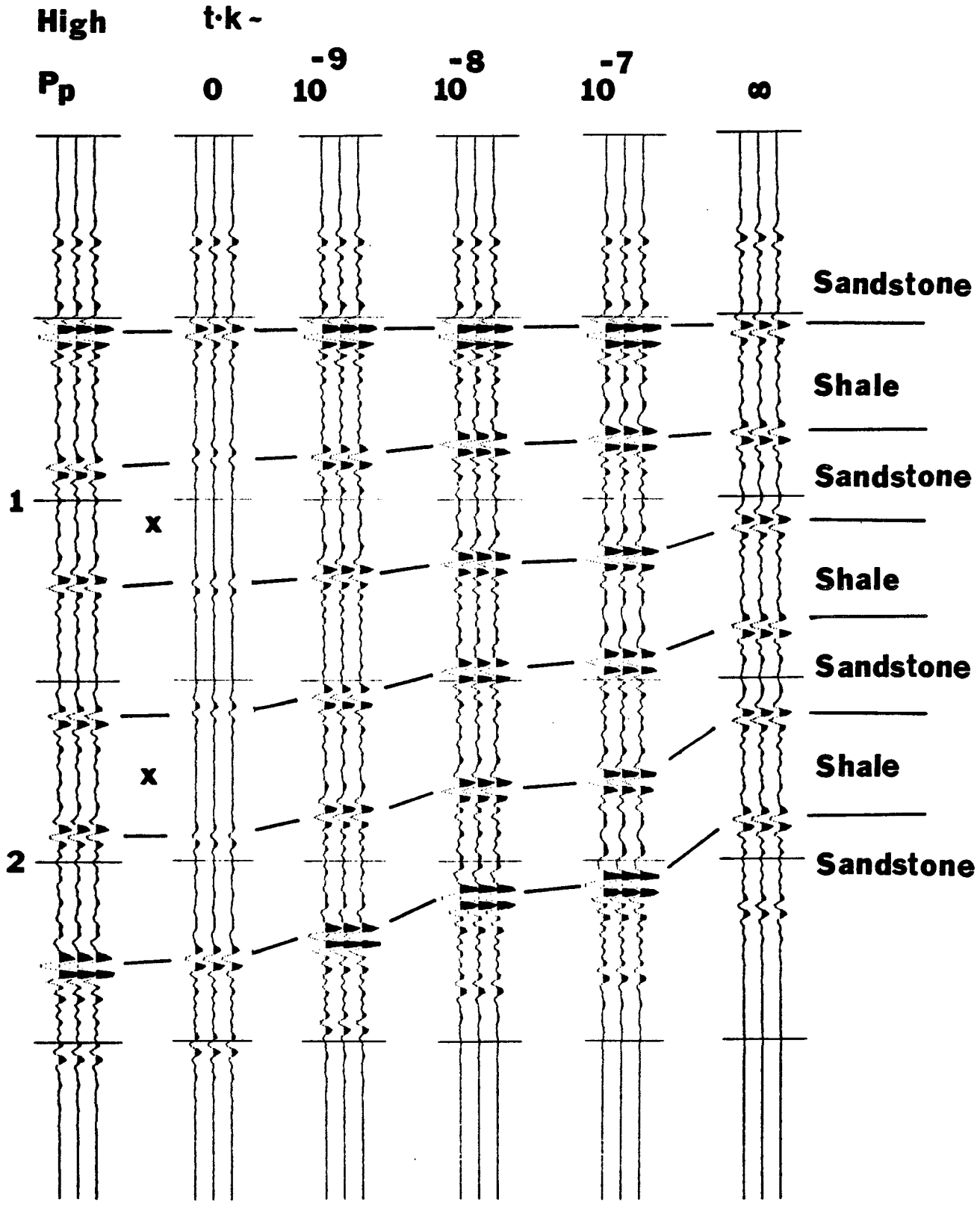

Figure 17. Synthetic seismograms computed for the interbedded sand-shale sequence as pore pressure decays. This case is for initial high pore pressure in the sandstone and low pore pressure in the shale.

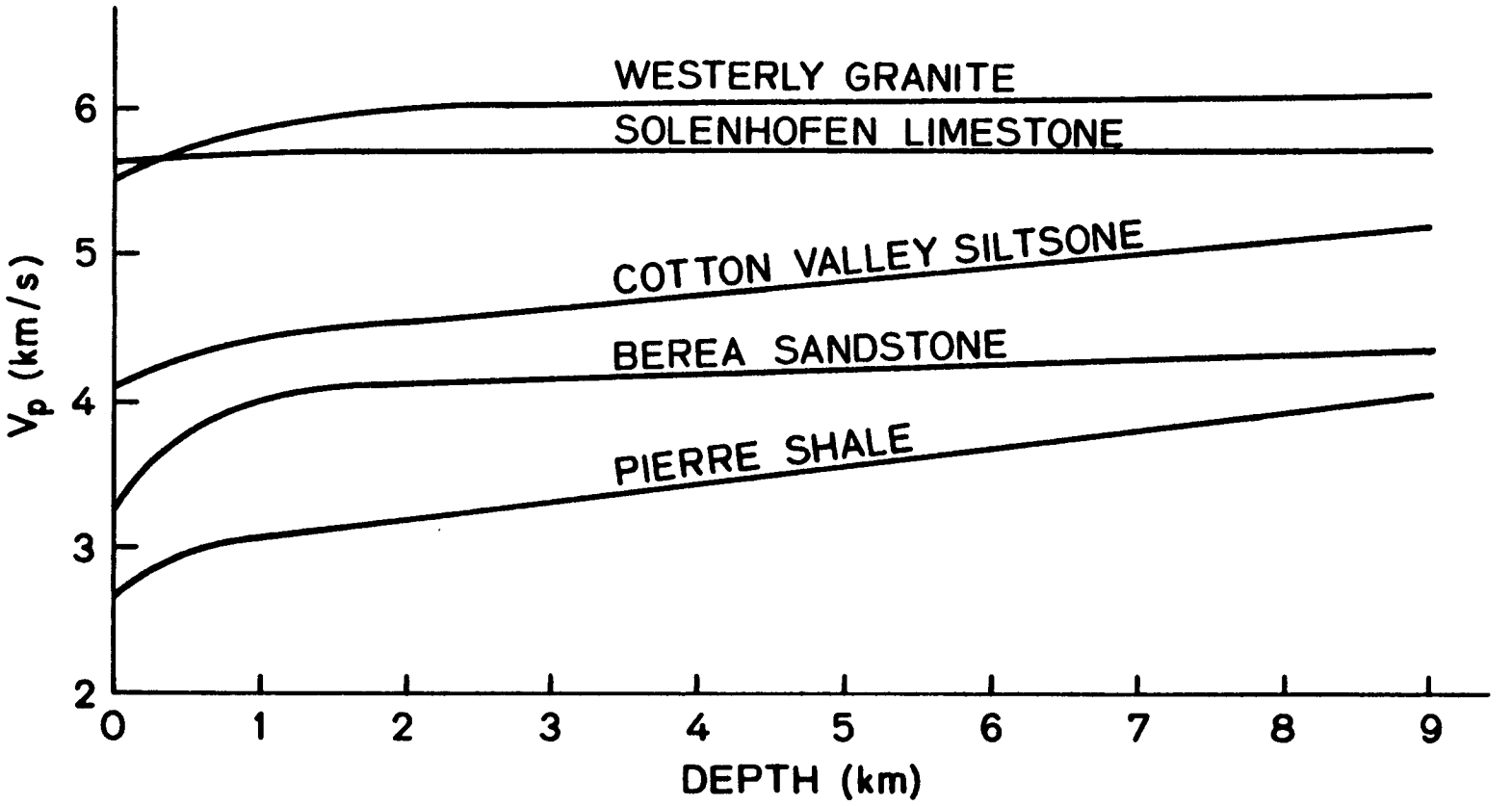

Figure 18. Velocity as a function of depth of burial for some typical crustal rocks.

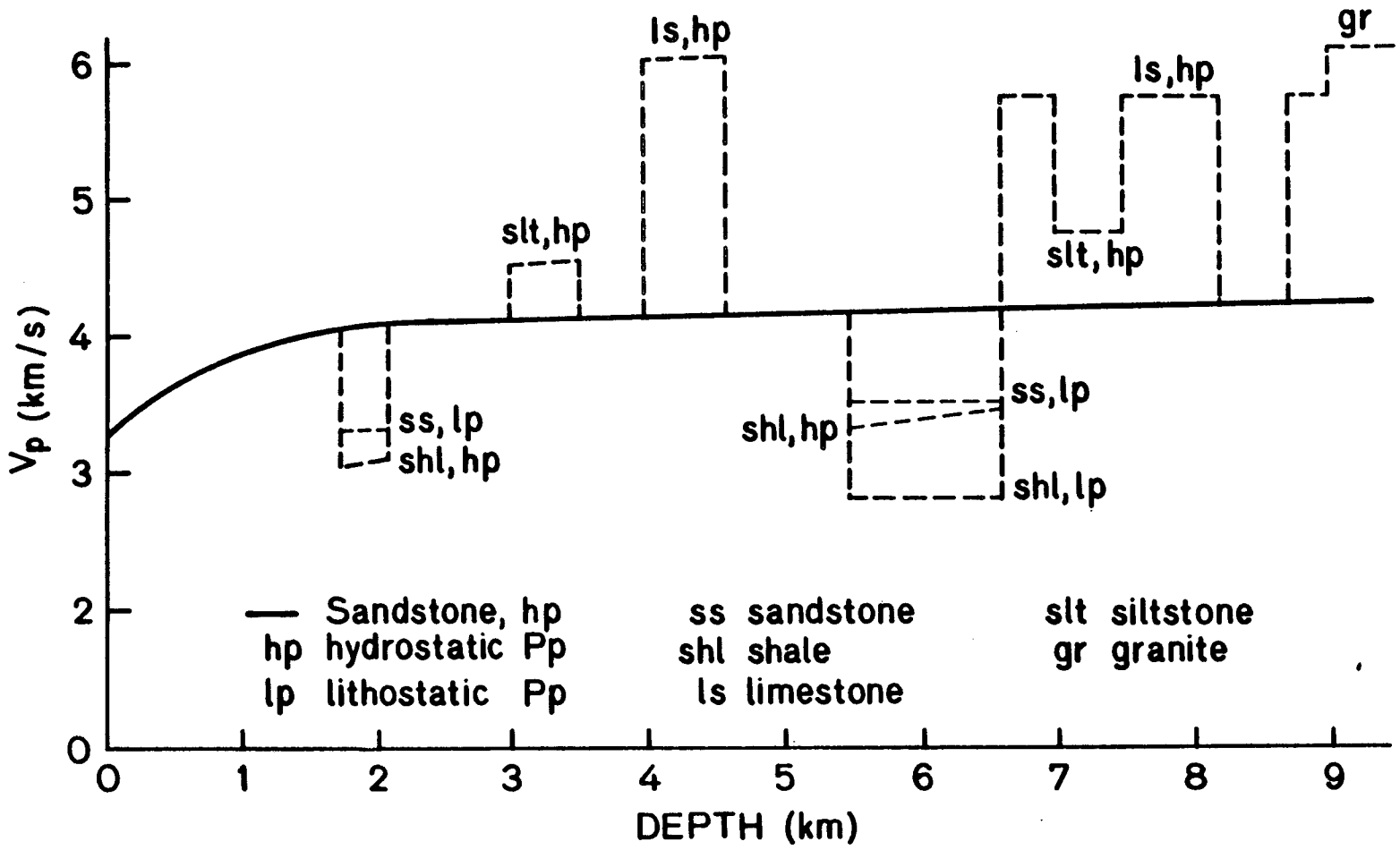

Figure 19. Model for the velocity structure of the Green River basin based on laboratory velocity data. The solid line is for a normally pressurized sandstone. The dashed lines show how departures from this velocity profile may be modeled by lithologic variations, or in the case of the low velocity zone at 5.5 to 6.5 kilometers, by a high pore pressure zone.

Chapter 5

THE NATURE OF SEISMIC REFLECTIONS FROM DEEP CRUSTAL FAULT ZONES

ABSTRACT

Deep seismic reflection profiles in many parts of the world have recorded reflections from ductile shear zones within the crystalline basement, in some cases below the brittle-ductile transition. Perhaps the best example is the COCORP Wind River Line in Wyoming. The Wind River thrust fault is a strong reflector from the surface to depths of 25 to 32 kilometers. Measurements of compressional wave velocity and velocity anisotropy are reported in a number of mylonites recovered from exhumed ductile shear zones in an attempt to identify the physical properties responsible for the seismic signal from fault zones. These rocks, which were deformed under greenschist grade conditions, are characterized by extensive ductile deformation of plastic minerals, brittle deformation of the more rigid minerals, a tectonically induced grain size reduction, and development of a strong fabric. Samples are subjected to a confining pressure of one kilobar, and measurements were done on both dry samples and water saturated samples at various pore pressures. Velocity and density were not found to change significantly between the mylonites and the adjacent undeformed protoliths. Seismic anisotropy of 7% or greater is present in several mylonites. Samples showing the strongest anisotropy have a high content of layered silicates, a low content of feldspars, and a uniformly aphanitic texture. Many mylonitic rocks studied do not have strong seismic anisotropy despite extensive deformation and a well developed macroscopic foliation. Samples with low anisotropy are characterized by low content of layered silicates, high content of feldspars, and a porphyroclastic texture.

Where anisotropy is present, velocities are slowest perpendicular to the foliation and fastest parallel to both foliation and lineation. Using our data on mylonite velocities and models for the crustal structure near the Wind River range, Wyoming, we compute true amplitude synthetic seismograms and compare them to true amplitude plots of the COCORP Wind River data to identify cases in which ductile shear zones may be strong reflectors at mid-crustal depths. When the fine layered structure of the fault zone is considered, as well as anisotropic effects, our laboratory velocity measurements indicate fairly strong reflections from mylonite zones in most cases. It is also shown that in some cases zones of near lithostatic pore pressure trapped in shear zones may produce strong reflections. However a permeability of the fault zone on the order of 10^{-16} darcy is required to maintain sufficient pore pressure to produce a velocity anomaly in a fault zone which has long been inactive.

INTRODUCTION

In recent years the seismic reflection technique has been applied with increasing success to the study of the entire thickness of the continental crust (Dohr and Meissner, 1975; Schilt et. al., 1979). One of the significant results of this work and problems in interpretation is the observation that zones of deformation or faulting are traceable throughout the thickness of the crust (Oliver, 1982), and in some cases major fault zones have been found which were previously unsuspected from geological investigations (Kaila et. al., 1979). Table 1 summerizes recent investigations which report possible seismic reflections observed from fault zones within the crystalline basement. These zones of strain localization were formed at depths within the crust where deformation was predominately ductile. Although many have since been uplifted into the brittle regime their petrogenesis is controlled by the synkinematic ductile deformation, hence when we are primarily concerned with the petrology and petrofabric of fault zones rather than their geometry we will refer to them as ductile shear zones.

Perhaps the most striking example of reflections from deep fault zones is the COCORP reflection survey in the Wind River mountains, Wyoming. Figure 1 shows a portion of COCORP Wind River line 1 in which the Pacific Creek thrust fault is seen as a strong reflector at 5.5 to 6.5 seconds. The layered sediments of the Green River basin are visible to about 4.4 seconds. Below is Precambrian crystalline basement. The Wind River thrust to the east apparently generates reflections through 20 to 30 kilometers of the crust. Lynn (1979) and Brewer et. al. (1982) discuss the general features of this line. Figure 2 is a portion of Wind River lines 1 and 1a showing the reflections from the Wind River thrust in the upper crust. The fault zone reflection is also strong in the mid-crust at 4 to 10 seconds two-way travel time (Figure 3). Approximate depth in kilometers may be estimated by multiplying the two-way travel time by 2.0 to 2.5 in the sedimentary section and by 3.0 in the crystalline section.

The continuation of the fault on line 2 to about 12 seconds is debatable. Lynn (1979) reports that the Wind River thrust may be traced on the migrated data from the surface to a depth of 32 kilometers where it flattens to near horizontal from its original dip of about 30 degrees and dies out. Figure 4 shows detail of the events in line 2 interpreted to be from the deeper portions of the Wind River thrust. Zawislak and Smithson (1981) believe that these events are multiples from the shallow sedimentary section of the Wind River basin. Modeling by Jones (1983) indicate these events most likely are not multiples and are due to horizons within the crystalline basement. Regardless, the evidence for seismic reflections throughout most of the crust is convincing. In Figures 1 through 4 it may be seen that the fault zone has a substantial thickness, up to 4 kilometers in places. Reflections are multicyclic, and the fault zone consists of multiple and anastomosing bands of reflections with considerable variation in amplitude. The total offset is only about 0.6 kilometers in the case of the Pacific Creek thrust, compared to 30 kilometers for the Wind River thrust (Lynn, 1979) yet they both cause very strong reflections. The faults offsets portions of the crystalline basement. We believe that the reflections are not caused by impedance contrasts across the fault due to juxtaposed blocks of different seismic impedances. The relatively

small offset on the Pacific Creek thrust makes it unlikely that large impedance contrasts could occur over such a small distance. The reflections apparently emanate from the fault zones.

Sibson (1977) has reviewed the structure and petrology of fault zones at various depths within the earths crust. Figure 5 (adapted from Sibson, 1977) shows schematically the deep structure of a fault zone as inferred from rocks presently exposed on the earth's surface. The depth boundaries of transition to different types of behavior are approximate, depending on rock type and mineralogy, strain rate, presence of fluids, heat flow, etc.

In the upper one to four kilometers brittle processes dominate and incohesive gouge and breccia are formed, often containing significant amounts of clays (Wu, 1978). We might expect these materials to have significantly reduced velocities due to the lack of cohesion, high clay content, and extensive fracturing. Indeed anomalously low velocities are observed in situ in the upper portion of the San Andreas fault (Mayer-Rosa, 1973; Healy and Peak, 1975; Aki and Lee, 1976; McEvilly, 1981) and laboratory measurements on fault gouge show a correspondingly low velocity (Wang et. al., 1978). Here we are primarily interested in the properties of the fault below the gouge zone. As the depth increases the confining pressure is such that although deformation is still predominately brittle the rocks become more cohesive and form relatively low porosity cataclasites, which have random fabrics and a reduced grain size. At still greater depths of 10-15 kilometers and 250–350°C, corresponding approximately to greenschist metamorphic grade, ductile processes begin to predominate over brittle ones and mylonites are formed. These are cohesive, low porosity rocks with well developed fabrics and a tectonically induced grain size reduction. Zones of mylonites are often several kilometers thick in surface exposures and consist of multiple and undulating bands of varying fabric and intensity of deformation (Higgens, 1971). The strain is gradational from the undeformed protolith to the highly deformed mylonites and discrete slip surfaces are not present unless they formed after uplift to more brittle conditions.

It has been suggested by Lynn (1979) and Smithson et. al. (1979) that these thick sequences of mylonites might be responsible for the seismic reflections if their seismic impedance has been altered during deformation. It has also been proposed that mylonites may cause seismic reflections due to elastic anisotropy, as their pervasive fabric (Kosada, 1980; Lawrence, 1978; Sibson, 1977; Higgens, 1971) is similar to fabrics in regionally metamorphosed rocks which are known to be seismically anisotropic (Birch, 1960; Kern and Richter, 1981; Kern and Fakhimi, 1975; Meissner and Fakhimi, 1977; Christensen, 1965; Johnson and Wenk, 1974; Wang et. al., 1975). If strong seismic anisotropy is present and suitably oriented within the fault zone it could cause reflections even if the average velocity had not changed during deformation. Seismic anisotropy has been observed in situ around fault zones (Rezanov and Galdin, 1967), and in terrains of schistose rock (Kitsunezaki, 1964) at shallow depths. Furthermore the complex structural layering often observed in thick mylonite zones (Higgens, 1971) is similar to that of cyclic sedimentary sequences which can produce anomalously strong reflections due to constructive interference for certain wavelength to thickness ratios (Morlet et. al., 1982).

Unfortunately there has as yet been no systematic study of seismic velocities in typical deep seated shear zone rocks to evaluate these possibilities. Jones and Nur (1982 and 1983) present preliminary measurements on mylonites in continental rocks and Karson (1982) reports measurements on some ultramafic mylonites. In this paper we present field observations of some well exposed continental ductile shear zones as well as velocity and velocity anisotropy data in mylonites and cataclasites and the surrounding undeformed rocks collected from exhumed ductile deformation zones. In collaboration with seismic modeling of reflections from fault zones in the COCORP Wind River line we can identify the conditions under which ductile shear zones are expected to be seismic reflectors deep in the continental crust.

Fault zones are of great importance as they are the localization of much of the earth's tectonic movements. They are also the source of earthquake

generation and the associated hazards. Can we always expect to observe deep crustal shear zones on seismic reflection data, and if so what physical properties of the ductile shear zone are responsible for the strong reflections, and what may be learned regarding the in situ state of deep crustal zones of deformation? If these questions may be addressed then we have an important tool for mapping and investigating these features in situ. This problem is also important for economic reasons. Extensive thrusting may cause basement shear zones to occur over sedimentary strata in overthrust belts, as does the upper portion of the Wind River thrust (Figure 2), and hence the shear zone must be penetrated in hydrocarbon exploration. Basement fault zones beneath sedimentary basins may be responsible for creating structures in the overlying sediments which form hydrocarbon traps, as in the case of the Pacific Creek thrust and the overlying Pacific Creek anticline (Figure 1). It also appears that the reflection signal from deformation zones in the crystalline basement may be mistaken for layered sedimentary sequences (Reif and Robinson, 1981). Finally these features may act as zones of hydrothermal mineral concentration (Park and MacDiarmid, 1975), and conduits for magma migration (R. Meissner, personal communication, 1982).

FIELD STUDIES AND SAMPLE DESCRIPTIONS

Samples of mylonites and their associated protolithic equivalents have been collected from three well exposed ductile shear zones, the Columbia River fault zone in southeastern British Columbia, the Winters Pass thrust in southeastern California, and the Goat Rock and Bartletts Ferry fault zones in eastern Alabama.

The most detailed sampling was done in the Columbia River fault zone. It is a zone of mylonites of about one kilometer structural thickness. In Figure 6 the large dots indicate locations of samples for detailed laboratory analysis of petrography and physical properties. The mylonites separate and incorporate two distinct protolithic units. Precambrian high grade gneisses and metasediments of the Monashee metamorphic complex to the west form the footwall. The hanging wall is Mesozoic granodiorite of the Clauchnacudainn

Salient to the east. Synkinematic mineral assemblages indicate the mylonites were deformed at greenschist metamorphic grade. (Read and Brown, 1981). The fault, which was active from mid-Mesozoic to Eocene, displaces metamorphic isograds 15 kilometers vertically, and likely has much greater total offset (Read and Brown, 1981). It probably represents a decollement zone upon which allocthonous units of the Selkirk terrain were thrust to the east over the Monashee complex (Read and Brown, 1981). The fault zone currently dips 10 to 30 degrees to the east. More recent deformation during uplift has produced small zones of fault gouge and cataclasite within the mylonite zone and locally has produced intense folding of the mylonitic fabric. Similar mylonite zones are commonly described bounding Precambrian core complexes throughout the Cordillera (Crittenden et. al., 1980).

Field relationships show a gradational strain which transforms the granodiorite of the hanging wall into a fine grained, intensely deformed mylonite. The mylonitic metasediments, which are derived from pelitic and semi-pelitic rocks of the Monashee complex are also highly strained. No samples of undeformed footwall rocks were obtained.

The mylonites have a compositional banding which is parallel to the boundaries of the shear zone and is formed by differentiation of coarse grained, porphyroclast-rich, quartzo-feldspathic layers from fine grained, mafic-rich, porphyroclast-poor layers (Brown and Murphy, 1982). A strong foliation (flattening fabric) is ubiquitous and is parallel or subparallel to the compositional banding. A stretching lineation is also frequently present (Brown and Murphy, 1982).

X-ray diffraction modal analysis for these samples and the ones to be described later are presented in Table 2. Details of the textural changes associated with mylonitization of the Columbia River rocks are illustrated by thin section photomicrographs shown in Figures 7 through 9.

The protolith (7a) has a coarse grained primary igneous texture exhibiting evidence of only minor strain. In the mylonitized granodiorite (7b) the quartz, biotite, and chlorite have been reduced to a very fine grained matrix which appears to flow around large broken fragments of feldspars.

Biotite and chlorite are strongly foliated and elongate quartz aggregates form a consistent lineation within the foliation plane. Deformation has been predominately ductile for the quartz and micas and brittle for the feldspars. The mylonitic metasediments (Figures 8 and 9) are shown under plane polarized light which emphasizes the texture due to the pleochroic layered silicates. The mylonitic metasediment lacks the large feldspar porphyroclasts present in the mylonitic granodiorite, but fine grained feldspars are present. The strongly anisotropic fabric has been produced by ductile deformation of the quartz and phyllosilicates which have been reduced to very fine grained layers. The feldspars deformed primarily by fracturing and rigid body rotation. The cataclasite (Figure 9b) is not significantly different than the mylonite in hand samples, having high cohesion and low porosity. However in thin section the deformation is seen to be predominately brittle and there has been little or no development of a fabric. Grain size reduction has been more uniform for all minerals.

CR 14 (Figure 8a) has a relatively weak fabric in thin section, although the compositional banding is striking in hand specimen. CR 16 (Figure 8b) has a strong phyllosilicate fabric. Compositional differentiation of quartzo-feldspathic layers (light bands) from mafic layers (dark bands) is pronounced in thin section although it is to small to see in hand samples. CR 17 (Figure 9a) again shows the quartz and biotite reduced to fine grained layers undulating about the much larger feldspar porphyroclasts.

The second fault zone sampled is the Winters Pass thrust, part of the Clark Mountain thrust complex in the Mojave Desert, east of Baker, California. The thrust forms the contact between Precambrian crystalline rocks of the hanging wall and Cambrian sedimentary units of the footwall. Both units have been mylonitized under greenschist facies conditions (Burchfiel and Davis, 1971).

A thin section photomicrograph of the mylonitized crystalline rock (WP 6, shown in Figure 10a) displays a classic flaser gneiss texture. A fine grained, highly deformed and foliated matrix of recrystallized quartz and biotite undulate around feldspar porphyroclasts. The micacous quartzite (WP 8,

Figure 10b) is very fine grained (blastomylonitic). The absence of feldspar porphyroclasts give it the most uniform and pervasive fabric of any rock examined. Both samples have a well developed foliation formed by parallel alignment of the phyllosilicates and a lineation formed by elongate quartz aggregates lying in the foliation plane.

We have also obtained samples from the Goat Rock and Bartletts Ferry mylonite zones in Alabama, as well as the gneissic rocks which are in contact with the mylonites (Figure 11). These faults are composed of thick sequences of highly deformed mylonites with steep dips. These samples are particularly intriguing as some interpretations (Cook et al., 1979; Cook and Oliver, 1981; Clark et. al., 1978; Harris and Boyer, 1975) indicate they may root in the master decollement underneath the Appalachians and hence may directly correlate to deep seismic reflections observed on the COCORP profile of the coastal plain of Georgia. In this line the decollement appears as a strong reflector at two-way travel times of 3 to 6 seconds. Splays off the decollement towards the surface correlate well with surface exposures of mylonite zones (Cook et al., 1981).

In thin section (Figure 12) the mylonites show textures similar to those previously examined. There is pronounced compositional banding, a strong foliation parallel or nearly parallel to banding, and sometimes a stretching lineation is present. Quartz and the layered silicates form extremely fine grained layers which undulate about the abundant and obviously brittle feldspar porphyroclasts. The protoliths in this case are gneissic metamorphic rocks of the Pine Mountain block of the Alabama Piedmont and are also strongly foliated and compositionally banded (Figure 13). They may be distinguished from the tectonically altered rocks by the larger grain size in the regionally metamorphosed rock.

In an attempt to obtain more quantitative information on the relative strengths of phyllosilicate fabrics in mylonitic rocks we have had x-ray goniometry analysis done on samples CR 1, CR 11, CR 12, CR 14, CR 15, CR 16, CR 17, CR 18, WP 6, and WP 8. The technique is described by Etheridge and Oertel (1979). Basically it measures the preferred orientation of c axes of

phyllosilicates. It was found that samples CR 1, CR 11, CR 12, CR 14, CR 15, CR 17, and CR 18 had a fabric which was insufficiently developed to measure by this method. Hence despite the striking fabric of many of these rocks in hand specimen the preferred orientation of phyllosilicates on the scale of these measurements (a few cubic millimeters) is rather weak. This is particularly true of samples containing large amounts of feldspar porphyroclasts which tend to disturb the phyllosilicate fabric.

Samples WP 6, WP 8, and CR 16 did produce usable pole figures which are shown in Figures 14, 15, and 16. Contours represent values of intensity of phyllosilicate c axes in multiples of a uniform distribution (Lipshie et al., 1976). Sample CR 16 has an extremely strong fabric and a near axial symmetry (Figure 14). Samples WP 6 (Figure 15) and WP 8 (Figure 16) have a well developed fabric and an orthorombic symmetry, with a secondary pole nearly parallel to the stretching lineation. These samples which have the strongest fabric have a relatively high phyllosilicate composition and little or no feldspars, hence the fabric is undisturbed by the presence of brittle porphyroclasts. This observation appears to be consistent with observations of thin sections where samples CR 16, WP 6, and WP 8 appeared to have the strongest foliation of layer silicates.

DETERMINATION OF PHYSICAL PROPERTIES

The parameters which control the reflection of seismic energy from interfaces within the earth are the thickness, density, and the complex and frequency dependent stiffness tensor of each unit. The thickness of mylonite zones may be estimated from surface mapping and the reflection data. Densities of crystalline rocks may be adequately determined by measurements at room conditions.

It is generally not practical to make complete measurements of the stiffness tensor in an anisotropic material. However for rocks with a high degree of symmetry velocity measurements parallel to the three principal axes adequately determine its properties. The mylonites examined here apparently display an orthorombic or higher symmetry. The planer fabrics are

parallel or near parallel to the regional trend of the fault zone. The linear fabric, where present, lies within the foliation plane. Furthermore for the relatively small amounts of anisotropy considered here small deviations from this simple symmetry pattern will not have a noticeable effect.

If we assume an orthorombic or higher symmetry of the stiffness tensor the complicated equations for reflection coefficients in a general anisotropic media (Daley and Hron, 1979) simplify greatly for normal incidence and for one of the principal axes parallel to the direction of wave propagation. We may then consider only the velocity or velocity contrast in the direction of wave propagation to compute the reflection coefficient. In the deep surveys of interest here all reflections will be very near normal incidence. The orientation of fabric elements parallel to the fault plane suggest that one of the principal velocity axes will be parallel to normally incident waves.

Hence for our velocity determinations we have measured the velocities in three orthogonal directions oriented with respect to the fabric elements of the rock where present and in three orthogonal directions oriented randomly for the undeformed rocks where no fabric is present.

Velocity was measured using standard ultrasonic techniques at a frequency of 500 kiloHertz. Under appropriate in situ conditions for these samples velocity dispersion is likely to be very small, and we are primarily interested in relative differences in the ultrasonic measurements. Attenuation contrasts may effect reflection coefficients as well (Kjartansson, 1979) but the contributions are negligible at mid-crustal depths.

Velocity was measured versus confining pressure up to one kilobar for dry samples and for water saturated samples at various pore pressures. Sample dimensions were 5 in centimeters in diameter and 7 centimeters long. While mylonite zones are subject to much greater pressures at mid-crustal depths it was decided that it was more important to use large samples and wavelengths relative to the strong heterogeneities of the mylonites rather than go to higher pressures and be forced to use correspondingly smaller samples and wavelengths. At one kilobar pressure much of the porosity is closed and the greatest portion of the velocity increase with pressure has occurred (Wang

and Simmons, 1979), hence these measurements should be a good indication of relative velocity values at depth.

Figures 17-46 show the compressional velocities plotted versus pressure for the samples described previously. Figures 17-21 are velocities for the Columbia River fault zone protolith, Figures 22-23 are for the Columbia River fault zone mylonitic granodiorite, Figures 24 and 25 and 27-29 are the Columbia River mylonitic metasediment, and Figure 26 is for the Columbia River cataclasite. For samples CR 7, CR 13, CR 16, and CR 18 (Figures 20, 24, 27, and 29) we also report shear velocity measurements. Figures 29 and 30 are velocity measurements in the Winters Pass mylonites WP 6 and WP 8. The Appalachian rocks are shown in Figures 32-37. Figures 32 and 35 are the mylonites. The remainder are for the adjacent regionally metamorphosed rocks. Figures 38 through 46 show velocity versus pressure in selected samples which have been water saturated and measured at various pore pressures up to 825 bars. For the saturated samples the velocity is plotted versus effective pressure, which is defined as confining pressure minus pore pressure. The velocity and density data for all samples at one kilobar is summarized in more concise form in Table 3.

INTERPRETATION OF VELOCITY MEASUREMENTS

The data do not indicate any striking change of seismic velocity or density accompanying mylonitization. The Columbia River mylonites formed from the granodiorite seem to have slightly greater velocities and densities than the protolith, but the variation is small compared to the variation of properties within the granodiorite body itself. Surprisingly, despite the development of a strong fabric accompanying mylonitization as described earlier, there is no large increase in anisotropy over the granodiorite of nearly isotropic fabric.

Velocity and density in the mylonitic metasediments and the Winters Pass mylonites are more variable, probably reflecting a greater variation of protolithic composition. No samples of the protoliths of these rocks were available, however the velocities are comparable to values commonly

measured in gneissic rock of similar composition (Meissner and Fakhimi, 1977; Kern and Richter, 1981).

The cataclasite also shows no strong change in velocity or density. Although deformation was predominately brittle, under high confining pressures the cataclasite maintains high cohesion and low porosity. Its random fabric produces no significant anisotropy.

The Appalachian rocks also display no strong variation in physical properties between the tectonically altered and the regionally metamorphosed samples. Sample A 3 has been extensively weathered which accounts for its anomalously low velocity. Otherwise velocities are normal for rocks of similar composition. The predominately ductile processes involved in mylonitization produce a cohesive, low porosity rock leaving no reason to expect a large change of velocity or density during mylonitization, as the measurements indicate.

The anisotropy of the mylonites at elevated pressure is generally small. Only one of the Columbia River samples (CR 16) has strong anisotropy. It has an aphanitic texture, is rich in chlorite, and was the only sample with a poorly developed macroscopic fabric. All other Columbia River mylonites exhibit anisotropy no more than 7%. Both Winter Pass samples are strongly anisotropic. They both contain large amounts of biotite, but WP 8 with the highest anisotropy has an aphanitic texture similar to CR 16.

The anisotropy of the Appalachian mylonites is generally smaller then the anisotropy of the adjacent coarser grained regionally metamorphosed rocks. It has been re-oriented however by the shearing parallel to the fault plane so there may be some contrast in physical properties across the fault zone due to re-orientation of fabric.

The elastic anisotropy of the mineral constituents, together with their concentration and preferred orientation determine the anisotropy of a rock at high pressure. Table 4 shows the theoretical anisotropy of some common minerals, computed from single crystal elastic constants (Simmons and Wang, 1971; Babuska, 1981). Also included in Table 4 are some brief comments regarding the primary deformation style in crustal rocks (Carter, 1976).

Although feldspars are strongly anisotropic, mechanically they are strong and brittle and are therefore deformed by fracturing and rigid body rotation under greenschist conditions. Hence they are not observed to develop a preferred orientation of crystallographic axes in mylonites examined here and are not expected to increase seismic anisotropy.

Quartz is readily deformed and recrystallized to form fine grained aggregates with a preferred orientation of the c axis. The maximum seismic anisotropy in quartz is 26%, which occurs at an angle to the crystallographic axes. The maximum anisotropy between crystallographic axes, which will control response to ductile deformation is only 11%, so even a very strong quartz fabric will not cause large anisotropy.

The phyllosilicates are strongly anisotropic, and are very ductile as shown by their fine grain size and preferred orientation of the c axis normal to foliation in the mylonites. The low velocity in pyllosilicates is parallel to the c axis. Hence we expect the seismic anisotropy in silicic and intermediate rocks to be controlled by the concentration and degree of orientation of phyllosilicates, as our data seem to support. The three samples with the highest anisotropy, CR 16, WP 6, and WP 8 are richest in phyllosilicates. These were also the only three samples with a sufficiently strong fabric to yield good pole figures in the x-ray goniometry experiment (Figures 12-14).

Another fabric element is important. WP 6 has less anisotropy than WP 8 although it has more biotite. WP 6 contains abundant feldspar porphyroclasts around which the foliation undulates (see Figure 9a), diluting the preferred orientation of biotite and producing lower anisotropy. The texture of WP 8 is uniformly aphanitic (Figure 9b) so the foliation is undisturbed by any porphyroclasts, hence higher anisotropy. Similarly CR 16 contains no porphyroclasts and has much higher anisotropy than CR 14, CR 17, and CR 18 which have nearly as much chlorite, but many feldspar porphyroclasts. Note also the strong preferred orientation of phyllosilicate c axes in Figure 14. The mylonitic granodiorites have a low content of phyllosilicates and many feldspar porphyroclasts, hence low anisotropy. The inability to obtain usable pole figures indicates low preferred orientation of anisotropic minerals.

Hence feldspars may actually reduce seismic anisotropy. In some cases higher grade rocks contain feldspars which have undergone ductile deformation (Goldstien, 1982) and have a strong fabric (Lawrence, 1978), so they may contribute to seismic anisotropy. With strong fabrics of mafic minerals in very high grade rocks significant anisotropy may also be present (Christensen, 1971; Karson, 1982).

In summary, our data shows that to produce strong overall seismic anisotropy requires a mineral which is strongly anisotropic, is a substantial component of the rock, deforms readily by ductile processes forming a strong preferred orientation of crystallographic axes, and whose fabric is undisturbed by a porphyroclastic texture. Furthermore it should be noted that macroscopic fabric anisotropy is not a reliable indicator of elastic anisotropy. The highly anisotropic sample CR 16 appeared only weakly foliated in hand specimen, in contrast to the very strong macroscopic fabrics in CR 14 and CR 17 which had much lower seismic anisotropy. The relationship of composition to seismic anisotropy is shown graphically in Figure 47, where we have plotted the percent seismic anisotropy versus the relative phyllosilicate to feldspar composition.

The orientation of the anisotropy is such that the slowest direction is generally parallel to the foliation. This is controlled by the preferred orientation of phyllosilicate c axes perpendicular to foliation (Figures 14-16), the c axis being the slow direction in phyllosilicates (Table 4). Many of the samples are also significantly anisotropic within the foliation plane, the faster direction usually parallel to the stretching lineation. We believe that this anisotropy may be due to subsidiary phyllosilicate c axis poles as seen on the pole figures in Figures 14-16.

The addition of water to the pore space increased the velocity in all samples, but did not change significantly the relative values of the velocities. The anisotropy decreased in some cases upon the addition of water (notably WP 6) and increased in one case (CR 17). The greatest effect of pore fluids on velocity contrasts in fault zones would likely be if a saturated rock was in contact with a dry samples or if a large gradient in pore pressure existed.

The effect of pore fluids in increasing velocity was greatest at low effective pressures where more porosity was open. After a rock is saturated increasing pore pressure at constant effective pressure caused further increase in velocity, indicating confining pressure is more effective in closing pores then pore pressure is in opening them.

Note that the addition of water at elevated pore pressure has the effect of flattening the velocity-pressure dependence, making it easier to extrapolate to elevated pressures, but making it less likely that pore pressure gradients may be responsible for large reflection coefficients.

MODELING OF FAULT ZONE REFLECTIONS

Laboratory data have been presented on mylonites thought to be analogous to the type of rocks which would be found at depth in the Pacific Creek or Wind River fault zones. The Precambrian basement of the Wind River range is very similar in composition (Bayley et. al., 1973), as well as velocity and density (Smithson and Ebens, 1971) to the samples from the Columbia River fault zone, particularly the granodiorites. Taken individually most of the measurements do not suggest a strong contrast of physical properties between the protolith and the mylonite. The anisotropy in the mylonitic granodiorite is only slightly greater than that of the protolith. Some of the Columbia River mylonitic metasediments are anisotropic and display variations in velocity, but likely little more than that found in an undeformed sequence of metasedimentary units. Likewise samples from the Winters Pass thrust show strong anisotropy, but not significantly more than has been measured on foliated, regionally metamorphosed rocks (Birch, 1960; Christensen, 1965; Kern and Fakhimi, 1975, Meissner and Fakhimi, 1977; Wang et. al., 1975). Anisotropy and velocity for the Appalachian mylonites is within the range of their protoliths. This led us to suggest earlier (Jones and Nur, 1982) that measured velocities might not account for observed reflections from ductile shear zones. Ignored in the earlier work was the effect of re-orientation of anisotropy and cyclic layering which could cause large amplitudes of reflected waves from a series of interfaces of relatively small

reflection coefficients.

Using models for the velocity and attenuation structure of the crust in this area (Jones, 1983) and our laboratory data on physical properties in mylonitic rocks we are now in a position to develop quantitative models to determine if a given velocity structure in a basement fault zone can account for the reflections from the Wind River line. We will approach this by generating true amplitude seismic sections of the Wind River reflection data where the amplitudes have been corrected for losses due to spherical divergence and attenuation (Jones, 1983). The synthetics are then gained using the same gain function as the data and the amplitudes may be directly compared (Jones, 1983).

We also note that spectral analysis of deep basement reflections, as well as the ringing character on the time section indicates they are not caused by a step discontinuity of velocity, rather by a series of alternating high and low velocity zones of thicknesses ranging from 100 to 300 meters (Jones, 1983). This is in the range of a quarter to a half wavelength which will produce anomalously large amplitudes due to constructive interference. This is a common observation in deep reflection data (Hale and Thompson, 1982). It is also a reasonable model for a fault zone from a geologic standpoint. Zones of ductile deformation commonly have a complex structural layering, analogous to stratification, due to variability of deformation intensity and composition across the fault zone.

Figure 48 shows a portion of COCORP Wind River line 1, stations 430 to 460, true amplitude record. The Pacific Creek thrust fault is the strong series of dipping reflections from about 5.5 to 6.5 seconds. A number of true amplitude synthetics are computed based on our data in an attempt to model the seismic reflections from a ductile fault zone. Synthetic A uses the data from the Columbia River fault zone. The mean velocity of the undeformed granodiorite was used for the basement velocity above the fault zone, and the velocities in the mylonites perpendicular to foliation were used for the fault zone. Synthetics B, C, D, and E were computed for anisotropies of 20%, 13%, 7%, and 4% respectively.

In a one dimensional model it is generally not possible to accurately model effects of anisotropy. However some simplifying assumptions allow us to include this effect. For rocks of orthorombic or higher velocity symmetry the velocities parallel to the principal axes are considered. As anisotropy in mylonites is effected principally by the phyllosilicate anisotropy and fabric, the slow velocity in mylonites is perpendicular to the foliation which is in general parallel to the regional trend of the shear zone. Since deep reflected waves will be very nearly normally incident due to the relatively small offset, we may consider the velocities in a mylonite zone to be effected only by the velocity measured perpendicular to foliation. The synthetics B through F are thus computed using an alternating series of layers, one having a velocity that of a sample perpendicular to foliation, the next having a velocity the mean of velocities measured in all three orthogonal directions. This is meant to correspond to zones of intensely deformed and anisotropic rock in contact with isotropic zones of less deformation or of lower phyllosilicate composition. Synthetic B is based on laboratory data for sample WP 8, synthetic C for CR 16, and WP 6, synthetic D for CR 13, 14, 18, and A 5, and synthetic E for samples with low anisotropy such as A1, CR 11, CR 12, and CR 17.

Synthetic F is computed based on data from the Appalachian mylonites. As deformation here occurs in a previously metamorphosed, foliated rock we have used an alternating series of thin layers, one having a velocity perpendicular to foliation (the mylonitic zone) in contact with a with a zone of velocity parallel to foliation (the metamorphic protolith). This obviously yields a larger velocity contrast at each contact and is meant to correspond to maximum re-orientation of anisotropy locally by deformation.

Based on this modeling we see evidence for seismic reflections from mylonite zones in some cases. For the Columbia River fault zone model (A) reflections are seen from the strongly anisotropic metasedimentary rock (CR 16). Considering anisotropic effects, strong reflections are seen from zones of 20% and 13% anisotropy. Less but still significant energy is reflected from zones of 7% anisotropy. Using an anisotropy of 4%, meant to correspond to that measured in mylonitic granodiorite of low phyllosilicate composition

reflections are also visible, although with much lower amplitudes than is indicated on the data.

Synthetic F shows strong reflections from a fault zone when the effects of re-orientation of fabric in a metamorphic terrain are considered, even though most samples did not in themselves have very strong anisotropy (sample A 3 was not used in modeling as it was felt its properties were overly influenced by weathering).

Figure 49 shows the spectral content of reflections from the Pacific Creek thrust fault (on the right), and for the synthetic models of the fault zone (on the left). The finely layered structure of the fault zone is required by the spectral modeling to get the sharp peaks at 10 to 15 Hz. This laminar structure also causes strong amplification of reflected wave amplitudes due to constructive interference. Hence the amplitudes in our models are highly dependent on layer thickness. Making the layers significantly thicker or thinner could significantly decrease the amplitudes of reflected energy from fault zones. A variation of thicknesses of principal reflecting units along the fault zone could be part of the reason for strong variation in character of reflected waves observed along the Wind River thrust (see Figures 2, 3, and 4) and for its complete disappearance in portions of the section.

Though shallow crustal velocity and attenuation control is not as complete in lines 1a and 2 we have computed models for the reflections from the Wind River thrust based on our data. Figure 50 shows a portion of line 1a, stations 650 to 680, true amplitude record. The Wind River thrust is the series of reflections from 6 to 8 seconds. The synthetics are computed for the same cases as in Figure 48, except that a thickness of 150 meters was used for the fault zone layers, and substantially more of them were required to model the greater apparent thickness of the fault zone on this line.

Both the Columbia River and Appalachian rocks generate strong reflections. An anisotropy of as low as 7% (synthetic D) generates strong reflections as well. Figure 51 shows the spectral content of reflections from the Wind River thrust as well as that of our synthetics based on a laminar model of the fault zone with a lamina thickness of 150 meters.

The continuation of the Wind River thrust on line 2 is controversial, but a series of reflections at 10 to 12 seconds has been interpreted (Lynn, 1979) as the thrust fault. Figure 52 shows a portion of Wind River line 2, stations 330 to 370. The events at 11 to 12 seconds are interpreted to be from the Wind River thrust fault. Our synthetics computed for the same cases as in Figure 50 and 48 show strong reflections from the Columbia River and Appalachian velocity data, as well as for 20% and 13% anisotropy. Modeling of the spectral content of these reflections (Figure 53) produces a reasonable match for a laminar structured fault zone with a thickness of each unit of 300 meters.

In a previous paper (Jones and Nur, 1982) we suggested that zones of anomalously high pore pressure associated with active faults might be partially responsible for the seismic reflections. Since the classic work of Hubbert and Rubey (1959) a near lithostatic pore pressure has been called upon to address problems regarding the state of stress on faults and the strength of rock (Raleigh and Evernden, 1982).

The mylonites we have examined owe their characteristic fabric and texture to predominantly ductile processes. Petrographic work (Murphy, 1980) indicates pore fluids were present at the time of deformation. If this is true, pressure solution of silica should have been active. This tends to reduce porosity (Sprunt and Nur, 1977) and likely have an even more profound effect on permeability by sealing major flow channels. The effect of permeability reduction due to ductile deformation has been observed in the laboratory (Bernabe et. al., 1982). It is also well known that increased pore pressure at constant depth can substantially lower velocities, even in low porosity crystalline rocks (Nur and Simmons, 1969).

Hence it does not seem unreasonable to postulate high pore pressures may exist, at least intermittently, along active fault zones. A problem is that the deformation associated with the Laramide orogeny has been inactive for about 40 million years. Assuming pore pressure was high during faulting, could it be maintained sufficiently high for this length of time after faulting, and presumably the fluid source, has stopped?

Figure 54 shows the transient solution to the diffusion of pore pressure in a medium of permeability k (Carslaw and Jaeger, 1959). Initially a pore pressure of P_0 exists in a zone from -x/L to x/L. The pore pressure at future times as the pressure front diffuses out is shown as a function of distance for the values on the graph times the parameter kt/L^2. Next we consider the effect of pore pressure on velocity. From the data presented here, and other data on crystalline rocks (Christensen and Salisbury, 1975; Nur and Simmons, 1969; Todd and Simmons, 1972) we have developed an empirical relation between velocity and pressure. For a saturated, low porosity crystalline rock of approximately gabbroic composition we use

$$V_p = 6.4 + P_e(.000045) - (0.7)e^{(-0.005P_e)}$$

$$P_e = P_c - \alpha P_p$$

$$\alpha = 1 - 0.5e^{(-P_p/400)}$$

Figure 55 shows the form of this equation for various pore pressures as a function of confining pressure. Combining Figure 54 and 55 we may compute the velocity profile across a zone of anomalous pore pressure as it decays with time. This has been done in Figure 56, selecting a zone of half width 55 meters, implied by spectral modeling of reflections for the Pacific Creek thrust (Jones, 1983). This allows us to plot the velocity profile across this zone for values of the product time (t in seconds) and permeability (k in cm^2). Using several of these zones to model the Pacific Creek thrust we can compute synthetic seismograms as the pressure decays.

Figure 57 shows again the reflections from the Pacific Creek thrust. On the right are five synthetic seismograms at various values of tk, computed as the pore pressure decays. Initially very strong reflections are apparent, which decrease with increasing tk until no energy is reflected.

If we consider that the Laramide thrusting has been inactive for about 40 million years (10^{+15} seconds) to maintain sufficient pore pressure for minimal reflected energy ($tk = 10^{-9}$), would require a permeability of $10^{-24} cm^2$ or 10^{-16} darcy. The lowest values of permeability found in the literature are about $10^{-20} cm^2$ or 10^{-12} darcy for intact crystalline rock (Timmer et. al., 1980). Hence it seems unlikely that permeabilities sufficiently low could be

maintained long enough to provide reflections from a high pore pressure zone along a long inactive fault. The permeabilities we would infer are on the order of those for volume diffusion in oxides and silicates (Brace et. al., 1968). If the thickness of the fault were on the order of one kilometer a permeability of $10^{-20} cm^2$ would be required to maintain high pore pressure for 40 million years, sufficient to cause a strong velocity contrast. This is in the range of the laboratory data of Trimmer et. al. (1980). However the reflection character of a zone of one kilometer would not match as well the reflections from the Wind River or Pacific Creek thrust. Furthermore if the excess pore pressure was distributed over a zone of a wavelength or greater thickness there would be insufficient velocity contrast to cause a seismic reflection.

CONCLUSIONS

In this paper we have combined field observations of ductile fault zones, laboratory measurements of physical properties of mylonites, and true amplitude seismic modeling to investigate the problem of seismic reflections observed from deep crustal shear zones.

Laboratory measurements indicate that the velocity and density of a mylonite is not strongly changed during deformation under mid-crustal conditions from that of the prctolith. Strong anisotropy may develop depending on the composition. Rocks of granodioritic composition have weak anisotropy (2% to 5%). Rocks with high content of phyllosilicates and low content of feldspars may develop substantially greater anisotropy (up to 21%).

The anisotropy is related to the composition and deformation style of the rock. Quartz and phyllosilicates are readily deformed ductilely to form a strong preferred orientation of crystallographic axes. However phyllosilicates have much greater single crystal anisotropy then quartz so the phyllosilicate composition and fabric will control seismic anisotropy. This causes the slow direction to be parallel to the foliation of the deformed rock, as this is parallel to preferred orientation of the phyllosilicate c axis, which is the slow direction in phyllosilicates. Feldspars have large single crystal anisotropy but are deformed primarily by brittle processes hence they do not form strong fabrics

in mylonites and do not contribute to anisotropy. They may in fact reduce seismic anisotropy as the brittle feldspar porphyroclasts dilute the phyllosilicate fabric.

Seismic modeling of the character of amplitudes and frequency content of reflections from the Pacific Creek and Wind River thrust faults indicates they are caused by a laminar structure of alternating high and low velocity zones. Thickness of these zones is about 100 to 300 meters. At this thickness strong constructive interference causes large amplitudes of reflections from zones of relatively small impedance contrasts.

When the Wind River lines are modeled using our data for velocities and densities in mylonitic rocks, strong reflections observed when the laminar structure and anisotropic effects are considered, for an anisotropy of 7% or greater. This is highly dependent on the thickness scale of the principal laminations in the fault zone and the seismic wavelength. If laminations become substantially thinner or thicker the observed reflections from fault zones would be weaker. Variation of thickness of major laminations along dip of the Wind River thrust may account for the change in reflection character with depth along the fault. Optimal layering to produce destructive interference could also account for the lack of reflections from the Wind River thrust at various portions of the record. Another possible cause for the change of character in the Wind River thrust reflections could be a change in content of phyllosilicates or feldspars. Re-orientation of anisotropy due to deformation in a foliated metamorphic terrain may also produce seismic reflections.

Zones of near lithostatic pore pressure have been postulated to control the strength of fault zones and the stress state of the crust. High pore pressure in thin zones along the fault could account for the reflected signal, but it would require permeabilities on the order of 10^{-16} darcy, likely too small even for low porosity crystalline rock, although it is on the order of volume diffusion in silicates with no connected porosity. However, high pore pressure and the resulting low effective pressure should also have the effect of increasing permeability (Brace et. al., 1968).

The interpretation of the reflection record from the COCORP Wind River lines as a zone kilometers in width of a complex, structurally layered, and anastomosing zone of mylonitic rocks of variable intensity of deformation and composition is consistent with field observations of exhumed ductile shear zones, laboratory measurements of physical properties of typical deformed rocks, and seismic modeling of the reflection character of deep crustal fault zone.

ACKNOWLEDGEMENTS

George Thompson and Don Murphy contributed ideas through numerous discussions. Don Murphy and Richard Brown patiently conducted a tour of the Columbia River fault zone. Greg Davis suggested the Winters Pass thrust fault for sampling and William Thomas supplied samples from the Goat Rock and Bartletts Ferry fault zones. Steve Lipshie carried out the x-ray goniometry measurements and the modal analysis was done by Reservoirs, Inc. Scott Waichler and Russell Gordon prepared the samples and carried out the velocity measurements. The synthetic seismogram program was written by Dave Hale. Dave Okaya discussed many of the aspects of seismic modeling and interpretation. Finally thanks are due to the Stanford Exploration Project and Jon Claerbout for the use of computing facilities. This research was supported by grant EAR80-18346 from the National Science Foundation.

REFERENCES

Aki, K., and W. H. K. Lee, Determination of three dimensional velocity anomalies under a seismic array using first P arrival time from local earthquakes, 1: A homogeneous initial model, J. Geophys. Res., 81, 4381-4399, 1976.

Allmendinger, R. W., J. A. Brewer, L. D. Brown, S. Kaufman, J. E. Oliver, and R. S. Houston, COCORP profiling across the Rocky Mountain front in southern Wyoming, Part 2: Precambrian basement structure and its influence on Laramide deformation, Geol. Soc. Am. Bull., 93, 1253-1263, 1982.

Babuska, V., Anisotropy of Vp and Vs in rock-forming minerals, J. Geophys., 50, 1-6, 1981.

Bayley, R. W., P. D. Proctor, and K. C. Condie, Geology of the South Pass area, Fremont County, Wyoming, Geological Survey Professional Paper 793, 39p., 1973.

Bernabe, Y., W. F. Brace, and B. Evens, Permeability, porosity, and pore geometry of hot pressed calcite, Mechanics of Materials, 1, 173-183, 1982.

Birch, F., The velocity of compressional waves in rocks to 10 kilobars, Part 1, J. Geophys. Res., 65, 1083-1102, 1960.

Brace, W. F., J. B. Walsh, and W. T. Frangos, Permeability of granite under high pressure, J. Geophys. Res., 73, 2225-2236, 1968.

Brewer, J. A., R. W. Allmendinger, L. D. Brown, J. E. Oliver, and S. Kaufman, COCORP profiling across the Rocky Mountain front in southern Wyoming, Part I: Laramide structure, Geol. Soc. Am. Bull., 93, 1242-1252, 1982.

Brewer, J. A., R. Good, J. E. Oliver, L. D. Brown, and S. Kaufman, COCORP profiling across the southern Oklahoma aulacogen: Overthrusting of the Wichita mountains and compression within the Anadarko basin, Geology, 11, 109-114, 1983.

Brewer, J. A., S. B. Smithson, J. E. Oliver, S. Kaufman, and L. D. Brown, The Laramide orogeny: Evidence from COCORP deep crustal seismic profiles in the Wind River mountains, Tectonophysics, 62, 165-189, 1982.

Brown, R. L., and D. C. Murphy, Kinematic interpretation of mylonitic rocks in part of the Columbia River fault zone, Shuswap terrain, British Columbia,

Can J. Earth Sci., 19, 456-465, 1982.

Burchfiel, B. C., and G. A. Davis, Clark mountain thrust complex in the Cordillera of southeastern California: Geologic summary and field trip guide, University of California, Riverside, Campus Museum Contribution no. 1, 1-28, 1971.

Carslaw, H. S., and J. C. Jaeger, Conduction of heat in solids, 2nd edition, London, Oxford University Press, 510 p., 1959.

Carter, N. L., Steady state flow of rocks, Rev. of Geophys. and Space Physics, 14, 301-360, 1976.

Christensen, N. I., Compressional wave velocities in metamorphic rocks at pressures to 10 kilobars, J. Geophys. Res., 70, 6147-6164, 1965.

Christensen, N. I., Fabric, seismic anisotropy, and tectonic history of the Twin Sisters dunite, Washington, Geol. Soc. Am. Bull., 82, 1681-1694, 1971.

Christensen, N. I., and M. H. Salisbury, Structure and constitution of the lower oceanic crust, Rev. Geophys. and Space Physics, 13, 57-86, 1975.

Clark, H. B., J. K. Costain, and L. Glover, Structural and seismic reflection studies of the Brevard ductile deformation zone near Rosman, North Carolina, Am. J. Sci., 278, 419-441, 1978.

Cook, F. A., D. S. Albaugh, L. D. Brown, S. Kaufman, J. E. Oliver, and R. D. Hatcher, Thin-skinned tectonics in the crystalline southern Appalachians; COCORP seismic-reflection profiling of the Blue Ridge and Piedmont, Geology 7, 563-567, 1979.

Cook, F. A., L. D. Brown, S. Kaufman, J. E. Oliver, and T. A. Peterson, COCORP seismic profiling of the Appalachian orogen beneath the Coastal Plain of Georgia, Geol. Soc. Am. Bull., Part I, 92, 738-748, 1981.

Cook, F. A., and J. E. Oliver, The late Precambrian-early Paleozoic continental edge in the Appalachian orogen, Am. J. Sci., 281, 993-1008, 1981.

Crittenden, M. D., Jr., P. J. Coney, and G. A. Davis, Cordilleran metamorphic core complexes, Geol. Soc. Am. Memoir 153, 490p., 1981.

Daley, P. F., and F. Hron, Reflection and transmission coefficients for seismic waves in ellipsoidally anisotropy media, Geophysics, 44, 27-38, 1979.

Dohr, G. P., and R. Meissner, Deep crustal reflections in Europe, Geophysics, 40, 25-39, 1975.

Etheridege, J. A., and G. Oertel, Strain measurements from phyllosilicate preferred orientation-A precautionary note, Tectonophysics, 60, 107-120, 1979.

Goldstein, A. G., Geometry and kinematics of ductile faulting in a portion of the Lake Char mylonite zone, Massachusetts and Connecticut, Am. J. Sci., 282, 1778-1806, 1982.

Hale, L. D., and G. A. Thompson, The seismic reflection character of the Mohorovicic discontinuity, J. Geophys. Res., 87, 4625-4635, 1982.

Harris, L. D., and K. C. Boyer, Sequential development of the Appalachian orogen above a master decollement-A hypothesis, Geology, 7, 568-572, 1975.

Healy, J. G., and L. G. Peak, Seismic velocity structure on a section of the San Andreas fault near Bear Valley, California, Bull. Seism. Soc. Am., 65, 1177-1197, 1975.

Higgens, M. W., Cataclastic rocks, Geological Survey Professional Paper, 687, 97p. 1971.

Hubbert, M. K., and W. W. Rubey, Role of fluid pressure in mechanics of overthrust faulting, I. Mechanics of fluid-filled porous solids and its application to overthrust faulting, Bull. Geol. Soc. Am., 77, 741-760, 1959.

Johnson, L. R., and H. R. Wenk, Anisotropy of physical properties in metamorphic rocks, Tectonophysics, 23, 79-98, 1974.

Jones, T. D., The nature of seismic reflections from the crystalline basement, chapter 3, this volume, submitted to Jour. Geophys. Res., 1983.

Jones, T. D., and A. Nur, Seismic velocity and anisotropy in mylonites and the reflectivity of deep crustal fault zones, Geology, 10, 260-263, 1982.

Jones, T. D., and A. Nur, Reply to comment, in press, Geology, 1983.

Kay, R. W., and S. M. Kay, The nature of the lower continental crust: Inferences from geophysics, surface geology, and crustal xenoliths, Rev. Geophy. Space Physics, 19, 271-297, 1981.

Kaila, K. L., K. R. Chowdhury, P. R. Reddy, V. G. Krishna, H. Narain, S. I. Subbotin, V. B. Sollogub, A. V. Chokinov, G. E. Kharetchko, M. A. Lazarendo, and T. V. Ilchenko, Crustal structure along Kavail-Udipi profile in the Indian Peninsular shield from deep seismic sounding, J. Geol. Soc. India, 20, 307-333, 1979.

Kaila, K. L., V. G. Krishna, and D. M. Mall, Crustal structure along Mehmadabad-Billimora profile in the Cambay Basin, India from deep seismic soundings, Tectonophysics, 76, 99-130, 1981.

Karson, J. A., Reconstructed seismic velocity structure of the Lewis Hills Massif and implications for oceanic fracture zones, J. Geophys. Res., 87, 961-978, 1982.

Kern, H., and M. Fakhimi, Effect of fabric anisotropy on compressional-wave propagation in various metamorphic rocks for the range 20-700 degrees Celsius at 2 kbars, Tectonophysics, 28, 227-244, 1975.

Kern, H., and A. Richter, Temperature derivatives of compressional and shear wave velocities in crustal and mantle rocks at 6 kbar confining pressure, J. Geophysics, 49, 47-56, 1981.

Kitsunezaki, C., Determination of seismic anisotropy of metamorphic rocks in natural conditions, Special Contributions, Geophysical Institute, Kyoto University, 4, 83-90, 1964.

Kjartansson, E., Attenuation of seismic waves in rocks and applications in energy exploration, Ph.D., Thesis, Stanford University, Stanford, California, 1979.

Kosada, K., Fault-related fabrics of granitic rocks, Jour. Fac. Sci., Univ. Tokyo, Sec. II, 20, 77-115, 1980.

Lawrence, R. D., Tectonic significance of petrofabric studies along the Chewack-Pasayten fault, north-central Washington, Geol. Soc. Am. Bull., 89, 731-743, 1978.

Lipshie, S. R., G. Oertel, and J. M. Christie, Measurements of preferred orientation of phyllosilicates in schists, Tectonophysics, 34, 91-99, 1976.

Lynn, H. G., Migration and interpretation of deep crustal seismic reflection data, Ph.D., Thesis, Stanford University, Stanford, California, 158p., 1979.

Mayer-Rosa, D., Travel-time anomalies and distribution of earthquakes along the Calaveras fault zone, California, Bull. Seism. Soc. Am., 63, 713-729, 1973.

McEvilly, T. V., Extended reflection seismic survey of the San Andreas fault zone, U. S. Geological Survey Open File Report no. 81-388, 28p., 1981.

Meissner, R., and H. Bartelsen, Seismic reflection and refraction studies for investigating fault zones along the geotraverse Rhenoherzynikum,

Tectonophysics, 64, 59-84, 1980.

Meissner, R., H. Bartelsen, and H. Murawski, Thin-skinned tectonics in the northern Rhenish Massif, Germany, Nature, 290, 399-401, 1981.

Meissner, R., and M. Fakhimi, Seismic anisotropy as measured under high-pressure, high-temperature conditions, Geophys. J. R. Astr. Soc., 49, 133-143, 1977.

Morlet, J., G. Arens, E. Fourgean, and D. Giand, Wave propagation and sampling theory-Part I: Complex signal and scattering in multilayered media, Geophysics, 47, 203-221, 1982.

Murphy, D. C., Mylonite genesis: Columbia River fault zone, British Columbia, M. A. Thesis, Stanford University, Stanford, California, 111p. 1980.

Nur, A., and G. Simmons, The effect of saturation on velocity in low porosity rocks, Earth and Planet. Sci. Let., 7, 183-193, 1969.

Oliver, J., Tracing surface features to great depths: A powerful means for exploring the deep crust, Tectonophysics, 81, 257-272, 1982

Park, C. F., and R. A. MacDiarmid, Ore Deposits, Third edition, W. H. Freeman and Company, San Francisco, 1975.

Pavlenkova, N. I., and T. V. Smelyanskaya, The nature of the group of reflected seismic waves from the base of the earths crust, Izv., Earth Physics, 1, 17-27, 1970.

Raleigh, B., and J. Everden, case for low deviatoric stress in the lithosphere, Mechanical behavior of crustal rocks, A. G. U., 173-186, 1982.

Read, P. B., and R. L. Brown, Columbia River fault zone: southeastern margin of the Shuswap and Monashee complexes, southern British Columbia, Can. J. Earth Sci., 18, 1127-1145, 1981.

Reif, D. M., and J. P. Robinson, Geophysical, geochemical, and petrographic data and regional correlation from the Arizona state A-1 well, Pinal county, Arizona, Ariz. Geol. Soc., Digest, 13, 99-109, 1981.

Rezanov, I. A., and N. Y. Galdin, Geological significance of anisotropy of seismic velocities in earths crust, Internat. Geology Rev., 9, 1424-1429, 1967.

Schilt, S., J. Oliver, L. Brown, S. Kaufman, D. Albaugh, J. Brewer, F. Cook, L. Jensen, P. Krumhansl, G. Long, and D. Steiner, The heterogeneity of the continental crust: Results from deep crustal seismic reflection profiling

using the vibroseis program, Rev. Geophys. Space Physics, 17, 354-368, 1979.

Sibson, R. G., Fault rocks and fault mechanism, J. Geol. Soc. Lond., 122, 191-213, 1977.

Simmons, G., and H. Wang, Single crystal elastic constants and calculated aggregate properties: A handbook, 2nd ed., The M.I.T. Press, Cambridge, Mass., 370p. 1971.

Smithson, S. B. and R. J. Ebens, Interpretation of data from a 3.05-kilometer borehole in Precambrian crystalline rocks, Wind River mountains, Wyoming, J. Geophys. Res., 76, 7079-7087, 1971.

Smithson, S. B., J. A. Brewer, S. Kaufman, J. E. Oliver, and C. A. Hurich, Structure of the Laramide Wind River uplift, Wyoming, from COCORP deep reflection data and from gravity data, J. Geophys. Res., 84, 5955, 5972, 1979.

Smythe, D. K., A. Dobinson, R. McQuillin, J. A. Brewer, D. H. Matthews, D. J. Blundell, and B. Kelk, Deep structure of the Scottish Caledonides revealed by the MOIST reflection profile, Nature, 299, 338-340, 1982.

Sprunt, E. and A. Nur, Destruction of porosity through pressure solution, Geophysics, 42, 726-742, 1977.

Todd, T., and G. Simmons, Effect of pore pressure on the velocity of compressional waves in low-porosity rocks, J. Geophys. Res., 77, 3731-3743, 1972.

Trimmer, D., B. Bonner, H. C. Heard, and A. Duba, Effect of pressure and stress on water transport in intact and fractured gabbro and granite, J. Geophys. Res., 7059-7071, 1980.

Wang, C. Y., W. Lin, and F. T. Wu, Constitution of the San Andreas fault zone at depth, Geophys. Res. Lett., 5, 741-744, 1978.

Wang, C. Y., W. Lin, and H. R. Wenk, The effects of water and pressure on velocities of elastic waves in a foliated rock, J. Geophys. Res., 80, 1065-1069, 1975.

Wang, H. F., and G. Simmons, Microcracks in crystalline rock from 5.3-km depth in the Michigan Basin, J. Geophys. Res., 83, 5849-5856, 1978.

Wu, F. T., Mineralogy and physical nature of clay gouge, Pure and Applied Geophysics, 116, 655-689, 1978.

Zawislak, R. L., and S. B. Smithson, Problems and interpretation of COCORP deep seismic reflection data, Wind River range, Wyoming, Geophysics, 46, 1684-1701, 1981.

TABLE 1

Seismic Reflections from Ductile Fault Zones

LOCATION	APPROXIMATE DEPTH OF FAULT REFLECTIONS	REFERENCE
West Germany (Rhinegraben)	5-35 km	Meissner and Bartelsen, 1980 Meissner and others, 1981 Dohr and Meissner, 1975
India (Shield)	0-40 km	Kailia and others, 1981 Kailia and others, 1979
U.S.S.R. (Ukraine)	0-40 km	Pavlenkova & Smelyanskaya, 1970
Great Britain	5-40 km	Smythe and others, 1982
Southern Arizona	3-10 km	Reif and Robinson, 1981
North Carolina (Brevard Zone)	2-5 km	Clark and others, 1978
Georgia (Appalachian Decollment)	5-20 km	Cook and others, 1981 Cook and oliver, 1981
Wyoming (Wind River Mts.)	0-30 km	Smithson and others, 1979 Lynn, 1979
Wyoming (Laramie Range)	10-15 km	Brewer and others, 1982
Oklahoma (Wichita Mts.)	5-15 km	Brewer and others, 1983

TABLE 2

MODAL ANALYSIS

SAMPLE	ROCK TYPE	QUARTZ	ORTHOCLASE	PLAGIOCLASE	MICA	CHLORITE	MAFICS	OTHER
CR 1	Granodiorite	42%	14%	24%	12%	6%	1%	1%
CR 5	Granodiorite	48%	17%	13%	12%	9%	-	1%
CR 10	Granodiorite	18%	21%	25%	32%	4%	-	-
CR 11	Mylonite	36%	4%	40%	9%	8%	2%	1%
CR 12	Mylonite	30%	21%	19%	9%	21%	-	-
CR 13	Mylonite	48%	9%	15%	12%	14%	2%	-
CR 14	Mylonite	35%	14%	19%	6%	23%	2%	1%
CR 15	Cataclasite	52%	20%	5%	9%	13%	-	1%
CR 16	Mylonite	49%	5%	6%	-	38%	2%	-
CR 17	Mylonite	69%	15%	8%	-	8%	-	-
CR 18	Mylonite	27%	18%	24%	24%	7%	-	-
WP 6	Mylonite	35%	8%	12%	45%	-	-	-
WP 8	Mylonite	55%	3%	1%	41%	-	-	-
A 1	Mylonite	56%	5%	23%	14%	-	2%	-
A 3	Gneiss	33%	24%	23%	17%	2%	-	1%
A 4	Gneiss	65%	1%	7%	27%	-	-	-
A 5	Mylonite	31%	11%	26%	19%	13%	-	-
A 6	Gneiss	21%	4%	40%	35%	-	-	-
A 7	Gneiss	27%	-	18%	54%	-	1%	-

TABLE 3

Measurements of Physical Properties

SAMPLE	POROSITY	DENSITY	Dry- Confining Pressure= 1 kilobar					Water Saturated P_c = 1 kilobar, P_p = 25 bars				
			MEAN VELOCITY	VELOCITY ⊥ FOL.*	VELOCITY ∥ FOL.* ⊥ LIN.	VELOCITY ∥ FOL.* ∥ LIN.	ANISOTROPY	MEAN VELOCITY	VELOCITY ⊥ FOL.*	VELOCITY ∥ FOL.* ⊥ LIN.	VELOCITY ∥ FOL.* ∥ LIN.	ANISOTROPY
CR 1	1.9%	2.63g/cc	5.65km/s	5.56km/s	5.67km/s	5.76km/s	3%					
CR 3		2.63	5.91	5.80	5.91	6.02	4					
CR 5	1.6	2.62	5.91	5.82	5.93	5.98	3	6.07km/s	6.09km/s	6.02km/s	6.10km/s	1%
CR 7		2.62	5.73	5.70	5.72	5.77	1					
CR 10		2.67	6.15	6.18	6.07	6.20	2					
CR 11	2.0	2.62	6.08	5.99	6.12	6.12	2	6.21	6.08	6.27	6.29	3
CR 12	1.2	2.66	6.15	6.11	6.33	6.01	5	6.24	6.18	6.39	6.16	4
CR 13		2.67	5.84	5.65	5.79	6.07	7					
CR 14	1.0	2.86	6.39	6.21	6.36	6.60	6	6.43	6.24	6.42	6.63	6
CR 15		2.68	5.76	5.70		5.82	2					
CR 16	1.3	2.77	5.88	5.36	6.09	6.20	13	5.97	5.42	6.26	6.22	14
CR 17		2.68	5.64	5.69	5.59	5.64	2	6.08	5.82	6.25	6.16	7
CR 18		2.68	5.90	5.74	5.86	6.10	6	6.20	6.00	6.35	6.24	6
WP 6	2.4	2.69	5.90	5.58	5.95	6.16	10	6.01	5.84	5.96	6.22	6
WP 8	0.6	2.68	6.03	5.25	6.31	6.53	21	6.08	5.36	6.32	6.56	20
A 1		2.67	6.18	6.01	6.29	6.24	4					
A 3		2.64	6.33	6.29	6.25	6.44	3					
A 4		2.66	5.34	4.98	5.29	5.76	15					
A 5		2.68	6.16	5.93	6.20	6.35	7					
A 6		2.67	6.30	6.12	6.30	6.47	5					
A 7		2.76	6.13	5.71	6.15	6.53	13					

* Orientation applies only to the mylonites and metamorphic rocks. In the ingeous samples (CR 1, CR 3, CR 5, CR 7, and CR 10) and the cataclasite (CR 15) velocities were measured in arbitrary orthogonal directions. Where no lineation was present the slowest velocity within the foliation plane is given as perpendicular to lineation.

TABLE 4

Physical Properties of some Common Crustal Minerals

MINERAL	DENSITY	AGGREGATE VELOCITY*	SINGLE CRYSTAL VELOCITY ALONG AXES** A	B	C	ANISOTROPY***	RHEOLOGY
Quartz	2.65g/cc	6.02km/s	5.66km/s	5.66km/s	6.30km/s	11%	Ductile-commonly deformed in greenschist grade rocks.
Calcite	2.72	6.36	7.10	7.10	5.39	26	Ductile-very easily deformed.
Biotite	3.05	5.26	7.81	7.81	4.21	54	Ductile-commonly deformed in greenschist grade rocks.
Muscovite	2.79	5.78	7.98	7.98	4.43	52	Ductile.
Garnet	4.06	8.44	8.47	8.47	8.47	0	Strong and brittle in crust.
Olivine (Fo_{93})	3.31	8.41	9.78	7.73	8.43	24	Brittle in mid-upper crust. Ductile in mantle.
Clinopyroxene (Diopside)	3.31	7.70	7.60	6.98	9.13	27	Strong and brittle-rarely deformed ductilly.
Augite	3.32	7.21	7.40	6.53	8.51	26	" "
Orthopyroxene (Bronsite)	3.34	7.84	7.84	7.84	6.80	8.21	18 " "
Horneblende	3.12	6.80	6.09	7.15	7.84	25	Very strong and brittle. Rarely deformed.
Labradorite (An_{40})	2.68	6.70	6.14	7.68	7.51	22	All feldspars are strong and brittle. Rarely deformed by ductile processes in the crust.
Microcline	2.56	6.01	5.09	8.17	6.89	46	
Oligoclase (An_{80})	2.64	6.22	5.52	7.86	6.86	35	
Albite (An_9)	2.61	6.06	5.36	7.26	7.03	29	
Sanadine (Or_{75},Ab_{22})	2.54	5.55	4.74	7.64	6.36	46	

* Voight-Reuss-Hill velocity in an isotropic aggregate (Simmons and Wang, 1971).

** Computed from single crystal stiffness tensor values tabulated by Simmons and Wang (1971).

*** Between crystallographic axis, maximum anisotropy for quartz and calcite is much greater

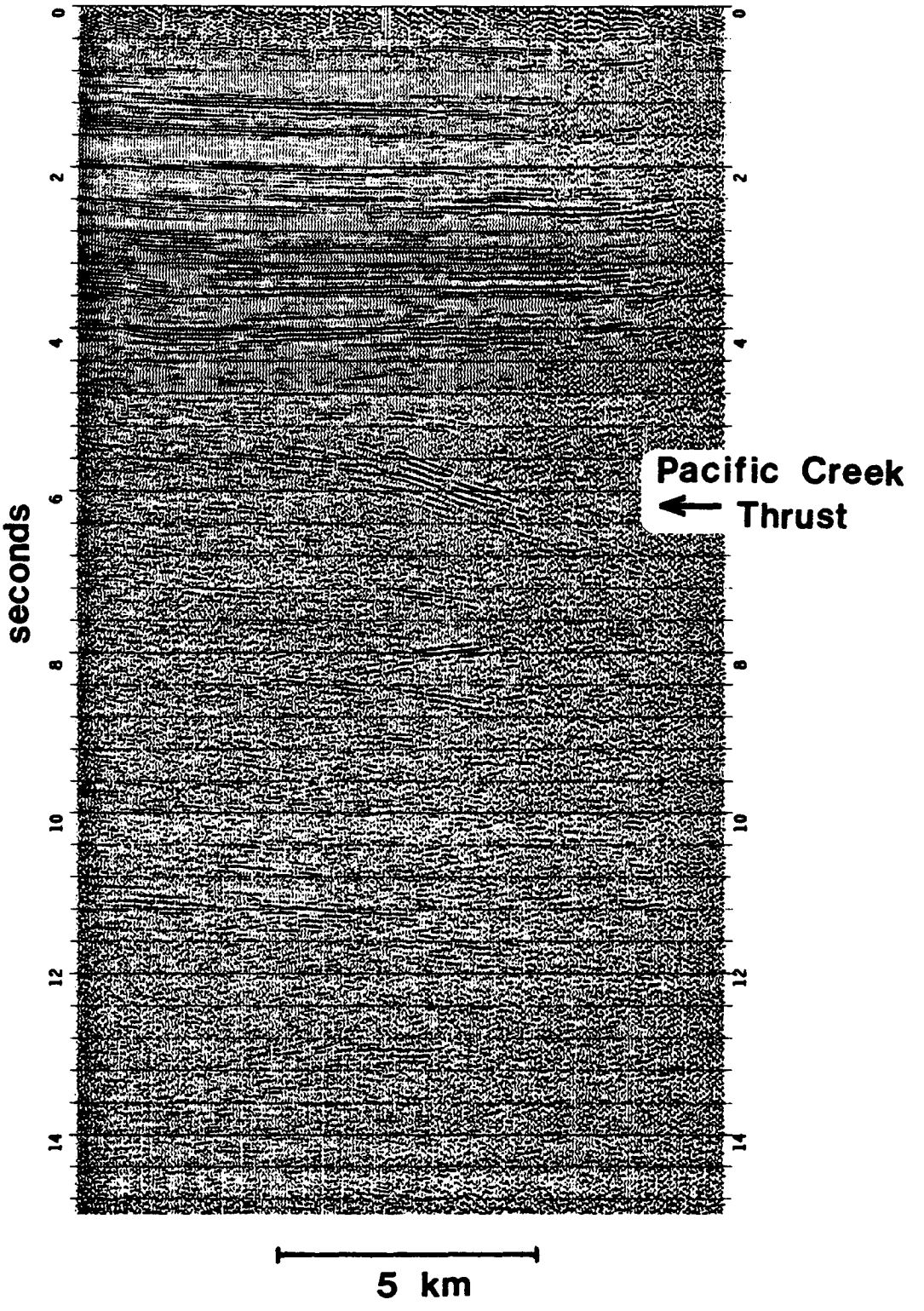

Figure 1. Portion of COCORP Wind River line 1. Vertical scale is two-way travel time in seconds.

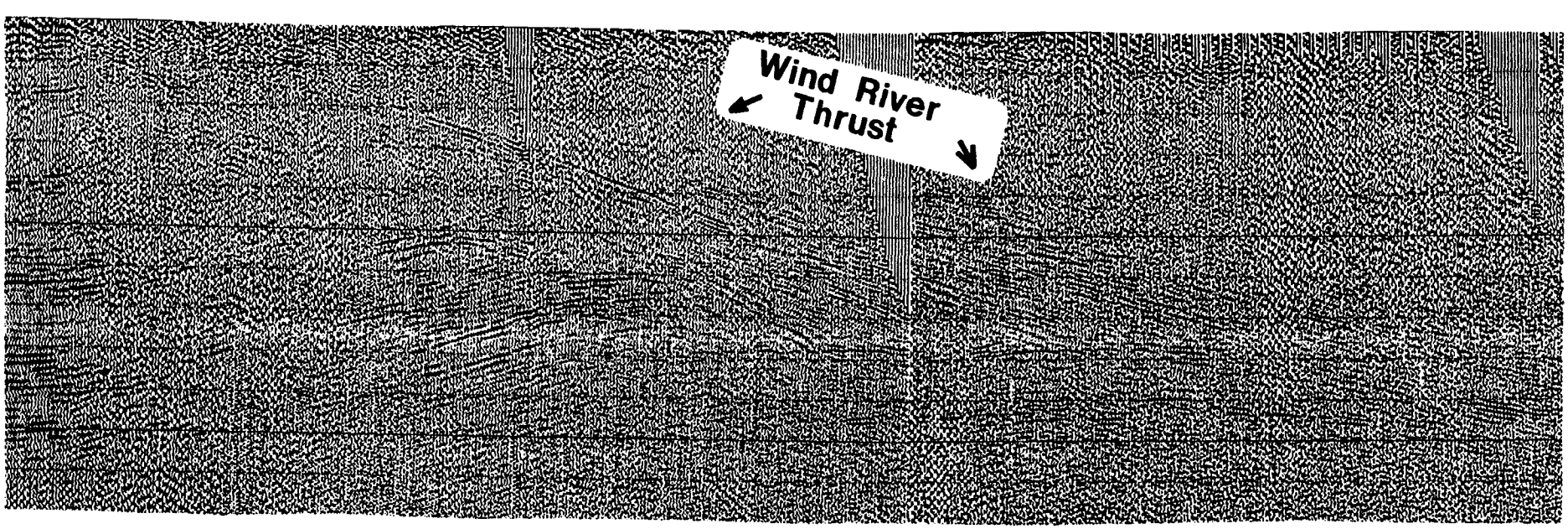

Figure 2. Detailed portion of Wind River line 1a showing the Wind River thrust fault at shallow depths.

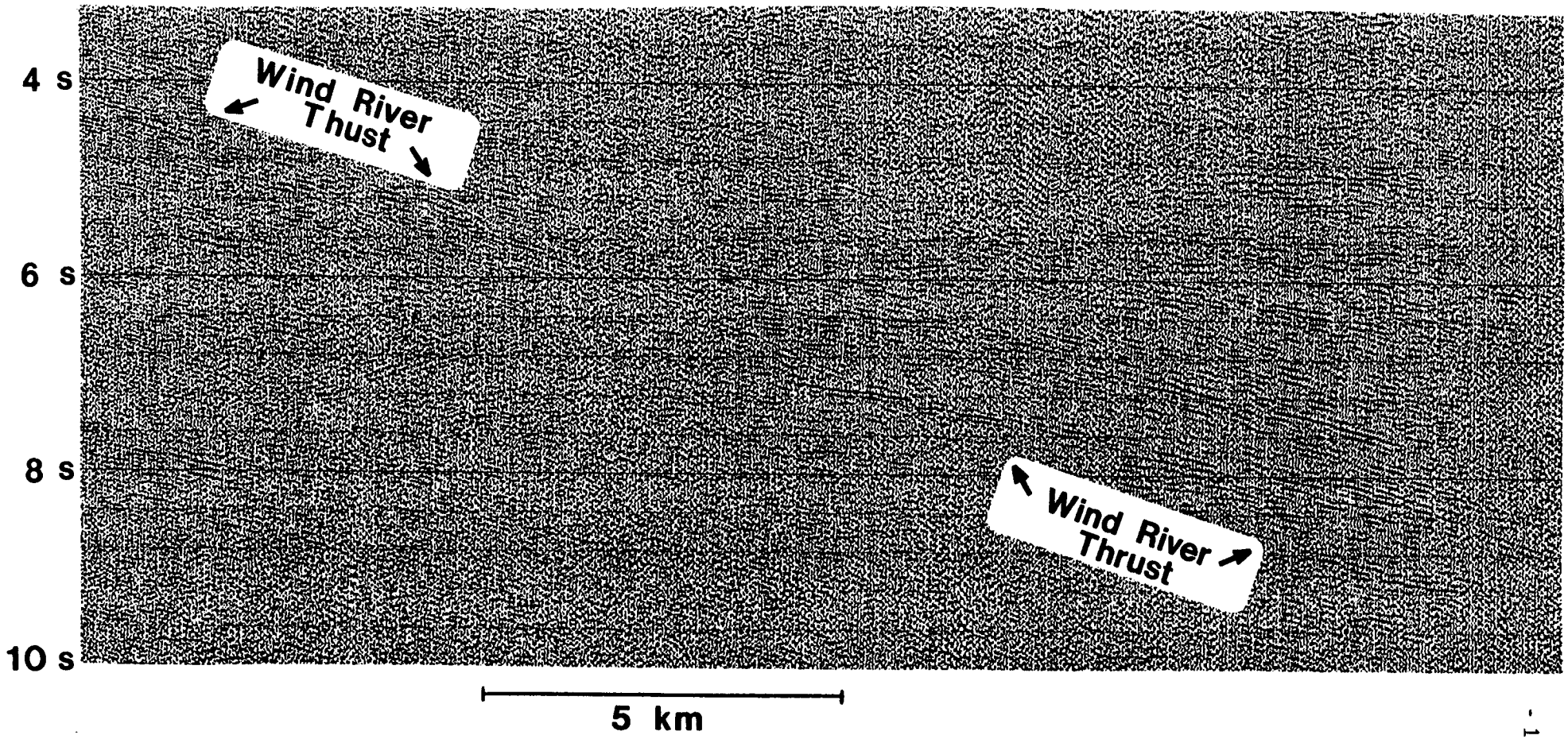

Figure 3. Portion of Wind River line 1a showing the Wind River fault zone at mid-crustal depths.

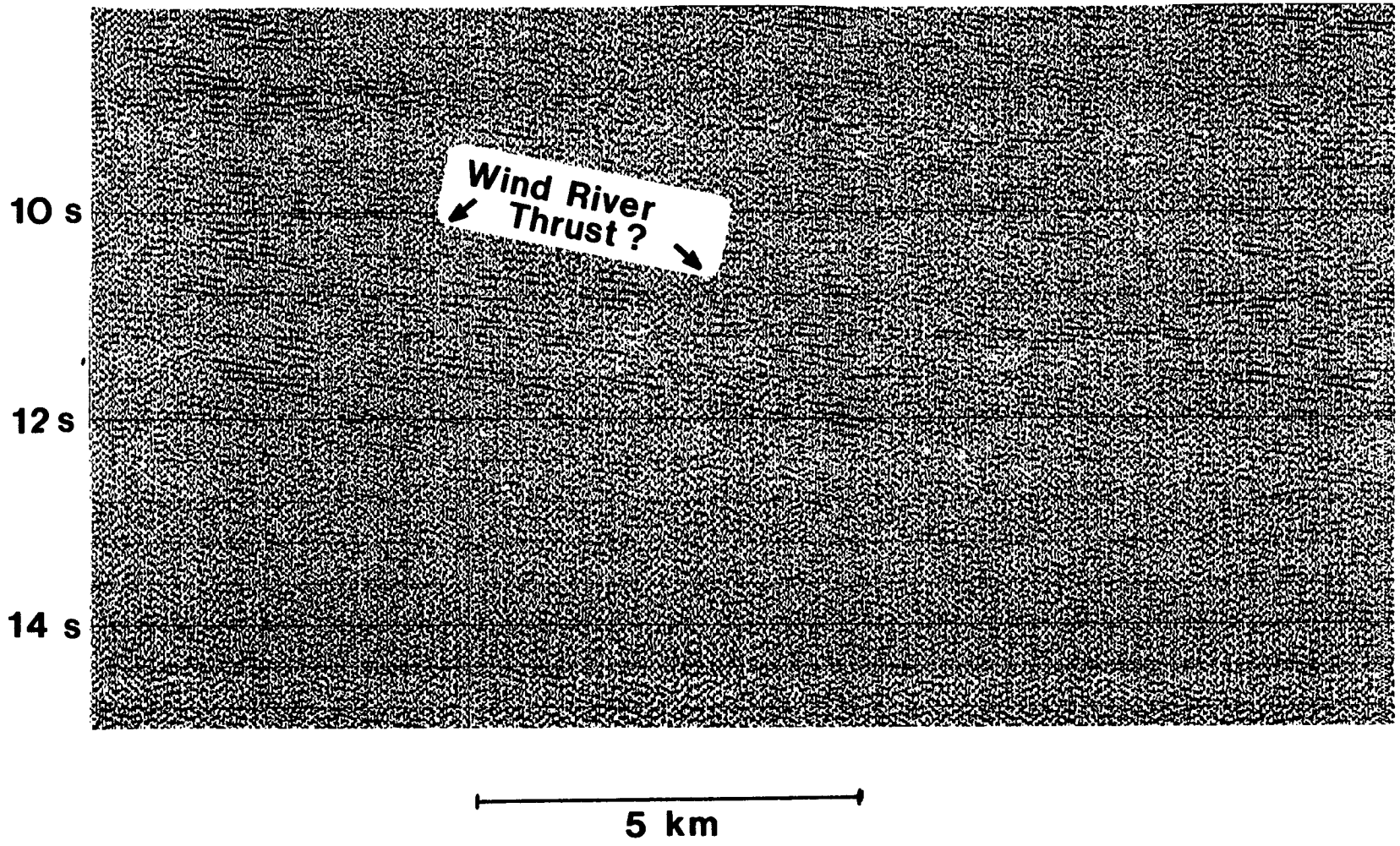

Figure 4. Detail from the deep section of Wind River line 2 shows possible reflections from the Wind River thrust in the lower crust.

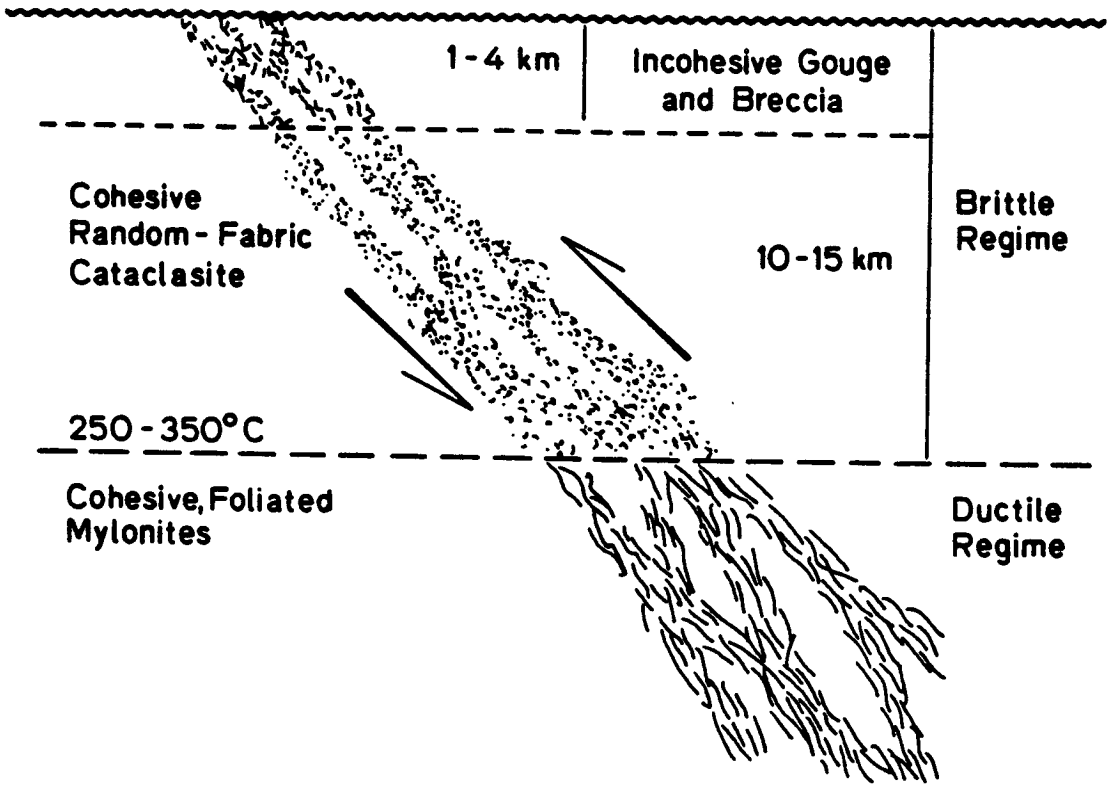

Figure 5. Inferred structure of a typical fault zone within the crust, adapted from Sibson, (1977).

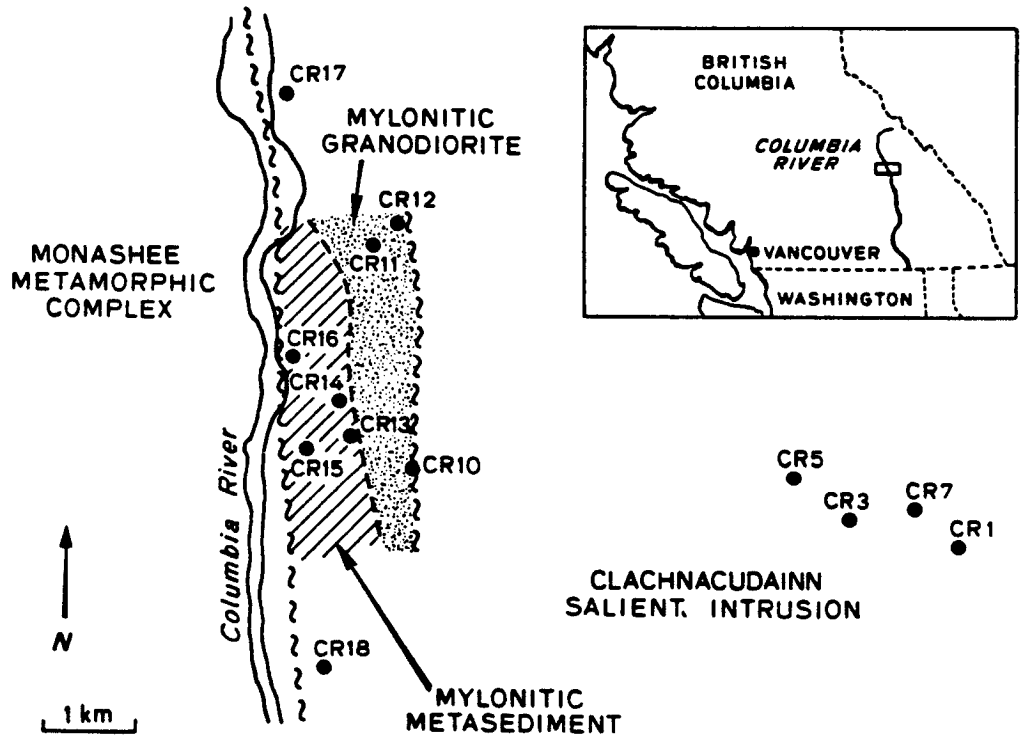

Figure 6. Geology of the Columbia River fault zone, southeastern British Columbia. The large dots represent sample locations.

a

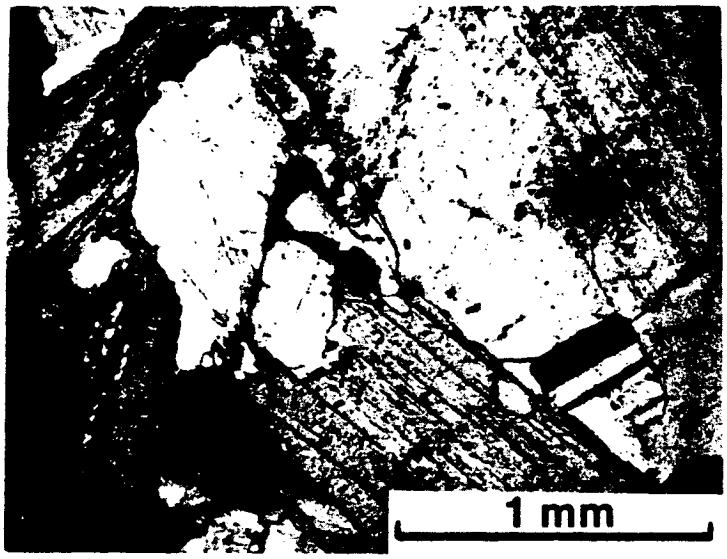

b

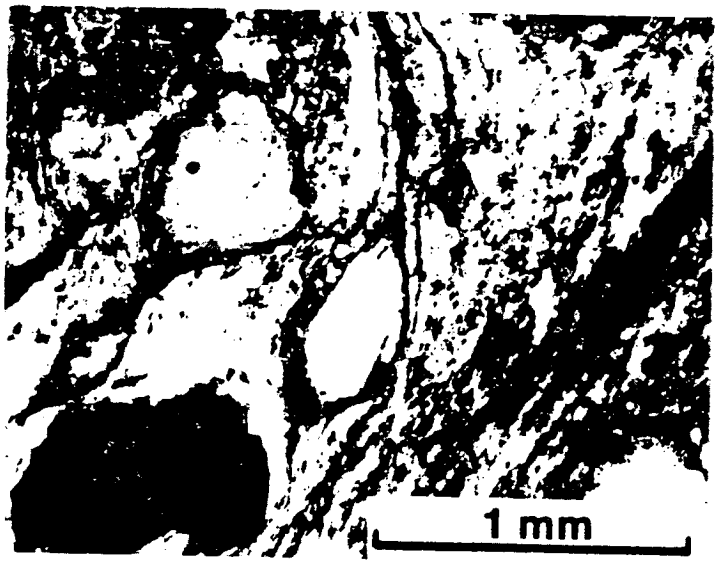

Figure 7. Photomicrographs of mylonitic textures cut perpendicular to foliation. Crossed polars. a: CR 5, coarse grained undeformed protolith. b: CR 11, highly deformed mylonitic granodiorite.

a

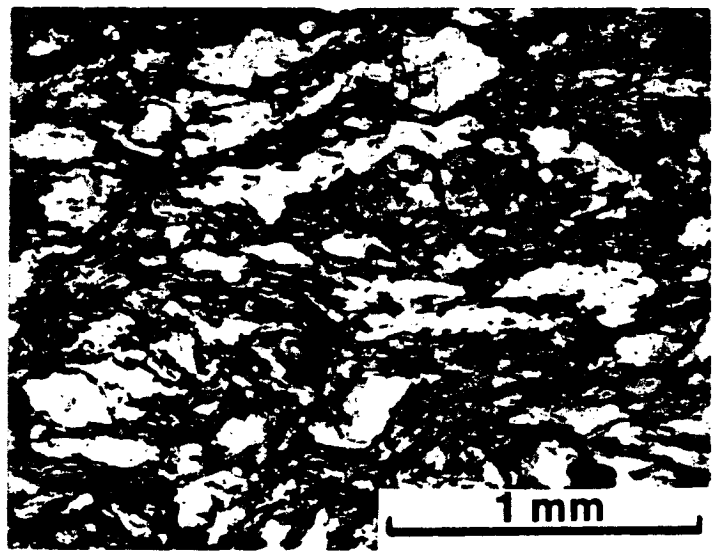

b

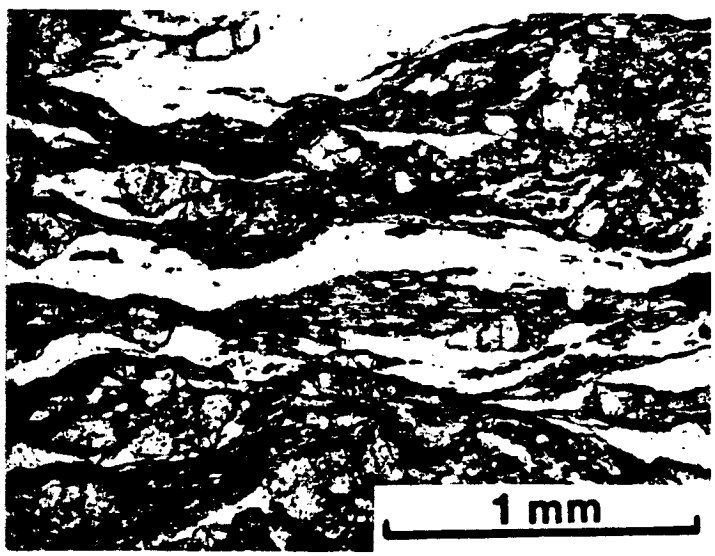

Figure 8. Photomicrographs of mylonitic textures in deformed metasedimentary rocks cut perpendicular to foliation. Plane polarized light. a: CR 14, Mylonitic metasediment. b: CR 16, Mylonitic metasediment.

a

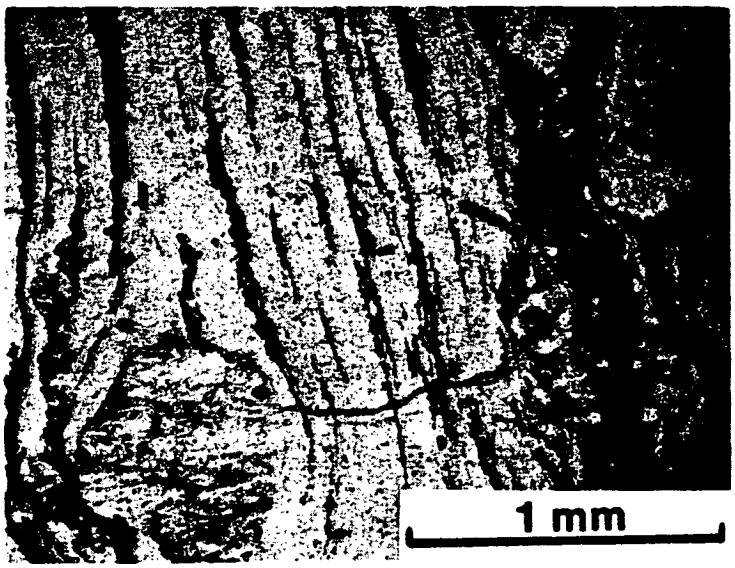

b

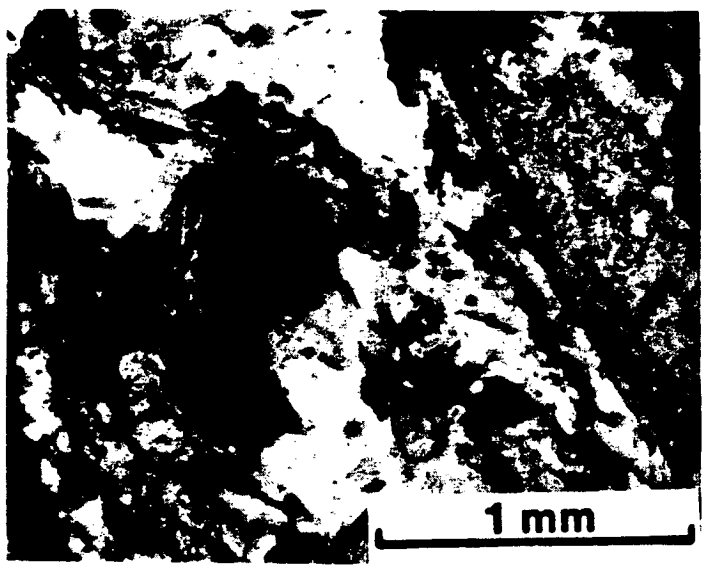

Figure 9. Photomicrographs of mylonitic textures in deformed metasedimentary rocks cut perpendicular to foliation. a: CR 17, Mylonitic metasediment. Plane polarized light. b: CR 15, Cataclasite. Crossed polars.

a

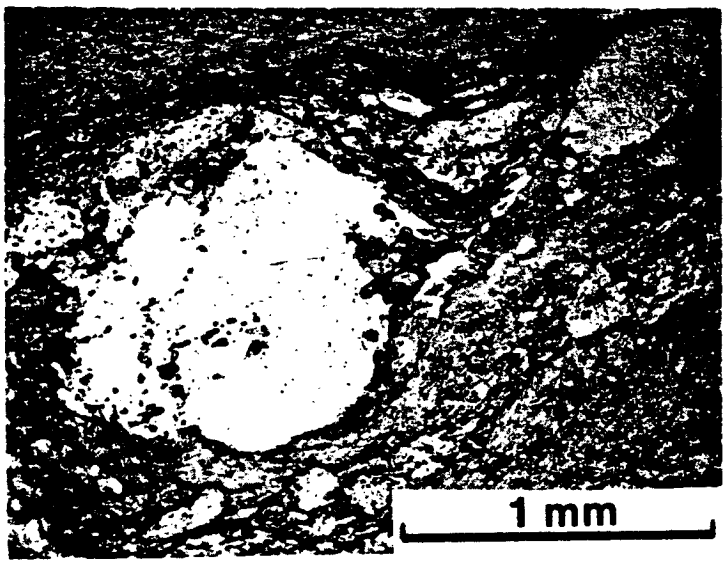

b

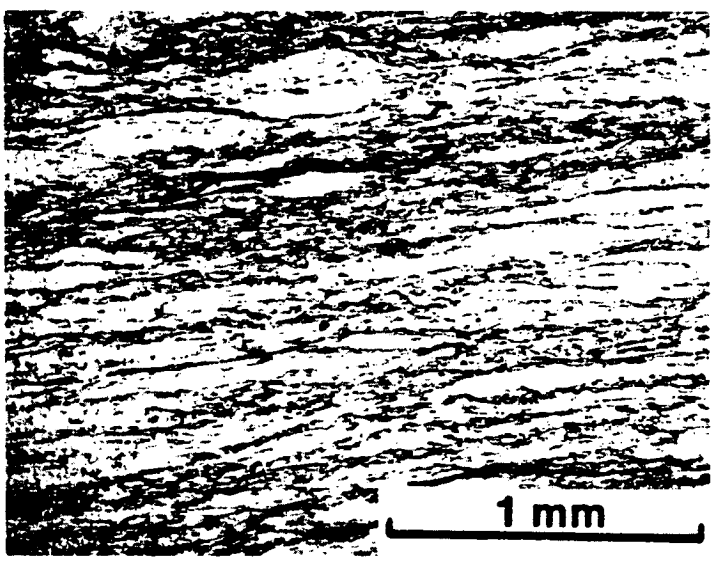

Figure 10. Photomicrographs of mylonitic textures in the Winters Pass mylonites cut perpendicular to foliation and taken in plane polarized light. a: WP 6, Flaser gneiss mylonite. b: WP 8, Blastomylonite.

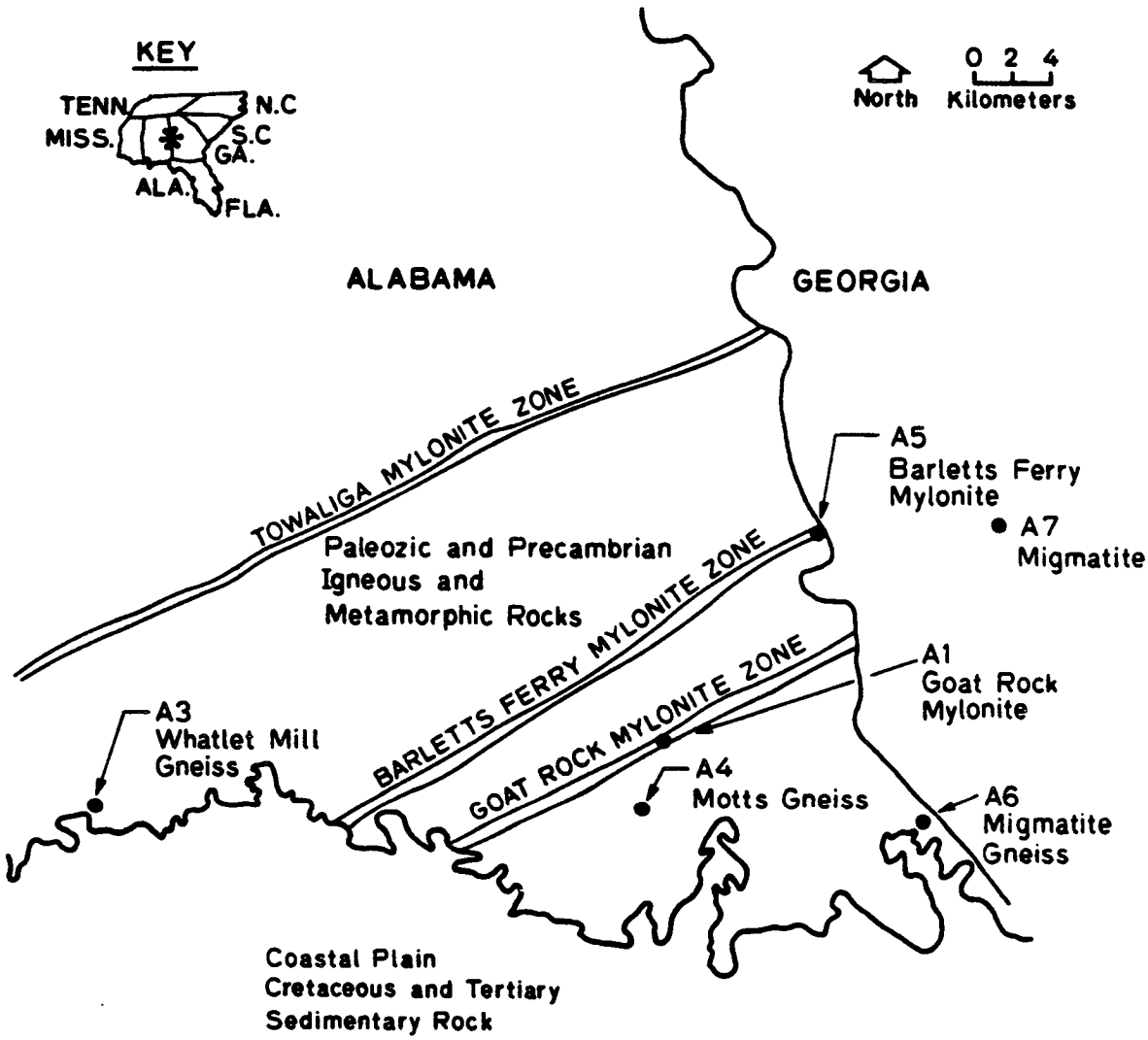

Figure 11. Geology of mylonite zones in the southern Appalachians. Dots represent sample locations.

a

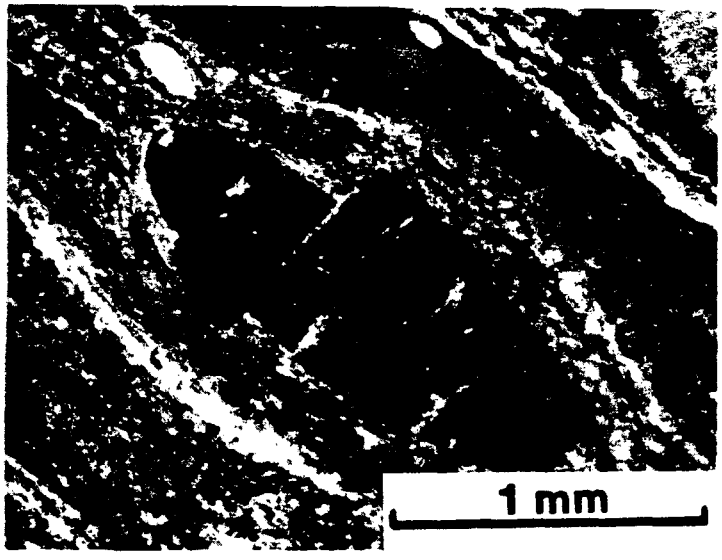

b

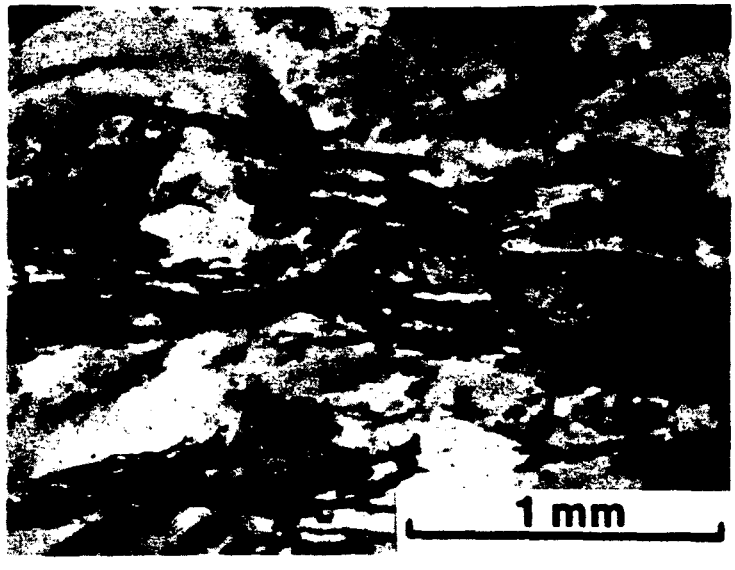

Figure 12. Photomicrographs of mylonitic textures in Appalachian samples cut perpendicular to foliation. Crossed polars. a: A1, Goat Rock mylonite. b: A2, Bartlets Ferry mylonite.

a

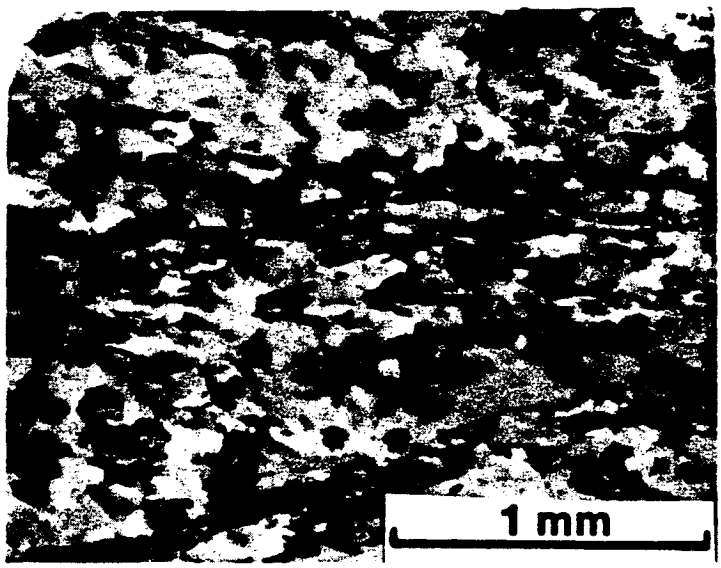

b

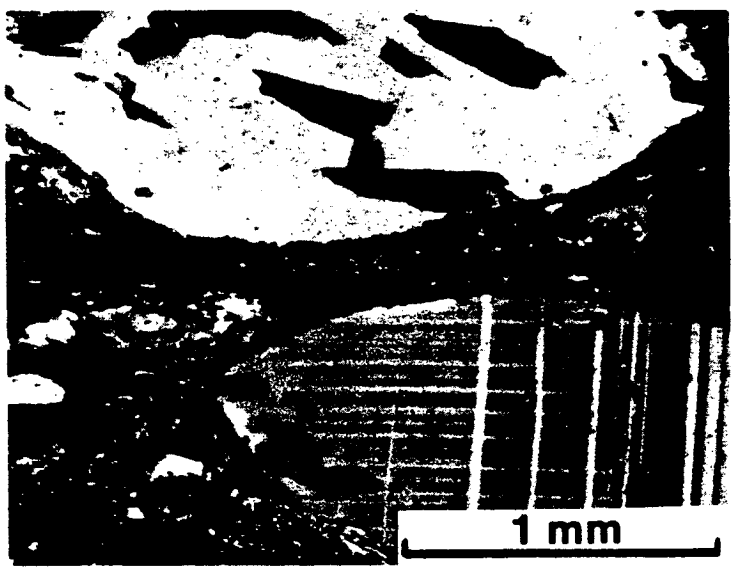

Figure 13. Photomicrographs of textures from Appalachian gneisses cut perpendicular to foliation. Crossed polars. a: A3, Whatlet Mill gneiss. b: A7, migmatite gneiss.

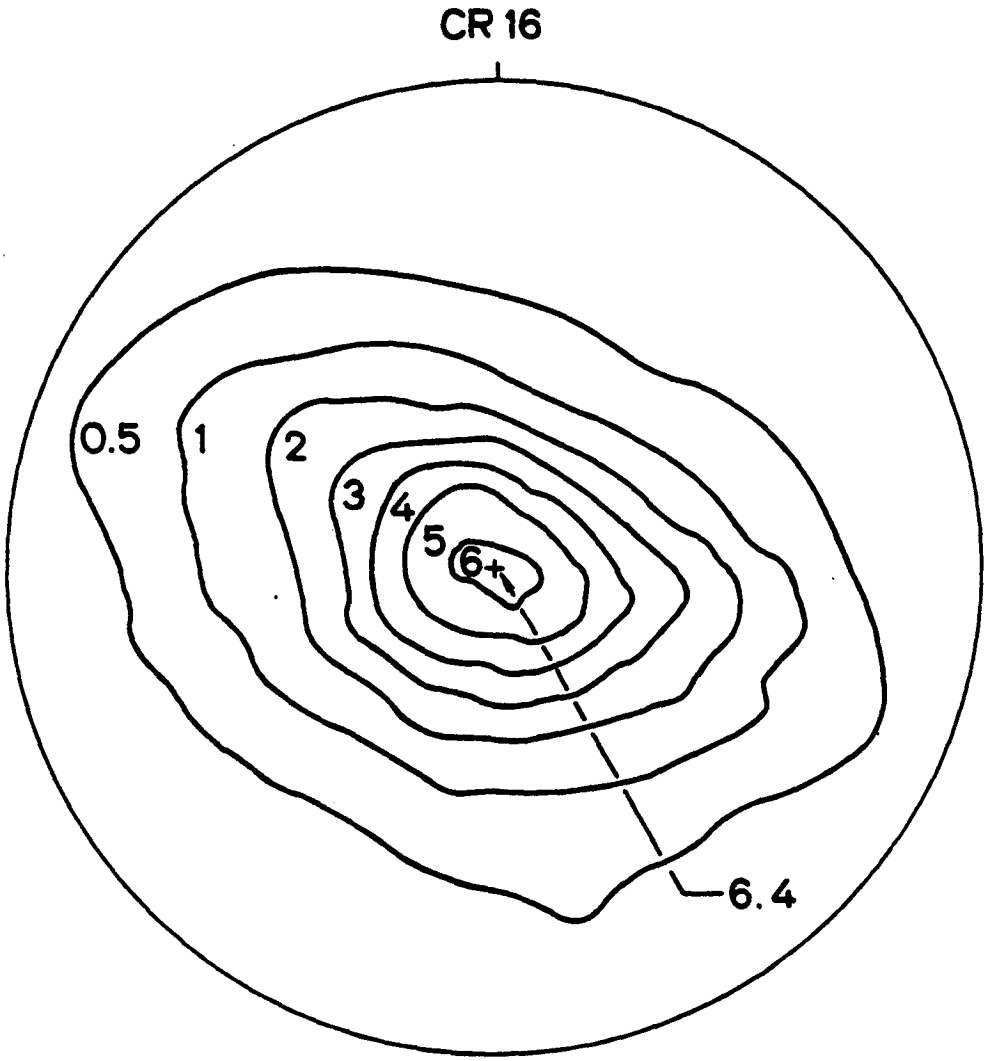

Figure 14. Pole figure for CR 16. Contours are preferred orientation of c-axis of phyllosilicate intensities in multiples of a uniform distribution. Foliation is parallel to the plane of the figure.

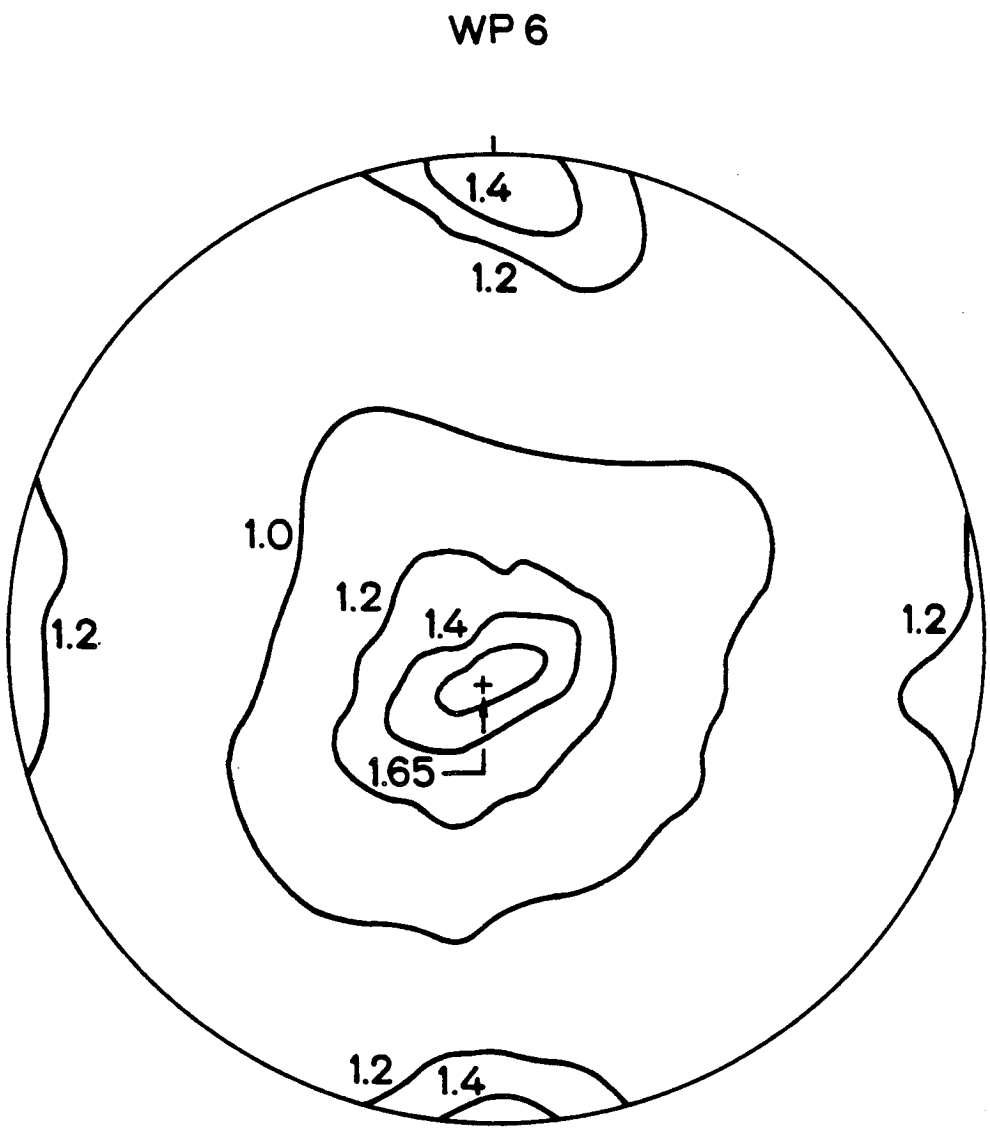

Figure 15. Pole figure for WP 6.

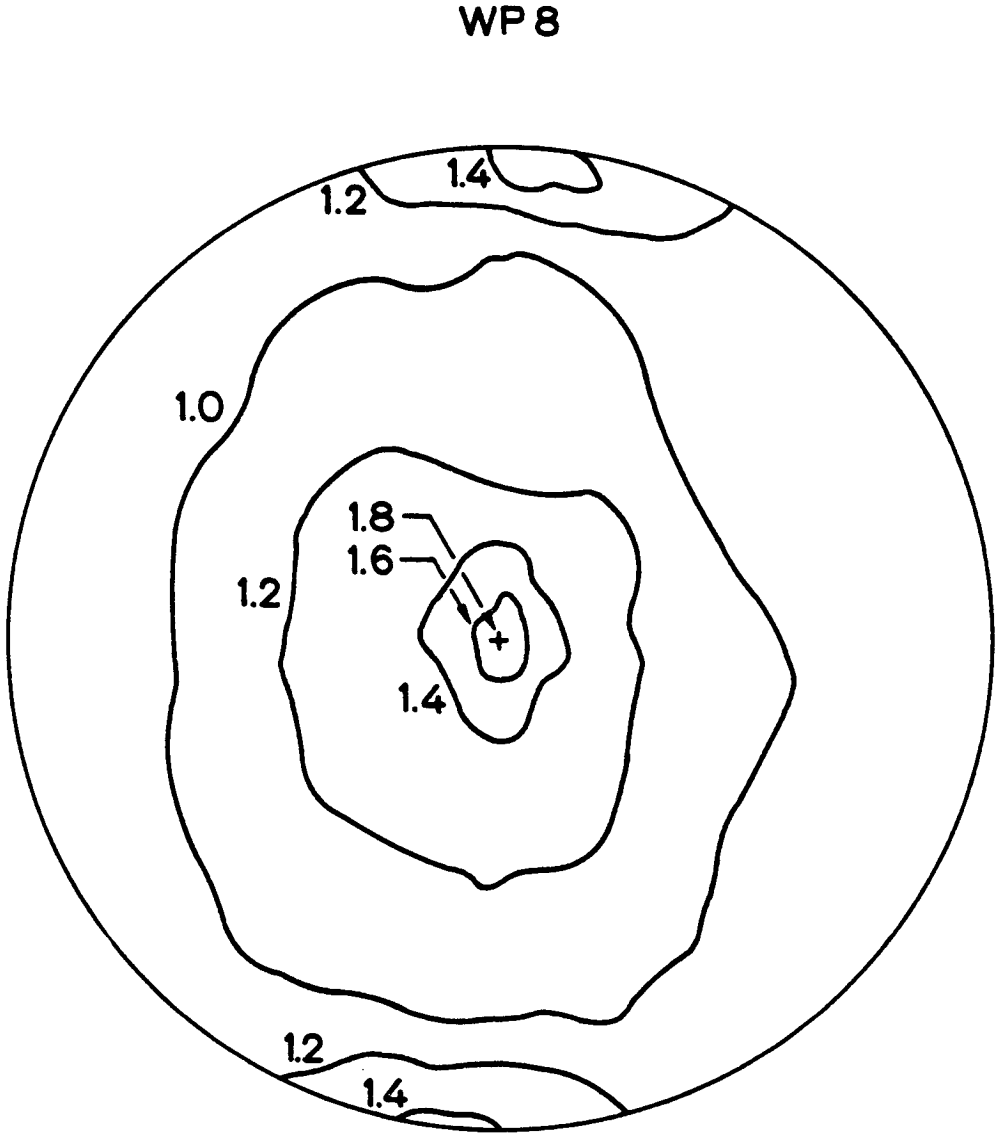

Figure 16. Pole figure for WP 8.

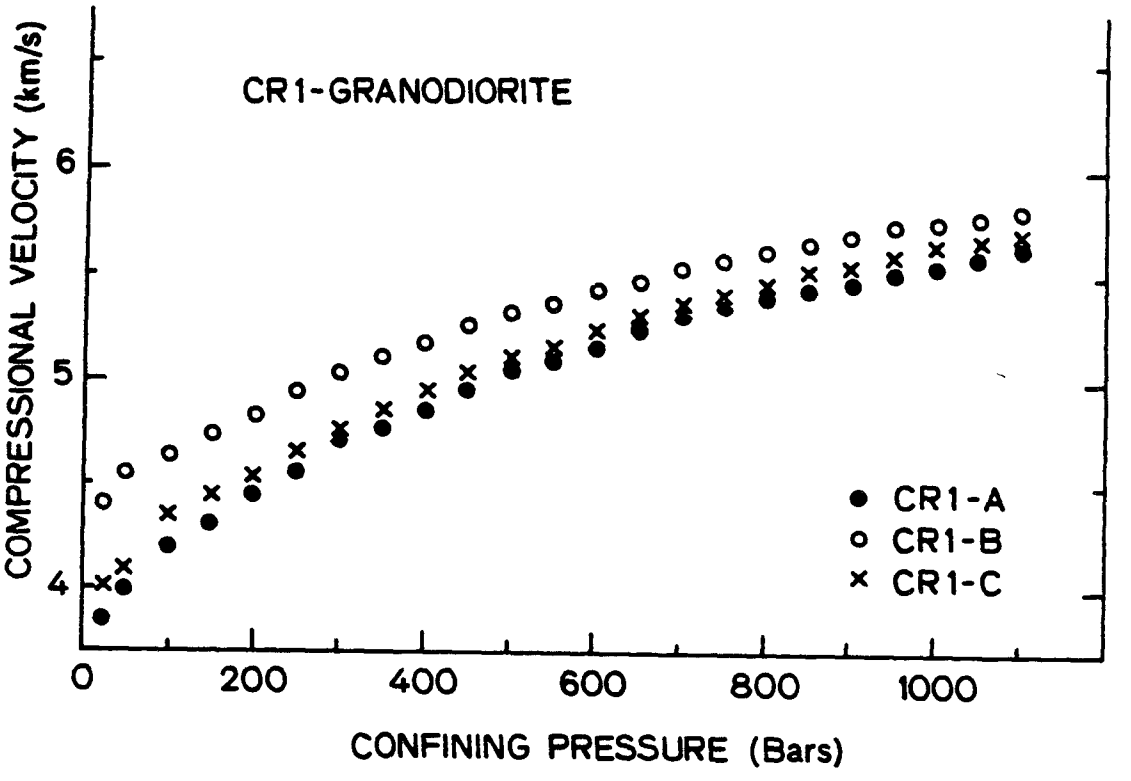

Figure 17. Compressional velocity versus confining pressure for three orthogonal samples of CR 1 (granodiorite). Dry conditions.

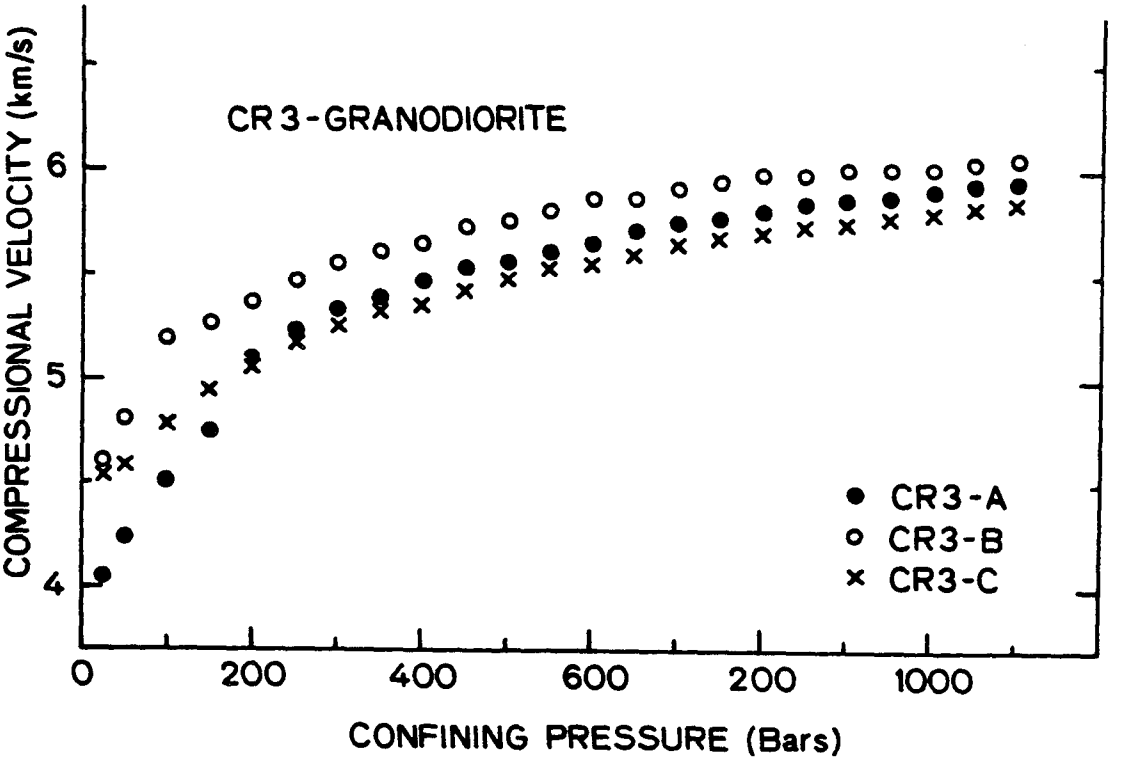

Figure 18. Compressional velocity versus confining pressure for three orthogonal samples of CR 3 (granodiorite). Dry conditions.

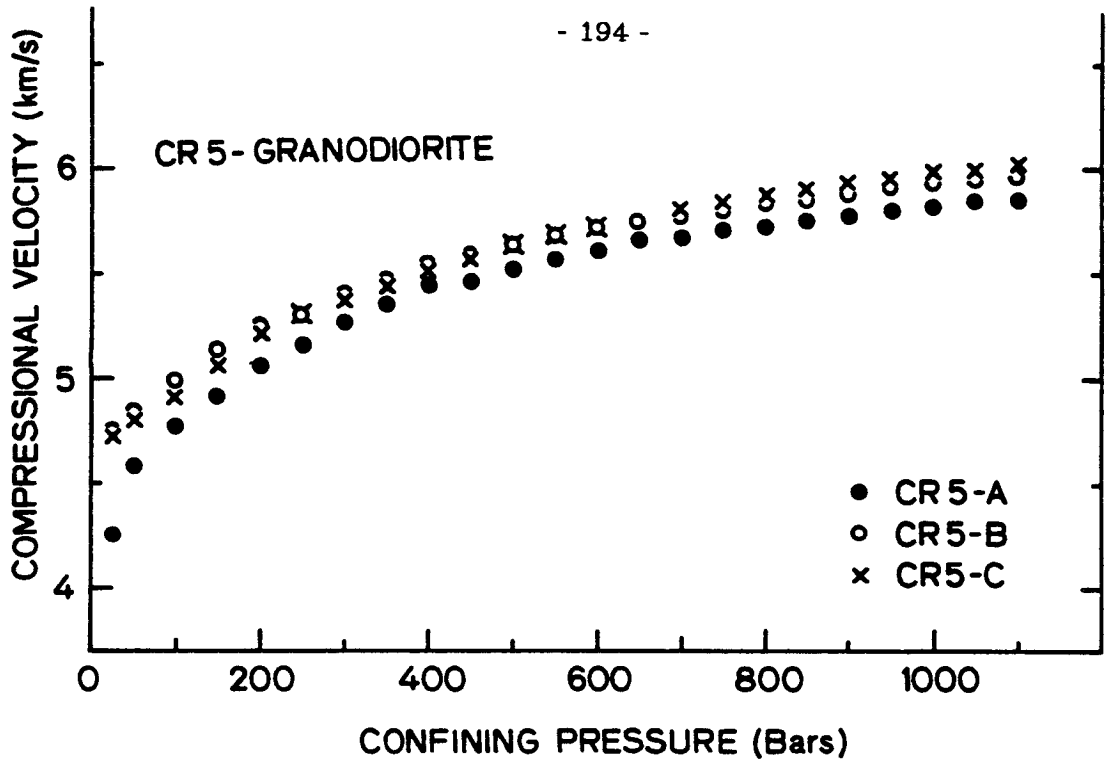

Figure 19. Compressional velocity versus confining pressure for three orthogonal samples of CR 5 (granodiorite). Dry conditions.

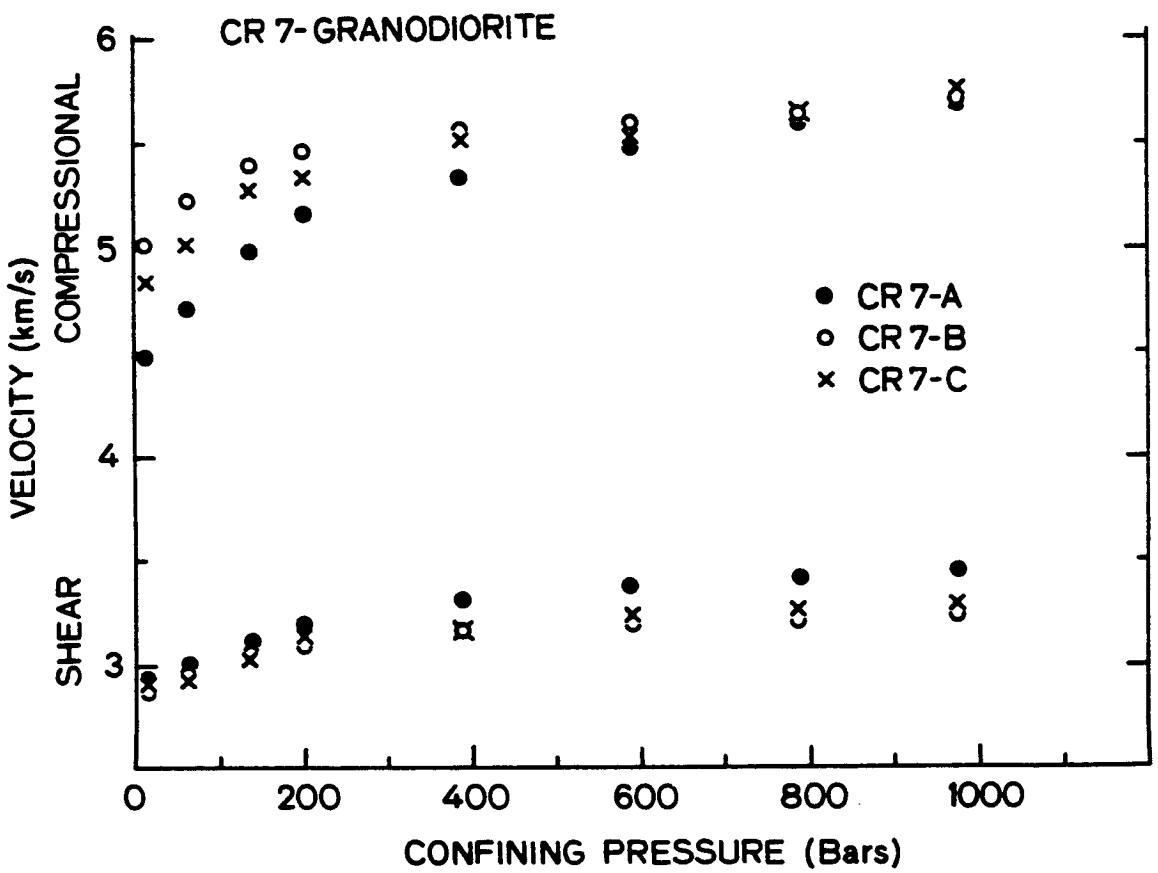

Figure 20. Compressional and shear velocity versus confining pressure for three orthogonal samples of CR 7 (granodiorite). Dry conditions.

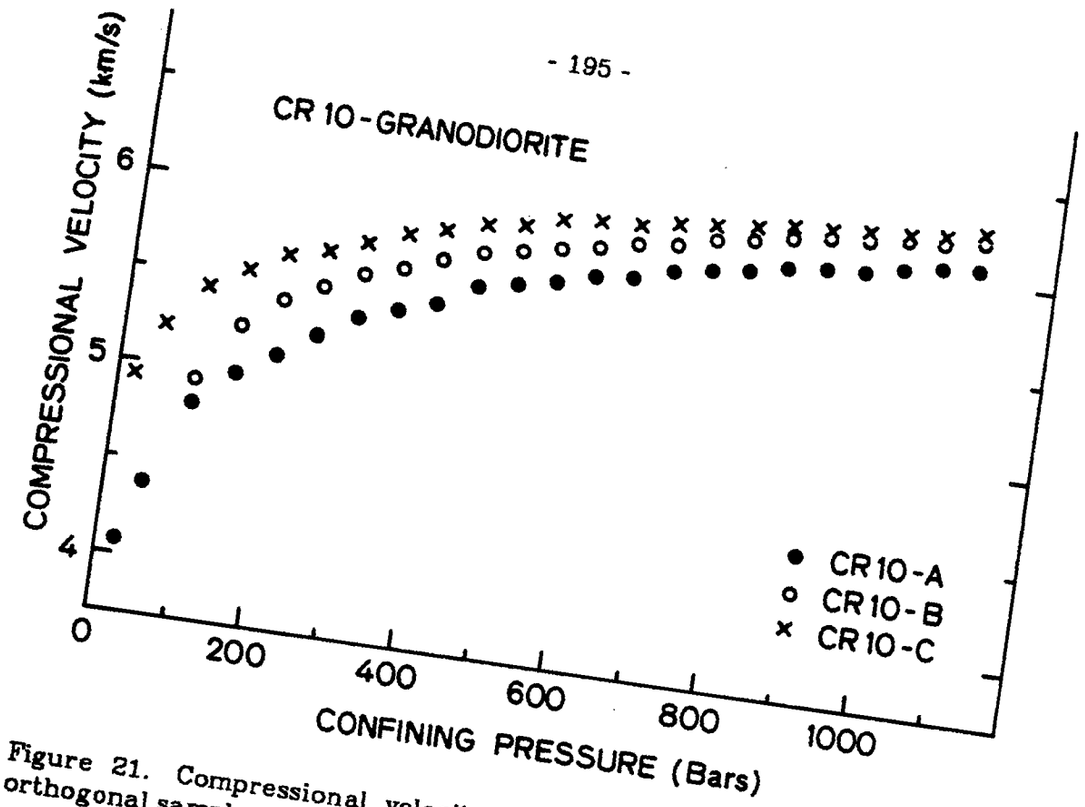

Figure 21. Compressional velocity versus confining pressure for three orthogonal samples of CR 10 (granodiorite). Dry conditions.

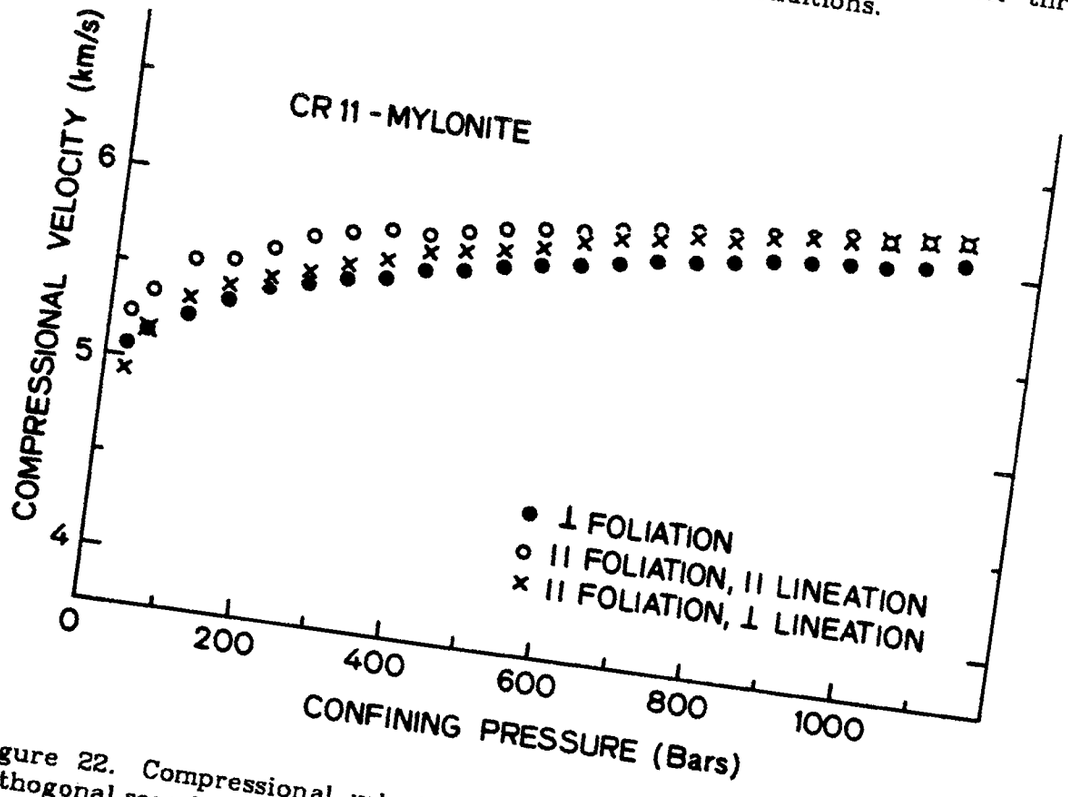

Figure 22. Compressional velocity versus confining pressure for three orthogonal samples oriented with respect to fabric as indicated. Rock is CR 11 (mylonitic granodiorite). Dry conditions.

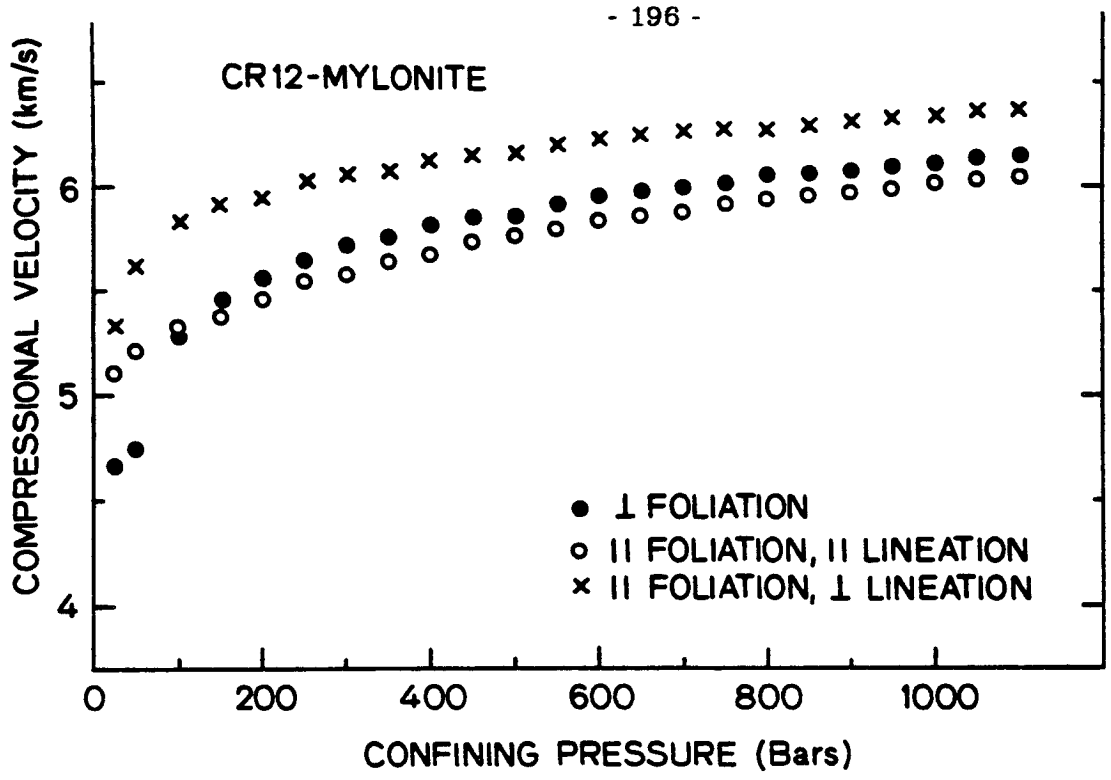

Figure 23. Compressional velocity versus confining pressure for three orthogonal samples oriented with respect to fabric as indicated. Rock is CR 12 (mylonitic granodiorite). Dry conditions.

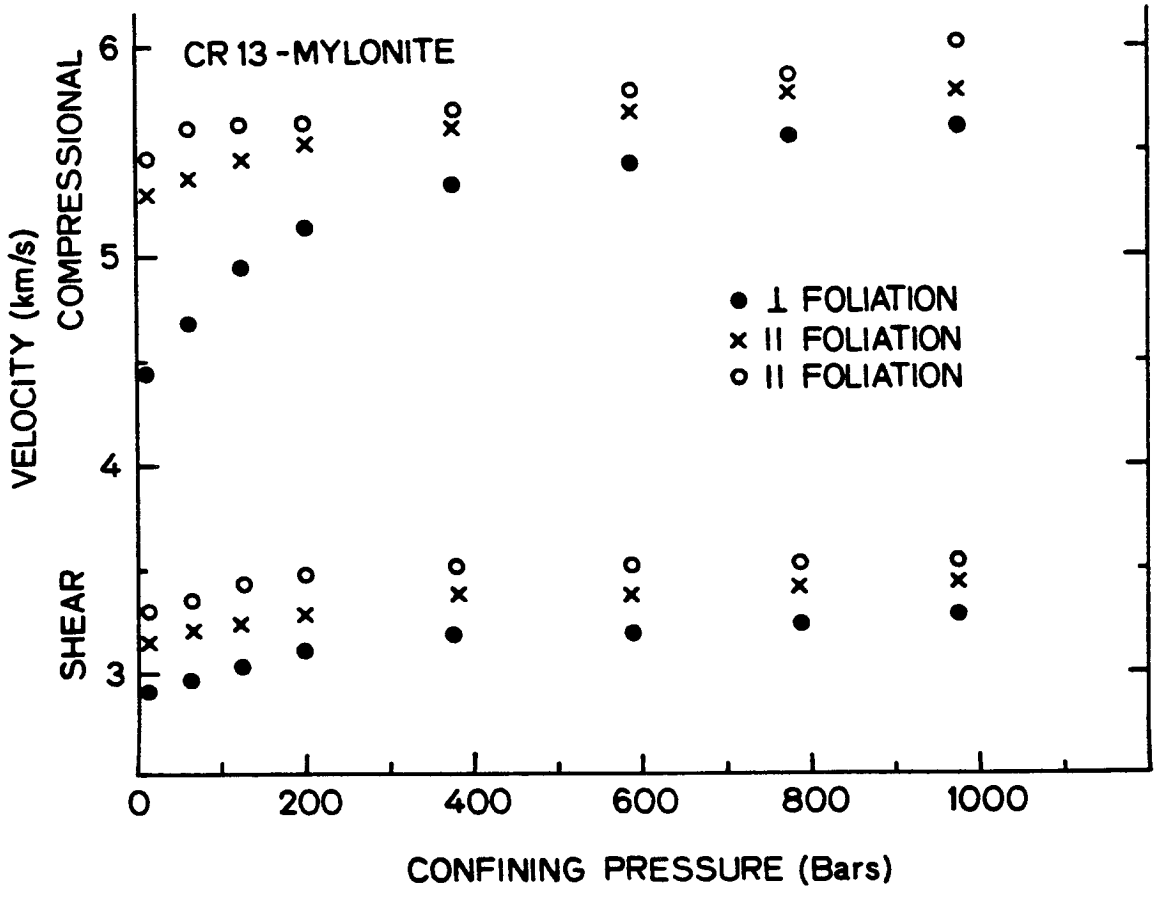

Figure 24. Compressional and shear velocity versus confining pressure for three orthogonal samples oriented with respect to fabric as indicated.

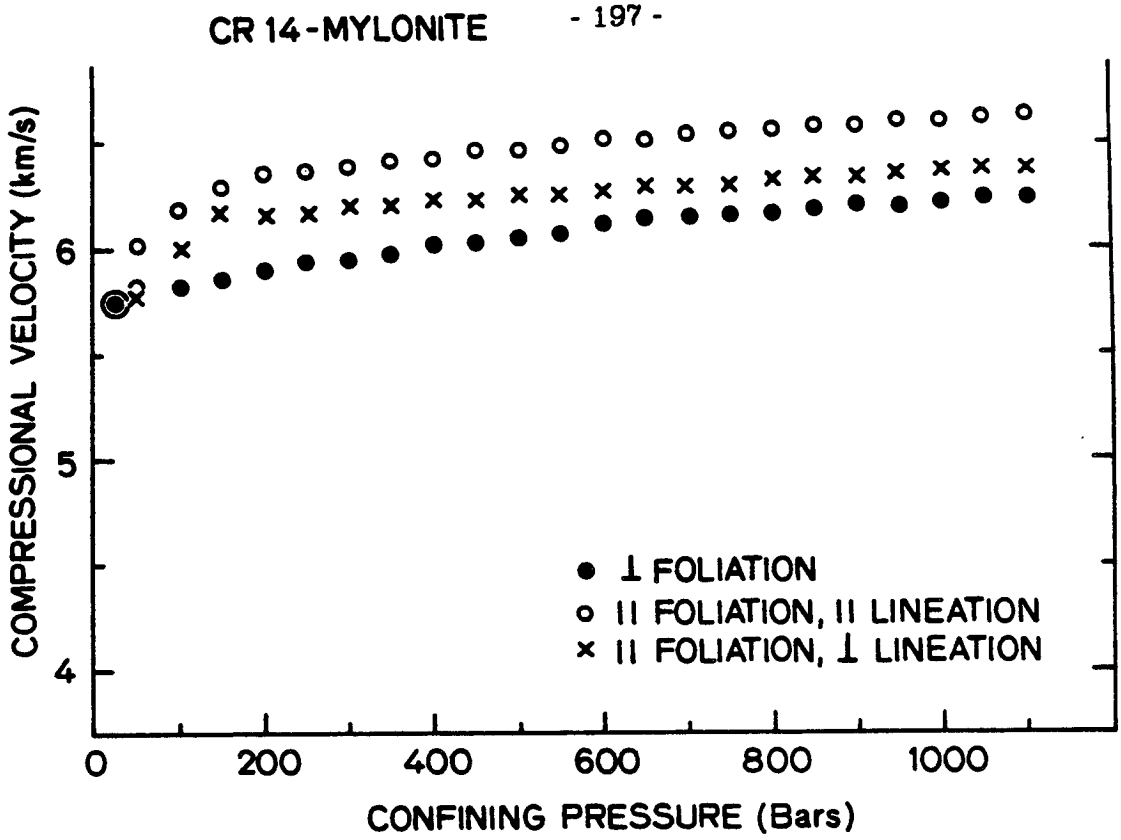

Figure 25. Compressional velocity versus confining pressure for three orthogonal samples oriented with respect to fabric as indicated. Rock is CR 14 (mylonitic metasediment). Dry conditions.

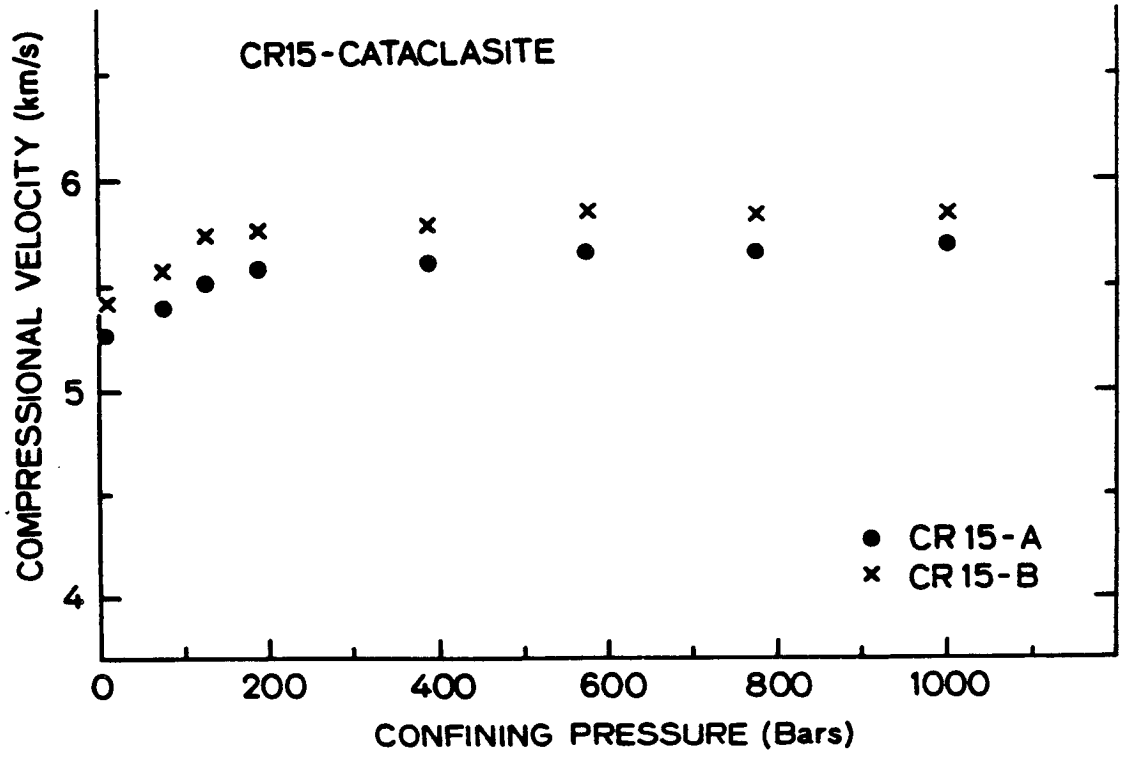

Figure 26. Compressional velocity versus confining pressure for two orthogonal samples of CR 15 (cataclasite). Dry conditions.

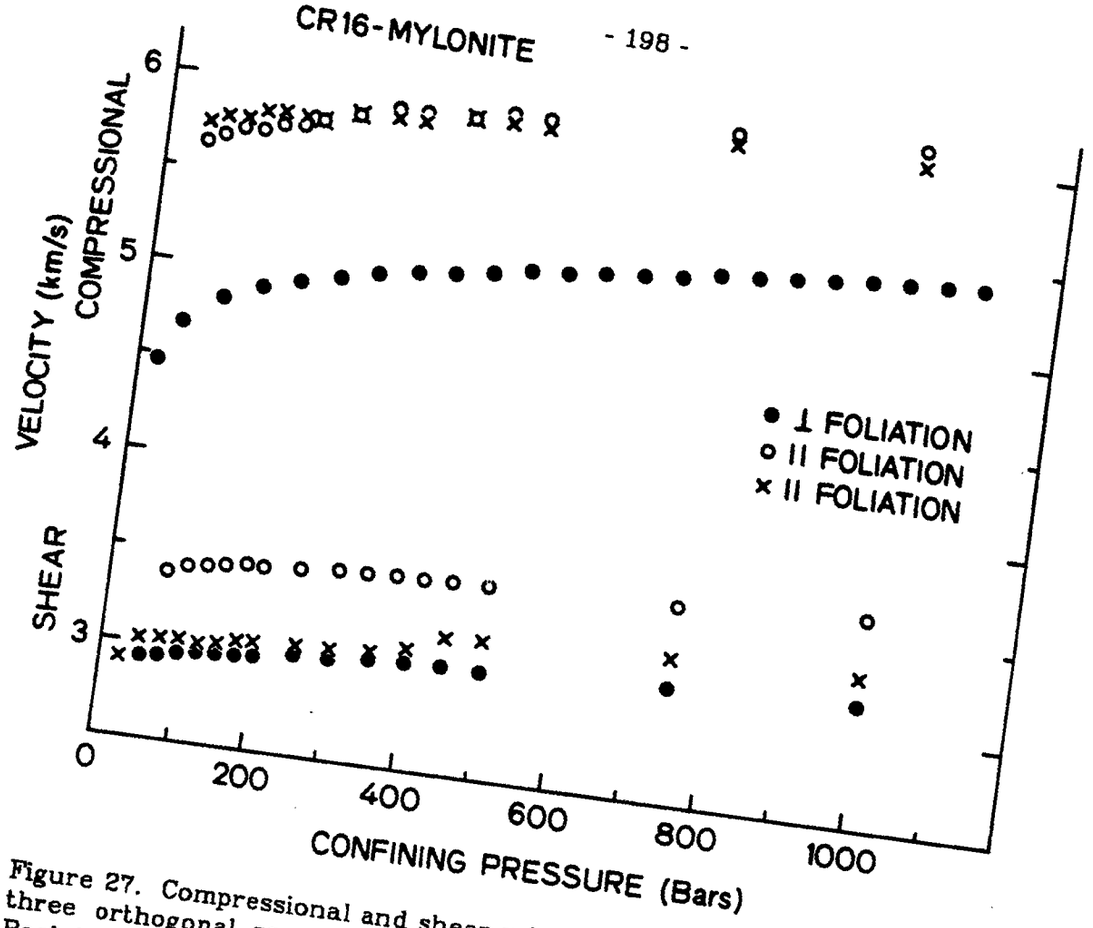

Figure 27. Compressional and shear velocity versus confining pressure for three orthogonal samples oriented with respect to fabric as indicated. Rock is CR 16 (mylonitic metasediment). Dry conditions.

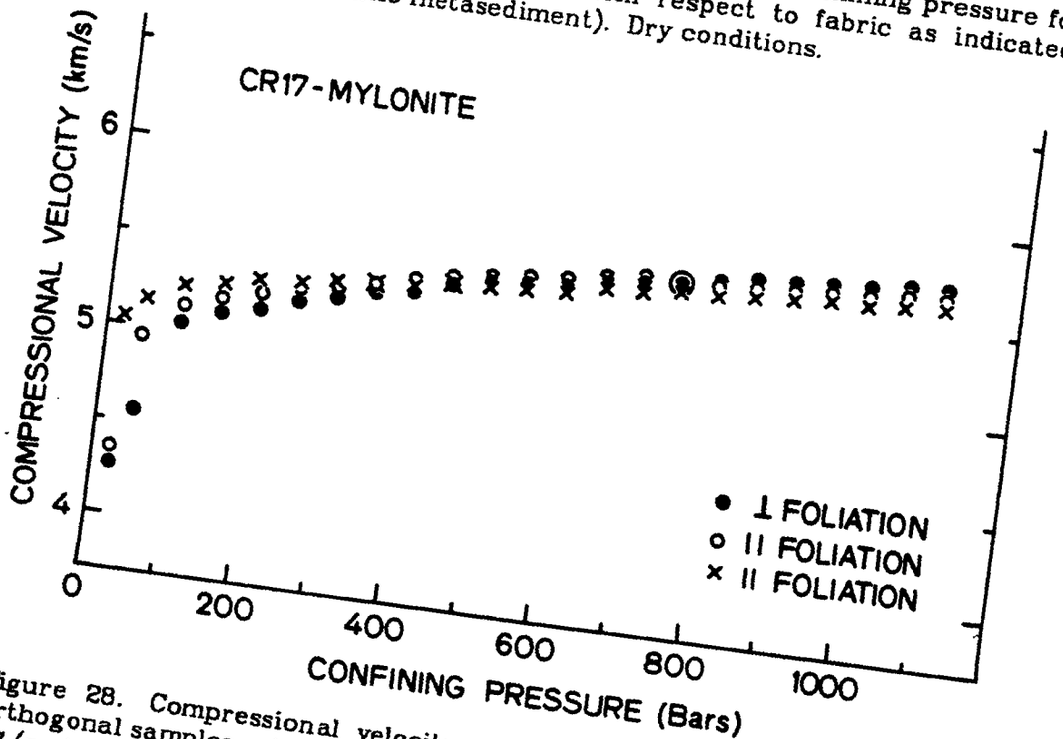

Figure 28. Compressional velocity versus confining pressure for three orthogonal samples oriented with respect to fabric as indicated. Rock is CR 17 (mylonitic metasediment). Dry conditions.

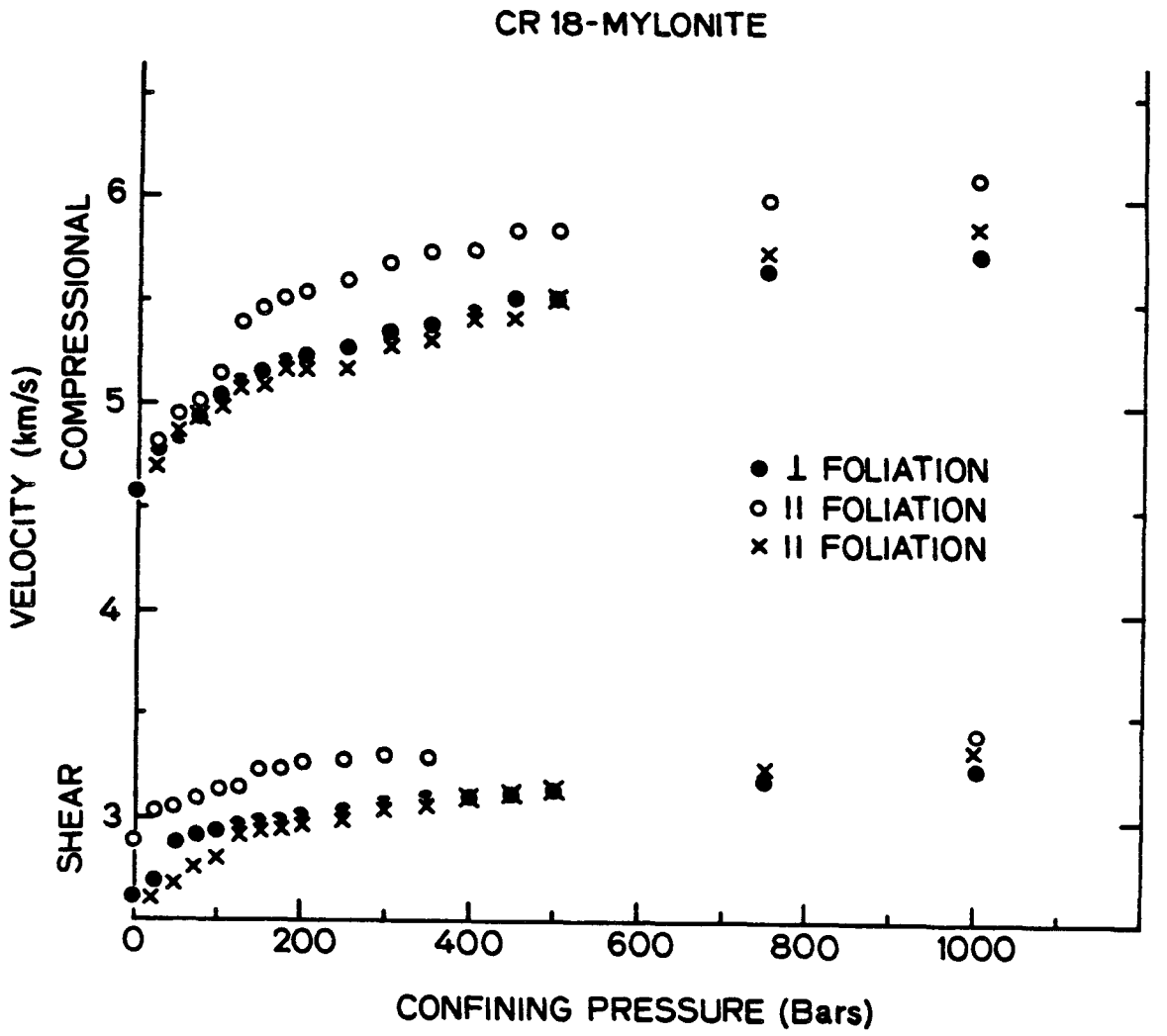

Figure 29. Compressional and shear velocity versus confining pressure for three orthogonal samples oriented with respect to fabric as indicated. Rock is CR 18 (mylonitic metasediment). Dry conditions.

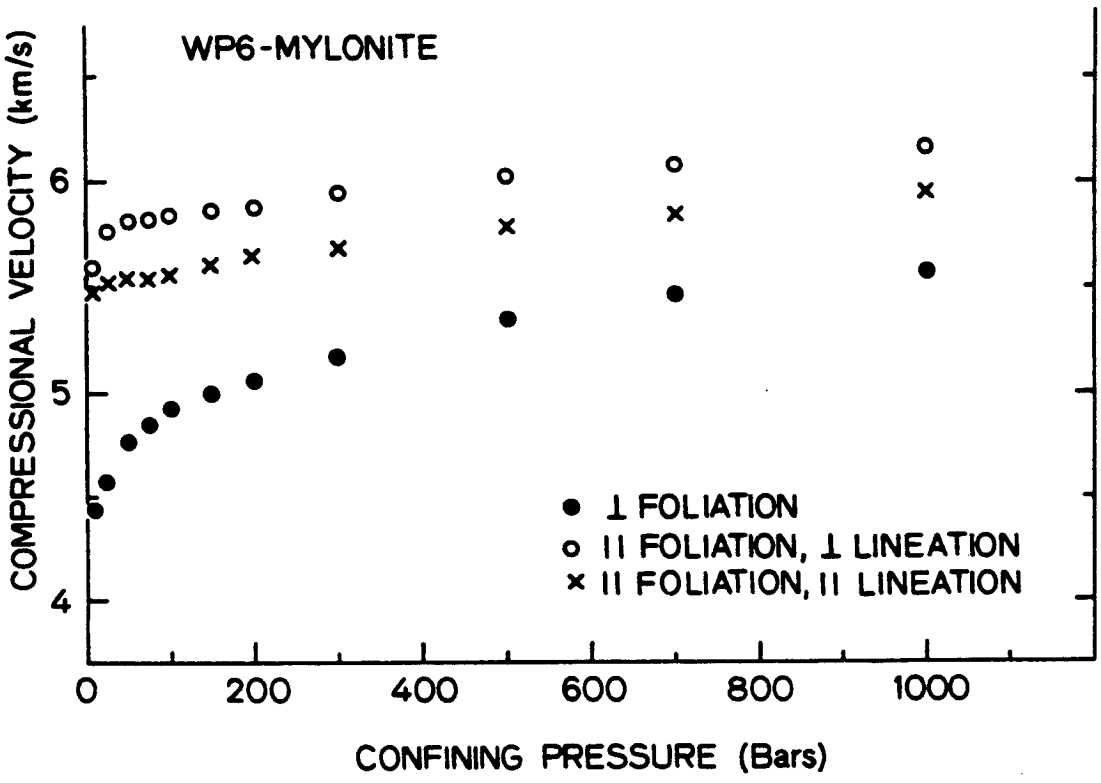

Figure 30. Compressional velocity versus confining pressure for three orthogonal samples oriented with respect to fabric as indicated. Rock is WP 6 (flaser gneiss mylonite). Dry conditions.

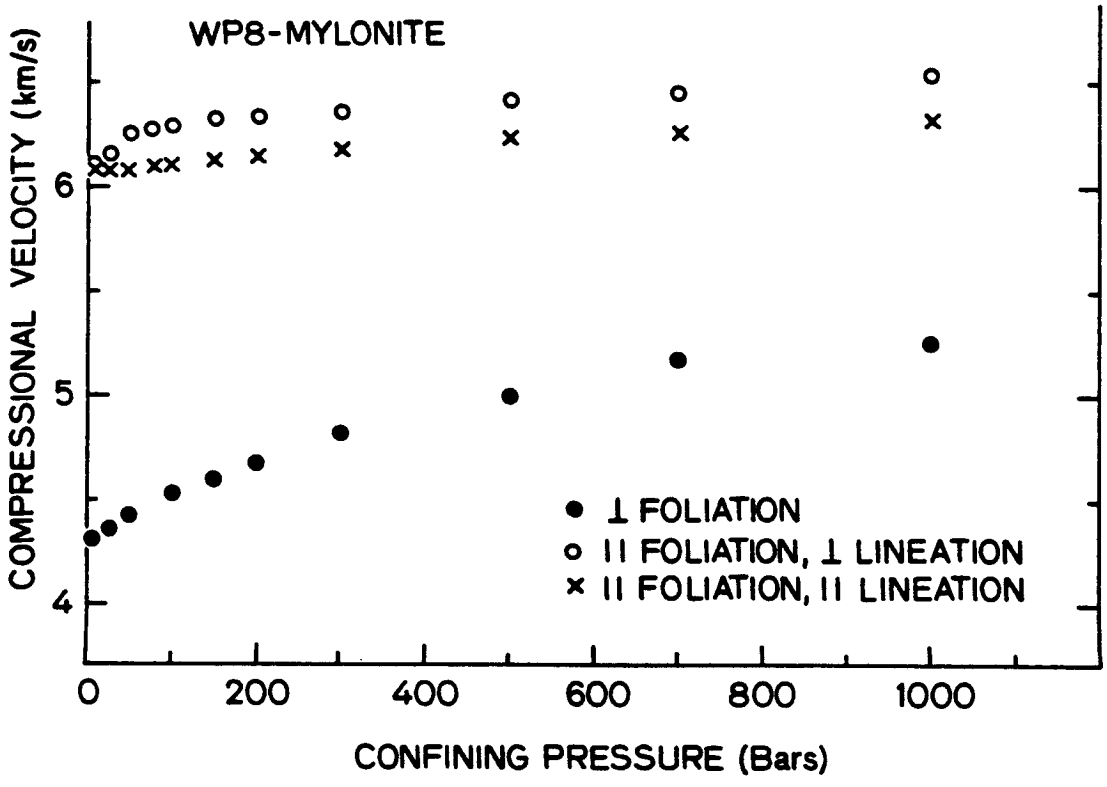

Figure 31. Compressional velocity versus confining pressure for three orthogonal samples oriented with respect to fabric as indicated. Rock is WP

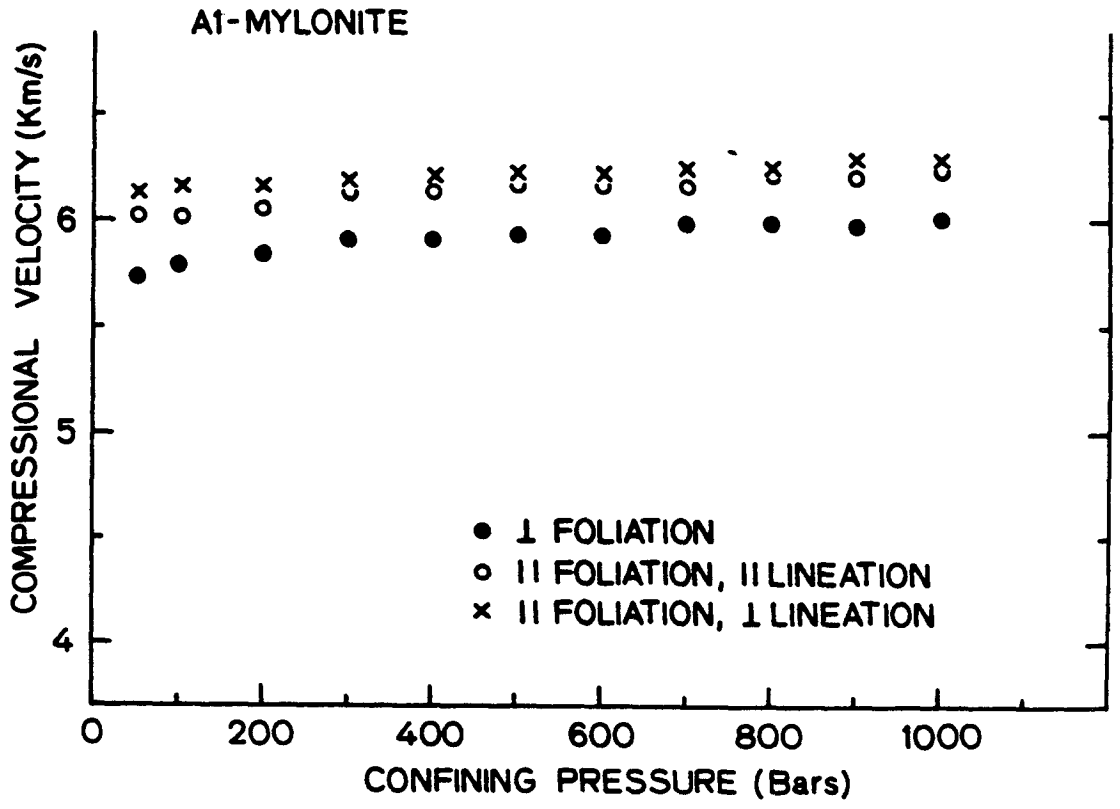

Figure 32. Compressional velocity versus confining pressure for three orthogonal samples oriented with respect to fabric as indicated. Rock is A1 (Goat Rock mylonite). Dry conditions.

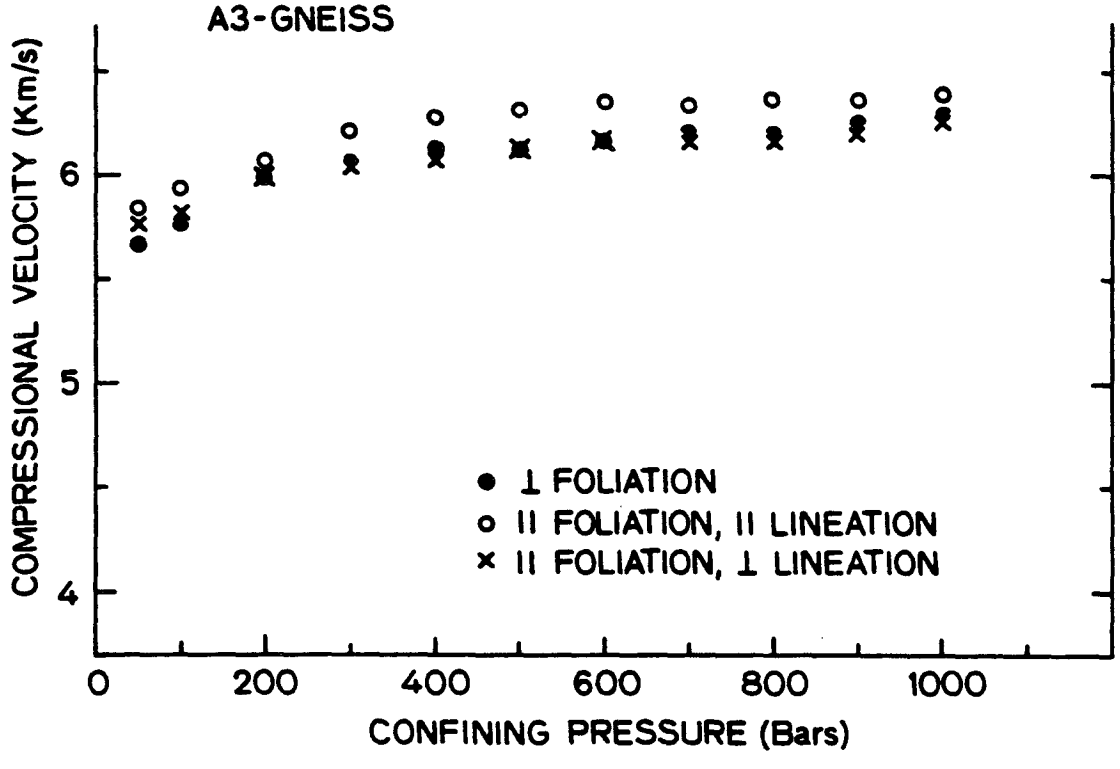

Figure 33. Compressional velocity versus confining pressure for three orthogonal samples oriented with respect to fabric as indicated. Rock is A3 (Whatlet Mill gneiss). Dry conditions.

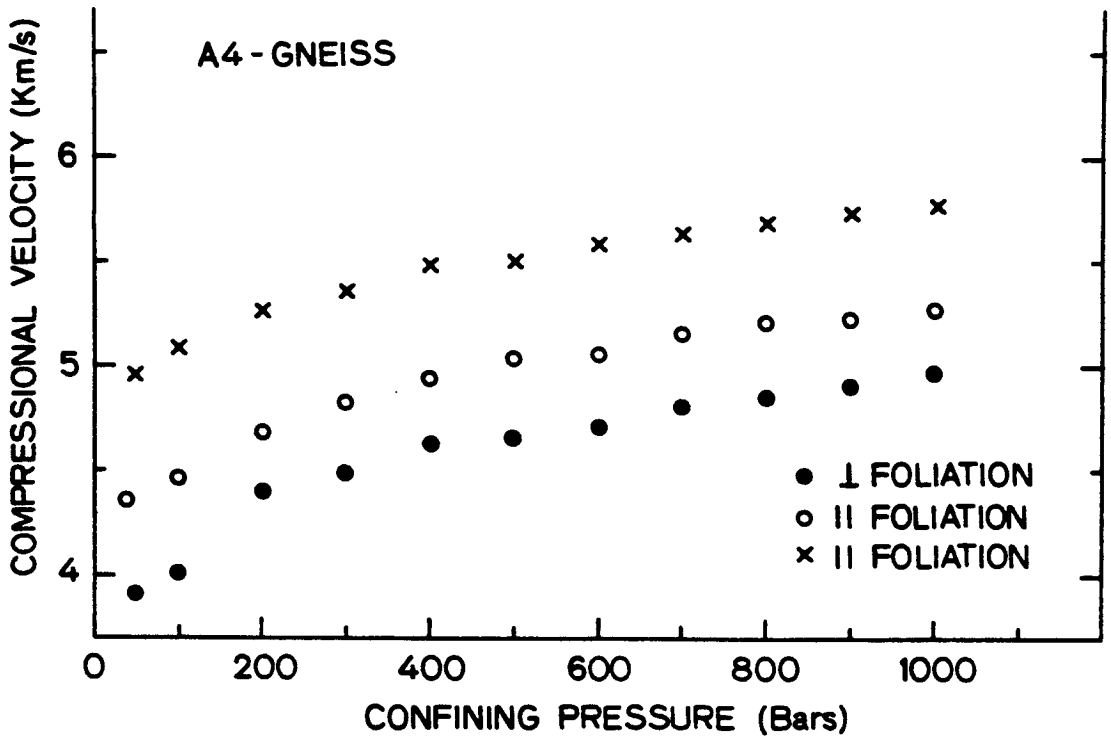

Figure 34. Compressional velocity versus confining pressure for three orthogonal samples oriented with respect to fabric as indicated. Rock is A4 (Mott gneiss). Dry conditions.

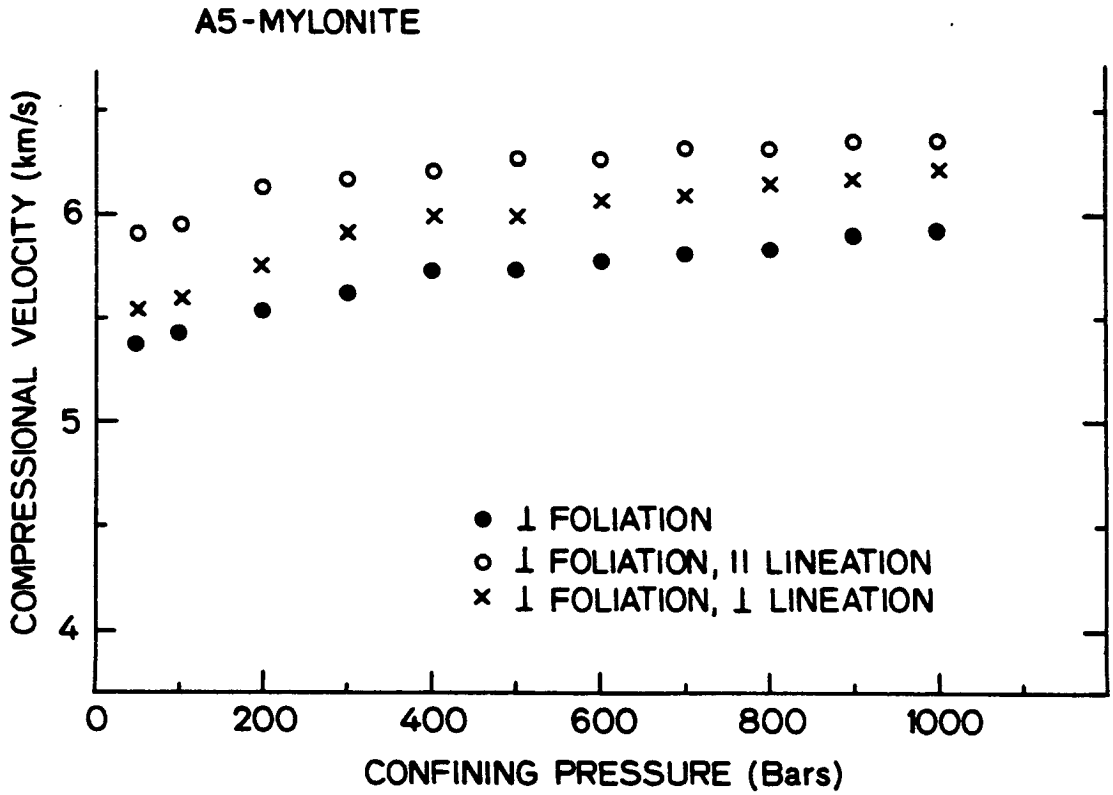

Figure 35. Compressional velocity versus confining pressure for three orthogonal samples oriented with respect to fabric as indicated. Rock is A5 (Bartletts Ferry mylonite). Dry conditions.

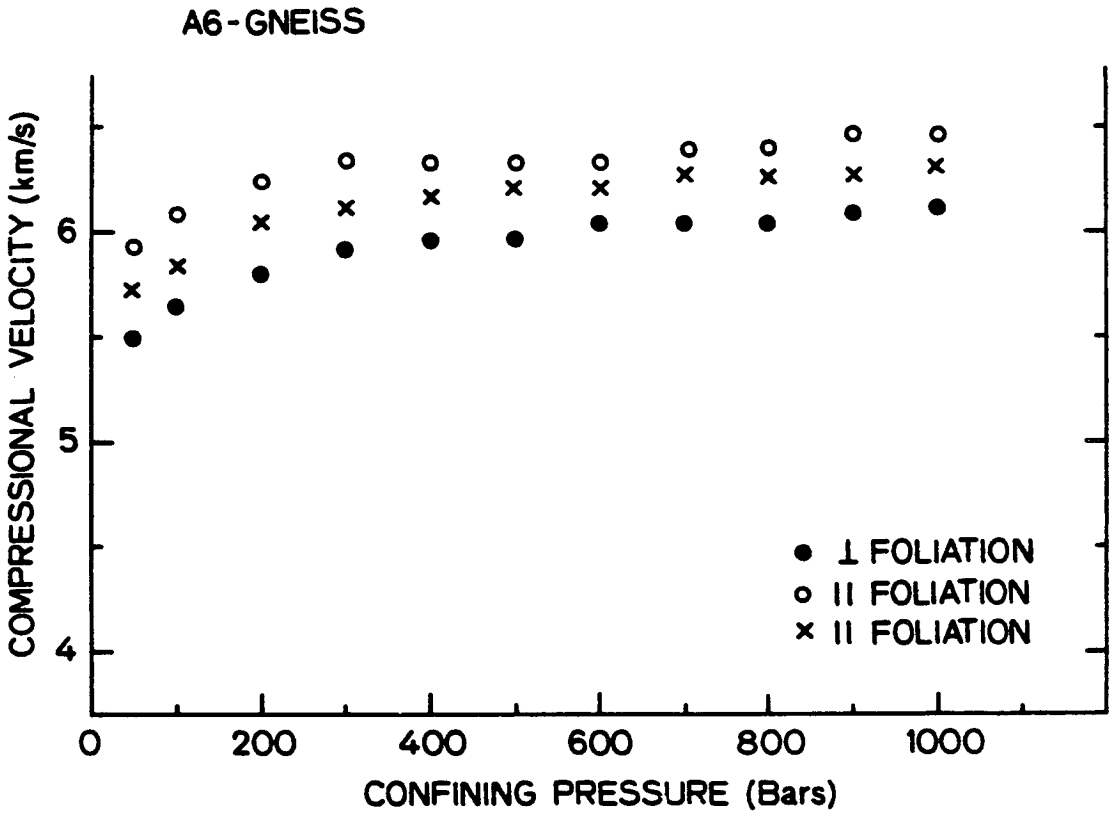

Figure 36. Compressional velocity versus confining pressure for three orthogonal samples oriented with respect to fabric as indicated. Rock is A6 (migmatite gneiss). Dry conditions.

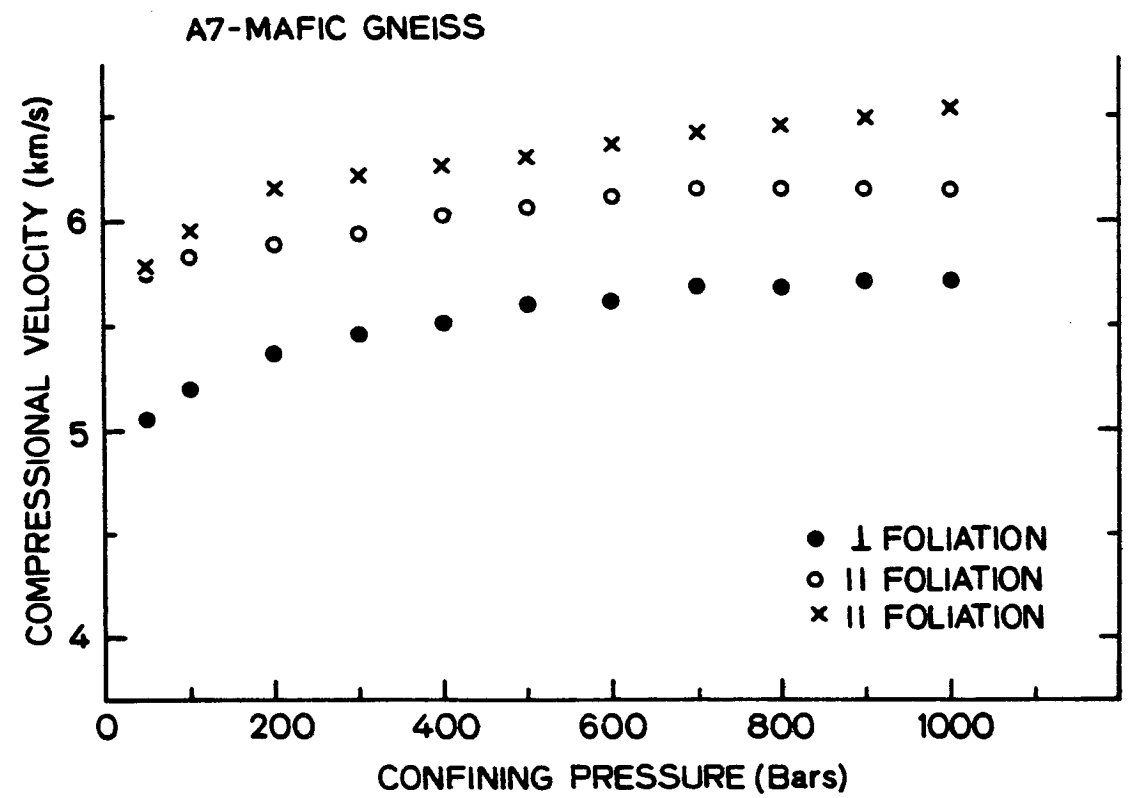

Figure 37. Compressional velocity versus confining pressure for three orthogonal samples oriented with respect to fabric as indicated. Rock is A7 (mafic gneiss). Dry conditions.

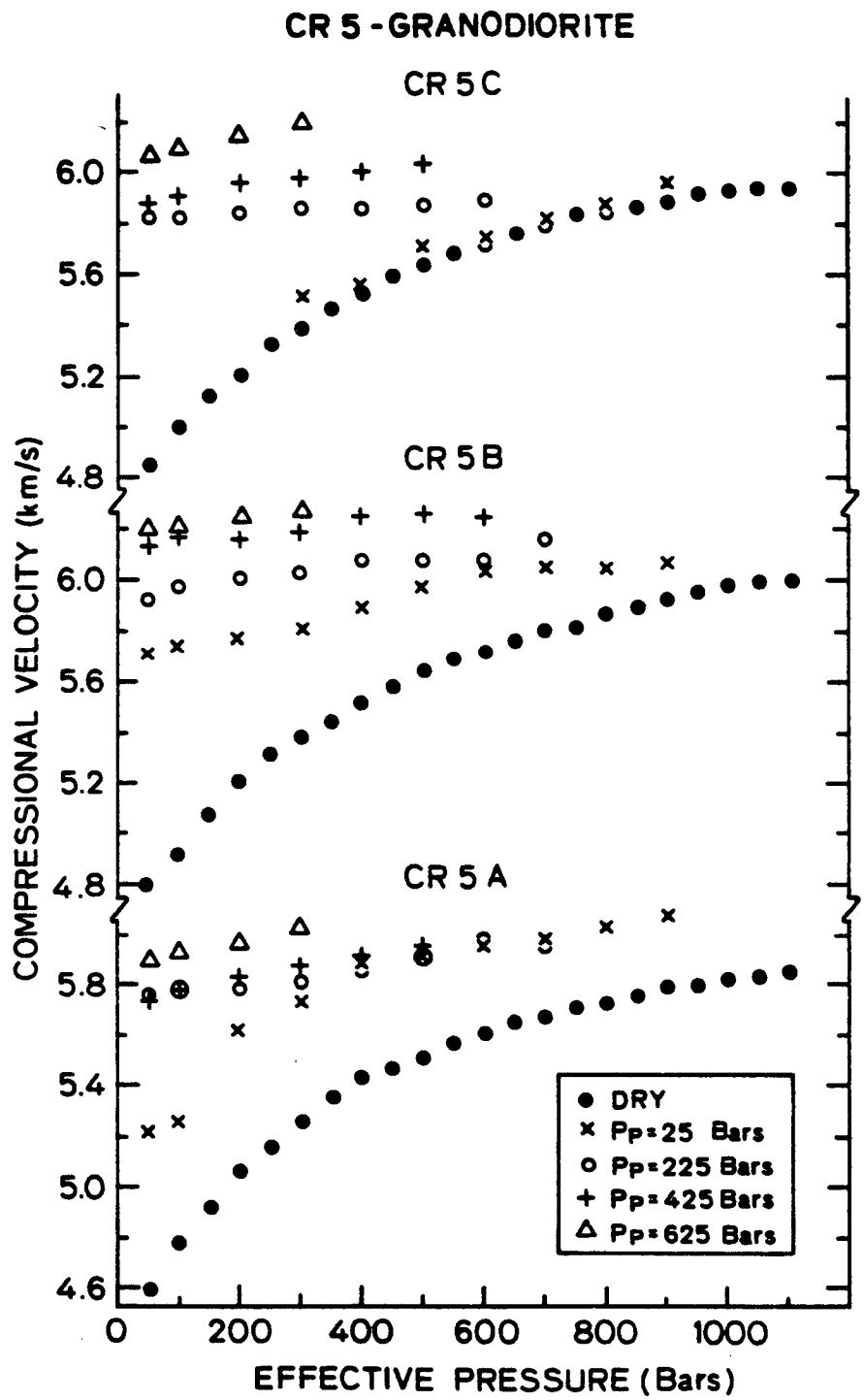

Figure 38. Compressional velocity versus effective pressure for three orthogonal samples. Rock is CR 5 (granodiorite). Sample was water saturated and velocity measurements were done at the indicated pore pressures.

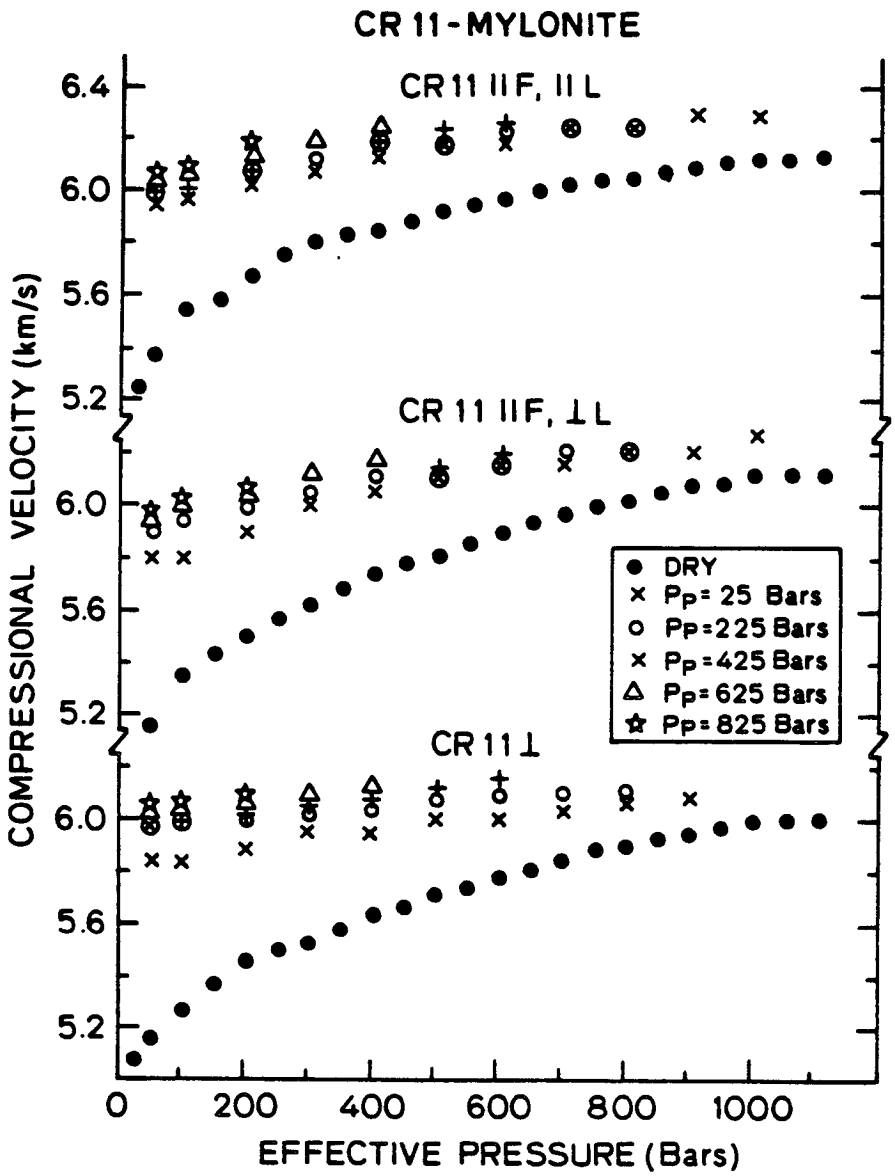

Figure 39. Compressional velocity versus effective pressure for three orthogonal samples oriented with respect to fabric as indicated. Rock is CR 11 (mylonitic granodiorite). Sample was water saturated and velocity measurements were done at the indicated pore pressures.

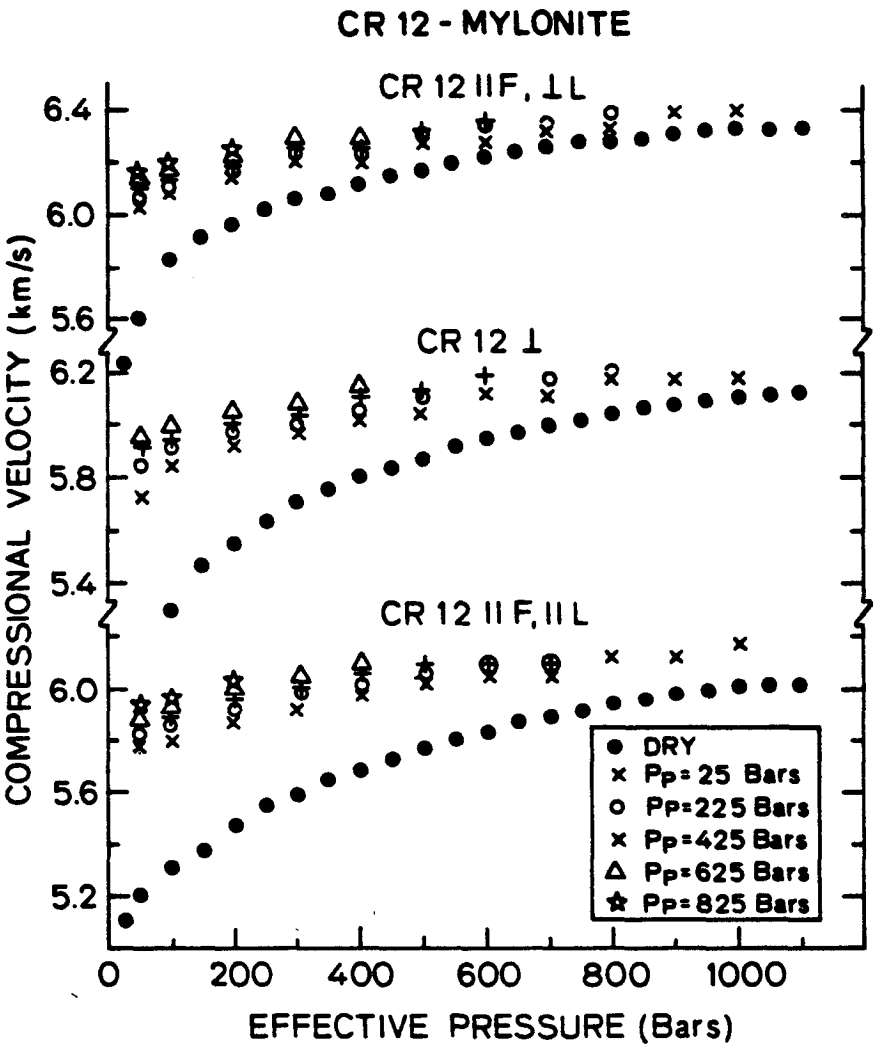

Figure 40. Compressional velocity versus effective pressure for three orthogonal samples oriented with respect to fabric as indicated. Rock is CR 12 (mylonitic granodiorite). Sample was water saturated and velocity measurements were done at the indicated pore pressures.

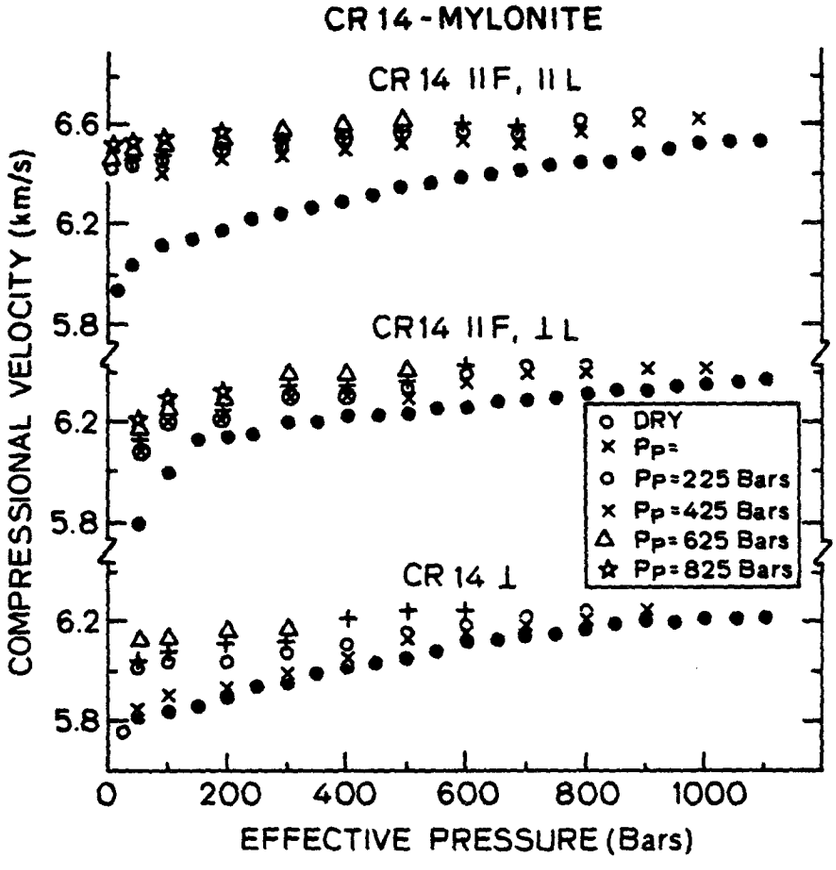

Figure 41. Compressional velocity versus effective pressure for three orthogonal samples oriented with respect to fabric as indicated. Rock is CR 14 (mylonitic metasediment). Sample was water saturated and velocity measurements were done at the indicated pore pressures.

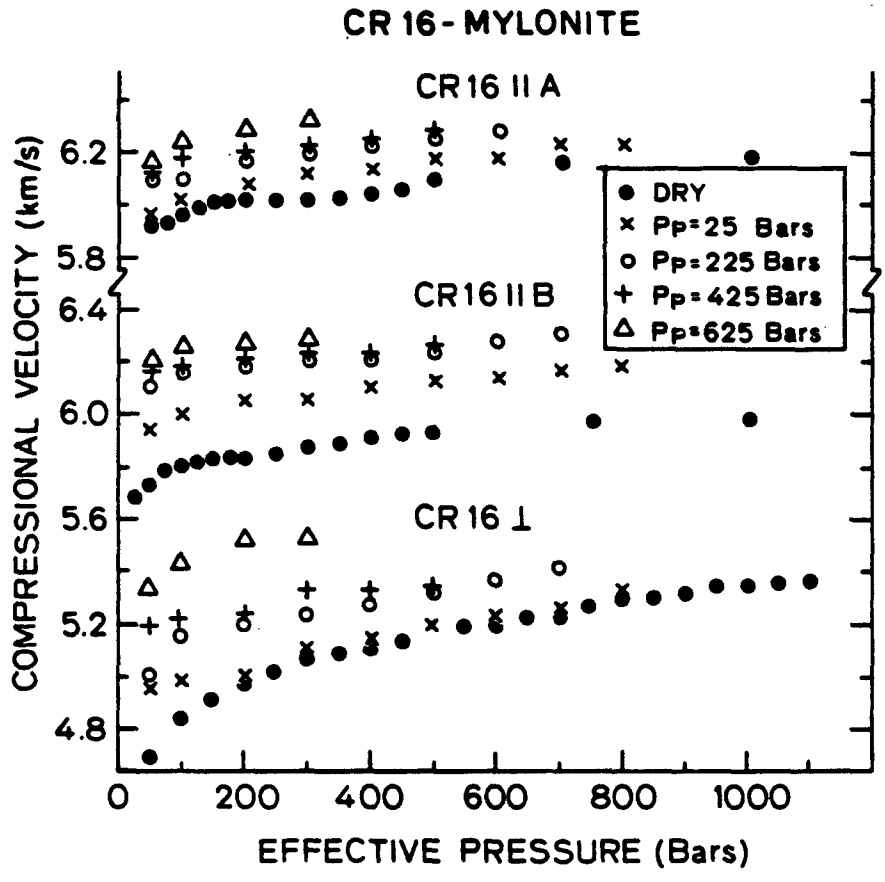

Figure 42. Compressional velocity versus effective pressure for three orthogonal samples oriented with respect to fabric as indicated. Rock is CR 16 (mylonitic metasediment). Sample was water saturated and velocity measurements were done at the indicated pore pressures.

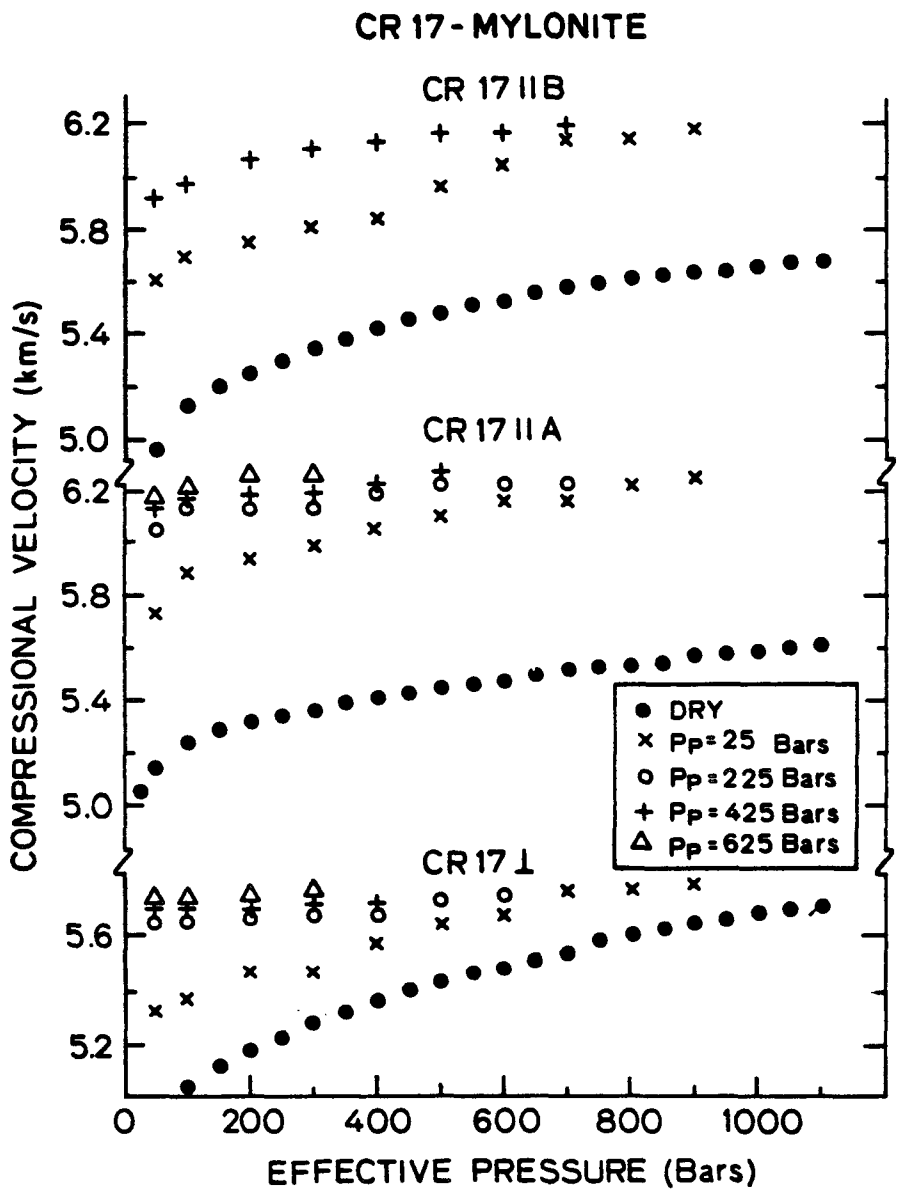

Figure 43. Compressional velocity versus effective pressure for three orthogonal samples oriented with respect to fabric as indicated. Rock is CR 17 (mylonitic metasediment). Sample was water saturated and velocity measurements were done at the indicated pore pressures.

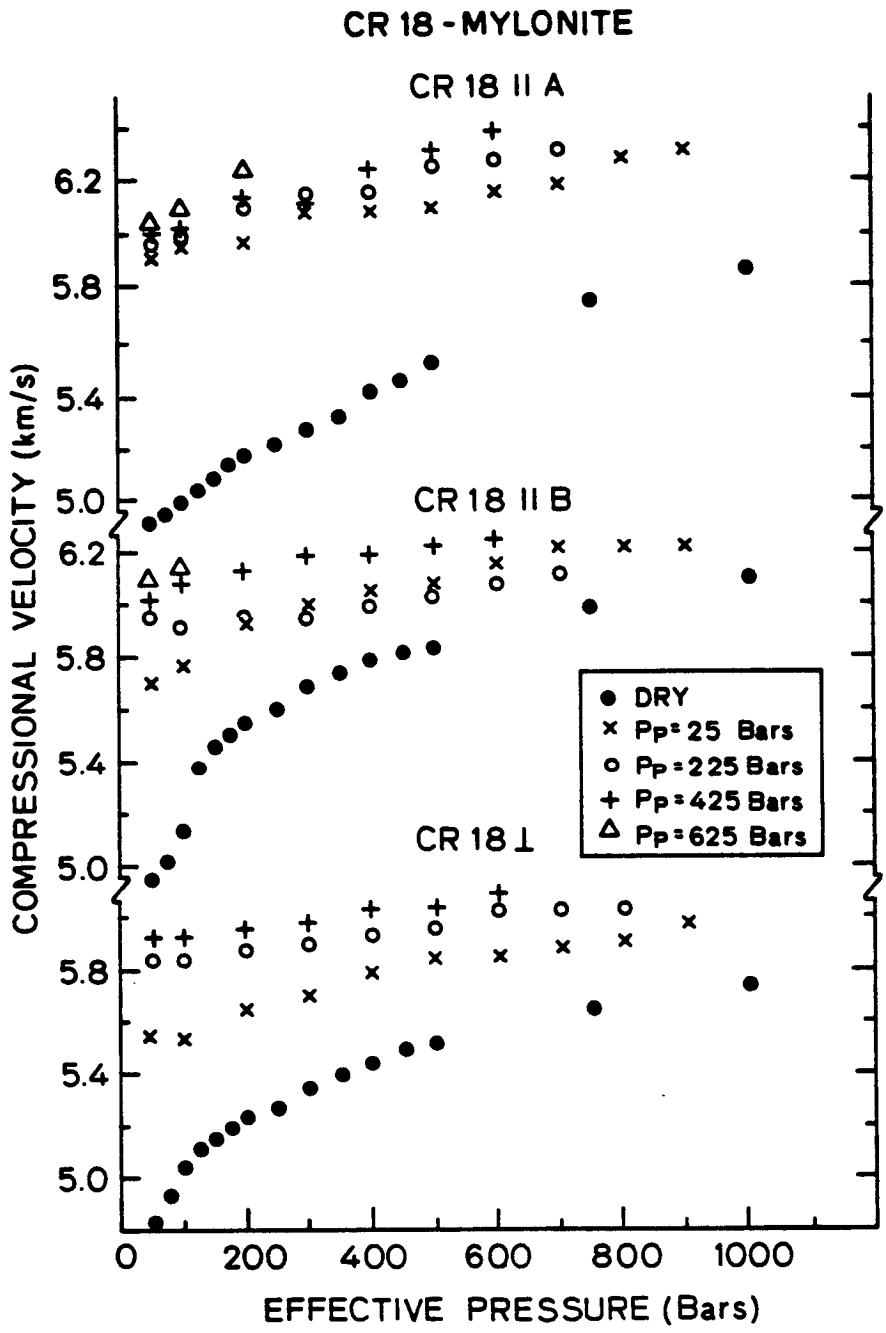

Figure 44. Compressional velocity versus effective pressure for three orthogonal samples oriented with respect to fabric as indicated. Rock is CR 18 (mylonitic metasediment). Sample was water saturated and velocity measurements were done at the indicated pore pressures.

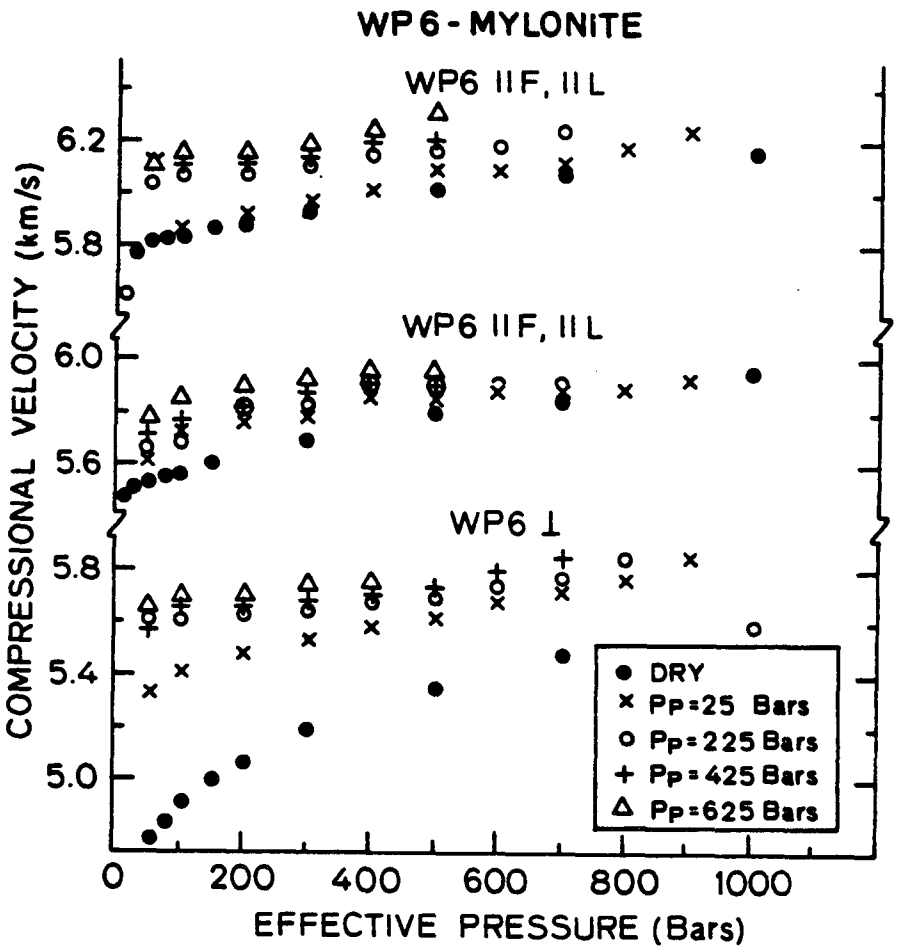

Figure 45. Compressional velocity versus effective pressure for three orthogonal samples oriented with respect to fabric as indicated. Rock is WP 6 (flaser gneiss mylonite). Sample was water saturated and velocity measurements were done at the indicated pore pressures.

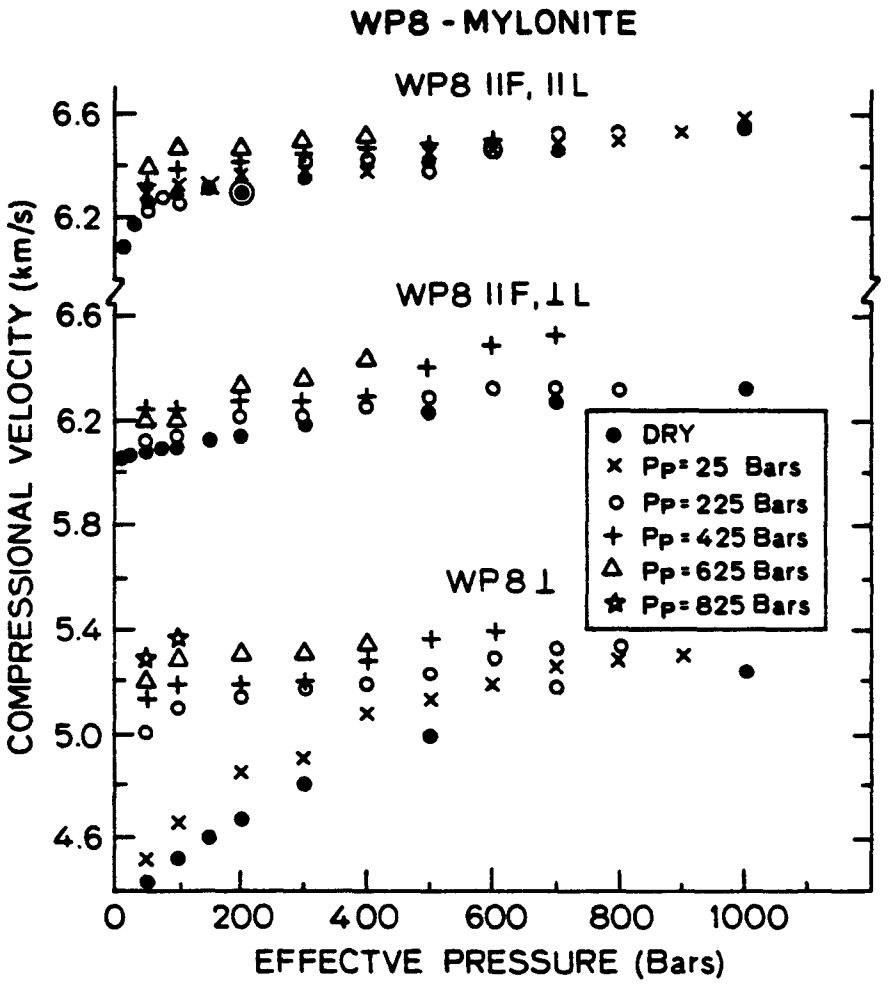

Figure 46. Compressional velocity versus effective pressure for three orthogonal samples oriented with respect to fabric as indicated. Rock is WP 8 (blastomylonite). Sample was water saturated and velocity measurements were done at the indicated pore pressures.

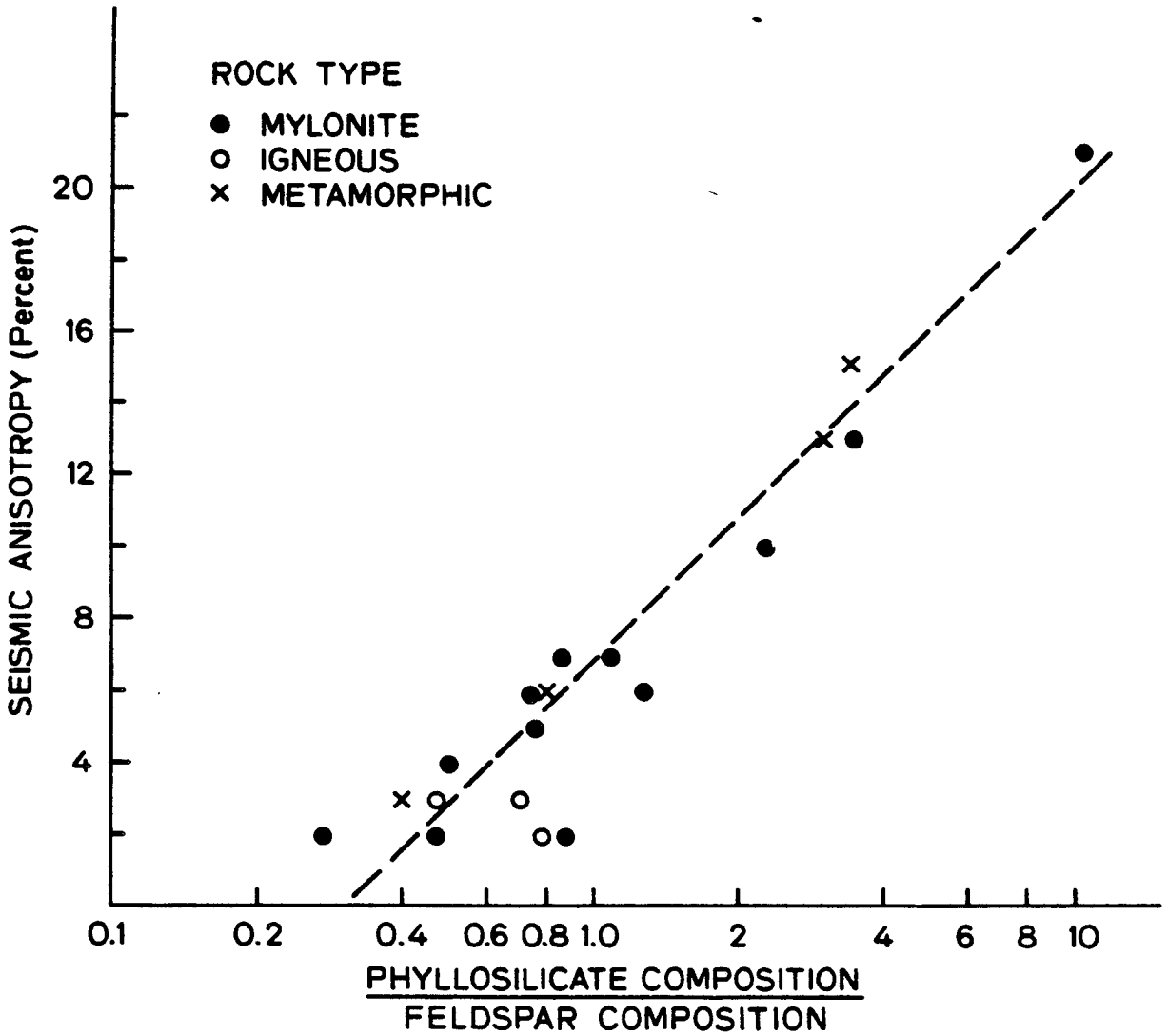

Figure 47. Percent seismic anisotropy plotted versus phyllosilicate composition divided by feldspar composition for all samples.

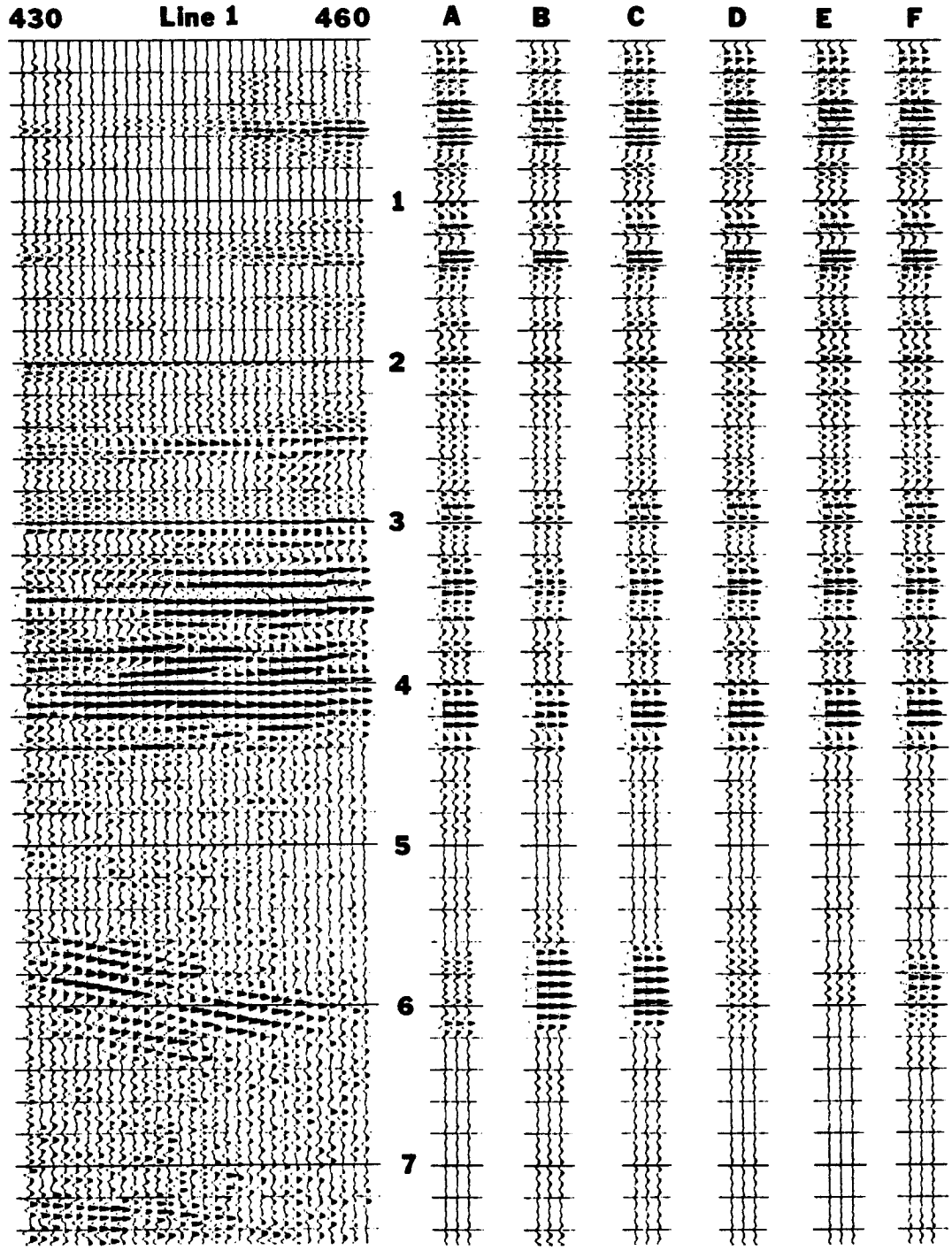

Figure 48. On the left if a portion of Wind River line 1 showing the reflections from the Pacific Creek thrust fault at about 6 seconds. On the right are synthetics computed for several cases based on our data. A: Velocities measured in mylonites from the Columbia River fault zone, including anisotropic effects. B: A series of alternating layers 110 meters thick, an isotropic layer in contact with a layer of 20% anisotropy. C: Same as case B but with an anisotropy of 13%. D: Same as case B but with an anisotropy of 7%. E: Same as case B but with an anisotropy of 4%. F: Velocities from Appalachian rocks, including maximum anisotropic effects, alternating layers of velocity perpendicular to foliation in contact with

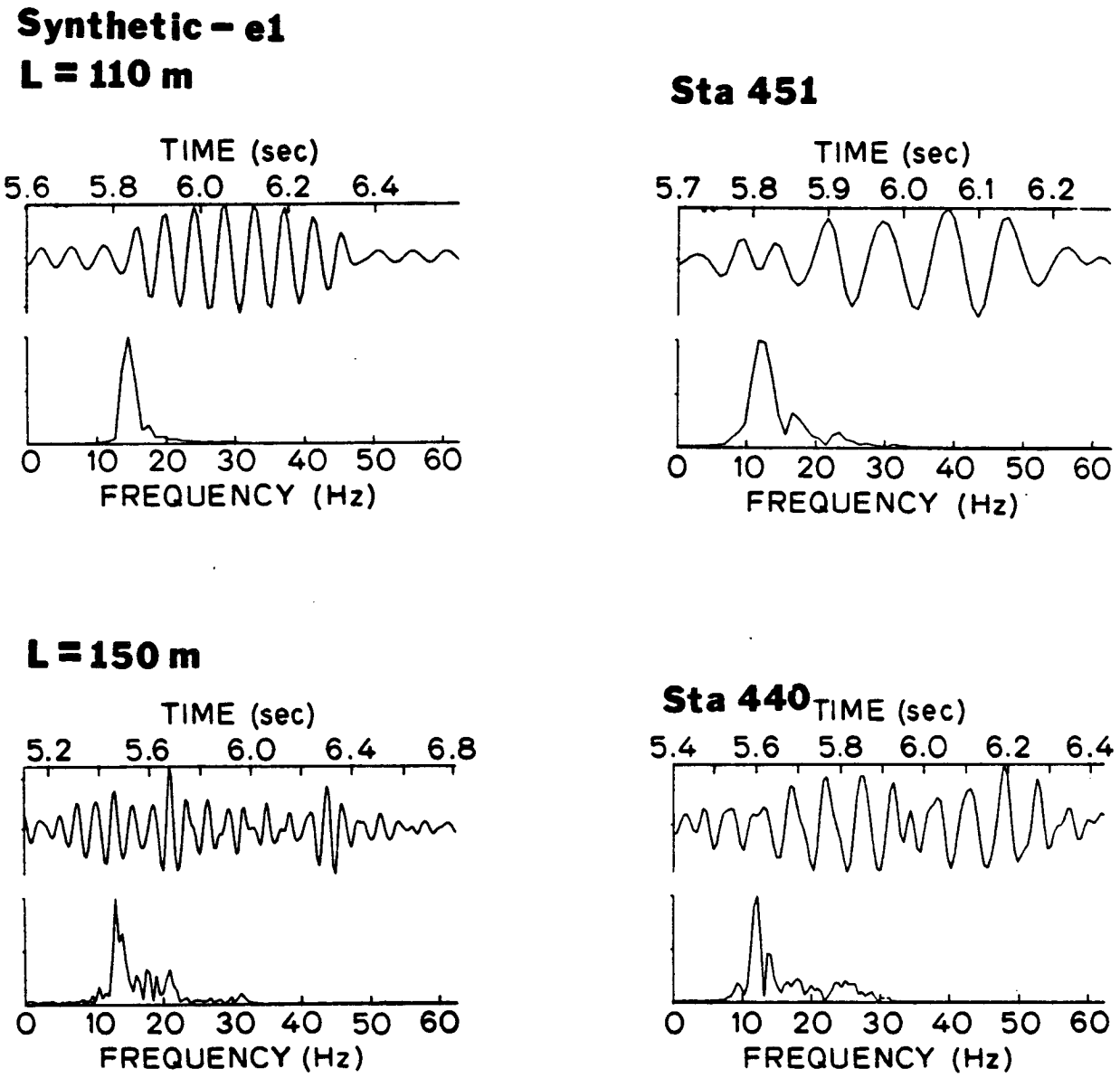

Figure 49. Frequency content of the reflections from the Pacific Creek thrust (right) and from the synthetics (left). Note change of time scale between the data and the synthetics.

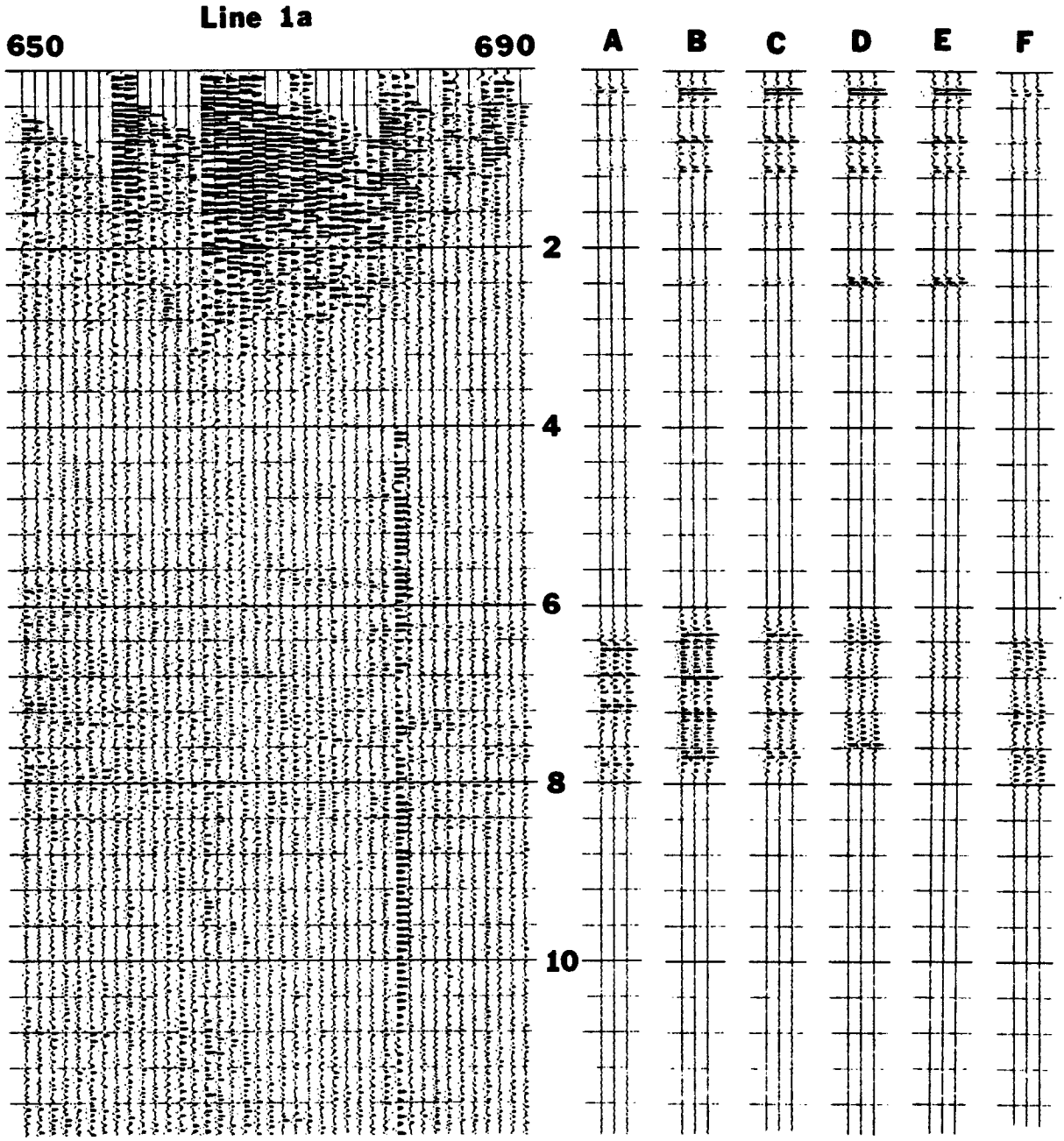

Figure 50. On the left is a portion of Wind River line 1a showing the reflections from the Wind River thrust at 6 to 8 seconds. On the right is a series of synthetics computed for the same conditions as for Figure 48, except the thickness is 150 meters and more layers are used to get a thicker series of reflections.

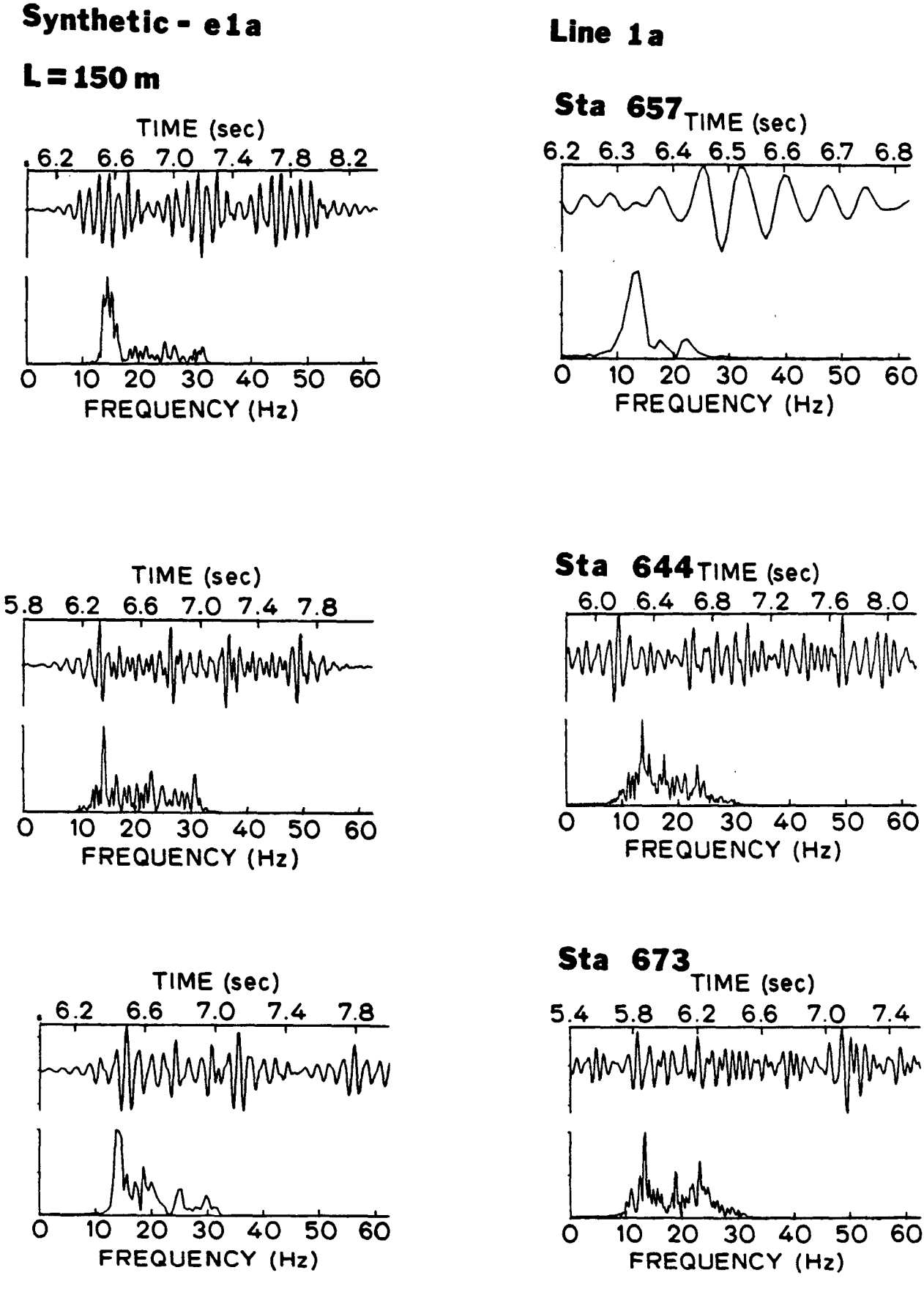

Figure 51. Frequency content of the reflections from the Wind River thrust fault (right) and from the synthetics (left).

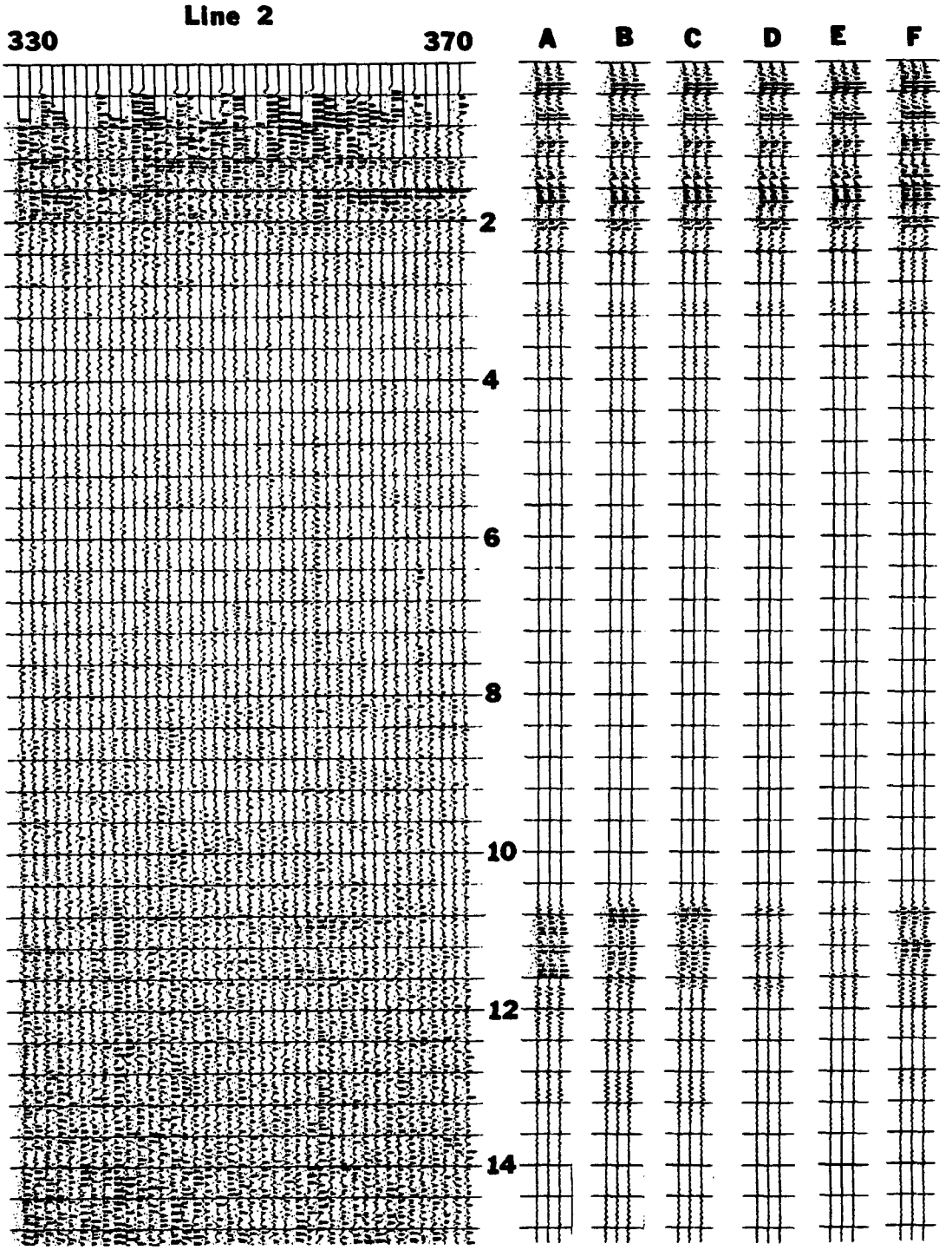

Figure 52. On the left is a portion of Wind River line 2 showing possible reflections from the Wind River thrust at 11 to 12 seconds. On the right is a series of synthetics computed for the same conditions as for Figure 48, except a thickness of 300 meters was used for the fault zone laminations.

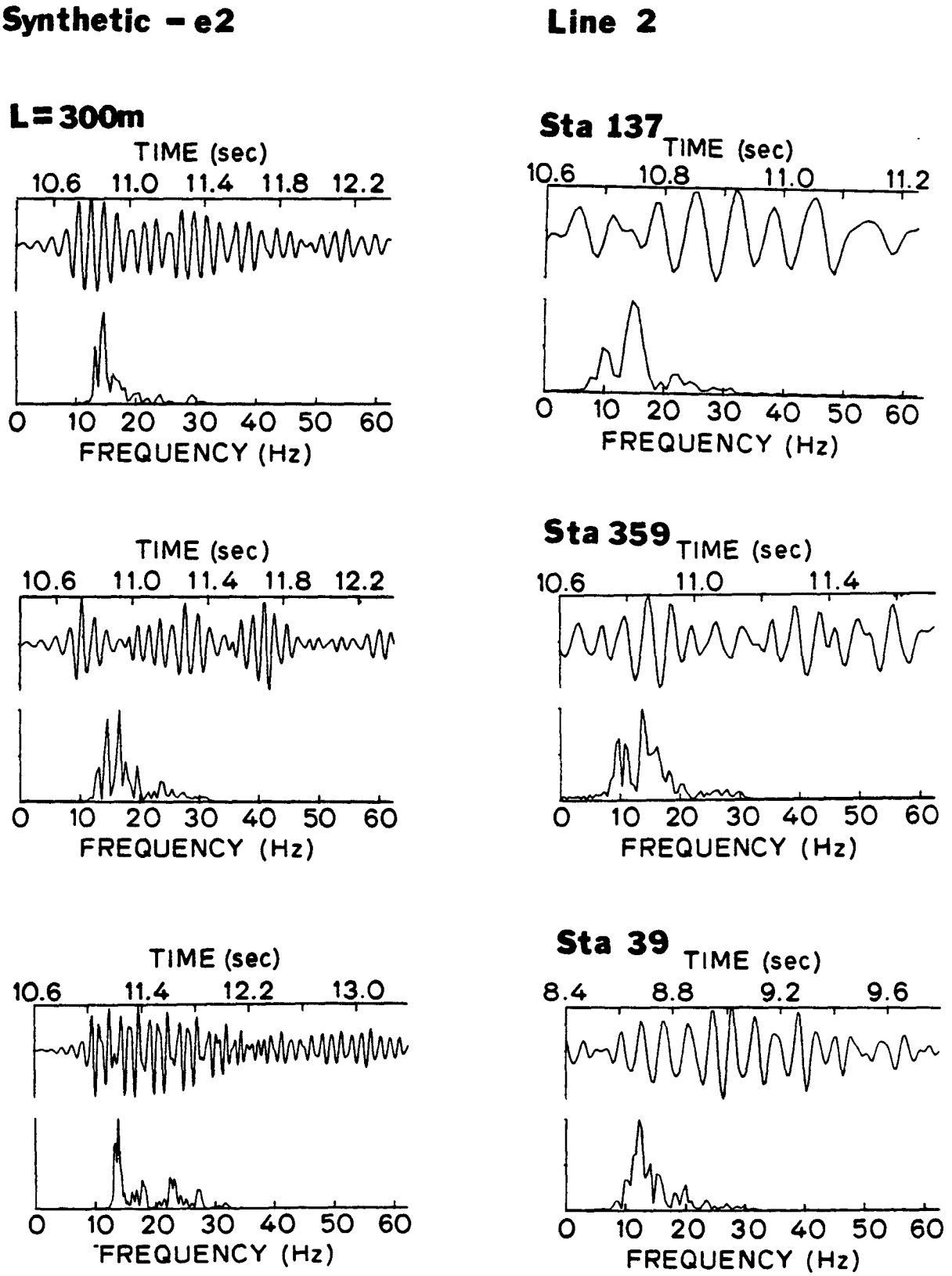

Figure 53. Frequency content of reflections from the Wind River thrust fault (right) and for the synthetics (left).

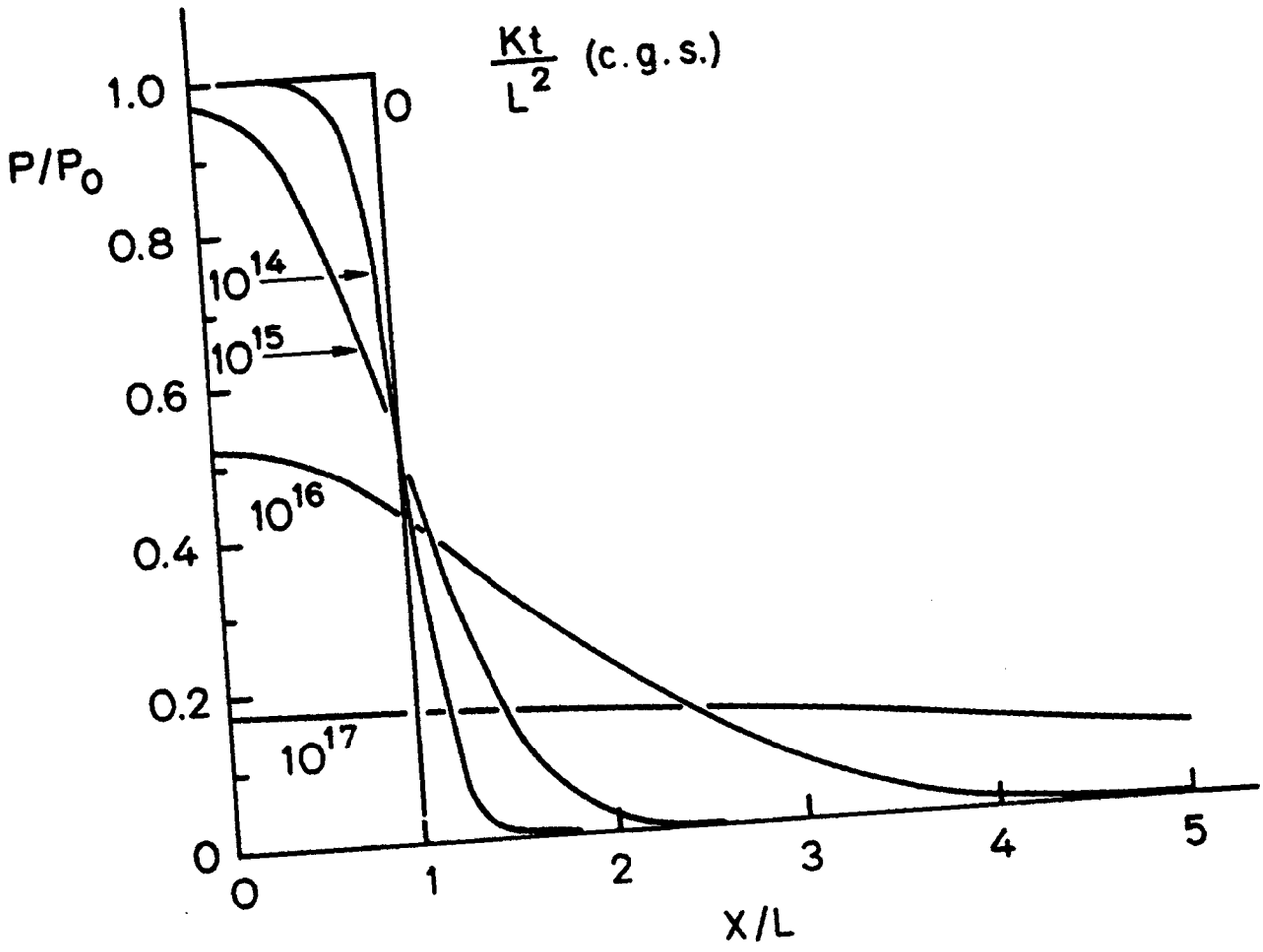

Figure 54. Transient solution for pore pressure in a material of permeability k. Initial conditions are pore pressure of P_0 at initial time in a zone of width 2L, and pore pressure of zero elsewhere. Curves plotted for given values times kt/L^2.

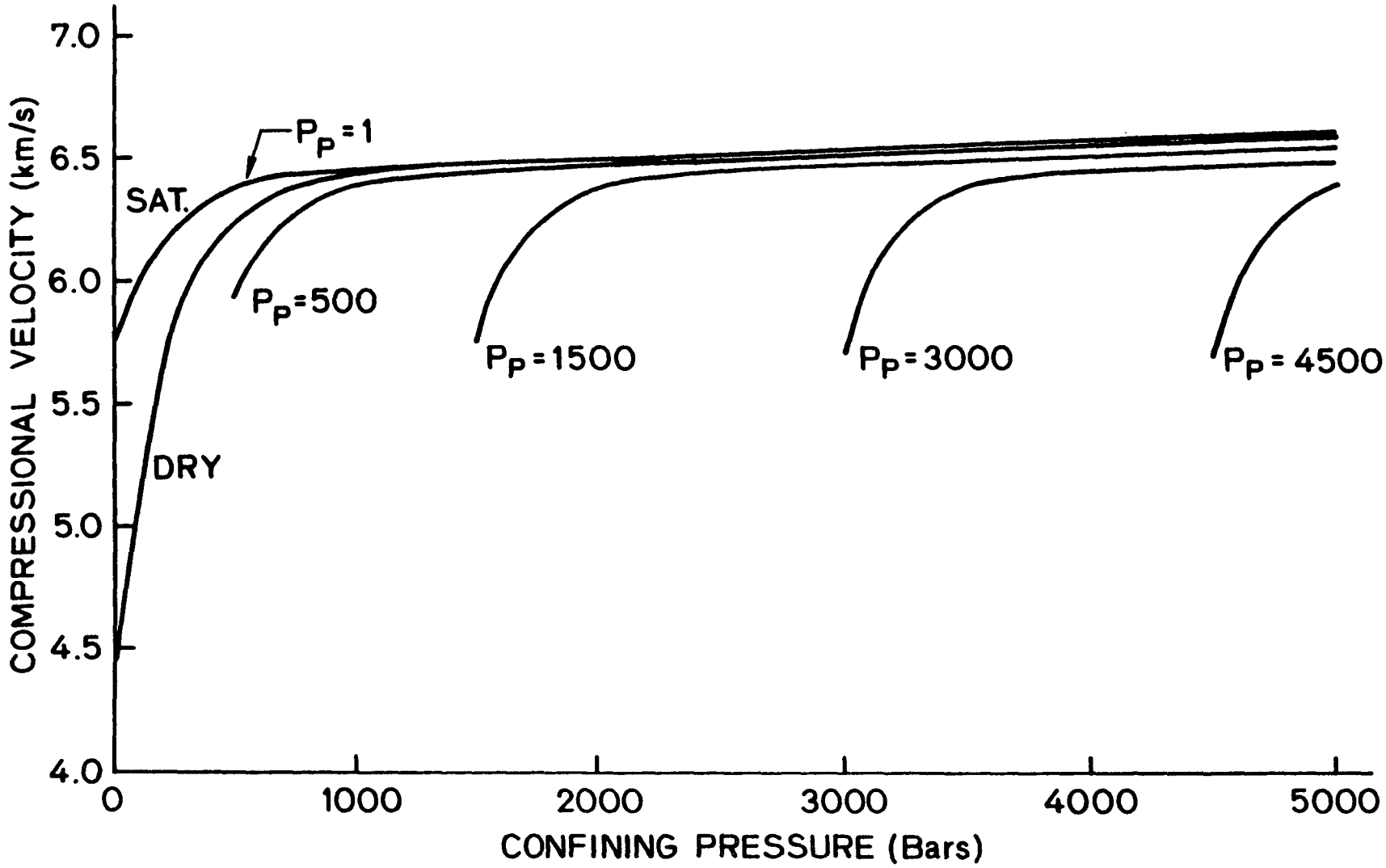

Figure 55. Empirical model for the effect of confining pressure and pore pressure on compressional velocity in a low porosity rock of approximately gabbroic composition.

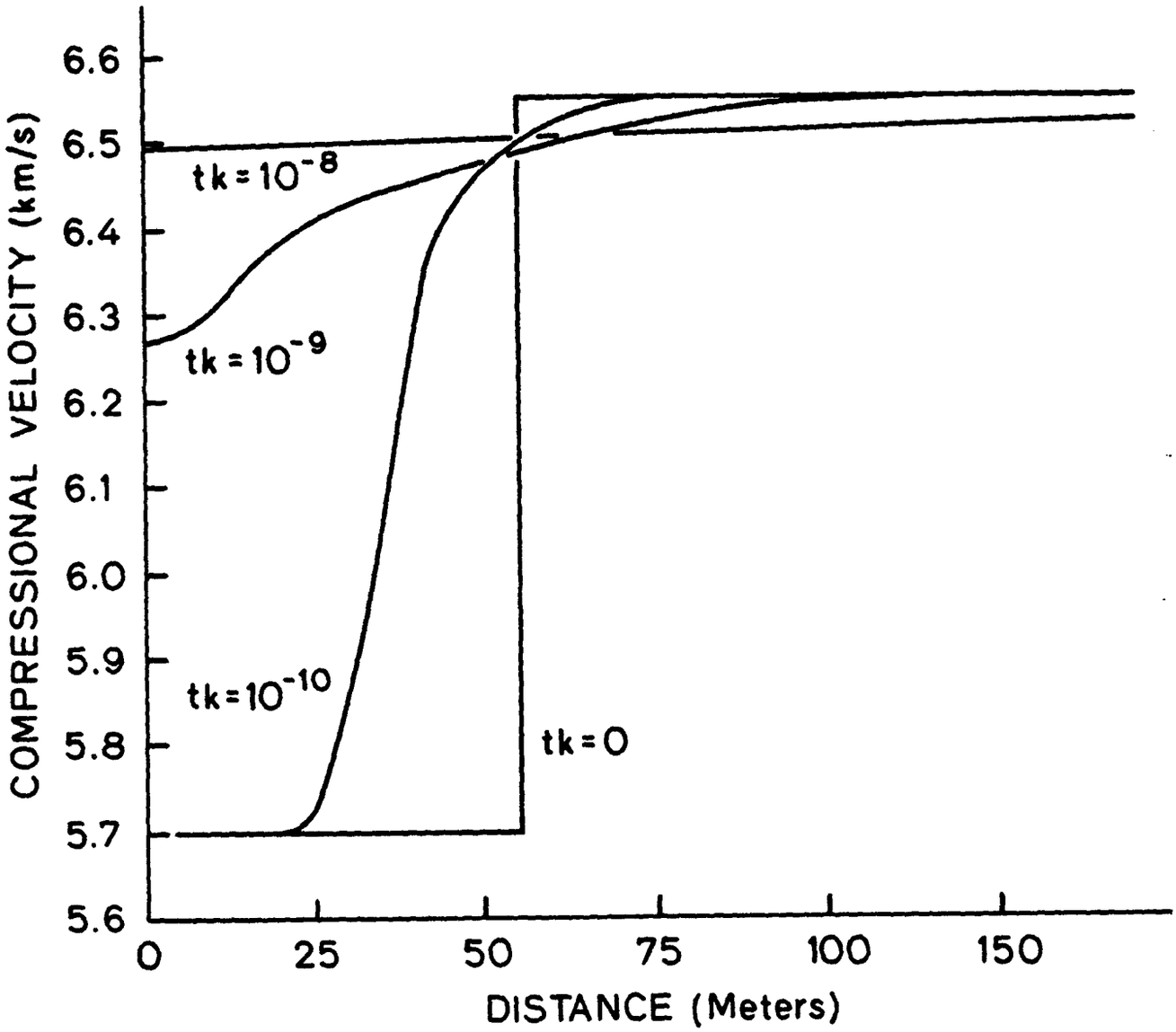

Figure 56. Velocity profile across a zone 110 meters thick as initial lithostatic pore pressure diffuses out. Pore pressure model based in Figure 54, and velocity model based on Figure 55. Curves are plotted for values of the product of time (in seconds) and permeability (in cm^2).

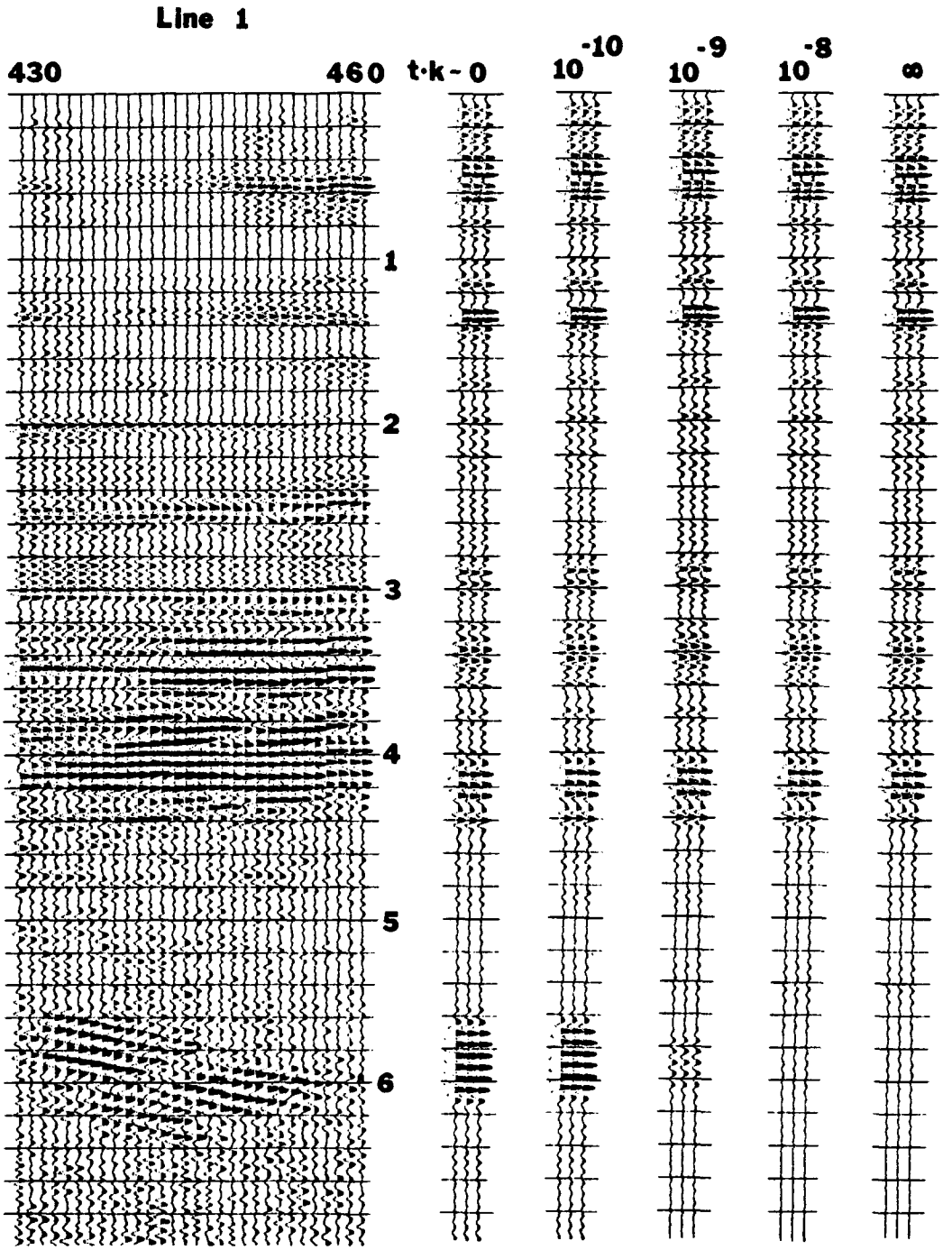

Figure 57. Portion of Wind River line 1 on the left, showing reflections from the Pacific Creek thrust at 6 seconds. Synthetics computed for a series of zones 110 meters in thickness, alternating ones which have an initial lithostatic pore pressure. Several cases show the change in reflectivity as the pore pressure diffuses out as the product tk increases.